Investigating the Eco-Hydrological Impact of Tropical Cyclones

in the Southeastern United States

by

Julien Brun

Department of Civil and Environmental Engineering
Duke University

Date:_____

Approved:

_____
A.P. Barros, Supervisor

_____
J. L. Evans

_____
R. B. Jackson

_____
M. A. Medina

_____
A. M. Porporato

Dissertation submitted in partial fulfillment of
the requirements for the degree of Doctor
of Philosophy in the Department of
Civil and Environmental Engineering in the Graduate School
of Duke University

2013

ABSTRACT

Investigating the Eco-Hydrological Impact of Tropical Cyclones

in the Southeastern United States

by

Julien Brun

Department of Civil and Environmental Engineering
Duke University

Date:_____

Approved:

_____
A.P. Barros, Supervisor

_____
J.L. Evans

_____
R.B. Jackson

_____
M. A. Medina

_____
A. M. Porporato

An abstract of a dissertation submitted in partial
fulfillment of the requirements for the degree
of Doctor of Philosophy in the Department of
Civil and Environmental Engineering in the Graduate School of
Duke University

2013

Abstract

Tropical Cyclones (TCs) intensity and frequency are expected to be impacted by climate change. Despite their destructive potential, these phenomena, which can produce heavy precipitation, are also an important source of freshwater. Therefore any change in frequency, seasonal timing and intensity of TCs is expected to strongly impact the regional water cycle and consequently the freshwater availability and distribution. This is critical as freshwater resources in the US are under stress due to the population growth and economic development that increasingly create more demands from agricultural, municipal and industrial uses, resulting in frequent over-allocation of water resources.

In this study we concentrate on monitoring the impact of hurricanes and tropical storms on vegetation activity along their terrestrial tracks, and investigate the underlying physical processes. To characterize and monitor the spatial organization and time of recovery of vegetation disturbance in the aftermath of major hurricanes over the entire southeastern US, a remote sensed framework based on MODerate resolution Imaging Spectroradiometer (MODIS) Enhanced Vegetation Index (EVI) was developed (Brun and Barros, 2012). The data show that in the first water year (October–September) after hurricane landfall, pronounced decreases in chlorophyll activity are found predominantly at very low elevations – including coastal marshes, wetlands, and the

floodplains aligned with drainage networks of major river systems along the storm track. Inland impacts are mainly located in agricultural areas and woody wetlands in the floodplains, and in forested headwater basins in the mountains.

At the SE scale, this framework was complemented by a water balance approach to estimate the spatial variability in hurricane groundwater recharge capacity and between events (Brun and Barros, 2013). The contribution of TCs (season totals and event by event) to the SE US annual precipitation totals from 2002 to 2011 was subsequently investigated using water budget approach applied at the drainage basin to characterize the partitioning of TCs' precipitation into surface runoff and groundwater in the direct aftermath of major TCs. This framework allows exploring the contribution of TCs to annual precipitation totals and the consequent recharge of subsurface reservoirs across different physiographic regions (mountains, coastal and alluvial plains) versus the fraction that is quickly evacuated through the river network and surface runoff. The data indicate that at the drainage basin scale, TC precipitation during the hurricane season can reach as high as 65% of the annual total of specific watersheds. In our period of study (2002–2011), Frances in 2004 was the hurricane which produced the highest amount of precipitation, producing up to 20% of the annual totals over coastal and mountain basins. The large precipitation deficit existing at the beginning of the 2004 and 2005 hurricane seasons was entirely redressed by the end of the season. In 2002 and 2008, the contribution of TCs in reducing the deficit was also significant. There is a strong

gradient in the runoff partitioning of precipitation across the different physiographic regions with the surface runoff being dominant in the mountains and the recharge to the groundwater system being dominant in Piedmont and Coastal Plains. Serial storms enhance runoff response highlighting the role of antecedent moisture conditions in rainfall-runoff processes, and consequently in the partition of TC precipitation between the surface and the groundwater system.

Finally a Land surface Eco-Hydrological Model (LEHM), combining water and energy budgets with photosynthetic activity, is used to estimate Gross Primary Production (GPP) over the SE US and the impact of TCs on the carbon budget at the seasonal and inter-annual scale over a 10-yer period. The model results are first compared to AmeriFlux tower data and MODIS GPP products over the SE United States in order to establish the model's ability to capture vegetation dynamics for the different biomes of the SE US. To evaluate the impact of Tropical Cyclones (TCs) precipitation over the SE US, various numerical experiments with the LEHM were conducted with and without TC meteorology (precipitation, wind and radiative forcing) by replacing the signature of TC forcing with NARR-derived climatology of atmospheric forcing ahead of landfall and along the TC terrestrial path. The comparison of these GPP estimates with those obtained with the normal forcing result in areas of discrepancies where the GPP was significantly modulated by TC activity. At the regional scale, the LEHM simulated GPP exhibits spatial variability related to water stress at inter-annual time-scales which is not

captured by the coarse MODIS GPP patterns. Inter-annual relative difference variations in the LEHM simulated annual GPP show that the impact of TCs on redressing meteorological, hydrological and eco-hydrological droughts occurs at different time-scales extending to periods of 1-3 months in the case of the latter depending on storm timing . The comparison of the 10-year simulations with and without TC meteorology has shown that the impact of TCs on soil water content as simulated by the LEHM can be as high as 8% of the annual average soil water content and up to 15% of the monthly average along the TC tracks. The excess soil moisture availability attributed to TCs is coupled to an increase of GPP over large areas ranging between 5 and 15%. Isolated events, such as tropical storms and generally weak TCs moving slowly across the SE US such as Bill (2003), Fay (2008) and Lee (2011) can have an important impact on GPP at the regional scale. The timing of the landfall is critical in terms of impact on the GPP, with early season TCs such as Alberto and Barry having a more significant impact on GPP than TCs happening near and past the mid-point of the hurricane season. Therefore any shift in season related to climate change should have an important impact on water availability and vegetation dynamics in the SE US.

Contents

List of Tables

List of Figures

Acknowledgements

This research was supported in part by a NASA Earth and Space Science Fellowship and by NOAA SARP-WATER grant NA08OAR4310701.

I use this opportunity to acknowledge and thank Dr. Ana P. Barros, my advisor, for giving me the opportunity to join the Civil and Environmental Engineering Department at Duke; for her support, guidance and keeping me going forward all along my PhD journey. I also thank the former and present members of the Barros' group - DK, Olivier, Prab, Wei, Xiaoming, Jing, Anna, Jessica, Lauren and Viola - for their help and laughs that made my stay at Duke a wonderful experience. You guys rock! A special thank you to Prabhakar for the interesting discussions while working on mapping aerosol intrusion in Himalayan valleys. I am also grateful to my PhD committee members - Dr. J.L. Evans, Dr. R.B. Jackson, Dr. M.A. Medina and Dr. A.M. Porporato - for their time and precious advice.

Thanks also goes to Dr. Jeffrey T. Morisette for his guidance on the MODIS NACP phenologically corrected products, to Michael E. Wieczorek (USGS) for sharing the watershed database and providing useful information on the watershed delineation process and to Dr. Stefano Manzoni for his insights on stomatal behavior and for sharing his database and thoughts, to Mathieu Therezien for being my friend and for his help.

Finally, I want to thank my family. My parents who always supported me even if it implied having their grandchildren far away. The two side projects I started along my PhD: my son, Eliott, for his joy and energy that he transmits to me. The first thing I do after my thesis defense is playing a game of giant Frisbee with you. Sophia, my little sunshine, who can warm up my heart with one smile (without teeth). Last but not least, my wife Karina for her constant and immutable support and without whom this work would not have been possible.

Overview

Climate change is expected to strongly impact the climatology of meteorological extremes in terms of intensity, frequency and timing. Despite their destructive potential, these extreme phenomena often produce heavy precipitation that is an important source of freshwater input to regional aquifers. The overall scientific goal of my research is to investigate the eco-hydrological impacts of extreme precipitation on the environment at the meso- and macro- scales. The applied goal is to develop monitoring and modeling tools that can be used in studies to plan and adapt for the consequences of changes in extreme hydrometeorological regimes.

The study area of interest is the southeastern United States, where the most intense and recurrent extreme precipitations are related to tropical cyclones (TCs) originating from the Atlantic basin. In particular, the focus is on the role of TCs in the regional hydrology of the SE US. To this end, a remote sensing monitoring framework to detect the location of vegetation disturbances along the terrestrial track of TCs and track the time necessary for recovery was developed (Brun and Barros, 2012). Besides the strong coastal disturbances close to landfall, persistent disturbances located along the alluvial plains of major rivers where intense cropland activity takes place were also detected. Additionally, vegetation disturbance clusters were identified in mountainous regions. These results motivated further work toward distinguishing, vegetation disturbances due to mechanical destruction of vegetation (by wind or water surge) from disturbances related to hydrological processes impacting soil-plant interactions. A watershed based

regional approach to estimate the contribution of TCs precipitation to fast and slow scales of basin response has been developed to address this question (Brun and Barros, 2013). This geographic information system (GIS) framework allows us to explore the contribution of TCs to the recharge of groundwater reservoirs across different physiographic regions (mountains, coastal and alluvial plains) at the watershed scale. Then, a hydrological model that also includes representation of vegetation dynamics has been enhanced, and used to investigate the physical processes leading to anomalies in vegetation photosynthetic activity in the aftermath of storm passage and how TCs contribute to recharge groundwater reservoirs and relief drought conditions. Combining these 3 techniques allows us to evaluate the relative impact of TCs on regional climatological stresses leading to vegetation disturbance. We will finally estimate how these processes impact the gross primary production (GPP) and therefore the feedback on the regional carbon cycle.

1 Introduction

1.1 Motivation

According to the Intergovernmental Panel on Climate Change (IPCC, 2007) the number of heavy daily precipitation events that lead to flooding have generally increased since 1950. In the southeastern US, the most powerful and recurrent meteorological phenomena are hurricanes and tropical storms (Kunkel et al., 2010). Tropical storm and hurricane frequencies vary considerably in time, but evidence suggests a substantial increase in terms of intensity and frequency (Karl et al., 2008; Knutson et al., 2010). During the summertime, Atlantic tropical cyclones can cause damages estimated to cost billions of dollars and loss of life along their track (Pielke et al., 2008) and these could rise in the near future (Mendelsohn et al., 2012). However, Tropical Cyclones also provide a significant influx of freshwater to the environment in a short period of time, replenishing aquifers in the recharge areas along the storm track.

In addition to climate impacts on water regimes, freshwater resources around the world are under stress due to population growth and economic development. This combination leads to a large range of physical and socio-economic impacts of a warming climate (Beniston, 2012). As summarized in the IPCC report "Working Group II: Impacts, Adaptation and Vulnerability" (Parry et al., 2007), freshwater resources in the US are under stress due to the population growth and economic development that create more demands from agricultural, municipal and industrial uses, resulting in frequent over-allocation of water resources (Colin and David, 2005). Thus, vulnerability to extended

drought is increasing across North America. Even if the Eastern US is less frequently impacted by drought than the West, droughts still handicap existing water resource management plans, posing difficult challenges in water allocation between anthropogenic and environmental needs (Dupigny-Giroux, 2001; Field et al., 2007). ***There is therefore a critical need to further investigate the role of extreme meteorological phenomena in the SE US water cycle and their resulting environmental impacts, to better understand and prepare for the potential effects that could be induced by climate and environmental change.***

Climate change could impact the path, frequency and/or strength of TCs (Emanuel, 2005; Michener et al., 1997; Pielke et al., 2005; Shepherd and Knutson, 2007). However, future trends in hurricane frequency and intensity remain very uncertain (Parry et al., 2007). Experiments with climate models at sufficient spatial and temporal resolutions to depict specific characteristics of individual hurricanes tend to project some increases in both peak wind speeds and precipitation intensities (Field et al., 2007). The pattern is clearer for extra-tropical storms, which are likely to become more intense, but perhaps less frequent (Meehl et al., 2007). Consequently any change in the track, frequency or strength of these phenomena could lead to significant impacts on regional hydrology.

Despite the efforts to better understand rainfall produced by TCs, little is known about the contribution of TCs related precipitation to extreme precipitation over North America (Barlow, 2011). Previous analyses of rain gauge time-series have shown that the proportion of extreme precipitation related to hurricanes is of large influence on the US hydrological cycle and not only the coastal zone as normally considered (Barlow, 2011;

Konrad and Perry, 2010) and that the spatial distribution of these extremes is not simply related to the track density, i.e. the number of events. Relying in the analysis of the Tropical Rainfall Measurement Mission (TRMM) 3B42 product from 1998 to 2009, Prat and Nelson (2012) estimated the TC contribution to reach locally 40% of seasonal totals (June to November) for year with major hurricanes with a peak close to 20% for the month of September. Using Stage IV precipitation products, Brun and Barros (2013) showed that at the watershed scale highly active hurricane seasons such as 2004, can bring up to 65% of the annual totals of precipitation. Recently, Kam et al. (2012) using offline simulations with a macroscale hydrologic model illustrated how the precipitation produced by TCs can impact drought through late initiation and early recovery, and smaller spatial extent.

Previous studies also suggest that the contribution of tropical cyclone precipitation to extreme precipitation has significantly increased both in magnitude and frequency during the last decades in Atlantic coastal states of the SE (Knight and Davis, 2009). Consequently, these changes in TC activity are expected to have a significant influence on the precipitation totals at the regional scale and therefore strongly impact the hydrological cycle. Besides the quantitative contribution of TC precipitation, its timing is also critical due to the peak in evapotranspiration during the summertime. At this time of the year, the vegetation needs a large amount of water to allow optimal photosynthetic activity, and it is therefore very sensitive to water availability. Although the amount of precipitation related to TCs can represent a large fraction of annual precipitation, there are only a few studies on how this episodic freshwater input

participates in recharging surface and subsurface reservoirs, especially at the regional scale with most of the studies focusing on fast hydrologic response (floods and flash-floods) and not on water cycle questions at seasonal and inter-annual time-scales (e.g. Smith et al., 2010; Tao and Barros, 2013; Villarini et al., 2011).

In fact, the eco-hydrological impacts of TCs precipitation are expected to change drastically between different physiographic regions, since the environmental response is strongly modulated by how water is stored and how it moves in the landscape. O'Connor and Costa (2004) computed the spatial distribution of the largest rainfall-runoff floods across a large range of basin sizes in the US. They proposed 2 factors to explain the observed distribution of high discharge watersheds (i.e. large runoff response): 1.) Presence of regional conditions that produce large precipitation; 2.) Steep topography, which enhances precipitation by convective and orographic processes and allows flow to be quickly concentrated into stream channels. They found that in the southeastern United States, watersheds with large discharge are concentrated along the Appalachians, where these two conditions are fulfilled. Despite similar regional meteorological conditions, high discharge watersheds are rare in the flat and permeable Atlantic coastal plains.

Tropical Cyclones do not only influence the water cycle through precipitation, they also modulate the response of the environment to future events by damaging the vegetation (by wind, storm surge, floods or erosion) and consequently modifying the land cover. For example, it has been shown that young fast-growing tree plantations use more water compared to native vegetation (e.g. Bren et al., 2010; Kagawa et al., 2009;

Licata et al., 2008). These changes in vegetation and land cover also feed back on plant–soil interactions and streamflow at the annual scale by changing vegetation water use (Asbjornsen et al., 2011).

On the coastal plains, TCs damage the environment close to the landfall through water surge and strong winds (Blake et al., 2007; Pielke et al., 2008; Zeng et al., 2009). Salt infiltration resultant from the surge can also induce a long-term disturbance in the ecosystem. Further inland, mechanical destruction due to winds is still present and local flooding, erosion and high soil moisture can damage vegetation roots. Finally, nutrients washout related to the flood and strong runoff can also impact vegetation activity (Burkholder et al., 2004; Heartsill-Scalley et al., 2007; Paerl et al., 2006).

The vulnerability of forested areas to hurricane destruction has been well documented, especially at the local scale (Basnet et al., 1992; Beard et al., 2005; Boose et al., 1994; Boutet and Weishampel, 2003; Brokaw and Jason, 1991; Brokaw and Walker, 1991; Chambers et al., 2007; Everham and Brokaw, 1996; Frangi and Lugo, 1991; Gresham et al., 1991; Lodge and McDowell, 1991; Oswalt and Oswalt, 2008; Pascarella et al., 2004; Walker, 1995; Wang and Xu, 2009; Wen et al., 2008). Although several studies have shown that damages are still visible several years after major hurricanes (Beard et al., 2005; Frangi and Lugo, 1998), a systematic quantitative assessment of landscape response at the regional scale is still lacking, especially in terms of long-term effects (Brun and Barros, 2012; Jacobs, 2007; Zeng et al., 2009).

There is therefore a critical need to develop the capacity to characterize the eco-hydrological impacts of TCs at regional scale to better understand: 1.) The time-rates and

strategies of landscape recovery in the aftermath of major TCs using vegetation activity as a proxy of ecohydrological disturbances; 2.) The causes of environmental disturbance persistence; 3.) The impact of such disturbances on Gross Primary Productivity (GPP); and 4.) The fraction of precipitation contributing to soil moisture and how this contribution relates to anomalies in vegetation activity. ***This quantitative understanding is critical to establish the basis for realistic assessments of the potential impacts of extreme weather changes (in frequency, location and/or intensity) on vegetation dynamics and the water cycle at regional scale***.

1.2 Research Objectives

I. ***To establish the spatial distribution and persistence of the impacts of land-falling hurricanes on the environment using vegetation activity as an indicator of disturbance.***

   Hypothesis: Coastal vegetation activity will be strongly affected close to the hurricane landfall due to wind and water surge causing mechanical destruction. Further inland, the disturbances should be less persistent as the storm intensity decreases. The time of recovery should be directly related to damage strength and strongly dependent on the vegetation type and local hydrometeorology.

II. ***To specify the hydrologic regimes among the watersheds of the SE US in the aftermath of major TCs, and to investigate the relationship between these regimes and the observed vegetation disturbances.***

Hypothesis: Persistent vegetation disturbance associated with hydrological processes is expected to be dominant over basins with large (small) direct runoff (recharge) fraction at the event scale.

III. ***To estimate how TC precipitation impacts the carbon cycle of the SE US by changing water availability and vegetation activity.***

Hypothesis: The direct GPP decrease associated with hurricane damages should be moderate at the regional scale due to localized nature of the damages. However, the indirect impact of TCs on GPP, as an important source of water availability, should be significant at the regional scale.

1.3 Approach

To achieve specific research goal I, a remotely sensed framework based on MODIS enhanced vegetation index (EVI) was developed to monitor the vegetation disturbance and its persistence (Brun and Barros, 2008, 2012). A new metric, the MODIS Vegetation Disturbance Persistence (MVDP), was introduced to measure the number of continuously disturbed 8-day periods during the hydrological year (Oct. to Sept. the next calendar year) following the hurricane season. Based on this new information, we investigated the causes of such disturbances using geostatistical analysis to compare the spatial correlation between the disturbances and different meteorological (storm related, such as wind speed, precipitation) and physical parameters (such as elevation, land cover, soil porosity). This work is fully described in Section 3 of this report.

To further investigate the hydrological processes leading to vegetation disturbance and establish in which areas these processes are expected to be dominant (research goal II), we have developed a water balance hydroclimatology relying on ~ 3,400 drainage basins monitored by the U.S. Geological Survey (USGS) streamgage network in the SE US (Brun and Barros, 2013). The specific objectives include establishing which fraction of precipitation is related to TCs with regard to the annual precipitation depth across the different physiographic regions, and the partitioning of TCs precipitation into surface runoff and groundwater recharge across the landscape. This work is described in Chapter 4. Finally, in Chapter 5, an eco-hydrological model combining water and energy budgets with photosynthesis activity (Garcia-Quijano and Barros, 2005; Gebremichael and Barros, 2006) is used to investigate the feedback of TCs on the SE carbon cycle (research goal III). Model simulated gross primary production (GPP) over the Southeastern US is used to investigate the role of TCs as a source of freshwater in the SE carbon cycle and to further investigate the link between vegetation disturbance persistence, hydrological processes, and basin hydrogeology.

2 Area of Study

The region of study encompasses the southeastern US, including Florida, Virginia, and Tennessee in addition to North and South Carolina, Georgia, Alabama, Mississippi and Louisiana (Figure 2-1). The regional climate is humid subtropical consisting of cool and mild winters with precipitation from big storms systems whereas summers are hot and humid with heavy precipitation from thunderstorm systems. The hurricane season takes place from June to the end of November with the peak activity usually taking place between August and October.

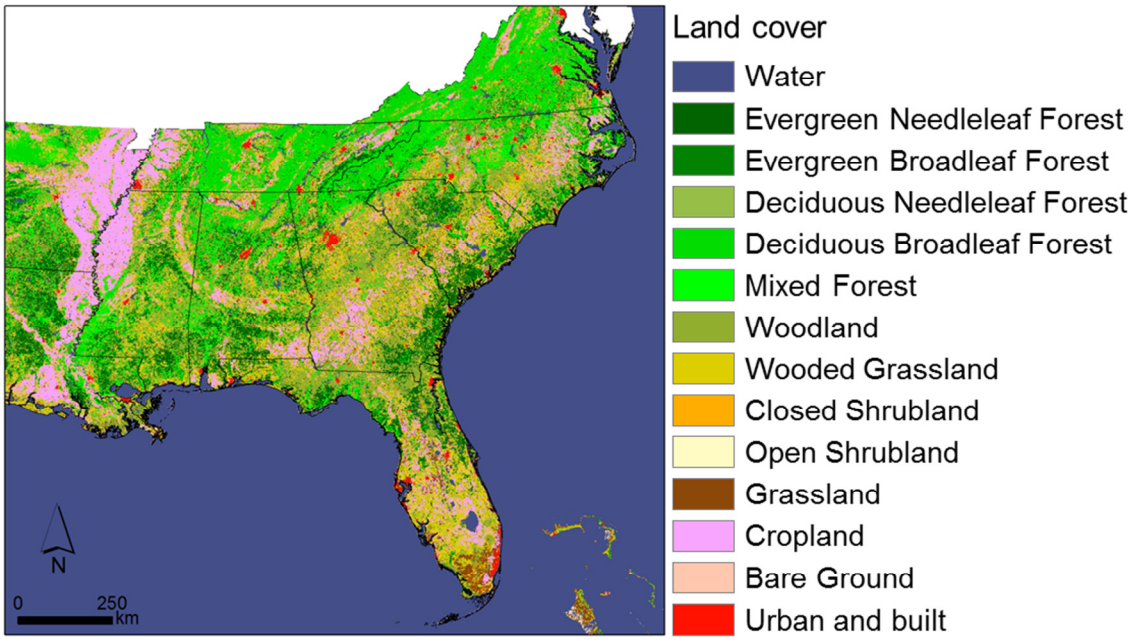

Figure 2-1: Overview of the area of interest for this study.

Tracks of all major hurricanes are available from NOAA's National Hurricane Center (NHC, http://www.nhc.noaa.gov). During the period of study (2001 to 2007), 2002 and especially 2004 and 2005 (Katrina) are the years with the highest number of TCs. In 2003, hurricane Isabel strongly impacted North Carolina and Virginia. Although

the number of events is important, the intensity of each event as measured by wind intensity and precipitation amount and extent should be key to understand the terrestrial impacts of hurricanes after landfall. In addition to the highest number of events, 2004 and 2005 were also the years with the strongest events on the wind-based Saffir-Simpson scale. Consequently, pronounced vegetation disturbances are expected during these two years and in the following years. The 2003-2007 period timeframe is therefore expected to be critical in this study.

3 Vegetation disturbance monitoring

In keeping with previous research, we use a remote sensing approach to describe the spatial heterogeneity of vegetation at regional scale (Chambers et al., 2007; Fisher and Mustard, 2007) based on the analysis of time-series of vegetation indices (Goward et al., 2008; Lunetta et al., 2006; Neigh et al., 2008; Potter et al., 2005). MODIS data were processed to detect areas subject to stress conditions in vegetation chlorophyll activity both in terms of biomass and phenology. In this section, we present the methodology used in the analysis of vegetation chlorophyll activity decrease and disturbance persistence along the track of major hurricanes between 2001 and 2007.

Currently, because of the diversity and quality of available remote sensing sensors, and despite the fact that not all time-series of satellite-based observations are long enough to establish baseline climatologies, high spatial and temporal resolution of remote sensing data are especially effective for environmental monitoring (Coppin et al., 2004; Kennedy et al., 2009; Lu et al., 2004; Mas, 1999), and consequently to evaluate the impact of natural hazards at large-scales (Barnes et al., 2007; Chen et al., 2007; Metternicht et al., 2005; Temesgen et al., 2001). The impact of hurricanes on ecosystems is well documented especially for forested areas (Basnet et al., 1992; Beard et al., 2005; Boose et al., 1994; Boutet and Weishampel, 2003; Brokaw and Jason, 1991; Brokaw and Walker, 1991; Chambers et al., 2007; Everham and Brokaw, 1996; Frangi and Lugo, 1991; Gresham et al., 1991; Lodge and McDowell, 1991; Oswalt and Oswalt, 2008; Pascarella et al., 2004; Walker, 1995; Wang and Xu, 2009; Wen et al., 2008). Although several studies have been conducted in the immediate aftermath of major hurricanes (Farris et al.; Wang

et al., 2010), a systematic quantitative assessment of landscape response at the regional scale is still lacking, especially in terms of long-term effects (Jacobs, 2007; Zeng et al., 2009).

In this section, the approach is to use remote sensing to monitor vegetation disturbances with a focus on their persistence in terms of green biomass variations, and also in terms of phenological shifts at regional and event-specific scales. The underlying premise is that it is critical to elucidate the time-scales that govern landscape recovery after a major disturbance in order to anticipate the impact and consequences of future changes in hurricane activity required for effective adaptation. To this end, Moderate Resolution Imaging Spectroradiometer (MODIS) vegetation products developed for the North American Carbon Program (NACP) at 500m spatial resolution were analyzed to detect patterns of inter-annual variability in the vegetation first, and second to conduct interpretive studies for specific extreme storms. The datasets used are described in the Section 4.1 and the methodology used for data analysis is described in Section 4.2. Evaluation of the proposed vegetation monitoring framework is presented in Section 4.3. Section 4.4 consists of interpretive case studies of two specific storms: Isabel in the eastern seaboard (North Carolina) and Katrina in the Gulf Coast (Louisiana). The final discussion is presented in Section 4.5.

3.1 Datasets

3.1.1 MODIS NACP

In particular, the 8-day EVI composite gap filled (MOD09A1G) product of the North American Carbon Program (NACP) was selected for this work because it was processed to remove erroneous and biologically implausible values from the original MODIS data. The asymmetric Gaussian function of the TIMESAT software is used to fill the gaps and find the best fit of the time-series with a specific weight given to the data based on the quality flag of the used MODIS dataset (Gao et al., 2008; Morisette, 2009)

3.1.2 EVI

The Enhanced Vegetation Index (Luzum et al., 2005; Shrestha et al., 2005) of the Moderate Resolution Imaging Spectroradiometer (MODIS) is defined as follows (Eq. 4.1):

$$EVI = (L+1)\frac{\rho_{NIR} - \rho_{RED}}{L + \rho_{NIR} + C_1\rho_{RED} + C_2\rho_{BLUE}} \quad (3.1)$$

where: ρ = Top-of-the atmosphere reflectance

L = Soil adjustment factor

C_1 = Atmosphere resistance Red correction coefficient

C_2 = Atmosphere resistance Blue correction coefficient

Due to the short satellite revisiting-period (one to two images per day are available for most of the Earth), MODIS products provide an ideal observational basis for

vegetation time-series analysis (Brown et al., 2006; Jin and Sader, 2005; Lunetta et al., 2006; Yilmaz et al., 2008). EVI was designed to address shortcomings of the popular Normalized Difference Vegetation Index (NDVI) by seeking increased sensitivity over dense vegetation regions, such as forests, and less sensitivity to atmospheric noise. This saturation effect is present over the region of interest (Brun and Barros, 2008). In addition, EVI was found to be the most consistent vegetation index product based on previous assessements of hurricane impacts (Rogan et al., 2010; Wang and Xu, 2009).

3.2 MODIS Vegetation Disturbance Persistence Index

3.2.1 Disturbance

The pre-processed 8-day composite images (46 per year) were stacked per "water year", with the "water year" defined as beginning in October of the current calendar year and ending in September of the next calendar year. This choice is motivated by the fact that the peak of hurricane activity tends to occur in late summer in the SE US. The immediate hydrological year should thus be optimal to detect the temporal evolution of hydro-ecological perturbations along the hurricane track. The 8-day standardized anomalies are calculated in the case studies reported in this manuscript for the available number of years n using the t-distribution as follows:

$$Z_{i,j} = \frac{X_{i,j} - \overline{X}_{i,n}}{SD_{i,n} / \sqrt{n}} \qquad (3.2)$$

Where i is the 8-day period index for each year (1, 46)

j is the year (2001 to 2007)

n is the number of years observed

The standardized value $Z_{i,j}$ is therefore calculated for the same 8-day calendar period across the years to remove the seasonal cycle. In addition, the normalization over the same 8-day period throughout the years enables detection of time shifts in the phenology. Subsequently, the pixels with negative anomalies and a cumulative probability of at least 95% [i.e. standardized value $Z_{i,j}$ lower than $t_{0.05}$ =-1.943 for 6 degrees of freedom] are identified, and a binary mask is generated where pixels with significant negative anomalies are given a value of 1 and zero otherwise. This approach is similar to the one used by Potter et al. (2005) for the detection of AVHRR FPAR anomalies.

3.2.2 Persistence

The MODIS Vegetation Disturbance Persistence (MVDP) metric is defined as the number of *uninterrupted* 8-day periods of significant anomalies (as defined above). It is obtained by summation of the binary values (1) for each water year at each pixel from the beginning of the disturbance to the end without interruption. That is, a period is only added to the sum if the previous period was also disturbed. This metric quantifies the duration of the disturbance during the water year, and the final value corresponds to the longest continuous disturbed period. Thus, in the case of the MODIS NACP product used here, the MVDP ranges from 0 (no anomalies) to 46 8-day periods corresponding to a continuously disturbed hydrological year. Note that due to the shorter growing seasons of crops, roughly three months shorter than natural vegetation on average, the

maximum possible MVDP in agricultural areas is expected to be lower (i.e. a difference of 11 on the MVDP scale).

3.3 Methodology Evaluation

3.3.1 Vegetation Index Sensitivity

Besides the MVDP based on the EVI (Figure 3-1a), we also computed the MVDP using the NDVI (Figure 3-1b) for the Southeast US. The difference in sensitivity between EVI and NDVI is apparent. The MVDP based on the NDVI appears to overestimate the occurrence of anomalies compared to the EVI based MVDP. This is due to the saturation of the NDVI index during summer time in dense vegetated areas (e.g. forests) as discussed earlier (see also Brun and Barros 2008). This tends to flatten artificially the standardized distribution, and therefore the spatial patterns associated with the criteria based on the 95% significance level for the t-distribution. Note that this saturation effect is further enhanced when the MODIS NDVI data are aggregated by simple averaging to 8km and to one month temporal resolution (Figure 3-1c) for intercomparison against the Global Inventory Modeling and Mapping Studies (GIMMS) NDVI data set (Tesoriero et al., 2004) used to assess the sensitivity of the MVDP to record length in Section 3.3.2 below. There is however very good agreement among the spatial patterns for MVDP values greater than six months.

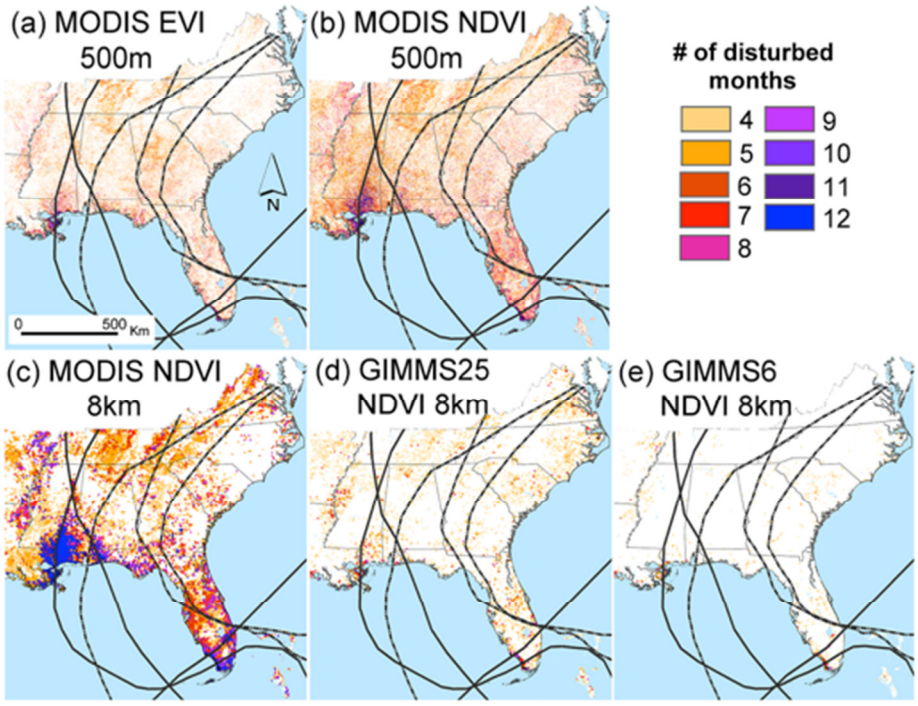

Figure 3-1: Comparison of VDP results computed from different datasets: (a) 8-day composite MODIS EVI at 500m resolution, (b) 8-day composite MODIS NDVI at 500m resolution, (c) monthly MODIS NDVI at 8km resolution, (d) monthly GIMMS NDVI at 8km resolution computed from the entire time-series (1982-2006), (e) monthly GIMMS NDVI at 8km resolution computed from 6 last years of the time-series (2001-06).

3.3.2 Statistical Robustness

MODIS begun to acquire data in March 2000, and the dataset used here (MOD09A1G) was only available from to 2001 to 2007 at the time this work was conducted. Due to this limitation, the sensitivity of the methodology to the length of the time-series was also investigated. As mentioned above, for this purpose, we relied on the Global Inventory Modeling and Mapping Studies (GIMMS) NDVI data set that consists of bi-weekly NDVI at 8km spatial resolution from July 1981 to December 2006. The GIMMS time-series has the great advantage that artifacts, such as solar zenith angle

errors introduced by orbital drift and atmospheric noise or other image defaults, have already been corrected (Tucker et al., 2005). The data set is freely available from the Global Land Cover Facility (http://www.landcover.org/data/gimms/), and it has been proven reliable for monitoring vegetation anomalies at large scales (Zhang et al., 2010). It is important to stress that the short length of the historical record of satellite-based products remains a major challenge, especially for characterizing landscape response associated with extreme events generally. This is further complicated by non-stationary in land-use and land-cover over time on the one hand, and in the frequency of hurricanes on the other as highlighted by Webster et al (2005), who reported an increase in major hurricane frequency over the Atlantic basin since mid-1990s. Nevertheless, much can be learned about landscape changes by careful analysis of relative if not absolute space-time anomalies interpreted in the light of the hydrologic processes that govern landscape response to such extreme events.

First, the GIMMS data were averaged to the monthly time-scale to avoid missing data. Next, in order to investigate the sensitivity to record length, MODIS EVI and NDVI time-series were aggregated by simple averaging to the GIMMS spatial and temporal resolutions. The GIMMS NDVI monthly mean from 1982 to 2006 was computed, and the monthly Vegetation Disturbance Persistence (VDP) was calculated first using the 25 years GIMMS product (GIMMS25, Figure 3-1d), and second using only a MODIS-like length time-series from 2001 to 2006 (GIMMS6, Figure 3-1e). The two records show consistent VDP patterns only in the areas where the highest values are clustered (i.e. MVDP > 6 months). Likewise, visual inspection shows there is close agreement between

the GIMMS25 and MODIS EVI VDP (Figure 3-1a and d)), again especially in the areas with high VDP clusters (> 6 months). The GIMMS25 NDVI VPD range is narrower and thus less sensitive to change than the MODIS EVI VDP as expected due to both the use of NDVI, and the difference in spatial and temporal resolutions. Also note that the aggregated 8km MODIS NDVI (Figure 3-1c) retains much of the spatial structure of the original 500m resolution product and exhibits the typical enlargement of spatial features associated with linear averaging in contrast with the GIMMS6 due to the spatial and temporal coarser resolution of the original AVHRR NDVI data.

Next, the coefficients of correlation between GIMMS25 and GIMMS6, and between GIMMS6 and the 8km MODIS NDVI were calculated for the years 2001 to 2006. In principle, besides the hurricane impacts that we seek to fingerprint in this study, any disagreements between the spatial patterns of GIMMS and MODIS VDP could be explained also by land cover change, fire, drought, and snow cover represented differently in the two products. MODIS land cover data (2003) was used to determine whether statistical agreements and disagreements are linked to certain land-cover categories (see Table 3-1). Across all land cover categories, the global mean coefficient correlation between GIMMS25 and GIMMS6 is around 0.76. The correlation is lower on average for croplands (0.747 ± 0.196) due to the modulation of the natural phenology through harvesting and culture rotation. The covariance shows a lager standard deviation to the mean compared to the correlation, with cropland also being the land cover with the lowest variability. Generally, however, there is very strong agreement between the two data sets, despite the different record lengths available to calculate the

anomalies: 25 years (GIMMS) and only 6 years otherwise. Note the very strong correlation between the two products in the case of wetlands in particular, which suggests that the vegetation disturbance in wetlands in the aftermath of the 2005 hurricane season is the strongest signal over the 25 years of GIMMS data.

Table 3-1: Correlation coefficients and covariance between VDP computed from different datasets: GIMMS with the entire times-series (GIMMS25), GIMMS overlapping MODIS era (GIMMS6) and MODIS NDVI aggregated at GIMMS spatial (8km) and temporal resolution (monthly).

	Coefficient Correlation VDP GIMMS6 and GIMMS25		Covariance VDP GIMMS6 and GIMMS25		Coefficient Correlation VDP GIMMS6 and MODIS 8km		Covariance VDP GIMMS6 and MODIS 8km		
Land cover	MEAN	SD	MEAN	SD	MEAN	SD	MEAN	SD	Samples used
forest	0.754	0.179	1.058	1.184	0.334	0.361	0.899	1.481	3370
cropland	0.747	0.196	0.893	0.762	0.314	0.362	0.760	1.120	4224
shrubland	0.784	0.182	1.082	0.989	0.307	0.370	0.956	1.694	3753
wetland	0.779	0.179	1.079	1.064	0.305	0.374	0.863	1.571	2487

This is consistent with the relative intensity of Katrina as compared with other storms during the period of record. On the other hand, the correlation between GIMMS6 and the 8km MODIS NDVI is much lower (Table 3-1), and agreement between the two is confined to coastal areas and floodplains (Mississippi) for VDP > 6 months (cf. Figure 3-1c and d). This suggests that inconsistencies in spatial and temporal sampling, and in particular the coarse resolution of the AVHRR NDVI, are more important to detect the range of space-time variability of vegetation disturbances than the length of the historical record.

3.3.3 Snow Cover Effects

Even if the Southeast US is not subject to regular snowfall, the effect of snow cover on the estimation of the MVPD must be assessed due to the reduction in EVI / NDVI values over snow covered areas, and the fact that the winter season is included in the calculation of the disturbance persistence metric. For this purpose, the GIMMS VDP was calculated separately for the warm season (April to October, when no snow on the ground is expected in the region) to determine whether a snow correction was necessary. Indeed, several years exhibited large spatial patterns with high VPD during the wintertime due to snow cover, and therefore the snow flag in the MODIS metadata should be used to trigger changes in the calculation of VDP. However, for the 2001-2006 period used in this study, no such widespread signal was detected, and therefore no correction is necessary. In addition, because the MVDP monitors only continuous disturbances and by imposing a threshold greater than 3 months for the data analysis (12 on MVDP scale), the local signature of snowfall is effectively removed on our methodology.

3.3.4 Regional Scale Evaluation

To evaluate the accuracy and sensitivity of the MODIS VDP (MVDP), the MVDP time-series were evaluated against ancillary data where and when available. First, we focus on the comparison against Landsat imagery before and after the hurricane processed by the USGS over the region of the Bayou national water reservoir in the aftermath of hurricane Katrina (Figure 3-2). The flooded areas are represented in red in the Landsat USGS analysis, and thus correspond to the potentially disturbed areas.

Visual inspection of the images shows there is good spatial agreement between the USGS high-resolution analysis and the MVDP results. The MVDP can detect therefore major disturbances, and generally the intensity of the disturbance and the duration of vegetation activity anomaly (MVDP) are well correlated spatially. Interestingly, there are two locations (identified by circles I and II) where the anomalies detected correspond to areas submerged by different flood mechanisms leading to different recovery time-scales: on the left (I), freshwater flooding shows very strong short-term impacts right after landfall, but recovery is fast taking place within 2-3 months; on the right (II), flooding due to the storm surge has limited impact initially, but erosion, washout of nutrients, and salt water intrusion delay recovery up to two years.

Second, the MVDP distribution in the SE was evaluated against the United States Forest Service (USFS) database of tree mortality aggregated to the county level (expressed in terms of dead wood volume in cubic feet). These data were normalized by the county fraction of forested area determined from the 2003 MODIS Land Cover (1 km resolution). To facilitate the inter-comparison, the MVDP fields were aggregated to the county level by first masking out non-forested areas using the MODIS Land Cover product, then summing all MVDP values for each county, and finally normalizing the county level sums by the fraction of forested area. Figure 3a shows the USFS data for 2006 as green filled circles (circle diameter is proportional to the volume of dead wood); whereas the color-coded county map corresponds to the aggregated and normalized MVDP (county color is indicative of VDP magnitude). Note that not all counties have ground survey data in the USFS database (the lack of a green dot over a specific county

indicates lack of data), and a detailed survey to clarify the relationship between the density of plots surveyed, forest fraction, and actual tree damage and, or mortality is not available. Nevertheless, these data provide a measure of the robustness of the VDP in forested areas in terms of co-localization between damaged areas.

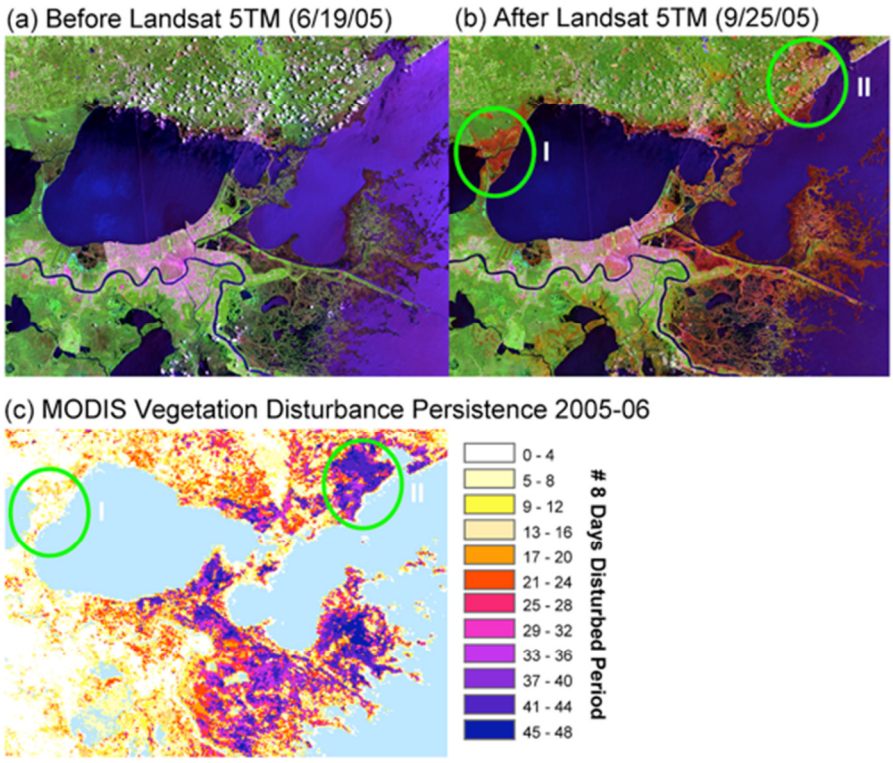

Figure 3-2: The top two Landsat images show healthy vegetation appears bright green (RGB composite using respectively Landsat bands 7, 4 and 2) before the storm (a) and bright red depicts vegetation mortality just after hurricane Katrina (b) Data courtesy USGS. MVDP over this area (c) displays similar patterns in general. However discrepancies exist (circled) suggesting that the disturbance can start later.

The spatial agreement between MVDP and FIA data can be assessed by cluster analysis using Z-score statistics to determine the most statistically significant clusters (hot spot analysis). The standard tool function "Getis-Ord Gi*" (with Euclidian distance) in ArcGIS was used to calculate the Z-score for each county. The Z-score plots

show counties with either strong (red) or weak (blue) clustering for both MVDP and FIA. A hot spot is defined as showing a cluster of adjacent counties with high Z-value. As shown in Figure 3-3c and d, there are 3 hot spots (2 circled green, and one circled cyan) that are present in both datasets including the Appalachians, North Florida, central Georgia, Mississippi and Alabama.

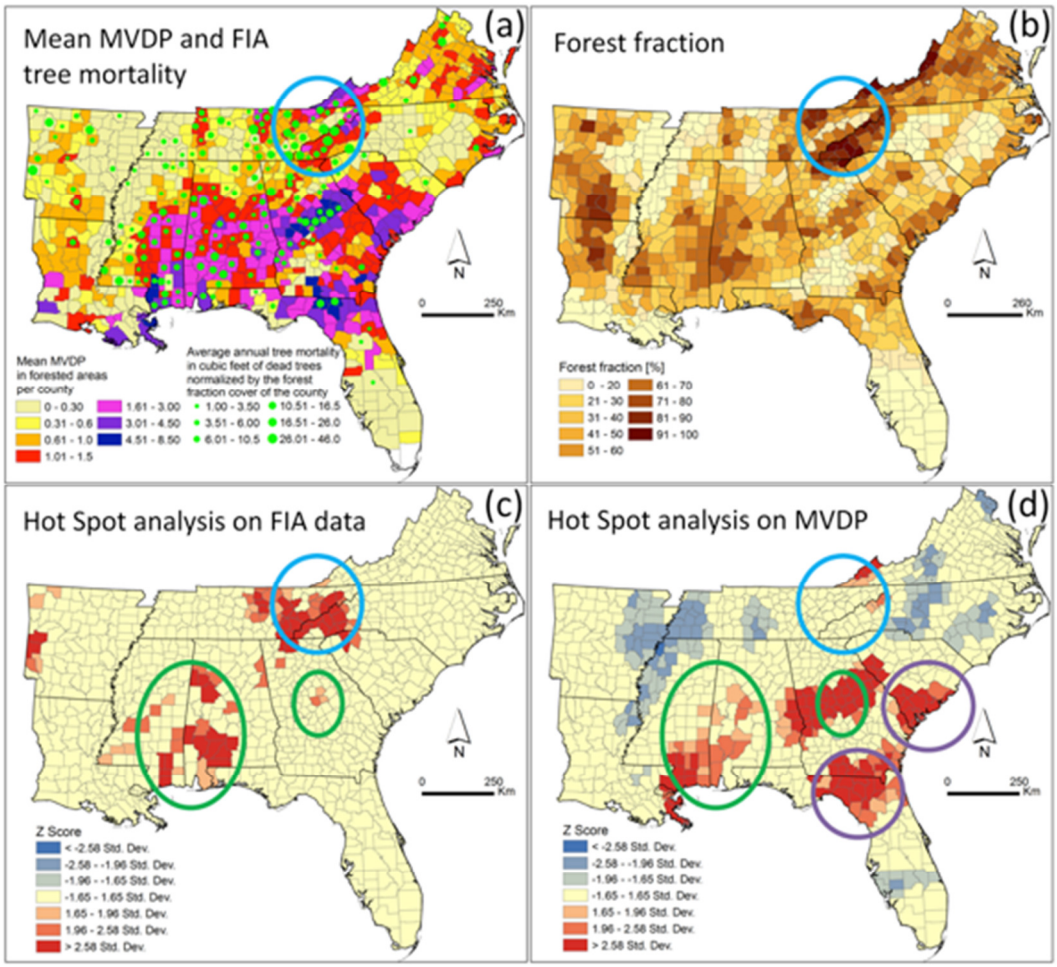

Figure 3-3: (a) the background colors display the average MVDP value per county. The dot size corresponds to the volume of dead trees (in ft³) extracted from the FIA database USFS (http://fia.fs.fed.us/tools-data/default.asp) normalized by the forest fraction of the county; (b) the estimated forest fraction of the county using MODIS land cover; (c) the hot spot analysis between FIA database and (d) averaged MVDP per county.

The 2 hotspots circled in purple on the MVDP map are missing on the FIA analysis due to the lack of data in the latter. This does not mean there is a lack of association, but rather it means that no data were collected. Note that there are some dispersed FIA data points along the eastern seaboard, but the number of samples is too small to conduct clustering analysis. The spatial extent of the cyan hot spot is much larger for FIA than for MVDP. The MVDP in that region detects disturbances with mid-range duration, which are not captured by the hot spot analysis that focuses on high values. In this region, most counties show areas with more than 90% fractional forest coverage (Figure 3-3b). So even if the volume of dead trees from individual surveys is high, when scaled by forest fraction and forest area the values are significantly lower compared to the total forested area, therefore not showing a strong signal when using the mean value of MVDP at the county level. In addition, this region encompasses the Great Smoky Mountains National Park and the adjacent foothills in Tennessee, and when damages are detected and access is possible they are surveyed by Park Management and the forest Service. However, because of high forest fraction, these surveys only target detected damaged areas, and therefore are not quantitatively representative of what goes on in large tracts of protected forest of difficult access, and which are rarely visited. On the other hand, the sampling frequency of damaged sites is higher than elsewhere including damages due to other causes, such as the natural variability of forest processes. Note that the very low MVDP values cluster (in blue in Figure 3-3d) along the Mississippi alluvial plain and east Tennessee correspond to predominantly agricultural land use (forest fraction < 20%, Figure 3-3b).

Overall, both evaluations show that the MVDP captures local and regional disturbances due to flooding and tree loss in agreement with ancillary data at the same spatial scale, and therefore should be useful for monitoring vegetation changes from space.

3.4 Results

3.4.1 Vegetation Monitoring

Figure 3-4 displays MVDP maps obtained for the SE. The spatial patterns of MVDP are dominated by hurricane impacts on the one hand, and drought on the other. Figure 3-5 shows the evolution of drought conditions over the southeast US according to the National Drought Mitigation Center (NDMC / NOAA) during the period of study. Recall that since the MVDP is based on the water year (Oct. – Sept.), the relevant signal in terms of vegetation activity takes place in the second calendar year of each water year. For example, drought in the calendar year 2002 is relevant to explain the 2001-02 MVDP patterns. There are clearly two wet periods (grey in Figure 3-5) during the calendar years 2003 and 2005 corresponding to low MVDP (white areas in Figure 3-4).

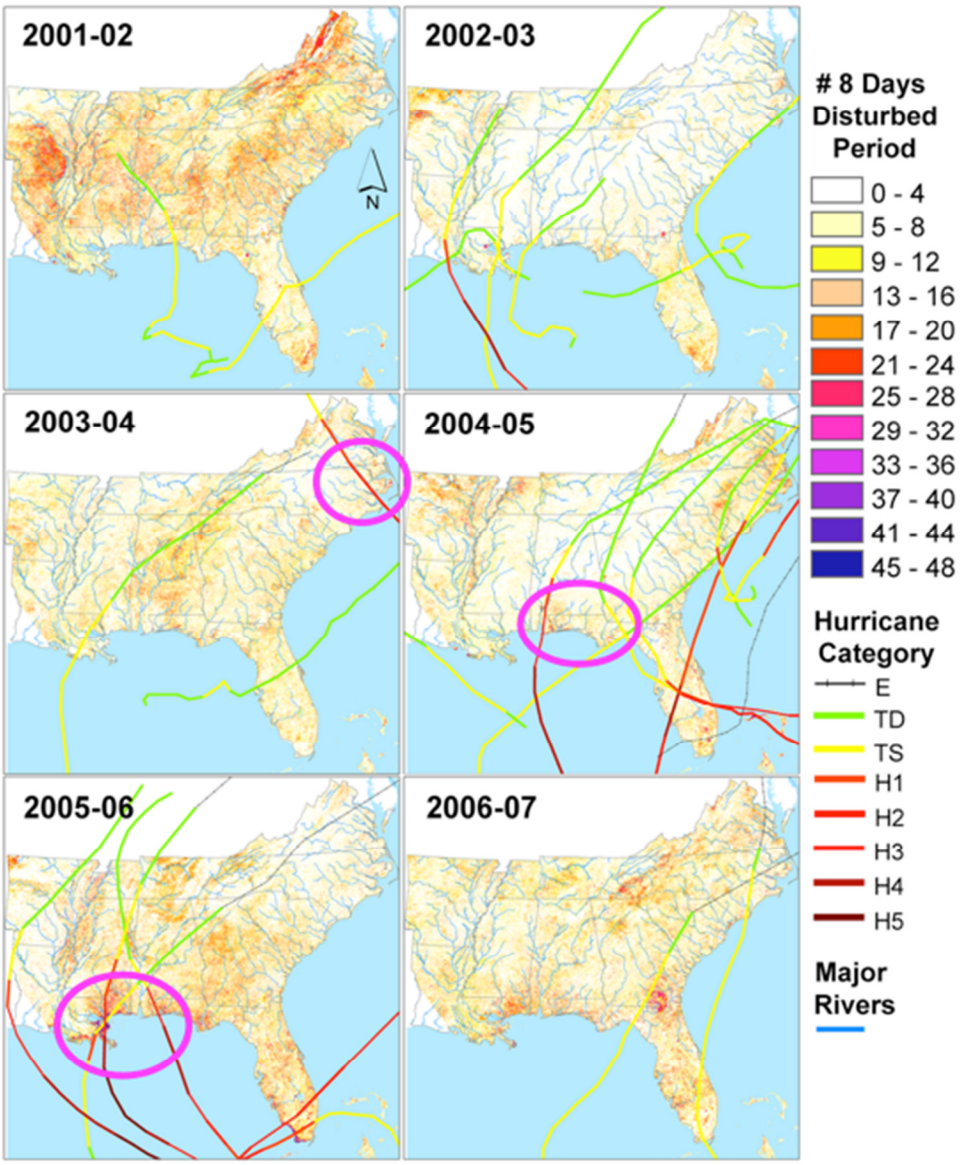

Figure 3-4: Vegetation disturbance persistence over the southeast US measured using the MVDP. Note the recurrence of widespread patterns of mid-range MVDP values organized by mountain and major river systems, such as the Mississippi and the Mist Rivers, which are indicators of hydrologic drought. Patterns corresponding to the longer persistence of vegetation stress (circled) are clustered at hurricane landfall sites. The hurricane categories (H1-5) correspond to the Saffir-Simpson scale as used by the National Hurricane Center (http://www.nhc.noaa.gov/sshws_table.shtml?large). E stands for extratropical storm, TD for tropical depression and TS for tropical storm.

Severe drought conditions were experienced in the summers of 2002, 2006 and 2007. This is consistent with the 2001-02, 2005-06 and 2006-07 MVDP exhibiting moderate values of 9 to 16 - corresponding to a disturbance that lasts 3-4 months - widespread over the entire region of study. In 2003-04, a drought pattern, especially over Alabama, is also visible during the summer 2004.

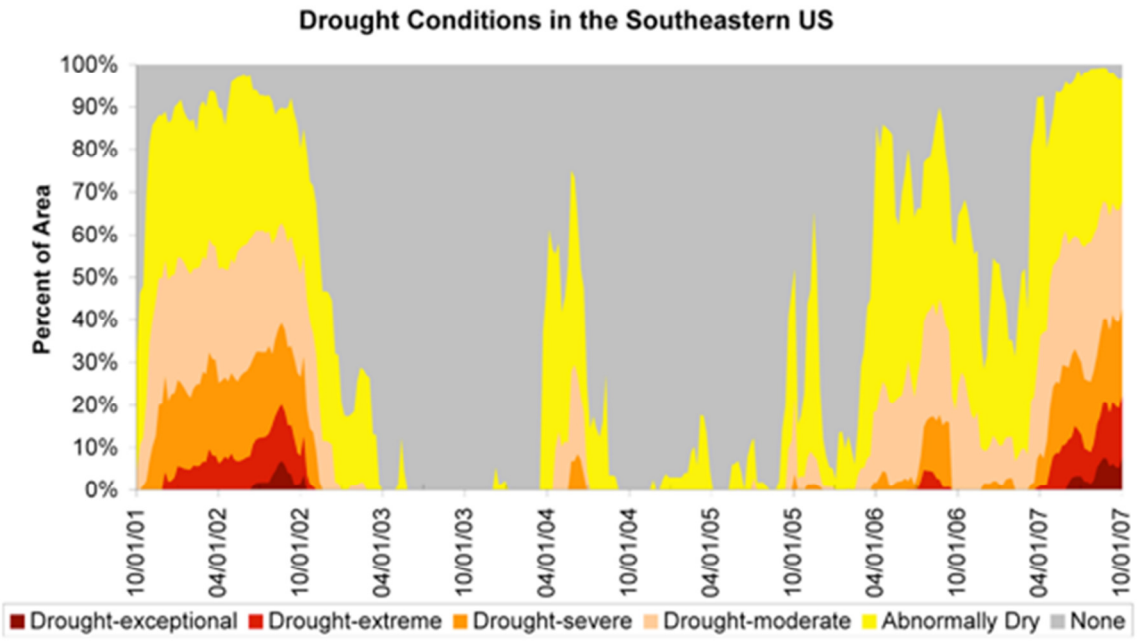

Figure 3-5: Drought patterns over the southeast US during the period of study (Data from the National Drought Mitigation Center, see http://drought.unl.edu/dm/index.html)

During the 2005-06 hydrological year, MVDP maps exhibit clusters of very high values around 40 and above, i.e. about 10 months (circled in Figure 3-4). These patterns are explained by the fact that 2004 and 2005 were the most active hurricane seasons in recent years both with respect to number (i.e. frequency) of hurricane events, as well as intensity (Ivan, Frances and Jeanne in 2004, Dennis and Katrina in 2005); indeed, the clusters match the landfall areas of these major hurricanes (category 3 to 4). Moreover,

long lasting disturbances due to flooding can be observed along coastal areas, estuaries, and the floodplains of major river drainage networks. Note the strong signal along the river valleys of the Mississippi, the Mobile and the Tennessee River systems. Cumulative runoff propagation through the drainage networks of large and small tributaries in response to the heavy persistent rainfall during the passage of major storms can lead to extended overbank flooding at lower elevations, impacting especially the areas of intense agriculture in the alluvial plains.

To better relate the MVDP to the regional river network, the average disturbance per USGS Hydrologic Unit (HU) was computed (HU are gauged watersheds corresponding to level 6 of the USGS catalogue; see, http://water.usgs.gov/GIS/huc.html) to create a simplified version of the MVDP that reflects the interconnectedness of the drainage network and the relationship between upstream and downstream impacts. The average values were aggregated to 8 levels of persistence with each level corresponding to a period of 2 weeks (Figure 3-6). The river network is represented using white lines, whose thickness is proportional to the mean flow computed from historical data (source: ESRI). On the coastal region, the Bayou and Mississippi delta (△) were strongly affected, as well as the Pearl (*) and the Pascagoula rivers (x) (warm colors). Inland, the alluvial plains of the Mississippi (m), the Tombigbee (o), the upper Pascagoula (v) and the upper parts of the Tennessee River (◎) were the most disturbed reflecting heavy precipitation in headwater catchments along the right flank of the storm track.

Disturbances along the Apalachicola River (circled in Figure 3-6) despite the fact that no hurricanes made landfall in this area during the 2005 hurricane season are indicative of long-term impacts of hurricanes Frances and Jeanne in 2004. Note also the combined effect of Ivan (2004) and Dennis (2005) along the Escambia River (+). Although Dennis was weaker than Katrina, the persistence of the disturbances is similar. Ivan made landfall at the estuary of the Escambia River in the previous year (2004) yielding MVDP values aggregated at the hydrological unit scale in the 7-16 range over the Escambia River (not shown), which correspond to much higher values on a pixel-by-pixel basis (25 to 46). Therefore, the ecological impact of Dennis' landfall at the same location one year later was amplified due to antecedent conditions.

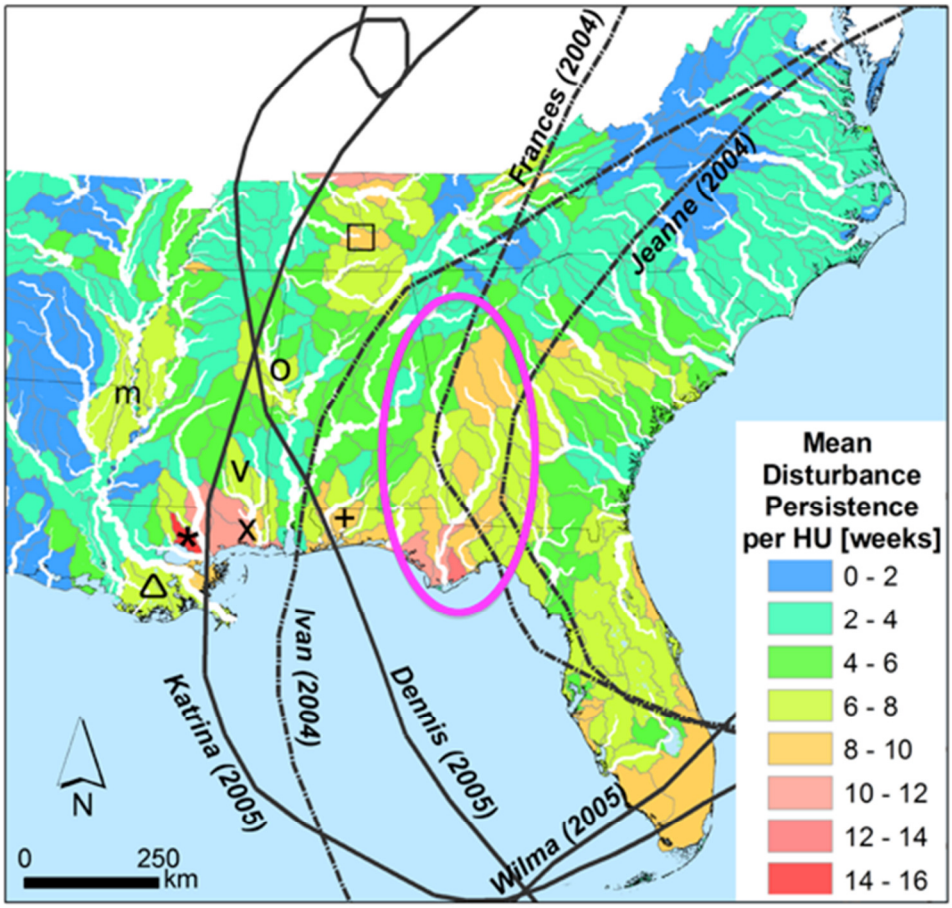

Figure 3-6: Simplified persistence of the vegetation disturbances during the following year of the hurricane Katrina (2005-2006) with respect to USGS hydrological units (gauged basins). Note the impacts along the tracks of hurricanes Frances and Jeanne in 2004 (dot-dashed lines) such as in the Apalachicola river basin (circled). Symbols indicate specific river systems: △ - Bayou and Mississippi delta; m- Mississippi Plains; * - Pearl River; X - Pascagoula River; o – Tombigbee River; □ - Upper parts of the Tennessee River; + - Escambia River.

3.4.2 Hurricane Case-Studies

Two specific case studies are presented in detail next. These two cases were selected among all others that were analyzed, because they illustrate two very different and yet representative track and landfall geometry: Atlantic ocean storm track and East

coast landfall - Isabel (2003); and Gulf of Mexico storm track with Gulf coast landfall – Katrina (2005). The terrestrial tracks of the former tend to stay on close to the Atlantic coastal plains; the terrestrial tracks of the latter tend to cross the continent slantwise with an S-NE orientation.

3.4.2.1 Isabel 2003

Hurricane Isabel made landfall at Cape Hatteras (NC) on September 18th 2003, when it was still a category 3 storm. Isabel strongly impacted the coastal plains of North Carolina and Virginia. Regional MVDP post Isabel as well as regional land-cover, wind fields and precipitation at landfall are shown in Figure 3-7a to f. Heavy precipitation and strong winds were co-located on the coastal sector of the landfall area. Three specific wetland regions are especially noteworthy in terms of long-term vegetation impacts.

One is the Great Dismal Swamp (marked 1 on Figure 3-7a) on the border between North Carolina and Virginia that is classified as a woody wetland in the National Land Cover Database 2001. The other wetland is the Alligator river wildlife refuge (marked 2 on Figure 3-7a) located between the Outer Banks of North Carolina and the Alligator River. The last one is the Chowan river estuary further inland from the coastal wetlands (marked 3 on Figure 3-7a). This region - as well as the other two - was strongly impacted by Isabel's storm surge (Reilly, 1991; Wang and Xu, 2009), which introduced salt in these wetland ecosystems where deep-rooted trees abound.

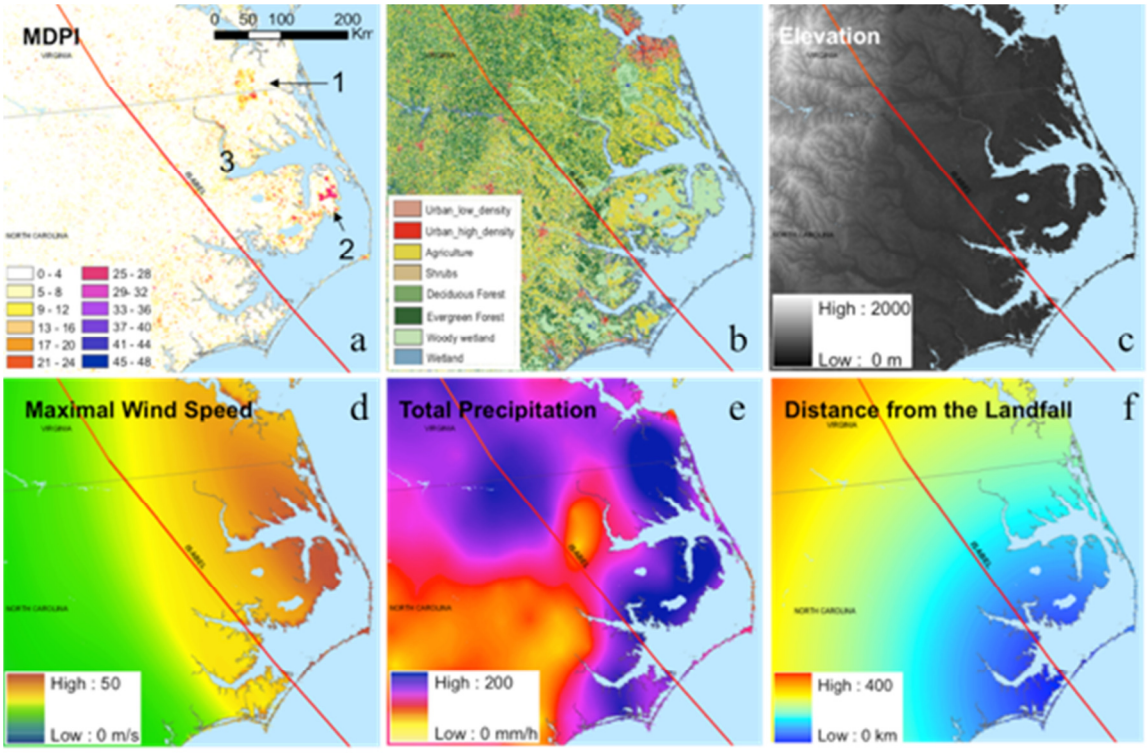

Figure 3-7: Impacts from Hurricane Isabel, 2003: (a) MVPD for vegetation; (b) land cover (NLCD01); (c) elevation; (d) maximum wind speed (NOAA); (e) estimates cumulative precipitation from TRMM 3B42; (f) distance from the landfall. The hurricane track colors correspond to the scale defined in Figure 3-4.

To better investigate the vegetation activity decrease, MVDP values were assessed as a function of local meteorological conditions during the event and environmental attributes. Different layers of information were used to extract statistics for each location with an EVI anomaly lasting longer than 3 months (i.e. a MVDP value higher than 12) in the following water year. This threshold was set to remove any potential drought signal that could interfere in the determination of hurricane driven vegetation disturbances. Density plots summarizing the analysis are presented in Figure 3-8. The X-axis is the MVDP of the hydrological year following Isabel landfall (2003-04), and the Y-axis corresponds to the different physical or meteorological parameters.

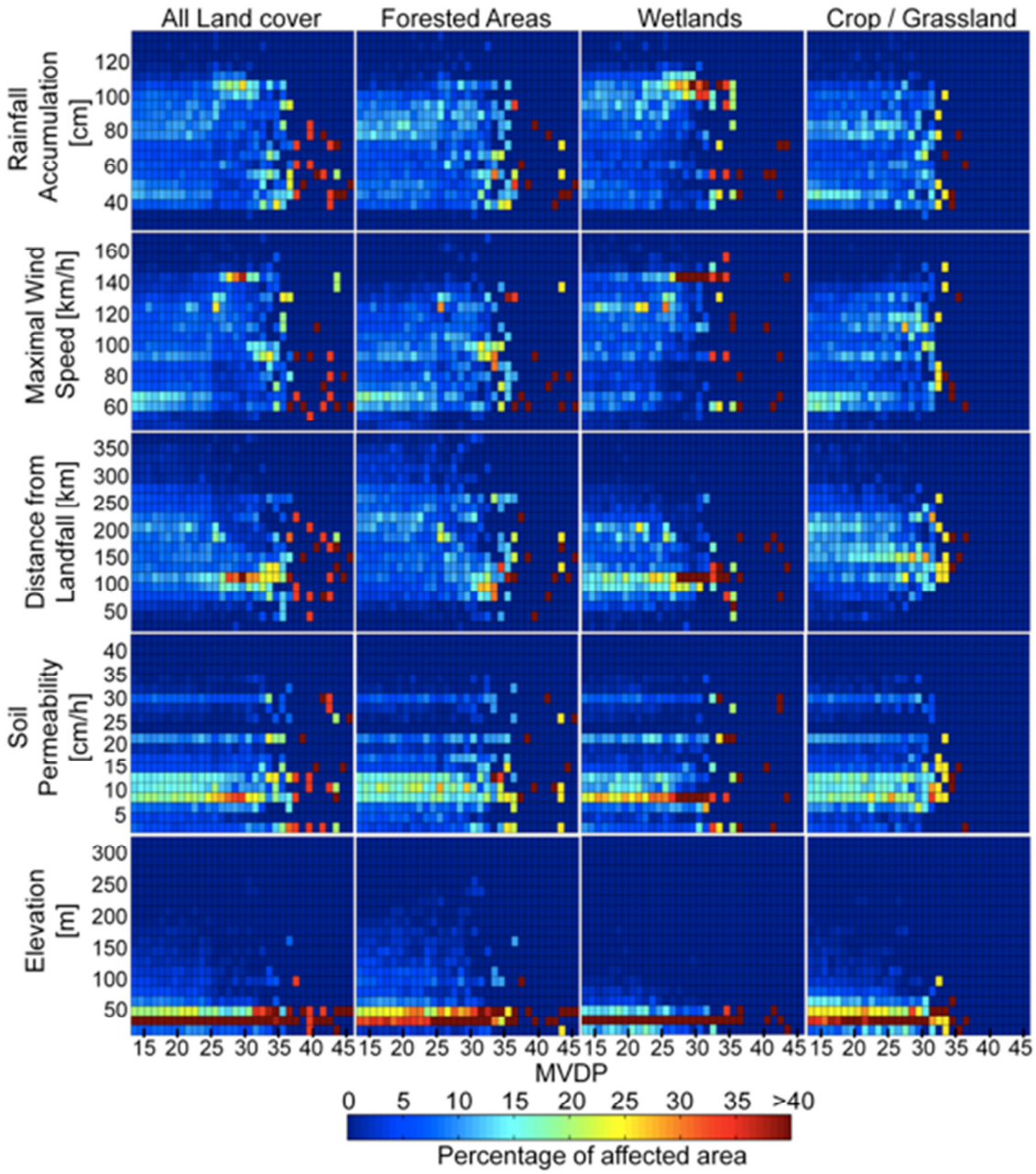

Figure 3-8: Density plots relating the percentage of affected area. On the x-axis the vegetation disturbances is expressed as MVDP during the hydrological year following the hurricane Isabel (2003-2004). On the y-axis, different storm and environmental characteristics: maximal wind speed, total accumulated rainfall, distance from the landfall, soil permeability and elevation. The first column displays then entire landscape and the followings major land cover themes. Note that only values of MVDP greater than 12 (> 3 months) are plotted.

The data presented in the plots in the first column of Figure 3-8 represent the entire landscape. The data in the following columns were separated according to major land cover themes. The color scale expresses the frequency of co-localization between a certain range of MVDP and the other parameter. The higher the percentage, the stronger is the spatial agreement (co-localization) of the parameters, and therefore the association between the disturbance persistence and the specific parameter. Summation for each column of boxes, i.e. for each MVDP value, corresponds to 100% of MODIS pixels, and therefore 100% area having this MVDP value. Each box represents the relative area of co-localization of a certain MVDP and parameter values. Note this is different from the "classical" 2D-histogram, which sums all the boxes on the plot to 100%. This choice was made because hurricanes cause by nature highly localized disturbances. Effectively, tropical storms have characteristics organized along their track, which change from quadrant to quadrant (winds are much stronger on the N-E sector of the storm), which vary sharply with distance away from the track (increasing first and then decreasing) and also weaken with time along track as the storm moves inland. Because our goal is to detect and attribute storm impacts at local places where damage is long lasting, even if these highly impacted areas are overall spatially more limited than areas exhibiting short-duration disturbances, we therefore decided to implement the frequency normalization with respect to each MVDP value and not based on the overall distribution. As expected, there is a direct association among wind speed, cumulative rainfall, distance from hurricane landfall and the MVDP. Highly disturbed areas are confined especially to very low elevations (below 25m) exposed to storm surge flooding.

Besides causing significant erosion, the hurricane storm surge introduces salt into the coastal ecosystem aquifer, either by salt-water infiltration from the surface or via underground diffusion transport further stressing vegetation (Baldwin and Mendelssohn 1998; Blood *et al.* 1991). The strongest co-localization of precipitation, maximum wind speed and distance to landfall occurs in wetlands for MVDP values between 25 and 35, which is the dominant signal when all the land cover categories are taken into account. In the case of forested areas, the signal is strongest for wind speeds of 100km/h and MVDP values between 30 and 35, consistent with mechanical tree damage. For this wind speed, note the association with low soil permeability (mostly clayey soils in this area). Forested areas are not only impacted close to the landfall, but also further inland though less and less as winds weaken along the terrestrial storm track. The lowest MVDP values are found in cropland due to the interruption of the phenological cycle of this land cover category by harvesting.

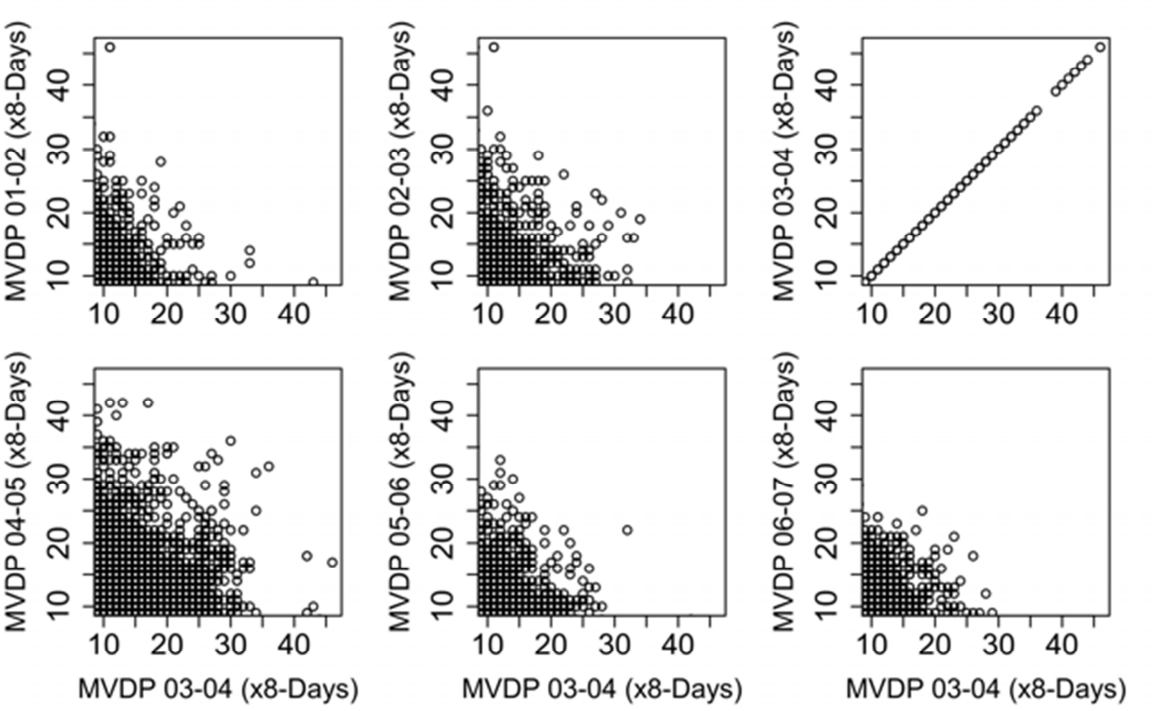

Figure 3-9: Scatter plots of vegetation disturbance persistence "normal years" versus the year in the aftermath of Isabel (2003-2004).

Figure 3-9 shows scatter plots of the MVDP values at each pixel in the post-Isabel water year against the MVDP values for all other years for the same region. Isabel was the only land-falling hurricane in this region during the period of study. In all scatter plots, the distribution is aligned with the (-1) slope, thus revealing strong disagreement between the locations of high MVDP values after Isabel (2003-04) and all others. This implies that the locations of long-term disturbance are different after landfall, whereas the location of moderately disturbed areas may remain the same from year to year. In other words, the driving causes of long-term disturbances in the years not affected by hurricane landfall and in the year after hurricane landfall are not the same (i.e. drought vs. hurricane impacts). This is confirmed by inspecting Figure 3-7 that shows that most

of the long-term disturbances are clustered in wetlands, woody wetlands and shallow water locations generally. The MVDP maps suggest that flooding impacts (erosion and salt intrusion) last longer than those caused by wind damage, especially in wetland regions. Indeed, in the second water year after Isabel (2004-05), the scatter plot shows an increase in the persistence of the disturbances compared to prior-Isabel conditions (2002-03), thus indicating that recovery time-scales are longer than one year in some of these low-lying areas.

To differentiate phenology shift effects from variations in the amount of green biomass activity due to tropical cyclones, the EVI difference between each two consecutive 16-day periods was calculated from January to August to identify the maximum value of this difference. The timing of the maximum difference is used to determine the beginning of the growing season (green-up date) for each pixel (Kaduk and Heimann 1996). Note that, for this step, the unprocessed EVI from MODIS (MOD13A1) was used to remove any potential smoothing effects in the processing of MOD09A1G. Finally, a land cover mask (NLCD01) was used to distinguish the natural vegetation phenology (Figure 3-10(*a*)) from agricultural activities (Figure 3-10(*b*)). In the post-Isabel water year (2003-04), the green-up took place in the 16-day period beginning on April 7th for the majority of the natural areas, and the spatial pattern of green-up date is very homogenous across the landscape in contrast to the previous growing season.

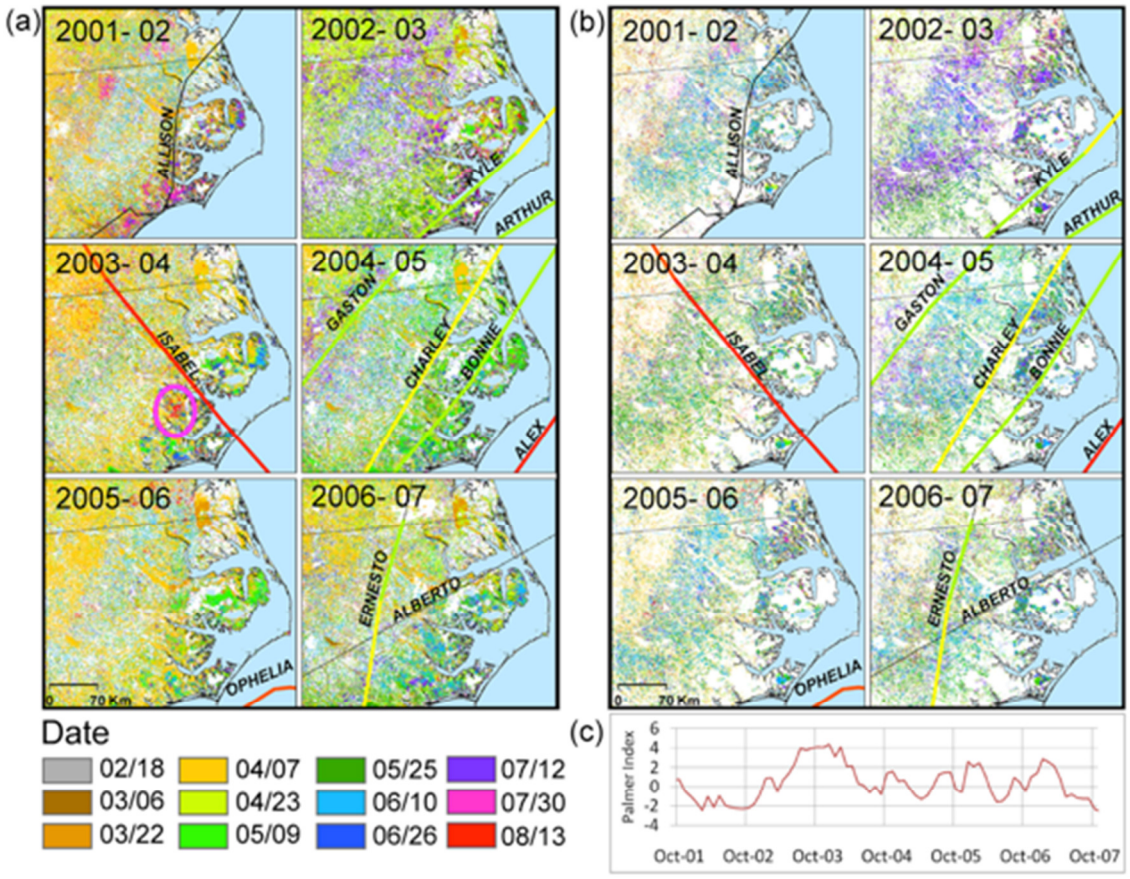

Figure 3-10: Green-up date in the growing season (second year in the hydrological year name) and the corresponding hurricane tracks of the previous year (first year in the hydrological year name): (a) for natural vegetation (forest, grassland and wetlands), (b) for cropland, and (c) the Palmer drought index for the same period over central coastal plain of North Carolina (http://nc-climate.ncsu.edu/climate/climdiv.php). The hurricane track colors correspond to the scale defined in figure 5.

This homogenization is even more marked in croplands of the Coastal Plain, with the green-up taking place on May 25th 2004, the earliest of the time-series. This homogenization of green-up onset could be explained by the relief of drought stress after Isabel in the fall of 2003. The Palmer drought index for the central Coastal Plain shows (Figure 3-9c) that heavy precipitation from Isabel recharged the groundwater

reservoirs leading to high water tables and increased soil moisture, which could explain this increased homogeneity in vegetation dynamics, especially for shallow rooted vegetation such as grasslands and cropland. In addition, water quality measurements suggest that the overall condition of the soil-water-vegetation ecosystem is improved in the aftermath of hurricanes in this region due to cleansing by runoff (Paerl et al. 2006). Despite this homogenization, Table 3-2 shows that the 16-day period starting on April 7th is the time when most of the natural vegetation green-up takes place during the duration of this study; therefore, the disturbance patterns captured by the MVDP are mostly due to a decrease in chlorophyll activity in the aftermath of Isabel than to a shift in the phenology. Nevertheless, what such statistics do not show is the spatial clustering of small areas close to the hurricane track and on the coast (e.g. the forested area circled in Figure 3-10a) that exhibit the latest green-up date from the entire time-series, due to the storm surge effects discussed above.

Table 3-2: Estimated Green-up period from MODIS EVI maximal difference for natural vegetation (Forest, grassland and wetland) over the coastal plains of North Carolina expressed as the percentage of area having a concurrent green-up. The bold numbers correspond to widest covered green-up date of the year. The shaded boxes correspond to coverage superior at 10%.

	2001	2002	2003	2004	2005	2006	2007
18-Feb	0.3%	0.1%	0.1%	0.2%	0.2%	0.3%	0.2%
6-Mar	0.5%	1.7%	1.6%	0.4%	0.6%	0.2%	6.5%
22-Mar	18.1%	13.2%	4.6%	4.7%	6.2%	4.0%	7.0%
7-Apr	**29.1%**	**45.8%**	5.6%	**58.1%**	**32.8%**	**57.8%**	**29.3%**
23-Apr	14.8%	9.4%	**44.7%**	9.3%	8.6%	11.7%	19.7%
9-May	11.9%	1.4%	5.9%	4.5%	20.0%	6.0%	8.7%
25-May	6.3%	3.5%	12.4%	6.6%	6.5%	3.6%	5.3%
10-Jun	8.1%	12.6%	1.7%	4.6%	14.0%	9.6%	13.5%
26-Jun	1.5%	3.1%	6.4%	4.3%	3.1%	2.5%	4.4%
12-Jul	5.0%	4.2%	12.5%	2.0%	6.0%	1.6%	3.5%
28-Jul	3.1%	4.3%	3.4%	1.9%	1.5%	0.9%	1.6%
13-Aug	1.2%	0.7%	1.1%	3.5%	0.5%	1.9%	0.3%

3.4.2.2 Katrina 2005

Katrina made landfall on August 29th 2005 in the New Orleans area when it was still a category-3 storm on the Saffir-Simpson scale. Regional MVDP post-Katrina as well as regional land-cover, wind fields and precipitation along the storm track are shown in Figure 3-11a to d on 29th August 2005. The maximum wind speed is higher and precipitation is heavier than in the case of Isabel. Note that in the case of Katrina there is substantial rainfall on both flanks of the storm track, which has implications for local hydrology. The MVDP range is also much larger, with the highest values clustered around New Orleans (MI) and extending northward into the Mobile River basin in Alabama.

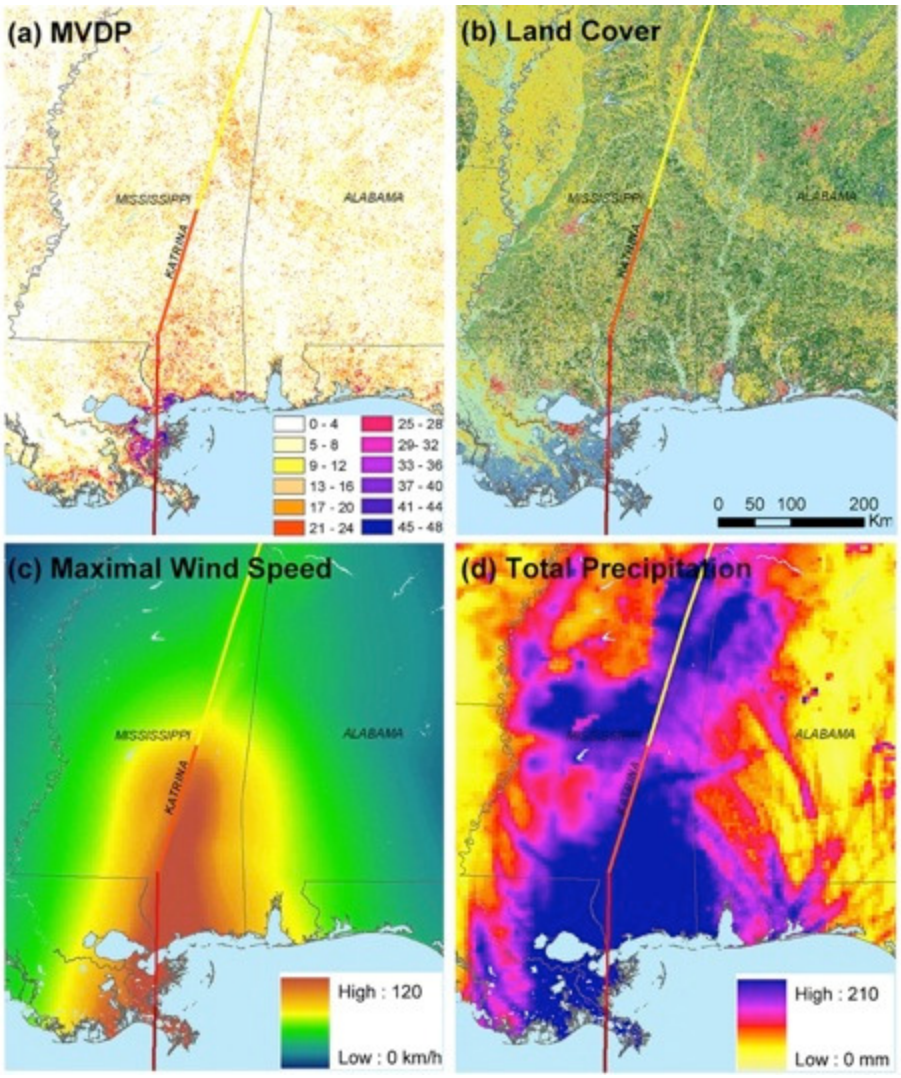

Figure 3-11: Impacts from Hurricane Katrina, 2005: (a) MVDP for vegetation; (b) land cover (NLCD01); (c) maximum wind speed (NOAA); (d) estimated cumulative precipitation from NCEP Stage IV. The hurricane track colors correspond to the scale defined in figure 4.

The density plots presented in figure 12 show two major patterns of disturbances. First, high MVDP values (> 35 on VDP scale, i.e. > 9 months) in wetlands (high soil permeability) and forests (low soil permeability) correspond to low elevation wetlands and forests in the coastal zone where rainfall and wind speed maxima were reached concurrently in the vicinity of landfall. A second disturbance pattern, with more

moderate MVDP values, is found in low-lying inland areas corresponding to the floodplains of major regional rivers, where overbank river flooding is the dominant hazard. Croplands typically located on these floodplains have MVDP values below 35 and a strong co-localization with low soil permeability. In forested areas, the MVDP spans the entire spectrum and shows strong spatial clustering.

Disturbances in agricultural areas are therefore not caused by the same processes as the disturbances in the coast. In the coast and near-coastal region, the most persistent disturbances are due to the hurricane intensity expressed through wind and precipitation, and the water surge via erosion of the shoreline and the introduction of salt in the environment. Therefore, before vegetation recovers, it is necessary to refill and wash out salts from the sediment beds. Regarding MVDP values below 9 months, disturbances are located more inland and mainly in croplands, where the storm intensity is significantly reduced. Due to the spatial organization of the disturbed areas along the alluvial plains of major rivers, these disturbances are attributed to overbank flooding that also washes out nutrients and top soil layers, therefore having an impact in the next planting season.

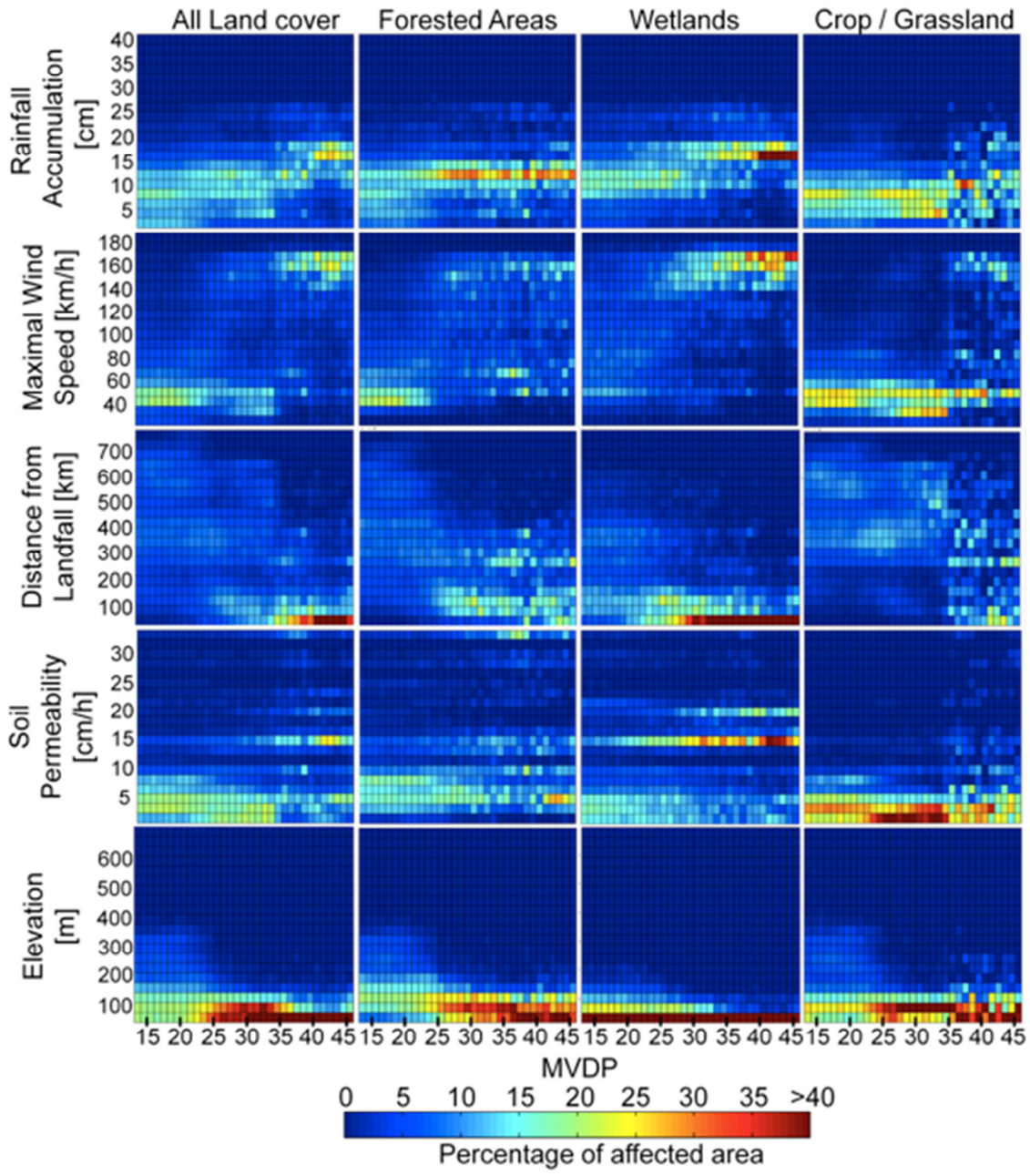

Figure 3-12: Density plots relating the percentage of affected area. On the x-axis the vegetation disturbances is expressed as MVDP during the hydrological year following the hurricane Katrina (2005-2006). On the y-axis, different storm and environmental characteristics: maximal wind speed, total accumulated rainfall, distance from the landfall, soil permeability and elevation. The first column displays then entire landscape and the followings major land cover themes. Note that only values of MVDP greater than 12 (> 3 months) are plotted.

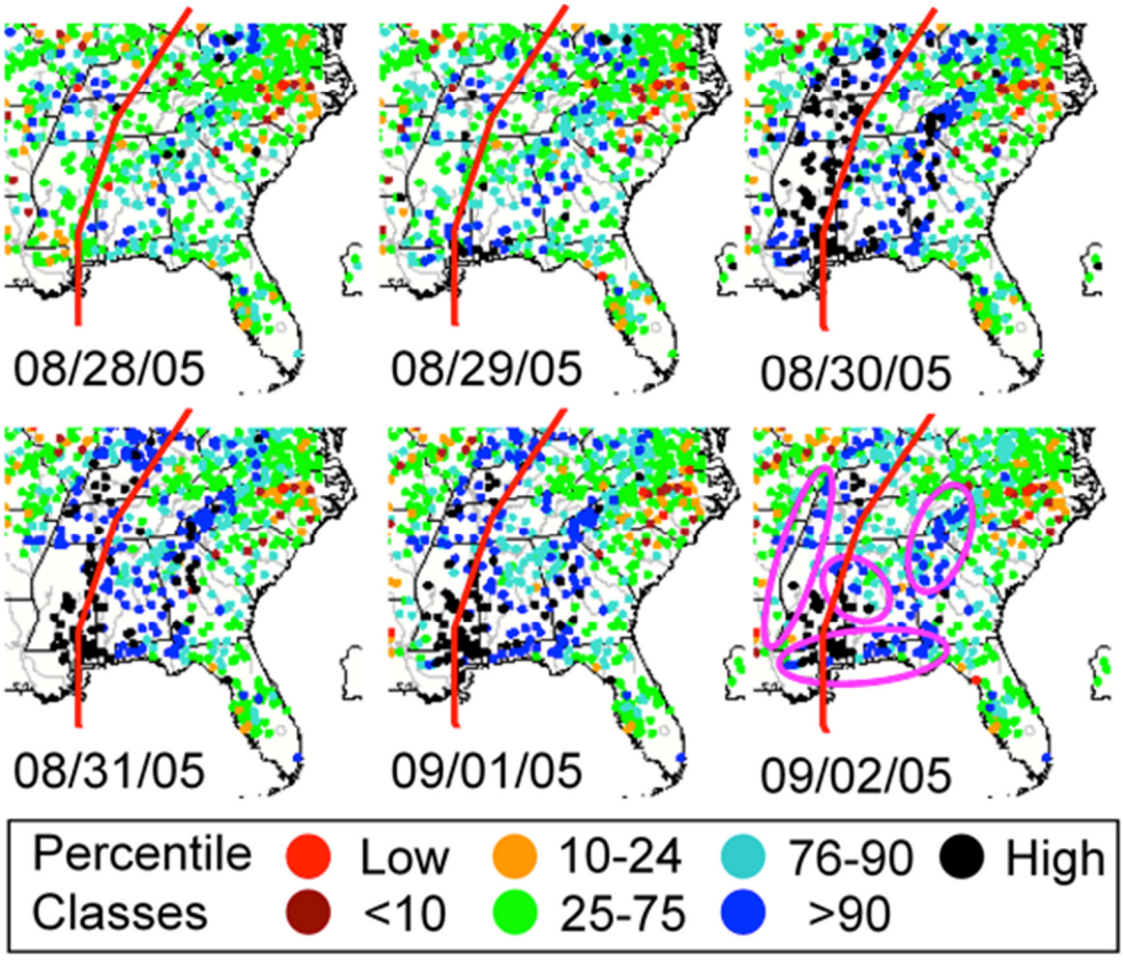

Figure 3-13: USGS streamflow data (http://waterwatch.usgs.gov/new/index.php) classified as percentile of the available time-series (more than 30 years) showing the flood propagation along the major alluvial plains in the aftermath of hurricane Katrina (estimated eye-track as red line). Black dots indicate the registered value is the maximum ever measured for this day of the year. Four distinct regions consistent with high MVDP values can be identified during the evolution of flood response (pink circles). Background images courtesy of USGS.

On August 31 and September 1st, overbank flooding remains only downstream of the regional drainage network toward the Mississippi and the Apalachicola and Mobile river mouths, and eventually is confined to the coastal zone. Note however that the water levels in most of the rivers in the region along the storm path are still in the top

10% of the historical record five days after landfall. River levels only returned to near normal conditions (< 75th percentile) over Mississippi and Alabama States on the 13th September (not shown). The MVDP patterns in the inland floodplains coincide with the locations were overbank flooding occurred, which correspond to areas where major agricultural activity takes place.

Figure 3-14 depicts scatter plots corresponding to the MVDP density distribution in the hydrologic year following Katrina in the x-axis against all other years in the period of study in the y-axis. As in the case of Isabel, before the 2005 hurricane season there are long-term disturbances present in all years but the locations of disturbances are not the same, except in 2004-2005 due to Frances and Jeanne, thus implying that the statistical signature of drought in the MVDP is different from that of hurricane impacts. In the second year after Katrina (2006-2007) the extent of disturbed areas is significantly larger than in the four preceding years, suggesting that vegetation in these locations has not yet returned to typical activity levels. Although the statistical analysis of hurricane Katrina suggests stronger impacts on the environment than Isabel in that the time-scale of recovery as measured by the MVDP is longer, vegetation impacts in the two studies do exhibit similar characteristics.

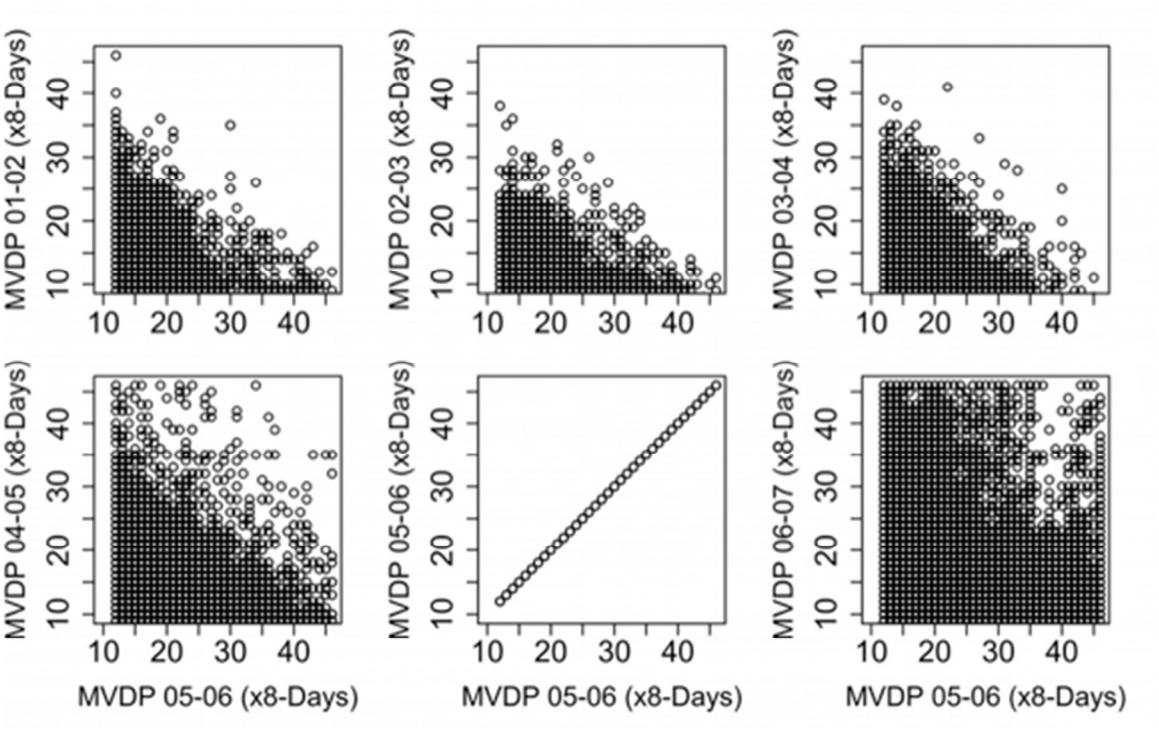

Figure 3-14: Scatter plots of vegetation disturbance persistence "normal years" versus the year in the aftermath of Katrina (2005-2006).

3.5 Discussion and conclusion

The proposed metric to monitor eco-hydrological impact of TCs shows good sensitivity to capture broad patterns due to drought stress conditions, as well as more strong organized disturbances due to specific storm events. The use of phenologically corrected data, combined with the fact that the climatological seasonal cycle is removed, allows detection of phenology shifts in addition to changes in vegetation activity. Certainly, further detailed attribution of the causes of the disturbances needs to be pursued, mostly due to the fact that several factors can concurrently affect vegetation dynamics.

The main cause of regional-scale vegetation disturbances during the three first years of the period of observation (i.e. 2001 to 2003) is water stress due to drought, which interestingly corresponds to years with weak hurricane activity. This pattern is expressed by values of MVDP in the low-range (10-16) and spans the entire southeast US, especially in areas of short rooted vegetation such as grasslands and agriculture. Regarding hurricane eco-hydrological impact assessment, we found that the magnitude of vegetation disturbances is larger than that for drought (high MVDP value in the range of 30 to 46) and spatially clustered and organized according to the governing hydrological process, that is overbank river flooding along the terrestrial drainage network. As expected, and consistent with previous work (e.g. Xiao et al., 2010), low elevation locations are significantly affected by hurricanes, and especially coastal areas are the most persistently affected in both case studies (Isabel and Katrina). Although hurricane impacts are expected to be higher on the coast, the temporal evolution of the recovery suggests that mechanical sediment removal and salt intrusion associated with the storm surge may be more important than tree uprooting and, or decrowning in terms of long term ecosystem recovery. Salt contamination during the storm surge appears to cause vegetation morbidity in the coastal zone for a period from 1 to 2 years.

The type and spatial extent of individual storms depends on their terrestrial track as shown by the two case studies: Isabel vs. Katrina. Generally, hydrologic units suffering major direct impact are aligned along the right flank of the storm track. In the case of large river basins with headwaters and major tributaries on the right flank, downstream floodplains along the left flank also show severe impact due to flood propagation (e.g.

Mississippi after Katrina). Alluvial plains with intense agricultural activities seem to be particularly vulnerable to flooding events in the aftermath of major tropical storms that last well into the year following the event.

In the case of moderate TCs, the time-series analysis suggests that the strong precipitation due to the event recharges groundwater and soil moisture reservoirs, erasing the signature of water stress that dominates in the absence of significant Tropical Cyclone activity. An interesting point to highlight is that the Saffir-Simpson scale does not take the amount of precipitation into account, therefore the classification of TCs through this scale is not pertinent to assess the potential of TCs to relieve drought and cause floods, or more generally to assess eco-hydrological impacts.

4 Contribution of TCs to the SE hydroclimate

Hurricanes, and tropical cyclones (TCs: hurricanes and tropical storms) more generally, are powerful meteorological phenomena that can cause massive wind and flood damages to natural and built areas. Along the storm terrestrial track, and especially at landfall, there is often debilitating economic impact locally and regionally (Blake et al., 2007; Pielke et al., 2008). On the other hand, TCs provide a significant influx of freshwater resources to surface and subsurface reservoirs during the warm season (10-25% of seasonal rainfall) (e.g. Konrad and Perry, 2010; Nogueira and Keim, 2011), which is critical to freshwater resources in the SE US. Although, the intra-seasonal frequency, timing and precipitation depth of TCs in summer is well documented from the local to the regional scales (Barlow, 2011; Jiang and Zipser, 2010; Knight and Davis, 2009; Konrad, 2001; Konrad and Perry, 2010; Kunkel et al., 2010; Nogueira and Keim, 2011; Prat and Nelson, 2012; Rodgers et al., 2001), still little is known on the role of TC precipitation in meteorological drought mitigation (Barlow, 2011; Maxwell et al., 2011).

Freshwater resources in the US, and in the SE in particular, are under stress due to population growth and economic development that increasingly create more demands for agricultural, municipal, recreational and industrial uses, resulting in frequent over-allocation (Parry et al., 2007). In addition, climate change could impact the path, frequency and/or intensity of TCs (Emanuel, 2005; Michener et al., 1997; Pielke et al., 2005; Shepherd and Knutson, 2007), which in turn can have a strong impact in regional hydrology. Although future trends in hurricane frequency and intensity remain very uncertain (Parry et al., 2007), experiments with climate models at sufficient spatial and

temporal resolutions to depict specific characteristics of individual hurricanes indicate increases in both peak wind speeds and precipitation intensities (Field et al., 2007). The pattern is clearer for extra-tropical storms, which are likely to become more intense, but perhaps less frequent (Meehl et al., 2007). Knight and Davis (2009) suggested that more of the heavy precipitation events can be attributed to TCs both in magnitude and frequency during the last decades in Atlantic coastal states of the SE relative to other types of heavy rain producing weather systems (thunderstorms, mesoscale convective systems). Note that the frequency of TCs is relatively high (every 1-2 years along the coast and 2-3 years inland) everywhere in the SE US (Knight and Davis, 2009; Konrad and Perry, 2010), and there have been no statistically significant changes in the statistics of the precipitation extremes proper (return periods > 25-30 years) during the same period (Douglas and Barros, 2003). Such changes in the statistics of TC related heavy precipitation are consistent with the significant increase in the 2-4 year variability of summer precipitation in JJA (June-July-August) in the last thirty years over the region documented by Li et al. (2012). Thus, from the hydrology and water resources perspective, that is the water quantity point-of-view, TCs are not extreme events in the SE, but rather a staple of the regional hydroclimatology. Because water resources management and water infrastructure decisions are made in the context of specific watersheds, the objective of this manuscript is to map the spatial and temporal variability of the contribution of these events to water budgets and hydrologic extremes at the watershed scale. At sub-regional scale, changes in the track, frequency and, or intensity of TCs could lead to significant impacts by either magnifying or mitigating

geophysical hazards (droughts, floods, debris flows). Mapping the range of such impacts on current climate is a necessary step to understand impacts of projected climate changes.

In this manuscript, similar to previous studies (e.g. Nogueira and Keim, 2011), we first examine the contribution of individual TCs to the annual and seasonal precipitation totals in the southeast US but instead of spatially interpolated fields of TC rainfall at the daily and monthly time-scales, the approach is to estimate the spatial distribution of TC hydroclimatology using basin integrated and basin-average TC precipitation for 3,211 watersheds over the 2002-2011 period. Second, a climatology of the contribution of TC precipitation to alleviate and, or terminate meteorological drought at the basin scale is presented. Third, the partitioning between surface runoff and groundwater recharge is quantified using the water-balance approach for each watershed (Palmroth et al., 2010; Schaller and Fan, 2009; Thompson et al., 2011). The focus here is to estimate the fraction of precipitation that can potentially recharge regional aquifers at short time-scales from the fraction that is quickly exported through the river network and surface runoff across different physiographic regions (mountains, coastal and alluvial plains). A complementary analysis of well data is presented at the end along with detailed analysis for the 2004 hurricane season.

4.1 Background

The spatial patterns of TC precipitation overland are complex (Jones et al., 2003; Matyas, 2010; Parodi et al., 2011) with heaviest rainfall occurring both close to and

hundreds of kilometers from the eye-track of the storm(e.g. Galarneau et al., 2010). This strong spatial variability in rainfall fields is mainly due to storm structural changes occurring after landfall, along the terrestrial track and during the extratropical transition (Evans and Hart, 2003; Matyas, 2010). For example, extratropical transition occurred in 50% of landfalling TCs from the Atlantic basin during the period 1950 - 1996 (Hart and Evans, 2001). These structural changes strongly impact the spatial distribution and intensity of rainfall relative to the track of the storm (Atallah et al., 2007; Atallah and Bosart, 2003; Sun and Barros, 2012; Villarini et al., 2011). In addition, environmental parameters such as synoptic meteorological conditions (e.g. presence of a front, location of the jet stream) and topography modulate these precipitation patterns, creating a widely variable distribution across the landscape (Barlow, 2011; Hart and Evans, 2001; Konrad, 2001; Konrad and Perry, 2010; Rodgers et al., 2001; Sturdevant-Rees et al., 2001; Sun and Barros, 2012). In the absence of direct measurements or high resolution simulations, it is therefore very difficult to diagnose the space-time evolution of rainfall produced by these storms at high temporal resolution, especially over land. Consequently, existing climatologies tend to rely on daily rainfall accumulations and, or storm total accumulations. Moreover, climatologies of the contribution of tropical cyclones (TCs) to the annual, seasonal, and monthly precipitation in the southeast US, as well their role from the perspective of extreme events were investigated using point rainfall observations.

Konrad and Perry (2010) conducted an analysis of the relationship between tropical cyclones and heavy rainfall in the Carolinas relying on 55 years of daily rainfall

observations from the Cooperative Observer Program (COOP) network and synoptic fields describing the storm environment including 200 hPa divergence, precipitable water, 700 hPa vertical velocities and 850 hPa moisture fluxes from the NCEP-NCAR Reanalysis data set at $2.5^{o} \times 2.5^{o}$ resolution. The COOP network is maintained on a volunteer basis to support National Weather Service (NWS) operational activities, but the spatial precipitation patterns during extreme storms should be reliable in the areas where the density of observations is highest, that is where people live. On the other hand, as pointed out by Knight and Davis (2007), large under catch errors should be expected because of strong winds if no corrections are applied, indicating that COOP observations can severely underestimate daily rainfall during the passage of TCs. Konrad and Perry (2010) found a strong E-W and ocean to land gradient in tropical cyclone frequency in the SE US with all locations being affected on average at least once every three years in the Southern Appalachians, and more than once a year along the Atlantic Coast, whereas Knight and Davis (2007) using more storm cases found that the return period was 1-year and more than twice a year along the coast, respectively. Note that, based on these return periods, TCs are common events in the SE climate. Konrad and Perry (2010) showed that tropical cyclones are responsible for the majority of the heavy precipitation events, and they identified two major groups of storms: early season storms (before mid-September), which tend to be smaller and produce rainfall over a narrower band along the track (roughly 200 km on either side of storm track, the storm half-width); and, late season storms, which tend to be much larger (four –six times the size of the early season storms) and produce much wider rainfall tracks (up to 400 km

half-widths). Early season storms tend to be mostly tropical storms and depressions, whereas hurricanes are more frequent in the late season. For both early and late season storms, the amount of rainfall produced by different TCs varied greatly among individual storms as a function of storm size and the overlap between the areas of 200hPa maximum divergence and maximum precipitable water (> 90% for TCs with the presence of a front). Note however, that at small scales close to the center of the storm, the distribution of rainfall is organized in well–defined bands of convective cells embedded in larger stratiform systems, and therefore high spatial variability of rainfall intensity and rainfall depth are expected independently of the size of the storm (e.g. Nogueira and Keim (2011) relied on HCN (Historical Climate Network) daily data over the eastern US to develop a climatology of TCs including the number of storm days, track densities and the TC contribution to monthly and seasonal rainfall, and compared results from a previous study (1931-1961) with results from 1960-2007. The spatial distribution of the relative contribution of TCs to the hurricane season rainfall (June-November) matches extremely well the results for Probable Maximum Precipitation (PMP) of Douglas and Barros (2003). Similar results were also reported by Barlow (2011), who studied the influence of hurricane-related activity on North American extreme precipitation using 25 years (1975-99) of rain gauge measurements to look at the proportion of extreme precipitation which fell within 500 km radius of the hurricane core when they occurred. He also found that heavy precipitation in the coastal zones of North and South Carolina was most directly linked to TC activity, and that that TC related extreme precipitation statistics away from the coast are not simply related to the

track density, but also modulated by the large-scale dynamics as pointed out by Konrad and Perry (2010) and Maxwell et al. (2011). On a seasonal basis, Nogueira and Keim (2011) estimates of the contribution of TCs to seasonal precipitation were lower (10-15%) than the (20-25%) values in Knight and Davis (2007) who also followed the storm track after extra-tropical transition. Nogueira and Keim produced monthly storm track density maps that highlight two major terrestrial corridors along the Piedmont-Atlantic Coastal Plain and the Gulf Coastal Plain and lower Mississippi valley with maxima also in August-October, during which the contribution of TCs to monthly rainfall varied between 10% in August up to 30% in September in the Carolina and Alabama coasts, while remaining generally above at least 5% everywhere in the SE during the hurricane season. Maximum values in September coincide with the increased frequency of larger storms in the late season.

Although the amount of precipitation related to TCs represents a significant fraction of the annual precipitation at regional, continental and even global scales (Barlow, 2011; Hart and Evans, 2001; Jiang and Zipser, 2010; Maxwell et al., 2011; Prat and Nelson, 2012), few studies have gone beyond the synthesis of precipitation-centered climatologies to characterize the role of TCs in warm season hydrology beyond river (and flood) response in the southeastern US. Not focusing specifically on TC activity, O'Connor and Costa (2004) computed the spatial distribution of the largest floods across a large range of basin sizes in the CONUS. They established 2 criteria to explain the observed distribution of high discharge units: 1) Presence of regional conditions that produce large precipitation; and, 2) Steep topography, that enhances precipitation by

convective and orographic processes and allows flow to be quickly concentrated into stream channels. The two criteria are met in the southeastern United States, where large specific discharges are organized along the complex terrain of the Appalachians. Despite similar meteorological conditions, and large floods in the historical record (e.g. Floyd and Isabel in coastal North Carolina), high discharge units are rare in the flat and permeable Atlantic coastal plains, where storm surge inundation and back water effects tend to dominate over rainfall-runoff response. Elsewhere, in Australia where TCs are also a key player in regional hydrometeorology, McGrath et al. (2012) conducted a trend analysis of water storage using water level estimates from the Gravity Recovery and Climate Experiment (GRACE) satellite and NDVI (Normalized Difference Vegetation Index) as a proxy of vegetation activity to study continental-scale drought. They were able to link ecosystem condition directly to water table levels, drought duration, and the frequency of land-falling TCs. In the Middle East, Macumber et al. (1995) used water isotopes to show that infrequent tropical storms over arid areas cause widespread sheet flooding and fast stream runoff response, which rapidly leaves the stream to recharge of the local groundwater. Abdalla and Al-Abri (2011) analyzed piezometer measurements in the aftermath of tropical cyclone Gonu, 2007 in Oman to study water table level changes. They found significant increases over the coastal plains in areas with high infiltration rate. Over less favorable soil hydraulic conditions, the water table changes were moderate. This is consistent with expected spatial variability in recharge rates induced by land cover, soil properties and underneath geology. For the case of large Tropical Cyclones such as those that tend to occur in the second-half of the hurricane

season (Konrad and Perry, 2010), the areas affected by TCs in the SE span a wide range of hydrogeological conditions, and consequently time-scales varying from days to months (Schaller and Fan, 2009).

Because of the extreme volume of rainfall produced by large TCs, it is expected that these events should make an important contribution to alleviate, or even terminate meteorological drought in the southeast US. Maxwell et al. (2011) used monthly PDSI (Palmer Drought Severity Index) and daily rainfall data from the COOP network to characterize the frequency with which TCs land-falling along the East Coast abruptly end drought conditions, so called drought busters) over 31 climate divisions (http://www.ncdc.noaa.gov/temp-and-precip/us-climate-divisions.php) in the states of Florida, Georgia, North and South Carolina, and Virginia over a 59 year period ending in 2008. They found that up to 41% of all droughts and at least 20% of droughts over 24 climatic divisions were terminated (50% redress of the antecedent precipitation deficit) by single TCs. Therefore, the underlying climate regime, and the timing along with the specific track of a TC are critical from the perspective of meteorological drought. Climate divisions correspond to homogeneous climate regions defined based on observational statistics of atmospheric variables, and thus do not reflect land hydrology constraints or processes. Nevertheless, the fundamental control volume of interest for water resources management is the watershed, and therefore actionable climate change projections must be developed at the watershed scale. A systematic examination of the role of these events in the SE US water cycle, and specifically on the watershed scale hydroperiodicity,

is critical in order to better understand and prepare for the potential effects that could be induced by climate and environmental change.

4.2 Data

The TC information data used in this study were extracted from the database (HURDAT) available from the National Hurricane Center (http://www.nhc.noaa.gov/pastall.shtml). The period of this study, which was limited by the precipitation dataset used for precipitation estimates, goes from 2002 to 2011. Over this period, all the TCs having made landfall in the southeast US were accounted for. Table 4-1 summarizes the dates and characteristics of each storm analyzed in this work.

In order to carry out the desired watershed-scale analysis, instead of relying on spatial interpolation of point-based raingauge observations to characterize TC rainfall patterns, we rely only on spatial data sets that result from the combination of raingauge data and radar observations (e.g. Stage IV data set, Section 4.3) and through data assimilation of NWP (Numerical Weather Prediction) simulations and observations (e.g., the North America Regional Reanalysis - NARR, Section 4.4) to calculate basin-scale estimates of precipitation. Note that although this addresses in part the question of spatial interpolation, such data sets are not immune to large errors and bias due to the lack of raingauge and radar observations over complex terrain for example in the case of Stage IV. Finally, the environmental response to the precipitation was monitored using USGS streamgage and wells networks.

4.2.1 Watersheds

Only USGS (United States Geological Survey) gauged basins were used for the catchment-based water budget calculations. The drainage area directly upstream of each streamgage was delineated using the National Hydrography Dataset Plus (NHDPlus) dataset and the accompanying DEM–based (Digital Elevation Model (DEM) flow direction information. Basin delineation was defined as successful when the computed drainage area was within 25% of the stream gauge drainage basin area reported in the USGS National Water Information System (NWIS) (Michael E. Wieczorek, USGS, pers. communication, 2012). This criterion was only necessary for watersheds in flat areas (white areas in Figure 4-1a), where the delimitation was often unsuccessful, restricting the analysis along the coastal wetlands such as the in the Florida Keys, and in the Mississippi alluvial plain. About 3,400 watersheds over a wide range of scales were delineated over the area of study. Smaller basins that could not be resolved at the spatial resolution of the Stage IV precipitation data were removed from the database, leaving 3,211 gauged basins to be systematically used in this study (Figure 4-1a-f).

Table 4-1: Landfalling Tropical Cyclones in the SE US during the period 2002-2011

	Year	Name	Landfall	Category at landfall	Exit	Category at SE exit	LF location Gulf / Atlantic
1	2002	BERTHA	5-Aug	TS	7-Aug	TD	Gulf
2	2002	EDOUARD	5-Sep	TS	5-Sep	TS	Atlantic
3	2002	HANNA	14-Sep	TS	--[1]	--	Gulf
4	2002	ISIDORE	26-Sep	TS	27-Sep	TD	Gulf
5	2002	KYLE	11-Oct	TD	12-Oct	TD	Atlantic
6	*2002*	*LILI*	*2-Oct*	*H1*	*4-Oct*	*TS*	*Gulf*
7	2003	BILL	30-Jun	TD	2-Jul	ET	Gulf
8	2003	HENRI	6-Sep	TD	7-Sep	TD	Gulf
9	*2003*	*ISABEL*	*18-Sep*	*H2*	*19-Sep*	*H1/TS*[2]	*Atlantic*
10	2004	BONNIE	12-Aug	TS	13-Aug	TD	Gulf
11	*2004*	*CHARLEY*	*13-Aug*	*H4*	*15-Aug*	*TD/ET*	*Gulf*
12	*2004*	*FRANCES*	*4-Sep*	*H2*	*8-Sep*	*TD*	*Atlantic*
13	*2004*	*GASTON*	*29-Aug*	*H1*	*31-Aug*	*TS*	*Atlantic*
14	*2004*	*IVAN*	*16-Sep*	*H3*	*18-Sep*	*TD/ET*	*Gulf*
15	*2004*	*JEANNE*	*25-Sep*	*H3*	*28-Sep*	*ET*	*Atlantic*
16	2005	ARLENE	11-Jun	TS	12-Jun	TD	Gulf
17	*2005*	*CINDY*	*5-Jul*	*H1*	*8-Jul*	*ET*	*Gulf*
18	*2005*	*DENNIS*	*10-Jul*	*H3*	*12-Jul*	*TD*	*Gulf*
19	*2005*	*KATRINA*	*29-Aug*	*H4/H3*	*31-Aug*	*TD*	*Gulf*
20	2005	TAMMY	5-Oct	TS	--	--	Atlantic
21	*2005*	*RITA*	*24-Sep*	*H3*	*25-Sep*	*TD*	*Gulf*
22	*2005*	*WILMA*	*24-Oct*	*H3/H2*	*24-Oct*	*H3*	*Gulf*
23	2006	ALBERTO	13-Jun	TS	14-Jun	ET	Gulf
24	2006	ERNESTO	29-Aug	TS	2-Sep	ET	Atlantic
25	2007	BARRY	2-Jun	TS	3-Jun	ET	Gulf
26	2007	GABRIELLE	9-Sep	TS	9-Sep	TS	Atlantic
27	2008	FAY	19-Aug	TS	27-Sep	ET	Gulf
28	2008	HANNA	6-Sep	TS	6-Sep	TS	Atlantic
29	*2008*	*GUSTAV*	*1-Sep*	*H2*	*4-Sep*	*ET*	*Gulf*
30	2009	CLAUDETTE	17-Sep	TD	--	--	Gulf
31	2009	IDA	10-Nov	TS/ET	--	--	Gulf
32	2010	BONNIE	23-Jul	TS	23-Jul	TD	Atlantic
33	2011	LEE	3-Sep	SS	--	--	Gulf
34	*2011*	*IRENE*	*27-Aug*	*H1*	*28-Aug*	*H1*	*Atlantic*

[1] Became a non-tropical system inside the area of study

[2] Transition occurred at the border

H1,2,3,4 = Hurricane of categories 1, 2, 3, 4; TS = Tropical Storm; TD= Tropical Depression; ET = ExtraTropical storm; SS = Subtropical Storm. Hurricanes are in italic.

This new dataset was generated for our study instead of the "standard" USGS Hydrological Unit (HU) delineation, because stream gauges are not always at the output of the standard HU basins leading to discrepancies between the drainage network and the HU areas. In the maps presented, small basins are nested within larger basins, and the spatial data are layered for display purposes such that smaller basins overlap larger basins similar to the strategy in Schaller and Fan (2009).Streamflow and Well Data

The surface runoff was derived from the USGS daily mean stream discharge available from the National Water Information System (NWIS) (http://waterdata.usgs.gov/nwis). All the stream gauge data of this database were extracted using a Latitude/Longitude box spanning 25-37.5°N and 95-75°W. If one day was missing during a storm event, the missing value was interpolated from the values from the day before and after using a spline function. When more than one daily value was missing, the stream gauge and the associated catchment were removed from the analysis for the specific event. In addition, data such as flood stage for example are not available at all gauged locations. To monitor water table variations in the direct aftermath of TCs, a data-base of daily data in the USGS NWIS database (http://waterdata.usgs.gov/nwis/dv/?referred_module=gw) from all wells within the study area and during the period of study was assembled.

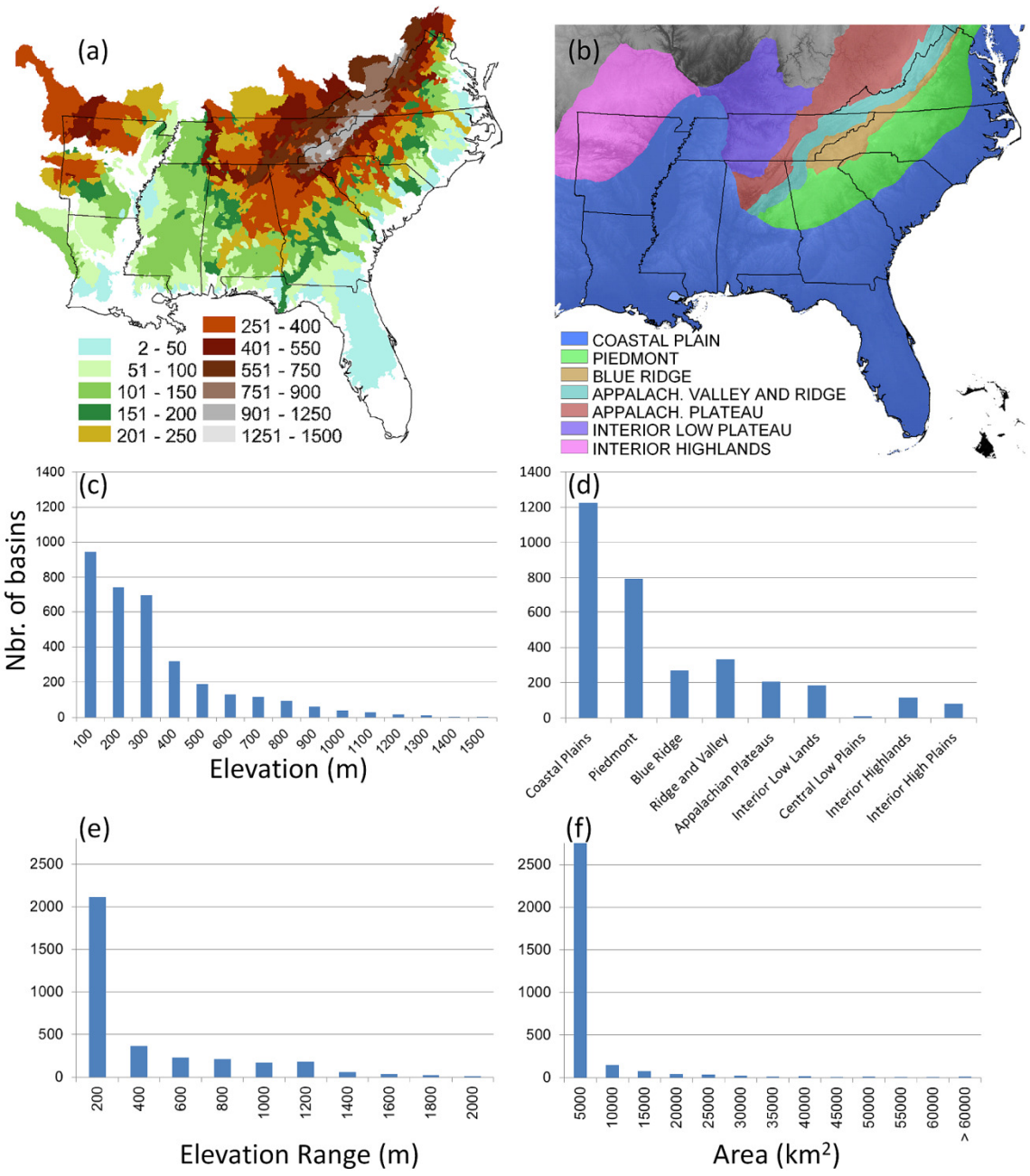

Figure 4-1: Characteristics of the SE US and 3211 watersheds used in this study: (a) map of watershed averaged elevation, (b) map of SE physiographic regions (elevation as grayscale background), (c) watershed distribution by elevation (d) watershed distribution by physiographic regions, (e) watershed distribution by elevation range and (f) watershed distribution by area.

4.2.2 National Centers for Environmental Prediction (NCEP) Stage IV Rainfall

The Stage IV multi-sensor (radar + raingauges) rainfall product produced by National Oceanic and Atmospheric Administration (NOAA) National Centers for Environmental Prediction (NCEP) (Baldwin and Mitchell, 1998; Lin and Mitchell, 2005) is available from 2002 onward, although 2002 was not fully operational. The data are mosaicked over the continental U.S. and bias-corrected using rain gauge observations. This product was selected due to its finest spatial resolution of 4km and because it has been previously shown to be suitable for TC precipitation quantitative and spatial distribution analysis (Villarini et al., 2011). However due to ground-clutter problems and the lack of raingauge observations over complex terrain, an underestimation of precipitation totals is expected (e.g. Prat and Barros, 2010; Sun and Barros, 2012). In this study, the daily precipitation accumulation product was used.

4.2.3 North American Regional Reanalysis (NARR) Rainfall Climatology

One goal of this study was to investigate the role of TC precipitation in alleviating meteorological drought (or precipitation totals deficit). Due to the relatively short record of the Stage IV time-series (~10 years at the time of this study), this product was not suitable in order to establish a precipitation climatology that could be used as reference to estimate meteorological drought during each specific year; therefore we relied on the North American Regional Reanalysis (NARR) climatology dataset (Mesinger et al., 2006). NCEP's Environmental Modeling Center (EMC) makes available the NARR climatology for the period 1979 to 2001 (25 years). The spatial resolution is 0.3 degrees and the temporal resolution is 3 hourly. From the provided 3 hourly data, daily rainfall

accumulations were independently calculated for each pixel of the NARR grid and then averaged at the drainage basin scale. Note that NARR does not account for rainfall intensities > 100 mm/hr, which can lead to severe underestimation of heavy TC rainfall (Nogueira and Keim, 2011; Sun and Barros, 2009, 2012) and is expected to have a similar problem with regard to rainfall underestimation in mountainous regions as Stage IV. Because of the coarser spatial resolution (0.3^{o}, or ~ 32 km), smaller drainage basins with an area less than 1024 km^2 were removed from the precipitation deficit analysis (see Section 4.3.2).

4.2.4 Gravity Recovery and Climate Experiment (GRACE) satellite

The Gravity Recovery and Climate Experiment (GRACE) satellite estimate the mass of water present in the environment by measuring small changes in the Earth gravitational field. Here we rely on the monthly gridded product of terrestrial water storage (TWS), which represents the difference in the masses for a specific month and the average over Jan 2004 to Dec 2009. This dataset has been corrected for signal modification due to filtering and truncation using simulations of terrestrial water storage variations from land-hydrology models to infer relationships between regional time series representing different spatial scales. These relationships, which are independent of the actual GRACE data, are then used to extrapolate the GRACE TWS estimates from their effective spatial resolution (length scales of a few hundred kilometers) to finer spatial scales (~100 km) (Landerer and Swenson, 2012; Swenson and Wahr, 2006). Therefore it is recommended to use this product only for regional to larger scale studies (Tapley et al., 2004). Reigger et al. (2012) have analyze the sources of

uncertainties in the different GRACE datasets by comparing GRACE mass changes to hydrological and hydrometeorological water balance equations combining ground observations and reanalysis data. They estimated the RMS on the residual to be ranging from 1 to 2cm over the SE US.

4.3 Methodology

The methodology developed to assess the contribution of TC in the SE hydrological cycle is summarized in Figure 4-2 and detailed in the next sections.

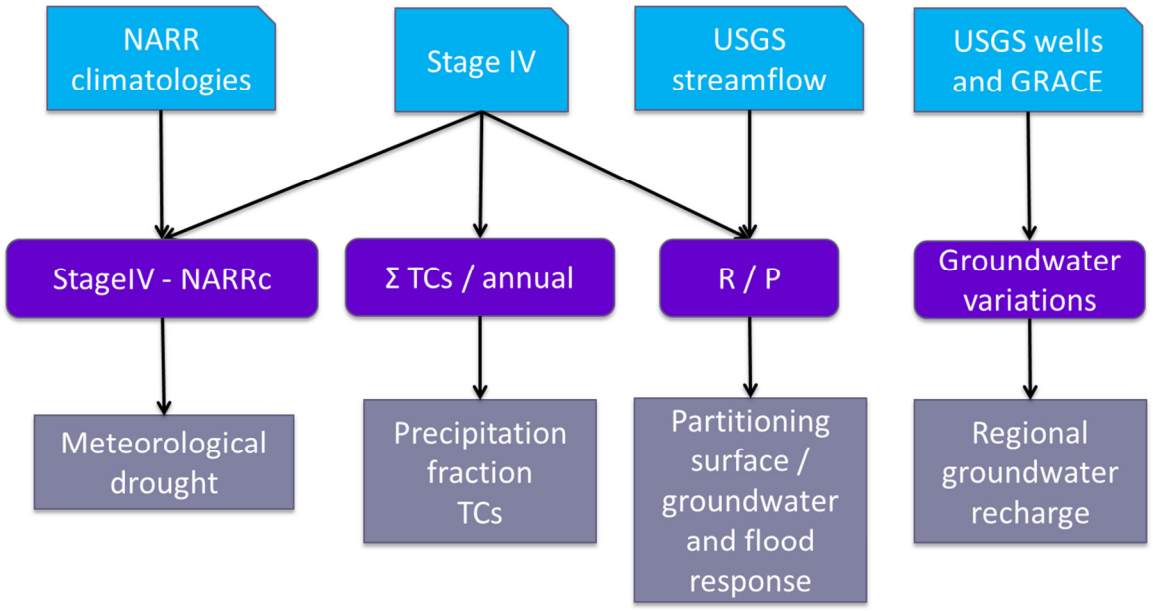

Figure 4-2: Chart flow describing the methodology used to assess the contribution of TCs to the SE hydrology at the watershed scale

4.3.1 Annual and Seasonal Precipitation Depth

The NCEP Stage IV daily cumulative precipitation depth data were used to compute the annual precipitation totals over the 3,211 drainage basins delineated in the southeast US. The 4km Stage IV data were interpolated using an Inverse Distance

Weighted (IDW) algorithm to create a regular grid of 1km×1km resolution, in order to fill potential missing values and improve the agreement between the rainfall fields and the watershed outline for the computation of the basin statistics, since the Spatial Analyst tools of ArcGIS does take into account any pixel overlapping a specific polygon when computing spatial statistics.

We also relied on this dataset to investigate the fraction of annual precipitation related to TCs at the hurricane season and event scale. The amount of TC-specific precipitation was computed by accumulating the precipitation from the day before landfall to the day after the hurricane track exited the SE US. Next, the cumulative sum of the events was computed to estimate the precipitation totals of the entire hurricane season. Finally, the ratio between this cumulative sum and the annual cumulative precipitation depth was calculated to evaluate the TC season contribution to the annual freshwater input.

4.3.2 Meteorological Drought - Precipitation Deficit

As mentioned above, the NARR climatology was used as reference to compute the temporal evolution of precipitation deficit (or surplus) for each drainage basin at daily time-scales for each year available in the Stage IV time-series (2002-2011). By considering the precipitation deficit or surplus just before and after each land-fallen TC, it is possible to quantify the contribution of each TC to mitigate meteorological drought. The integration at the drainage basin scale, combined with the use of daily totals, is expected to reduce the impact of the different spatial resolution between the two data sets (32km for NARR vs. 4km for Stage IV). Nevertheless, to limit the impact of this

spatial resolution discrepancy, the basins with an area smaller than 1,024 km^2 (i.e. 32x32 km^2) were removed from this analysis yielding finally a total of 1,517 watersheds for this portion of the analysis.

Two types of deficit accounting were conducted. First, the deficit was calculated based on cumulative annual precipitation 3 days before the first TC of the hurricane season for each drainage basin and for all years. The choice of a 3–day period was made to assure that the initial conditions reflected the state of the environment before any precipitation related to the first TC of the season was registered, i.e. before any front preceding the organized system has reached the coast. Then, the ratio between the total precipitation produced by TCs and this deficit was computed to quantify the relative contribution of the hurricane season as a whole to mitigate drought. Second, the analysis was repeated for specific TCs considering the change in precipitation deficit before and after each event. In order to highlight spatial and temporal variability patterns within the hurricane season, detailed results are presented for the most active hurricane seasons (2004 and 2005).

4.3.3 Event Water Budget Analysis

Rainfall-runoff ratios were the metrics used to map runoff and recharge fractions of TC rainfall. To this end, the spatial distribution of the ratio between the total surface runoff (R) and the total precipitation (P) during each TC was estimated. Assuming that evapotranspiration during the storm is negligible compared to the other water fluxes, the runoff fraction provides a metric of the recharge contribution of each TC across the entire landscape: a ratio R/P of 1 means that all the precipitation turned into surface

runoff, whereas a low R/P ratio indicates areas were the precipitation contribution to local soil moisture reservoirs and groundwater recharge is dominant. For each event, the watersheds affected by the TC were identified using a buffer of 500 km half-width to the right and left of the storm the storm track. For each basin, the cumulative stream discharge was estimated by searching the peak flow value in the 10 days after landfall. From this maximum, the inflexion points corresponding to the rising and falling limbs of the hydrograph were identified. The discharge at the lowest inflection point is subtracted from the other daily values during the time integration. The runoff depth was calculated by dividing the integrated discharge volume by the area of the basin. Consequently, R is defined as:

$$R = \sum_{d=m}^{n} (Q_d - Q_i) / A_{drain} \tag{4.1}$$

Where Q_d is the daily streamflow average for a specific day *d*; *m*, *n* correspond to the days when the inflection point of the rising and falling limb were reached, respectively; Q_i is the streamflow at the inflection point corresponding to the beginning of the rising limb of the hydrograph before hurricane landfall; and A_{drain} is the drainage area.

The event cumulative precipitation was computed from the daily NCEP Stage IV processed using the same method described in Section 4.3.1. The precipitation accumulation was conducted from the day before landfall (l) to the day after the storm has left the SE region (q).

$$P = \sum_{d=1}^{q} P_d \tag{4.2}$$

Where P is the accumulated precipitation during the storm overland path and P_d is the daily precipitation for a specific day *d*. Finally, the runoff ratio R/P is calculated for each drainage basin.

Using an approach similar to that for the streamgage data processing, a search for the maximum change in water table height in the 10 days following TC landfall and within a radius of 500km from the estimated track was conducted to focus on local groundwater response as opposed to large regional transfers which would require complex groundwater modeling out of the scope of this work (see Schaller and Fan, 2009 for insight). The water table level the day before landfall was used as reference and subtracted from the maximum measured value to compute the absolute change. This water table level change provides an estimate of water table recharge in the direct aftermath of the TC. The use of the 10-day interval insures that the water budget analysis remains local, that is at the watershed scale. Brun and Barros (2012) mapped vegetation disturbances due to flooding in the alluvial margins of rivers in the Gulf Coastal Plains that occurred several weeks later and could be traced back to hydrograph propagation and augmentation in the Tennessee and Mississippi river network systems, but these are not considered here.

4.3.4 Flood Frequency Analysis

Flood frequency analysis was conducted on the outlet stream gauges using the maximum annual flood series (USGS peak-Flow database) and fitting a log-Pearson Type III distribution following Kite (1977). The frequency factor (K_T) is estimated as follow:

$$K_T = z + (z^2 - 1)k + 1/3(z^3 - 6z)k^2 - (z^2 - 1)k^3 + zk^4 + 1/3k^5 \quad (4.3)$$

Where $k = \frac{C_s}{6}$ and Cs is the coefficient of skewness.

The standard normal z-values of the log of the streamflow data are estimated using a numerical approximation of the normal distribution (Abramowitz and Stegun, 1972):

$$z = w - \frac{2.515517 + 0.802853w + 0.010328w^2}{1 + 1.432788w + 0.18929w^2 + 0.001308w^3} \quad (4.4)$$

Where $w = \left[\log\left(\frac{1}{P^2}\right)\right]^{0.5}$ with P being the probability of exceedance of a specific return period.

The return periods for the peak discharge for each TC in the period of study were subsequently estimated, and the spatial distribution was examined in the light of river stage records (where available) from the NWIS. Note that flashfloods, i.e. floods with response times less than 6 hours typical in small basins (< 1,000 km^2), and floods in strongly urbanized watersheds (i.e. cities) are not included in this study.

4.3.5 Water Table Change

In order to examine the contribution of tropical cyclones precipitation to recharge groundwater reservoirs, changes in wells depth was computed by taking the well depth the day before the landfall and subtracting it from the highest well height observed in the 10 days following the landfall of specific storms. Only wells in a radius of 500km of the storm track were extracted from the USGS data base.

4.4 Results

4.4.1 Annual Precipitation

Figure 4-3 shows clearly the low spatial distribution of basin averaged annual precipitation depth during the years 2006 and 2007 leading to extreme drought over large parts of the SE During the period of study 2002 and 2009 are the wettest years despite low TC activity in the latter. The year with most TC activity during the period covered by Stage IV data is 2004. 2005 shows lower total precipitation than 2004 despite a high number of very intense storms (cat. 3 and above).

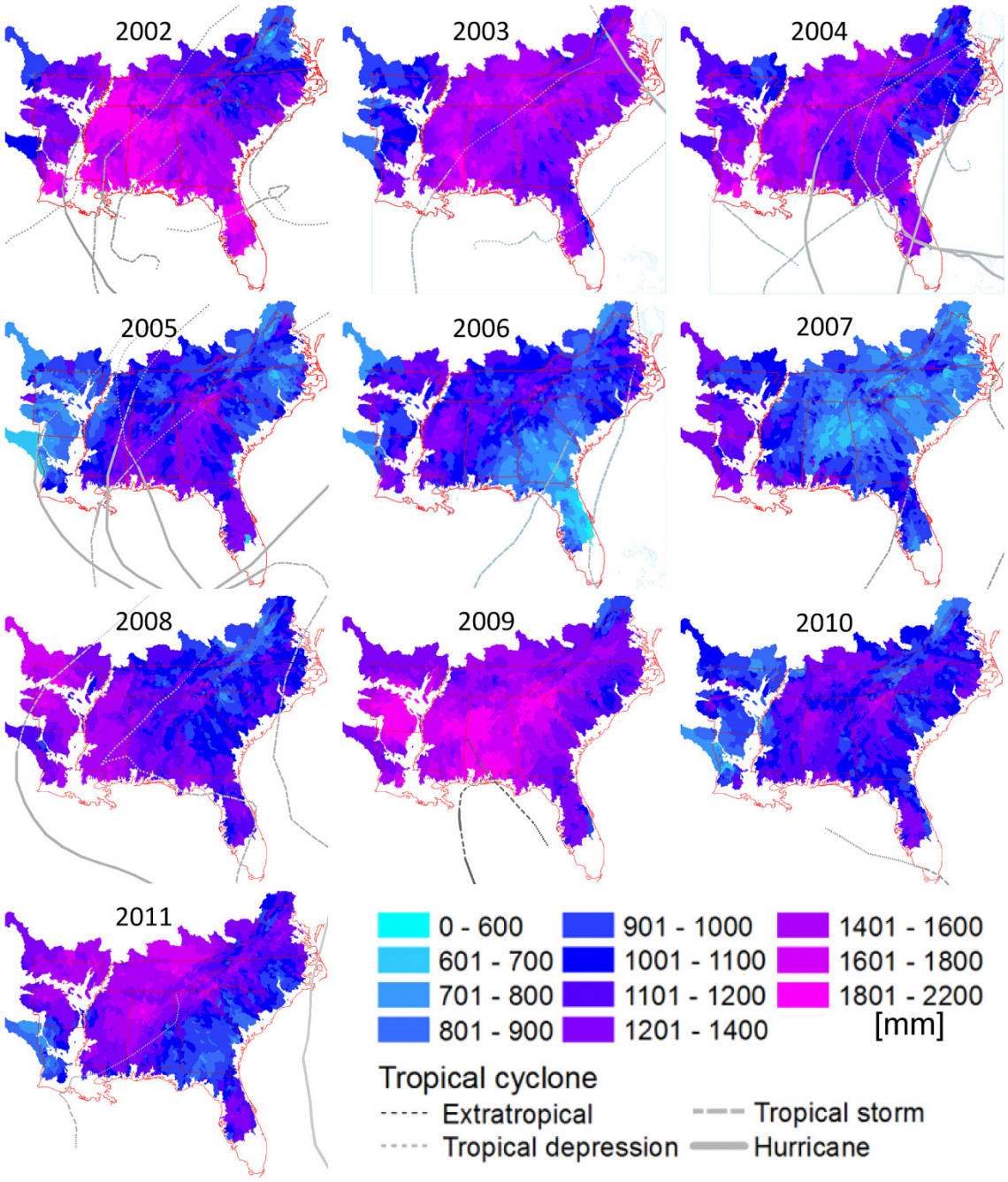

Figure 4-3: Basin averaged annual precipitation depth for the years 2002-11 computed using the Stage IV daily product. The lines mark the track of the tropical cyclones making landfall during each specific year.

In the same year, note the orographic enhancement of Cindy's precipitation close to the border of North and South Carolina and Georgia. A similar enhancement is also visible

for Fay in 2008 over the same area. In 2011, the Coastal Plains received significantly less precipitation than the inland areas (cf. Figure 4-3). In terms of spatial distribution, specific patterns of high precipitation totals are generally arranged along TC tracks, but not systematically. Storm category (tropical cyclone intensity, Table 4-1) is not a governing factor in explaining the observed spatial patterns (no clustering is observed) as opposed to within-season storm frequency and track density (2004 vs. 2005). Note the difference between years with predominant Atlantic Coast (AC) tracks such as 2004 as compared to years such as 2005 with Gulf Coast (GC) landfall and continental tracks along the Mississippi Alluvial Plains (MAP) and the Appalachian Mountains (AM) as also pointed out early by Nogueira and Keim (2011).

4.4.2 TC Contribution to SE Precipitation

4.4.2.1 Seasonal Scale

The contribution of TCs to annual precipitation totals at the watershed scale was estimated by summing the precipitation during each specific event (from the day before landfall to the day following the storm exit from the SE region), and by dividing this amount by the annual precipitation over each drainage basin. Figure 4-4 shows that 2004 was clearly the year when AC TC activity had a larger impact on precipitation, with TC fractions of annual precipitation exceeding 60% of annual totals for some watersheds, both close to and remote from landfall, the latter aligned with the Appalachian Mountains.

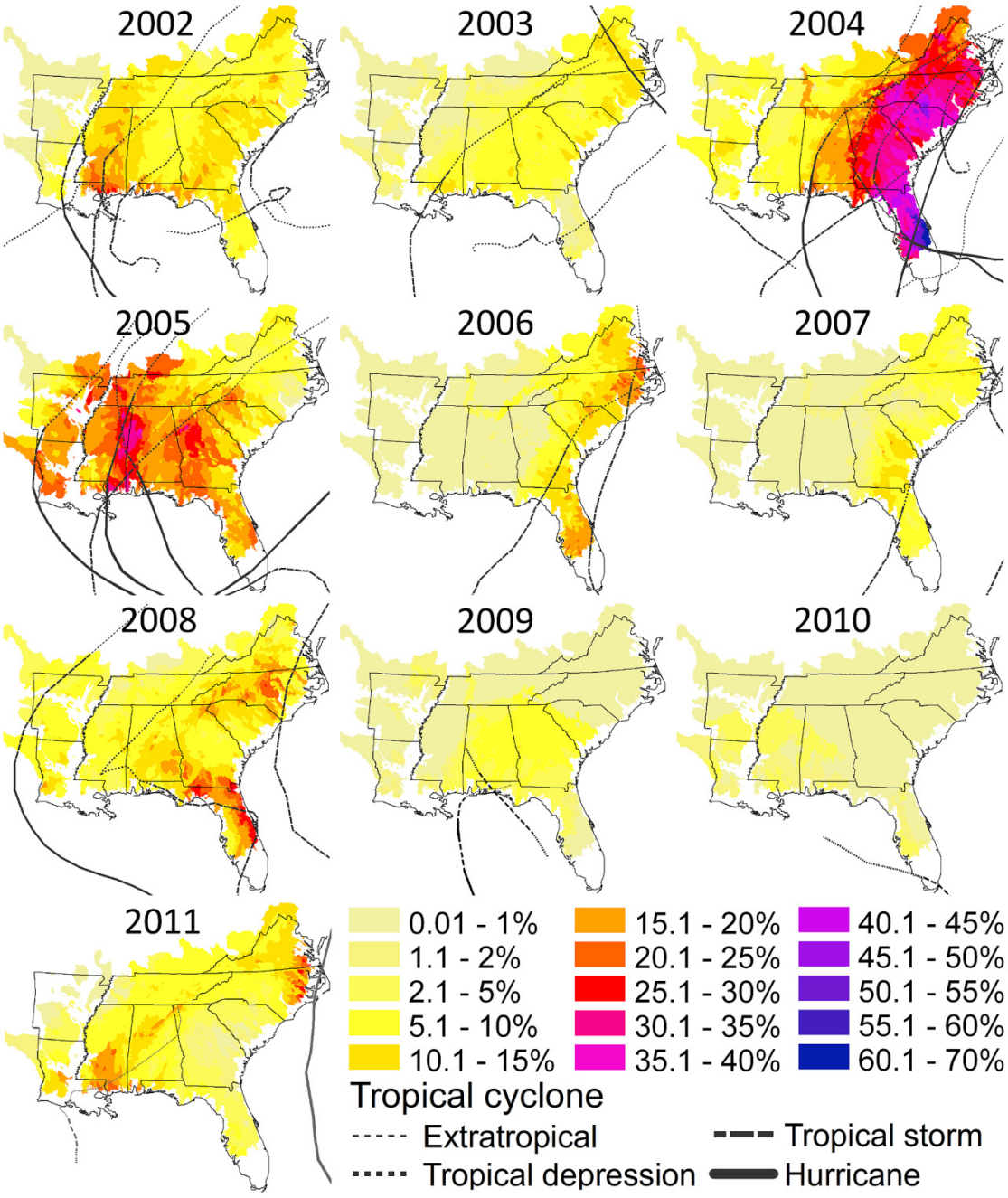

Figure 4-4: Annual precipitation fraction (%) due to TC activity estimated at the watershed scale unsing Stage IV daily product (2002-2011). The lines mark the track of the tropical cyclones making landfall during each specific year.

Despite the landfall of 4 major hurricanes in 2005 (Dennis, Katrina, Rita and Wilma), the contribution of TCs to the annual precipitation is moderate with maximum values of 25-

30%. In 2005, landfalls occurred along the Gulf of Mexico; and consequently, the TC rainfall maxima were located on the eastern side the Mississippi alluvial plains consistent with the storm tracks. In 2004, most landfalls occurred directly from the Atlantic basin with tracks on the Atlantic Coastal Plains, Piedmont and over the Appalachians, with larger precipitation totals as compared to 2005. The strong signal of 2006 in the NC coastal plain is attributed to the lower overall annual precipitation rather than to a high number or intensity of land falling tropical storms during this year (see Figure 4-3). By contrast, the low relative signal of hurricane Isabel in 2003 is due to the fact that the precipitation totals over the Coastal Plains of North Carolina were high for that year (see Figure 4-3). The intensity of the storm appears to be secondary in terms of seasonal precipitation fraction. For example in 2008, Fay was classified only as a tropical storm but it was a slow moving storm (Table 4-1) and produced large rainfall depths over large areas of the SE, mainly due to its specific track including orographic effects over the Southern Appalachians which caused multiple flashfloods (Tao and Barros, 2013).

Figure 4-5 shows histograms of annual rainfall at the watershed scale with and without TC contribution. The gap between the medians of the two histograms is indicative of the regional contribution of the TCs to annual precipitation: 2004 clearly is the year when most of the basins were significantly impacted by TC precipitation followed by 2005, 2008 and 2002.

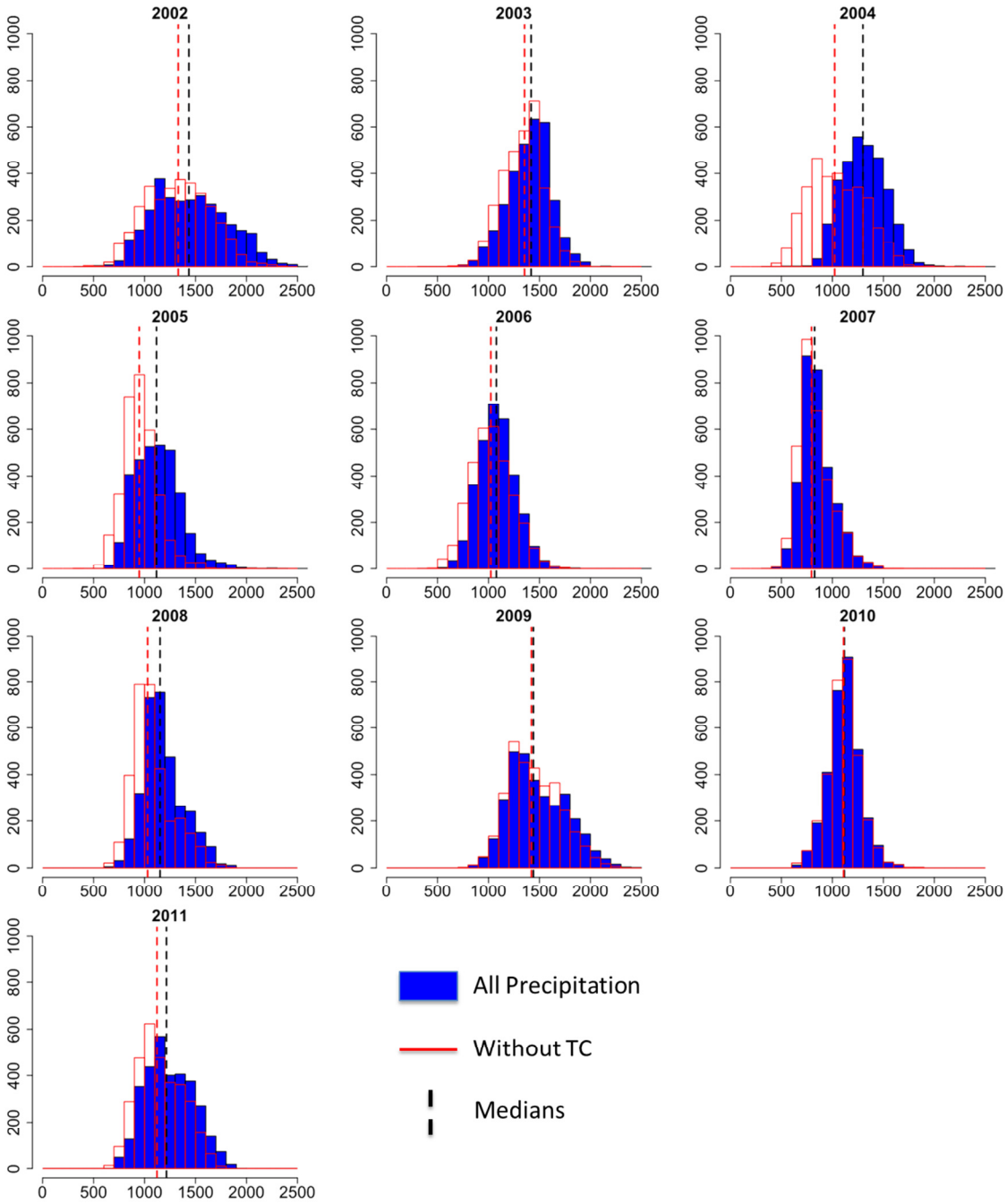

Figure 4-5: Frequency analysis of the annual precipitation depth over 3211 gauged watersheds. The plain histogram was computed with all the precipitation and for the red lined histogram the precipitation from TCs was removed. The dashed lines represent the two medians.

Interestingly, when the precipitation related to TC activity is removed from the annual totals in 2004, the median of the distribution is close to the median of the driest years for

the period of study, indicating that before the peak of the hurricane season in August – September, 2004, the Southeast was experiencing extensive meteorological drought (see also Figure 4-10). A similar pattern in distribution change is observed in 2005 and 2008. These statistics illustrate the significant role of TCs on the regional hydroclimatology, but do not elucidate the importance of intra-seasonal variability of TC precipitation contribution, and timing, which requires storm scale analysis.

4.4.2.2 Storm Scale

Due to the high TC activity in 2004 and 2005, specific events are examined in detail in order to characterize their individual contributions (Figures Figure 4-6 and Figure 4-7 respectively). Bonnie, a tropical storm at landfall, did impact all the southeast Atlantic Coast states, but produced only moderate precipitation amounts. Next, Charley, a very small system with extreme winds confined within only about 10 km of the center at landfall (Franklin et al., 2006), and yet an intense hurricane, (category H4 at landfall), exhibited similar behavior but it produced heavier precipitation up to 10% of the annual mean in the Coastal Plain of North Carolina. In the last days of August, Gaston a tropical storm, which reached shortly the hurricane category H1 before landfall in South Carolina, curved quickly over the Coastal Plains to exit the southeast though east Virginia. Gaston therefore mostly impacted the Coastal Plains in the Carolinas. Frances, the first large hurricane of the 2004 season followed a terrestrial track that veered away from the coast toward the Appalachian Mountains producing heavy precipitation to the right of the track exceeding 20% of the annual mean in the Piedmont and Blue Ridge watersheds. Frances was followed by Ivan, likewise a large storm, which had landfall in

the Gulf Coast and then veered northeastward with a continental track more or less aligned with the Southern Appalachians.

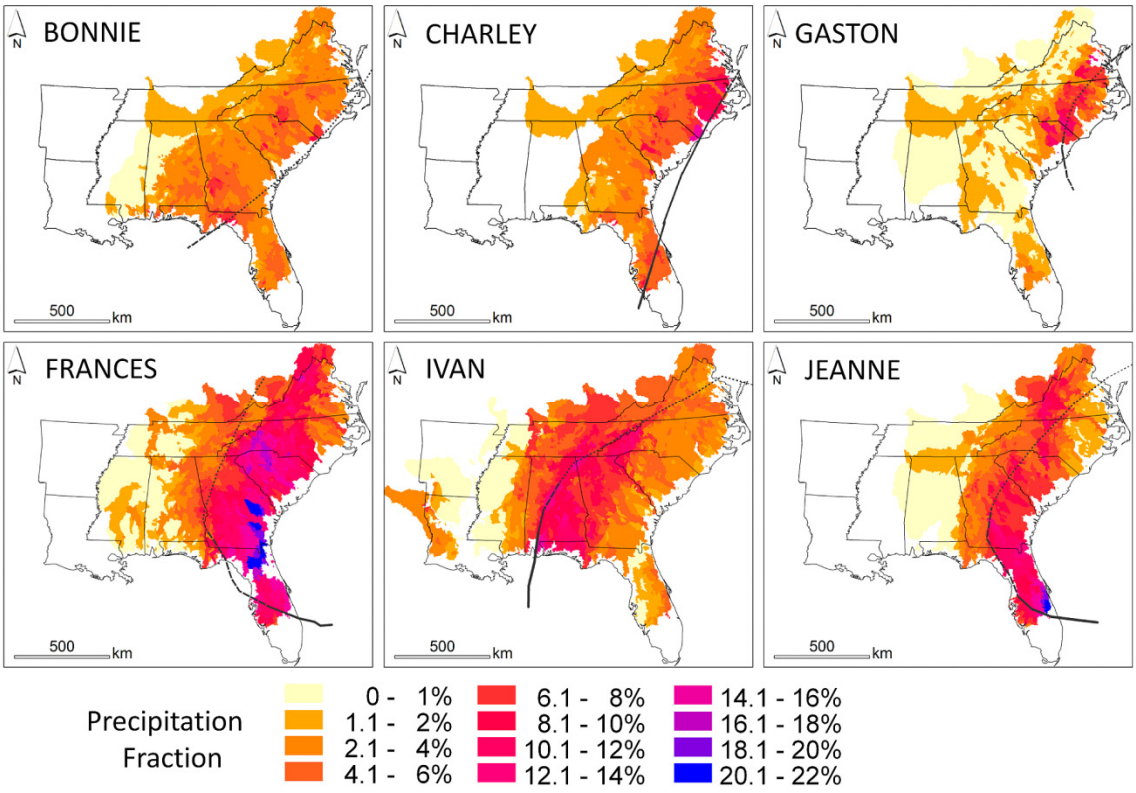

Figure 4-6: Contribution from individual TCs to the annual precipitation totals of 2004. Precipitation fraction computed at the watershed scale.

The Stage IV data indicate that Ivan produced about 15% of annual precipitation over a large fraction of the southeast region. However observations of several landslides and debris flows, and ten deaths in the mountains of western North Carolina as well as raingauge data at a limited number of locations (Wooten et al., 2008) indicate that Ivan's rainfall environmental impacts were enhanced by the high soil moisture levels due to the passing of hurricane Frances nine days earlier. Finally, Jeanne, the last hurricane of the season, produced heavy precipitation close to landfall and within a narrow swath

along track in the Piedmont region. Frances and Jeanne are the two hurricanes with the two closest landfall locations on record, and the cumulative effect of the two storms accounts for the 60-70% of the annual mean rainfall in Central Florida for the 2004 hurricane season (Figure 4-5).

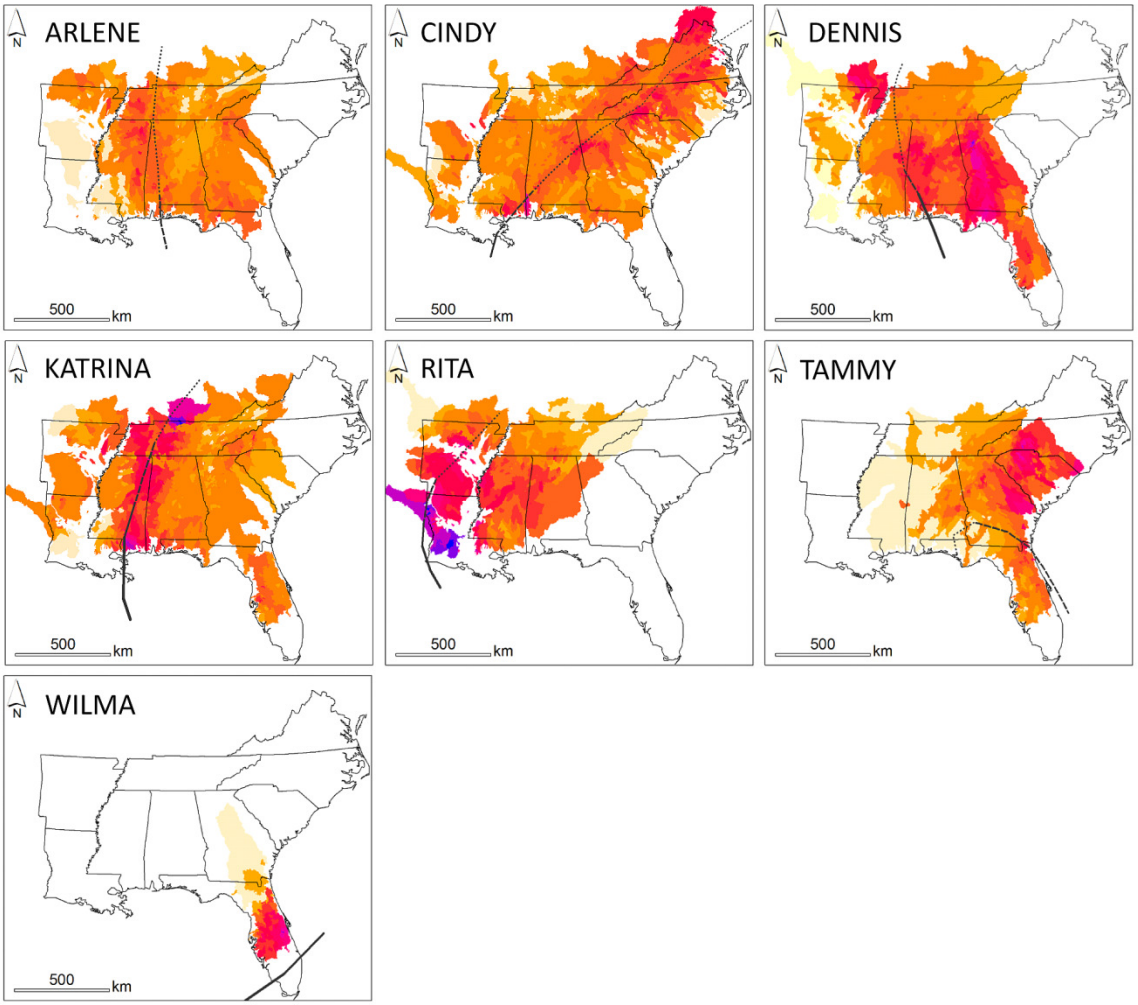

Figure 4-7: Same as Figure 4-6 during the hurricane season 2005

Arlene and Cindy were the two first TCs of the 2005 hurricane season and impacted large areas in a moderate way (Figure 4-7). Again note the orographic enhancement over the Blue Ridge and Ridge and Valley regions on the left hand side of

Cindy's track. Dennis was an intense (category 4 at landfall) but a very small hurricane at landfall with sustained hurricane-force wind within only 25-30 km of the swath center (estimated from *H*Wind* fields of the Hurricane Research Division (HDR), NOAA). The large precipitation fraction observed over Georgia and North Florida is not directly produced by Dennis, but by precipitation from the large leading cloud shield associated with the tropical cyclone outflow. Katrina produced large precipitation at landfall, but the overall contribution to the annual freshwater input over the Mississippi valley is not as significant as that for Frances in 2004. Further inland, and close to the extratropical transition region at the border between Kentucky and Tennessee, the precipitation fraction was over 16% of the annual values close to the track. In the aftermath of Katrina, Rita, a hurricane of category 3 at landfall, produced close to 20% of annual precipitation totals close to landfall and over the western flank of the Mississippi valley with a maximal relative contribution exceeding the one of Katrina. Rita was followed by Tammy, already a tropical storm at landfall, which produced heavy amounts of rainfall in the Piedmont region upwind of the Appalachians consistent with orographic enhancement effects of precipitation bands away from the storm center. Finally, although Wilma was one of the most intense hurricanes on record at landfall, and it did impact Florida significantly; however its regional impact was very limited due to a short overland track.

The detailed analysis of the contribution of specific storms in the context of the annual climatology of precipitation in the region shows there is large variability in the spatial distribution of precipitation between storms at the watershed-scale, even among

adjacent watersheds. The large range of storm-to-storm variability is not directly related to the storm intensity, as it varies with geometry and the length of the storm's terrestrial path. Storms with Atlantic Coast landfall tend to produce more precipitation during the period of study, although orographic enhancement in the Appalachian Mountains is consistently present. Nevertheless, storms with landfall along the Gulf Coast and more continental tracks tend to produce rainfall over the entire region, whereas recurving TCs with AC landfall have little impact westward of Alabama.

To examine further the spatial distribution of tropical cyclone precipitation, the basin data were clustered by physiographic regions as defined by the USGS (see Figure 4-1b). Figure 4-8 shows scatterplots of basin averaged annual precipitation depth (in mm) versus the basin averaged precipitation depth produced by all TCs (in mm) during the hurricane season. A diagonal line connecting the origin to the top right corner in each plot corresponds to a relationship of 1:4 (25% fraction) between the hurricane season TC rainfall and the annual total precipitation. Two regions stand out where the hurricane season precipitation exceeds 25% of the annual amount: the Coastal Plains and the Piedmont. For the Blue Ridge and the Appalachian Plateau, the inter-annual variability is not only associated with storm frequency but also with storm track (compare 2004 and 2005). In 2005, rainfall enhancement associated with landfall along the Gulf Coast and southerly continental tracks is apparent by the clustering of the Interior Plains and the Interior Highland basins above the 25% seasonal contribution.

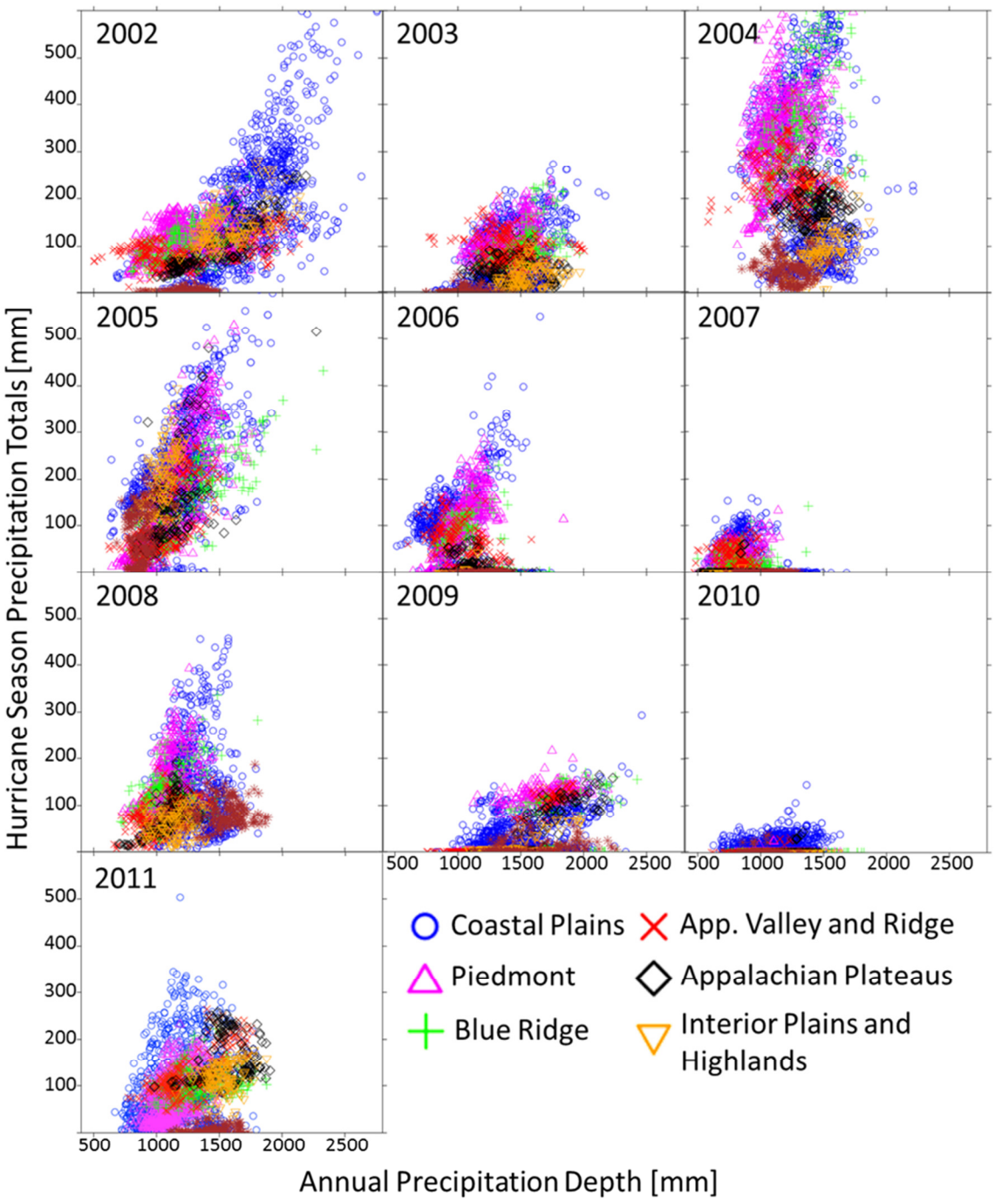

Figure 4-8: Scatterplots of basin averaged annual precipitation depth (in mm) versus the precipitation depth produced by all the TCs (mm) of the hurricane season as a function of physiographic regions. Note the importance of orographic effect (Blue Ridge) in 2004, 2008 and 2009.

Finally, the contribution of two weak, but slow moving tropical storms, Fay in 2008 and Irene in 2011, which caused widespread flooding, are clearly dominant during two otherwise average hydrometeorological years in the Coastal Plains and in the Blue Ridge for the case of Fay. Note the signature of orographic enhancement of Fay rainfall for Blue Ridge watersheds lining up well above the 25% line in 2008. Figure 4-9 shows boxplots of precipitation fraction distribution across physiographic regions for specific years: 2004 (Atlantic tracks), 2005 (Gulf tracks) and 2010 (low activity).

4.4.3 Meteorological Drought and Precipitation Deficit Mitigation

Despite high spatial and inter-annual variability as depicted in Figure 4-4,it is clear that warm season rainfall, and TC rainfall in particular, represent a substantial fraction of the annual meteorological freshwater input in the southeast and must play an important role in modulating meteorological drought the extent and intensity of which also peaks in the summer season, especially drought retreat in the second half of the hurricane season when larger storms (drought busters) are more frequent (e.g. see Sections 4.4.1 and 4.4.2 above, as well as Maxwell et al. 2011). Note that although the mitigation of meteorological drought, and by extension hydrological drought, is a valuable service of TCs, whether there is a benefit in terms of agricultural drought during the mid-summer season strongly depends on TC activity in the first-half of the season, which tends to be weaker according to climatology.

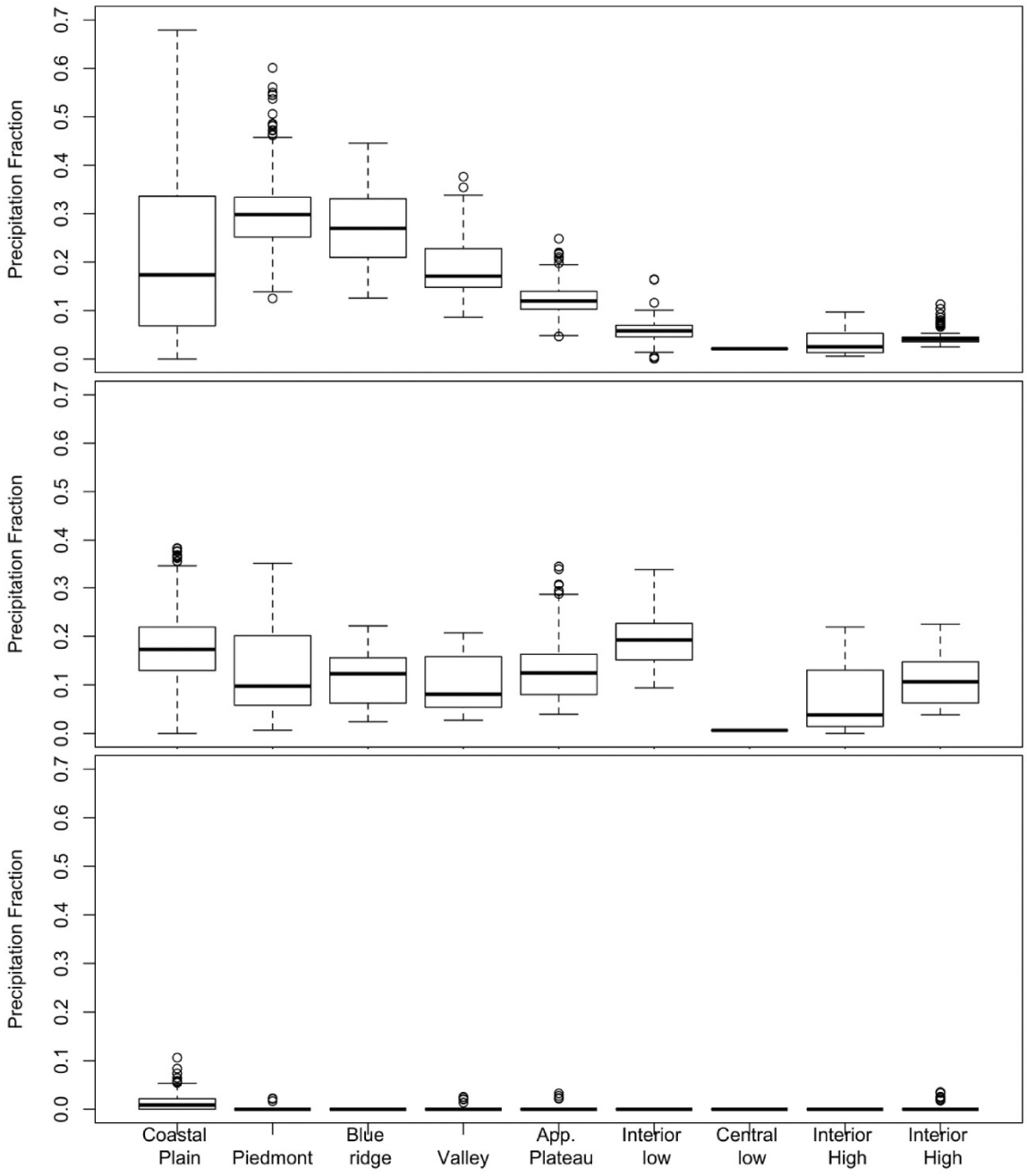

Figure 4-9: Boxplots of annual precipitation fraction due to TCs during the years 2004, 2005 and 2010 for the different physiographic regions.

Toward mapping the space-time relationship between drought and TC activity, basin-scale daily cumulative precipitation deficits of the Stage IV data with respect to the

NARR climatology were calculated assuming that no significant trends in annual precipitation amounts occurred in the region in the last thirty years. Maps of the spatial distribution of precipitation deficit at the onset of the hurricane season that was mitigated by TC rainfall over the course of the hurricane season are presented in Figure 4-10. The light green areas represent basins where there was no deficit for the specific year, meaning they were not in drought. The brown areas correspond to basins that were not impacted by TCs, in other words where hurricane season precipitation from TC activity is null. The purple areas correspond to basins where antecedent meteorological drought was fully redressed by TC precipitation during the hurricane season.

Figure 4-10 shows that every year a significant fraction of the southeast is in drought to some degree and every year tropical cyclone activity makes an important contribution to reducing drought intensity. Interestingly, the two years with higher number of TCs (2004 and 2005) were also years in which the larger areal extent of drought was remedied. Yet, even in the dry years of 2006 and 2007, TC rainfall was critical in alleviating meteorological drought in the Atlantic Coastal Plain (20-40% deficit reduction in 2007), and especially for specific watersheds in the Carolinas (50-90% deficit reduction in 2006). These effects are evident in vegetation activity disturbance patterns extracted from satellite based EVI imagery (Enhanced Vegetation Index) examined by Brun and Barros (2012). By contrast, over the Piedmont and Appalachians the contribution of TCs to drought reduction was below 20% of the precipitation deficit. In 2008, there is large spatial variability in TC rainfall consistent with the different paths of

the three TC storms on record, with deficit reductions on the order of 50 to 100% over large areas.

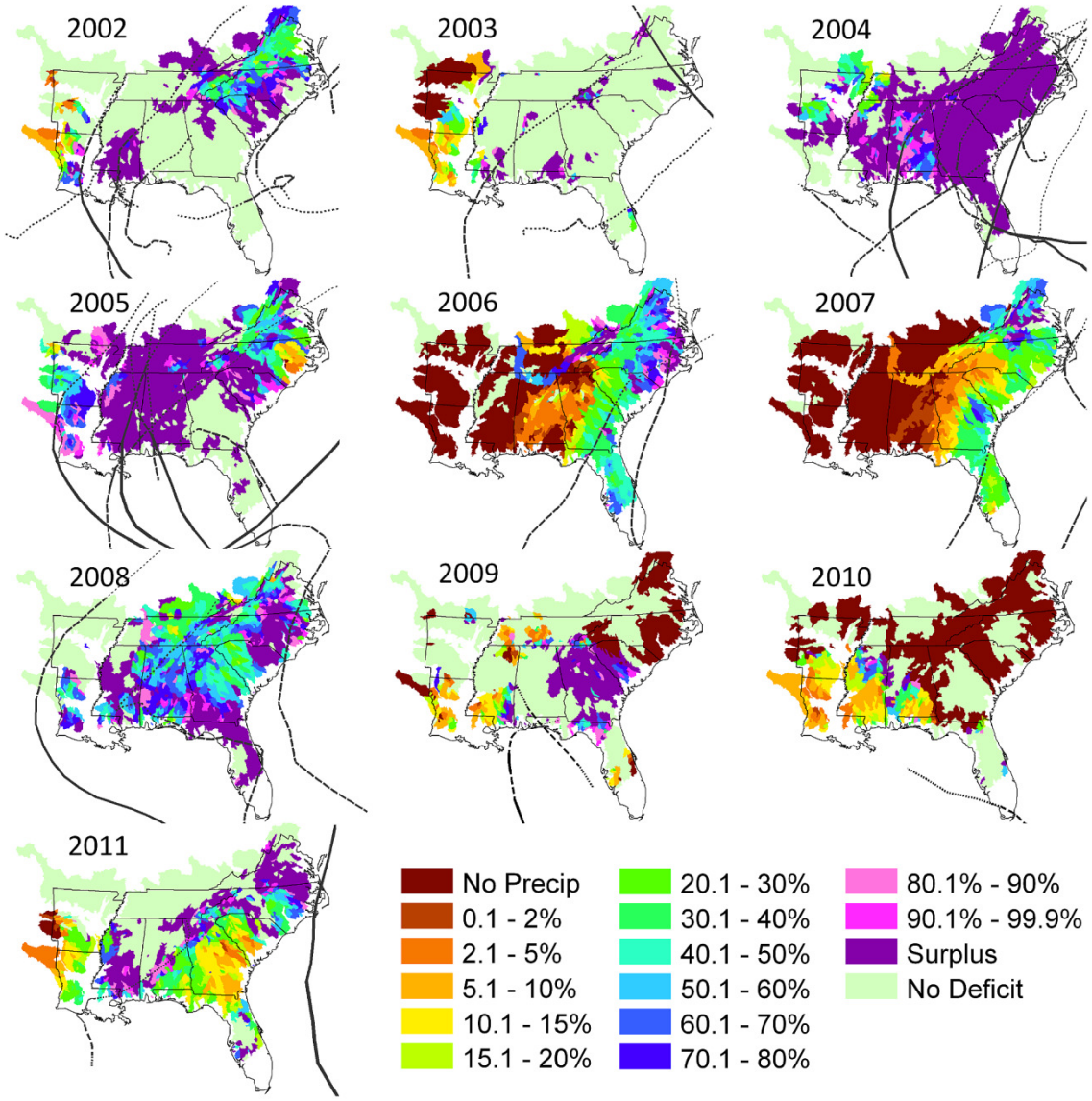

Figure 4-10: Fraction of the precipitation deficit at the beginning of the hurricane season (computed as the Stage IV cumulative precipitation average depth minus the NARR precipitation depth climatology for each basin) reduced by TC precipitation during the hurricane season.

Nevertheless, in years with less TC activity than 2004 and 2005, meteorological drought persistence (and mitigation) tends to have a strongly localized rather than

regional expression. Case in point is the drought in isolated watersheds east of the Mississippi that was completely mitigated by TC activity in 2002, though severe drought remained to the west. The redress of drought conditions over Georgia reflects weak drought conditions in 2009 (small deficit) not TC activity. In 2010, there was no relevant TC in the Piedmont and in the Atlantic Coastal Plain, but also no drought. Finally, the moderate precipitation deficit present over the Coastal Plains (Atlantic and Gulf of Mexico) was closed by Hurricane Irene over North Carolina and Virginia, and by Tropical Storm Lee over the Mississippi and the Appalachians in 2011.

The spatial distributions of the relative contributions of individual TCs to reduce the basin-scale precipitation deficit at the time of landfall which cumulatively explain the corresponding seasonal-scale spatial pattern in the 2004 season discussed above are depicted in Figure 4-11. Note that in this case the precipitation deficit with regard to climatology is updated just before storm landfall, and therefore summing these maps does not match quantitatively the previous seasonal analysis due to non-TC rainfall in-between TC events. As expected, these storm specific maps show large storm-to-storm spatial variability that is consistent not only with the storm rainfall but also antecedent weather. Defining a drought buster as a storm that redresses meteorological drought by 50%, one can see that all storms can be considered drought busters locally at the watershed scale, though at the regional scale only Ivan and Frances in 2004 qualify. Before Frances, Bonnie and Charley (not shown), and Gaston also contributed to reducing the precipitation deficit, but to a lesser extent. Jeanne closely followed Frances track and eliminated the rainfall deficit in the remainder basins over the Coastal Plains

of Florida and Georgia, and the Piedmont region of Georgia South and North Carolina by the end of the hurricane season. Indeed, by October 4th, there was a precipitation surplus compared to climatology over more than 65.5% of the SE area in contrast to a 79.5% areal extent of drought on August 1st.

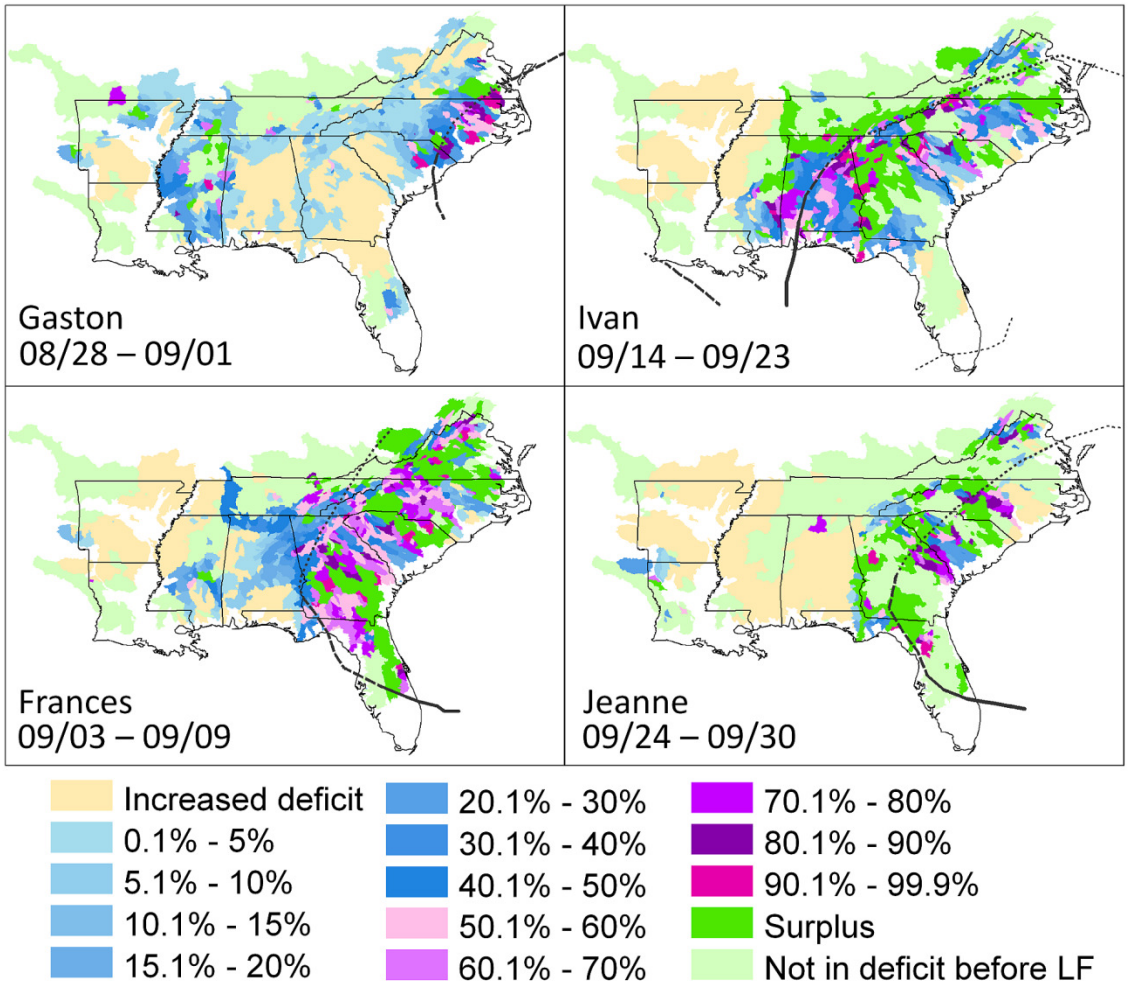

Figure 4-11: Fraction of precipitation deficit reduced by individual TC during the hurricane season 2004. The dates under the storm name correspond to the one used for the relative difference calculation. The mentioned dates were used to compute the deficit change. The light green color indicates gauges watersheds that were not in deficit before the TC landfall (LF).

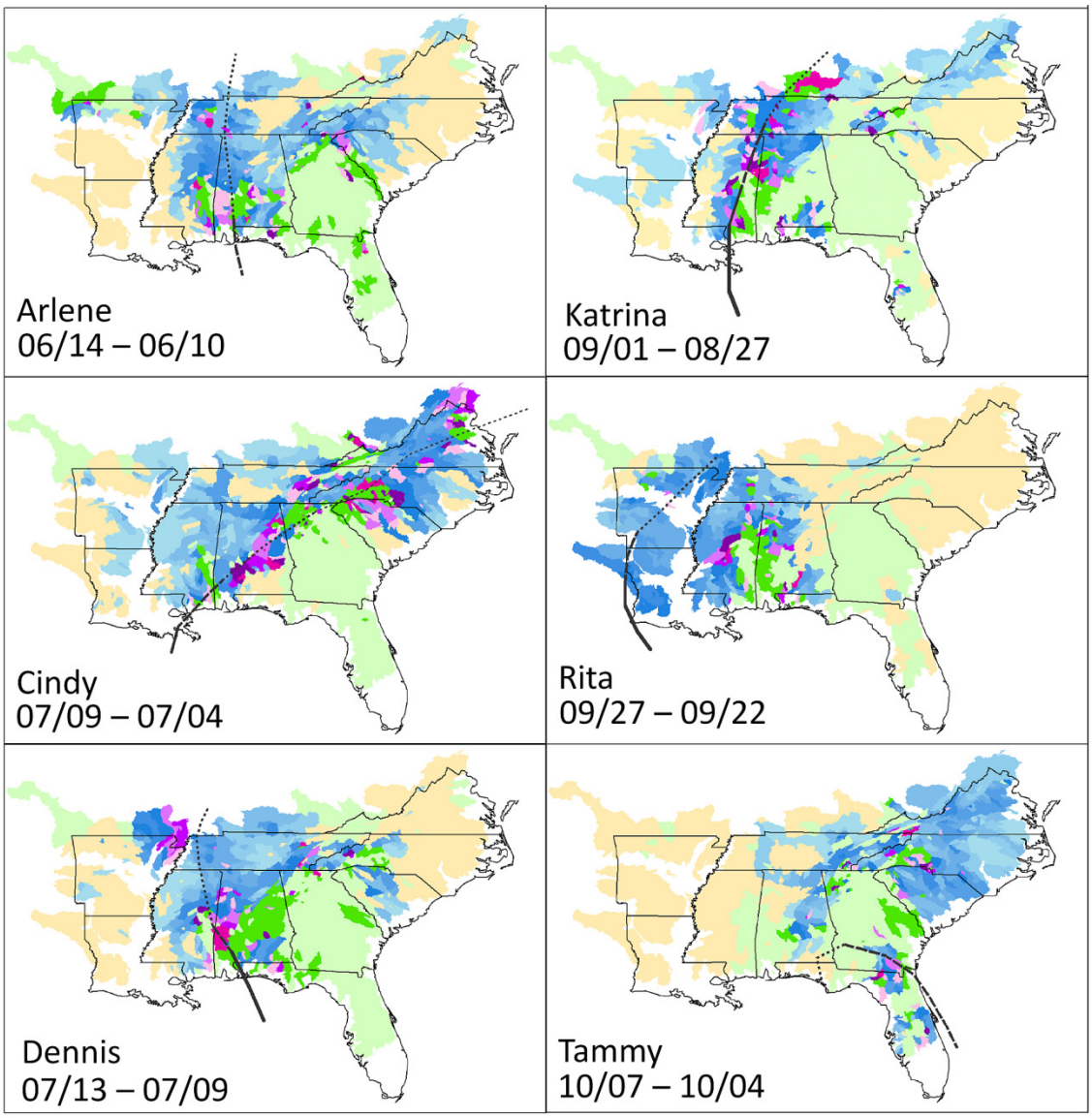

Figure 4-12: Same as Figure 9 for the year 2005.

Similar analysis conducted for 2005 is presented in Figure 4-12. The first thing to notice is that in 2005 most of the Georgia and Florida were not in meteorological drought before the beginning of the hurricane season (striped basins in Arlene's map). Quantitatively the precipitation deficit at the beginning of the 2005 hurricane season (67.2 ± 133.3 mm across the SE) was smaller, but more spatial heterogeneous than in 2004

(80.0 ± 97.4 mm). Arlene was a Tropical Cyclone at landfall and produced significant rainfall close to landfall. Cindy, presenting a track similar to Ivan in 2004 (but a less intense and smaller storm) produced rainfall over a large areal extent, including mountain watersheds. Dennis was a hurricane of category 4 at landfall but with a very small radius, and thus its major drought mitigation impact was limited to Alabama as the heavy rainfall produced by the associated cloud shield fell mostly over an area that was not in drought (cf. Figure 4-7). Katrina had a limited impact mainly constrained to a narrow along-track corridor in Tennessee, Mississippi and Alabama in spite of its size and intensity. As discussed earlier, Rita remedied the seasonal precipitation deficit by 15 to 40% over the western part of the region of study with much wider impact than Katrina. Late in the hurricane season, in October, Tammy busted the drought that was developing in southern Georgia and northern Florida since July, and by then Hurricanes Dennis, Katrina and Rita notwithstanding drought was already re-intensifying over most of Alabama. Before the first TC made landfall (June 10, 2005), watersheds in precipitation deficit covered about 79.5% of the SE area. At the end of the hurricane season, over 26.6% of the southeast region had a precipitation surplus. However, the area at the border of Mississippi and Alabama, which was impacted by all land-fallen TCs in 2005 except Tammy, was still in surplus despite general drought conditions in its surroundings.

The storm-scale analysis illustrates well the challenges in downscaling climate projections to the watershed scale, the control unit for water management decision-making. There is large spatial and temporal intermittency, and beyond and in addition

to timing, track and intensity, the specific intra-seasonal sequence of TC arrival on a watershed by watershed basis controls the effective contribution of TCs to the basin water budgets, even in favorable large scale conditions. That is, although TCs are largely regional scale phenomena, the impacts are mainly local.

4.4.4 Runoff Response

Maps of peak flow return periods and inundation (as determined by river stage levels of the National Weather Service (NWS) where available) are presented in Figure 4-13 and Figure 4-14 in the aftermath of individual TCs in 2004 and 2005, respectively. For the most part, and without including flashfloods and urban floods, the peak flows do not exceed the 2-year event, which typically corresponds to bank-full discharge for all watersheds as corroborated by a visual inspection of Figure 4-6a and Figure 4-6b. Floods with magnitude exceeding the 25-year event are restricted to landfall watersheds in Florida (Frances and Jeanne) and on the upwind slopes of the Southern Appalachians (Frances) in 2004. Despite causing various debris flows and landslides in headwater catchments (Wooten et al., 2008), Ivan floods did not exceed the magnitude of 5-10 year event for the non-urban watersheds considered here (area > 1,000 km^2). In 2005, several streamgages reached flood stage along the storm tracks, but the actual discharge is relatively moderate. These patterns correspond to floodplains with intense agricultural activity and compromised land-margins consistent with vegetation disturbances detected by Brun and Barros (2012).

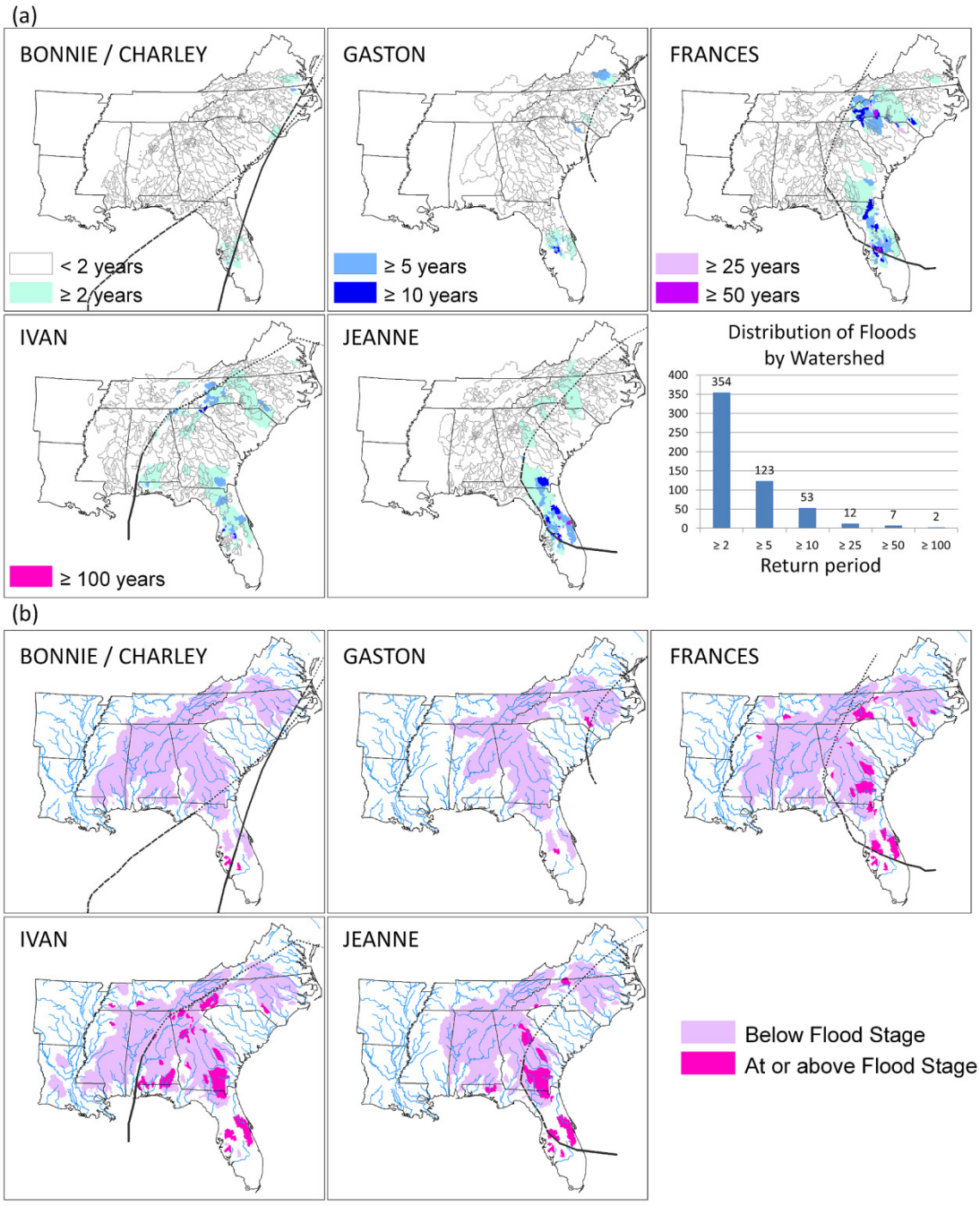

Figure 4-13: Stream flow response at the outlet of the gauged watersheds in the direct aftermath (10 days following the landfall) of major TCs during the 2004 season: (a) Return period of the observed peak flow; (b) flood stage at the watershed outlet. The withe areas correspond to watersheds either outside a 500km radius from the track or where no flood stage threshold was determined by the National Weather Service (NWS). The blue lines represent the major rivers and the thick lines the TC track.

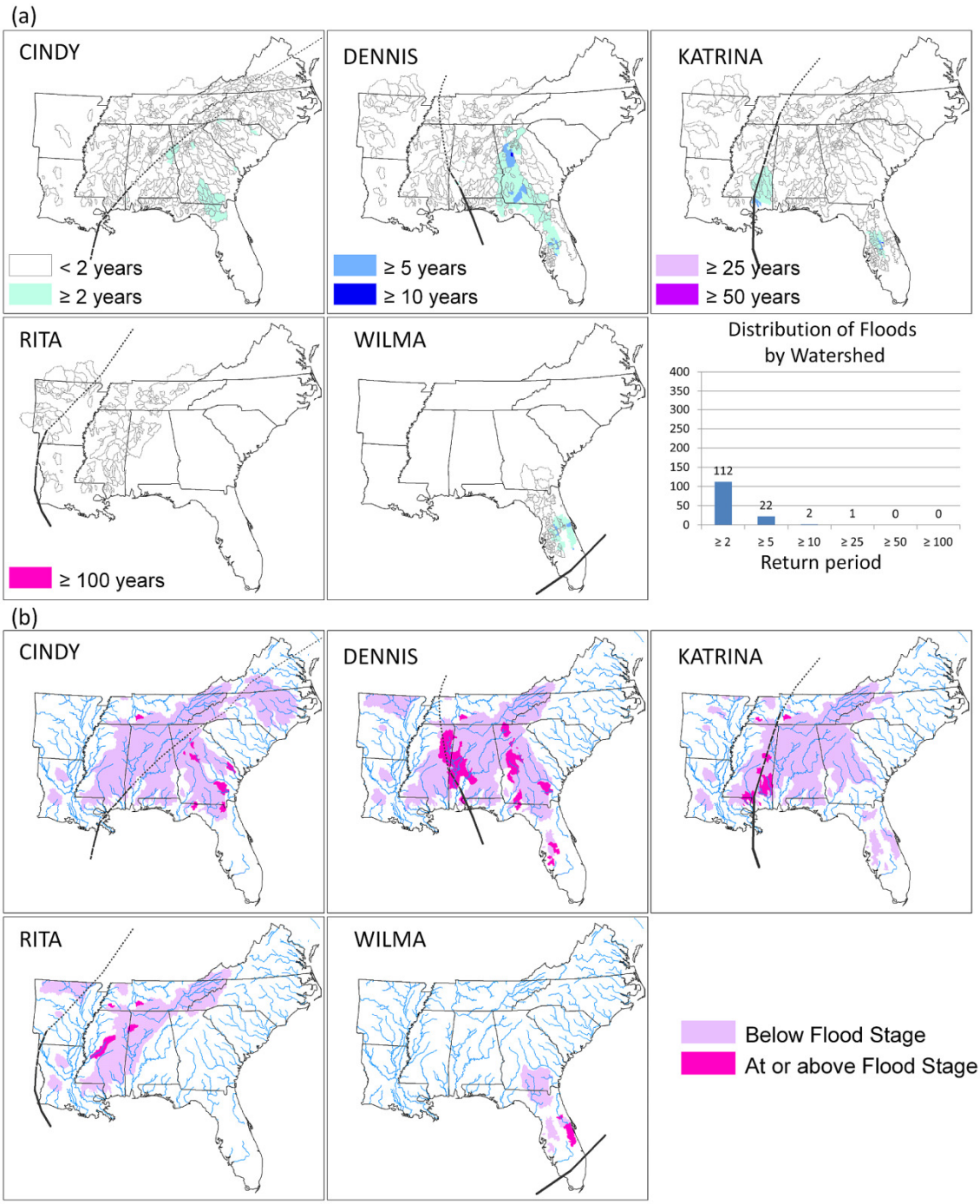

Figure 4-14: Same Figure 4-13 but for the 2005 season.

The spatial distribution of watersheds that experienced peak flow equal or larger than a 2-year event and river bank inundation match well with the watersheds in

precipitation surplus (Figure 4-11 and Figure 4-12), suggesting that flooding is more likely to take place where precipitation totals are large, and meteorological drought has been fully redressed. That is, where landscape infiltration and available storage capacities are low.

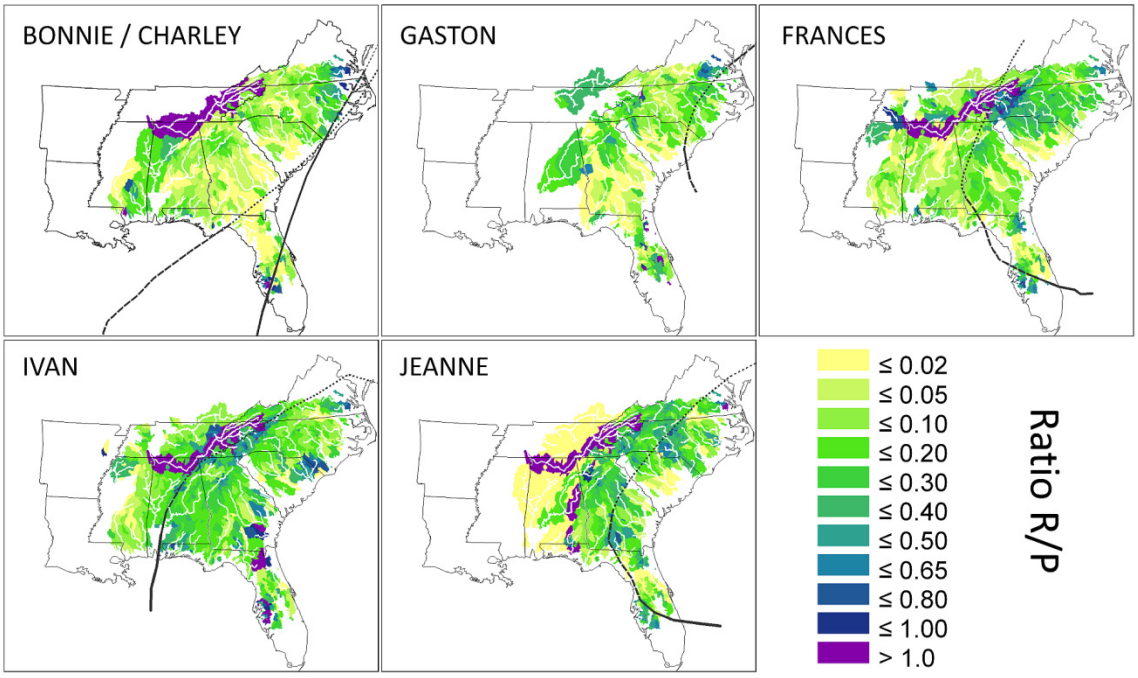

Figure 4-15: Runoff response expressed as the ratio between the total storm runoff (estimated from streamflow at the basin outlet) over total depth of storm precipitation. The black lines mark the storm track and the river network is marked by white lines. Note the difficulty with the R/P ration (R/P >1) for basins where overbank floods are observed (as marked in Figure 11b) as well as in Tennessee River dam system.

Figure 4-15 and Figure 4-16 show the maps of runoff ratios R/P for each of the major storms in 2004 and 2005 respectively. In Figure 4-15, values above 1 on the Tennessee River basin are attributed to anthropogenic streamflow regulation through the Tennessee Valley Authority (TVA) system of dams. The computed ratio is also

slightly over 1.0 for other basins where dams exist. Nevertheless, recall that the precipitation datasets used here underestimate rainfall over complex terrain, and therefore the actual runoff ratio in mountainous basins should be smaller than that estimated here. Relatively large errors in Stage IV precipitation should also be expected for low rainfall amounts and for heavy rainfall events due to measurement errors. When the total precipitation is very small, the Stage IV relative error becomes significant, leading to an unrealistic runoff ratio larger than 1.0 (but generally lower than 1.2). To address this problem, basins with precipitation depth lower than 1mm were removed from the analysis. Note that besides anthropogenic regulation, subsurface transport across basins can also explain ratios over 1.

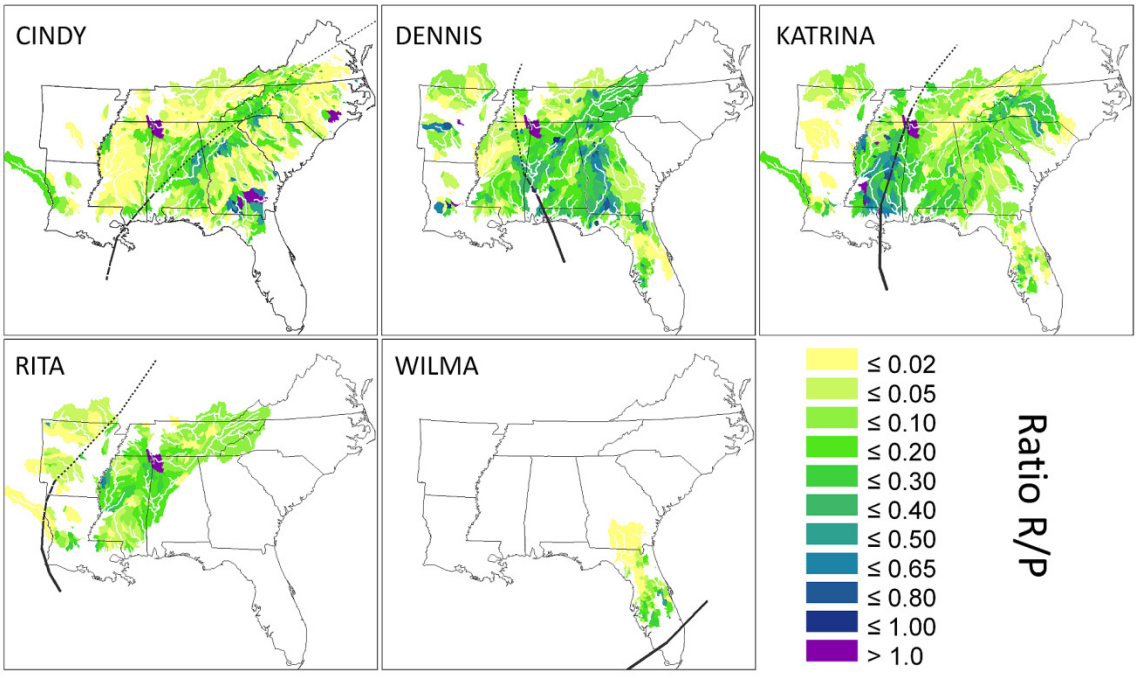

Figure 4-16: Same as Figure 4-15 but for the season 2005.

In 2004, the combined runoff response for Bonnie and Charley is depicted since Charley was entering the SE in the same day that Bonnie was exiting (Figure 4-15). Strong runoff response is aligned mostly with Charley's track, and higher runoff rations are consistent with watersheds where flood stage levels were exceeded (Figure 4-13). Charley was an intense but small storm; therefore its impact is local and intense, leading to strong rainfall-runoff response as indicated by discharge. The runoff ratio over the headwaters of the Appalachians generally shows high values consistent with regional topography and hydrogeology. Abstracting from the runoff ratios greater than one, the values in the region vary between 0.3 and 0.6 with higher values for Frances and Ivan as expected. Over the coastal plains and the Piedmont, the signals are more complex with some areas exhibiting low ratios and others high values, exhibiting a more complex hydrologic response as the topography becomes less dominant in the runoff response. In 2004 Frances, Ivan and Jeanne are the hurricanes that produced the most rainfall and generated the strongest runoff (see alsoVillarini et al., 2011). Among them, Ivan is the TC that has produced the most extensive runoff response despite the fact it is not the storm that produced the most rainfall (see Figure 4-6), or most severe flooding as noted earlier (see Figure 4-13). We hypothesize there are two main reasons to this. First, due to its track, Ivan first generated heavy precipitation over the coastal plains of Alabama, and as it moved farther inland it crossed over the Southern Appalachians twice and produced rainfall in the headwaters of streams on the east and west slopes, whereas Frances mostly affected the eastern slopes and the Piedmont. Second, Frances generated a very large amount of precipitation over most of Georgia and South Carolina 9 days before

Ivan (Figure 4-11). Therefore, saturated and wet antecedent soil moisture conditions were conducive to fast rainfall-runoff response and high runoff ratios at the time of Ivan landfall. This intra-seasonal enhancement of runoff production due to serial storm activity is also visible for Jeanne, which generated similar runoff response over the Piedmont and the Atlantic Coastal Plain as Frances despite producing less precipitation over these areas (see Figure 4-6 and Figure 4-13).

In 2005, runoff response to hurricane Dennis was generated east from the storm track (Georgia). As mentioned earlier, inspection of satellite imagery of the HURSAT database (http://www.ncdc.noaa.gov/oa/rsad/hursat/index.php) suggests that this precipitation is related to the cloud shield in front of the storm and not by its core. This area was previously hit by Cindy precipitation 5 days earlier, and thus antecedent landscape wetness played an important role in rainfall-runoff response. In contrast, Katrina generated its heaviest precipitation very close to the track with streamflow in the Mississippi alluvial plain often reaching the 90th percentile discharge for the same day in the historical records (Brun and Barros, 2012). Despite its significant contribution to drought reduction, runoff response to Rita was limited especially east of the Mississippi river valley, and no floods were recorded for the watersheds in this study. A more significant response was expected on the western side of the Mississippi, since the annual precipitation fraction was over 12% and up to 20% over this area. The fact that this area was not impacted by previous storms and that a large precipitation deficit was estimated before landfall (Figure 4-14) explains the low runoff yield. Also note the agreement between the spatial patterns of contribution to precipitation deficit reduction

(Figure 4-14) and the maximum runoff response (Figure 4-16), notwithstanding the mismatch relative to the spatial distribution of precipitation intensity (Figure 4-7). Wilma was one of the most intense hurricanes at landfall on record. However, its short path across Florida combined with the delineation failure of the flat drainage basins in south Florida limits our analysis. The numerous wetlands in this area are expected to play an important buffer role in terms of streamflow response, and could explain the moderate surface flow response.

To further characterize the spatial patterns of runoff production, cross-sections of runoff ratio data were examined across the different USGS physiographic regions for the 2004 and 2005 hurricane seasons. Specifically, Figure 4-17 shows the R/P ratio of watersheds within a 100 km of the points of intersection with the red-lined cross-sections highlighted in the inset map. In 2004, the runoff generated in the direct aftermath of Frances is stronger over the Blue Ridge region (Figure 4-17a). Despite very similar tracks, Jeanne seems to have generally produced stronger runoff response in the Piedmont than Frances, and this despite significantly less precipitation produced over this region, thus reflecting antecedent high wetness conditions later in the season. The signal in the Coastal Plains is not as clear, with Frances, Ivan and Jeanne presenting a similar distribution, Gaston's response being more moderated across all regions. However, from visual inspection of Figure 4-16 watersheds in the Coastal Plain in Georgia and North Carolina also show stronger runoff response in the aftermath of Jeanne. Note that the high R/P values generated by Ivan over Costal Plains correspond

to a specific cluster at the border of the Carolinas consistent with inland wetlands and lakes in the Pedee river basin, and thus near-surface water tables (Figure 4-16).

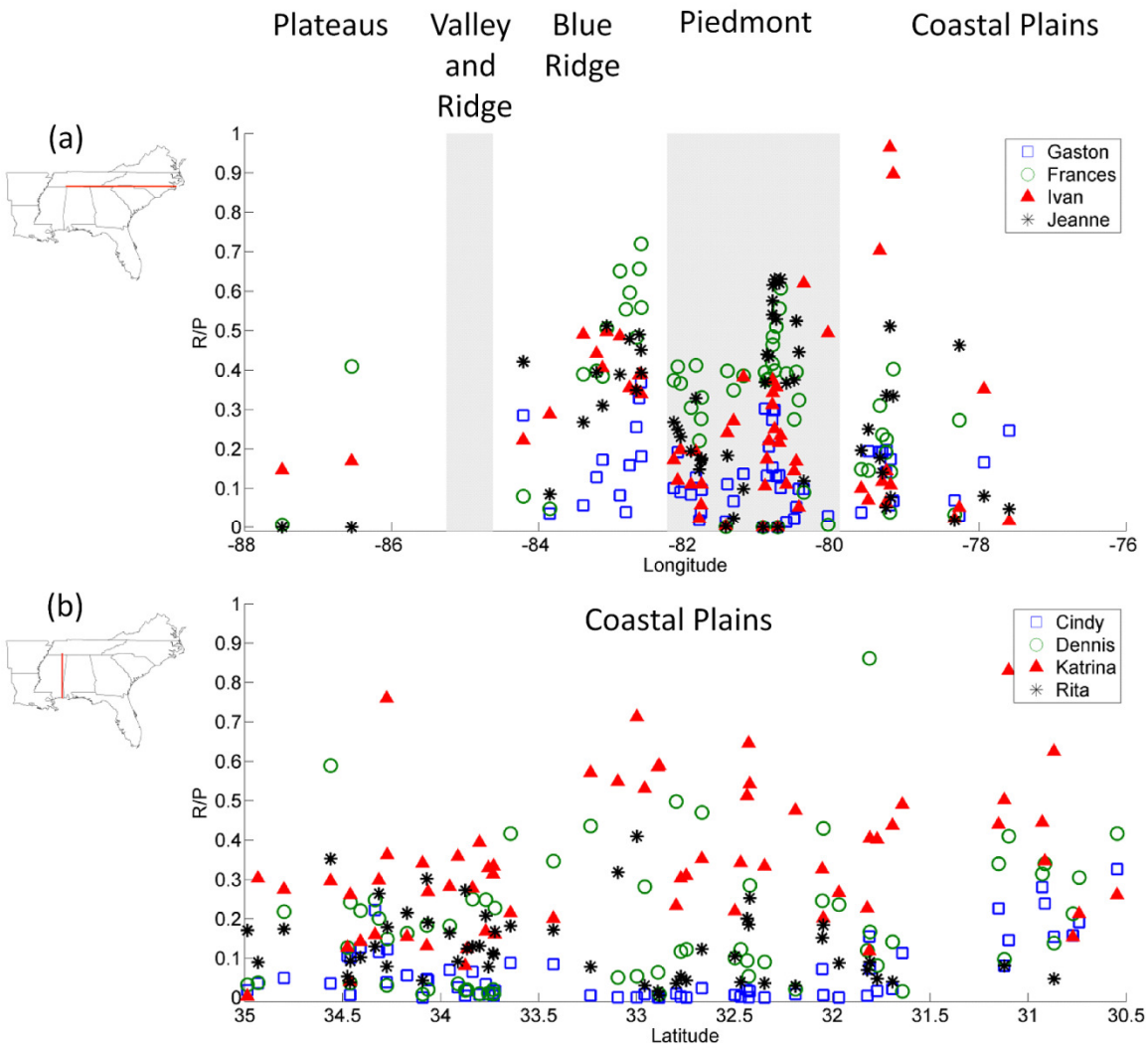

Figure 4-17: R/P ratio of watersheds intersecting 2 different cross-sections: (a) longitudinal cross-section at the south border of Tennessee and North Carolina crossing several physiographic regions; R/P in direct aftermath of major TCs during the hurricane season 2004; (b) latitudinal cross-section at the eastern border of Mississippi; R/P in direct aftermath of major TCs during the hurricane season 2005.

In 2005, due to the track geometry, the cross-section spans only the Gulf Coastal Plains, but it does cross several major river basins. Dennis and Katrina yield the larger

R/P ratios overall. Due to the rainfall produced by the TC cloud shield, Dennis produced high precipitation and strong runoff response in the Piedmont and in particular in the Atchafalaya basin which are not captured in this cross-section. Cindy generated the lowest runoff, except close to the coast. Rita's runoff response is more important in the northern part of the cross-section, but this effect is more related to its western landfall.

Overall, there is large spatial variability of runoff-rainfall response for each storm, showing the signature of timing and path in determining antecedent moisture conditions where there is landscape storage: Piedmont and Coastal Plains. In the Atlantic Coastal Plains away from the maritime fringe of lowlands and wetlands, there is significant storage as compared to the Piedmont, Blue Ridge and other Appalachian physiographic regions and thus R/P tend to remain low depending on local groundwater levels. Comparatively, the Gulf Coastal Plains show less storage capacity and therefore consistent increases of R/P values over time during the hurricane season. Thin soils and regolith explain limited low local storage capacity in the Appalachian region, which explains the higher R/P values which tend to peak around 0.5-0.7 reflecting recharge and groundwater flow into and through interconnected fractures in the bedrock system.

4.4.5 Water table height variations

In order to further examine the contribution of tropical cyclones to recharge, changes in groundwater levels that peaked within 10 days of the passage of specific storms in a radius of 500km of the storm track were extracted from the USGS data base and compared to climatology.

Figure 4-18 shows the spatial distribution of water table response in the aftermath of the 4 major hurricanes of the hurricane season 2004. The size of the circles is indicative of the magnitude of the maximum water table rise within 10 days; longer durations were not considered due to the difficulty in distinguishing the signatures of regional groundwater transport from outside the catchment from local recharge (Schaller and Fan, 2009) and the frequency of landfall during active hurricane season such as 2004. The wells have different depths and often there are three or more wells clustered together that are measuring water levels at different depths.

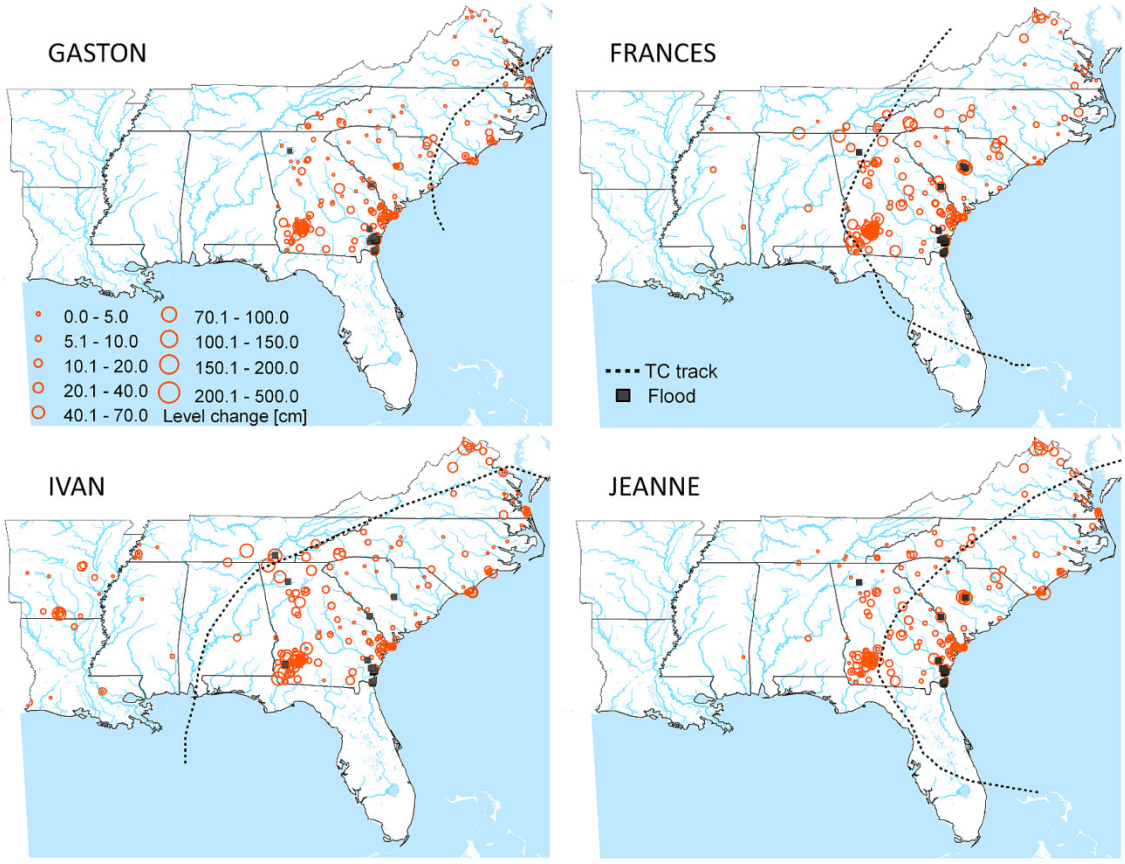

Figure 4-18: Water level changes in wells after major TCs during the 2004 hurricane season.

In 2004, the response to Gaston was weak except for shallow wells especially along the coast. However, wells along the border between the Carolinas in the Little Pee Dee River watershed show strong response even for relatively deep wells (80-100 m). The Little Pee Dee is a backwater river within a swamp area intersected by many natural lakes, and thus there is vigorous surface-subsurface exchange in the area. The strong response to local TC rainfall in contrast with small response elsewhere in the Coastal Plain is a constant feature in the Little Pee Dee as it can be seen in Figure 4-18 and Figure 4-19. Frances made landfall around one week after Gaston. Due to its track over the Appalachians, there are large increases in water table levels in the Blue Ridge and Ridge and Valley regions consistent with fast subsurface flow through fractures consistent with the regional geohydrology (e.g. Swain et al., 2004). Large response is also shown in the karst terrain of southwest Georgia, as expected. Water table levels show large increases after Ivan on the western sector of the Blue Ridge area at the border of Tennessee and North Carolina. From Figure 5, the Stage IV data suggests that Ivan may not have produced especially heavy precipitation over this area. However, model simulations by Sun and Barros (2012) show heavy rainfall in the second day of the storm passage over the region. Jeanne made landfall twenty days later. Its more Coastal track did not impact mountainous regions and the largest water table variations are located over Georgia and South Carolina. The lack of consistent wells data over Florida does not allow us to investigate impacts close to Jeanne landfall. Likewise, similar patterns can be found in 2005, not shown here due to the small number of wells in the regions most affected by the 2005 storms.

To illustrate further the relationship between recharge water table variations across different aquifers and physiographic regions, a W-E cross-section along the Tennessee and North Carolina south border was selected. Figure 4-19a-c displays the location and topography as well as wells within 100km of the cross-section. Figure 16a shows the mean topography and maximum and minimal elevations along the cross-section, and the dots represent the depth of the different wells as projected on the cross-section. Figure 16b shows that in the Valley and Ridge and Blue Ridge region the water levels in shallow and moderately deep wells increased significantly in the 10 days following Frances and Ivan landfalls. In the deeper wells, the water table rise was more moderate at least in the direct aftermath. Over the Piedmont, where Frances precipitation was heavy (Figure 4-6), the response of deeper wells is generally of the same magnitude as shallow wells everywhere, consistent with a faster recharge rate. Over the Coastal plains, the deep wells as well as shallow wells show changes in water levels despite lower precipitation depths. The sandy soils of this area facilitate infiltration and recharge. The water table variations over the Coastal Plains are of the same order as for Ivan and Frances, suggesting that the succession of heavy precipitation over this physiographic region does not seem to create a cumulative effect on infiltration capacity as long as storage is available (water table remains below the land surface). Generally, water level changes are dramatically different westward and eastward of the Blue Ridge–Piedmont transition, with large responses to the west consistent with shallow regolith and fractured bedrock (Swain et al., 2004).

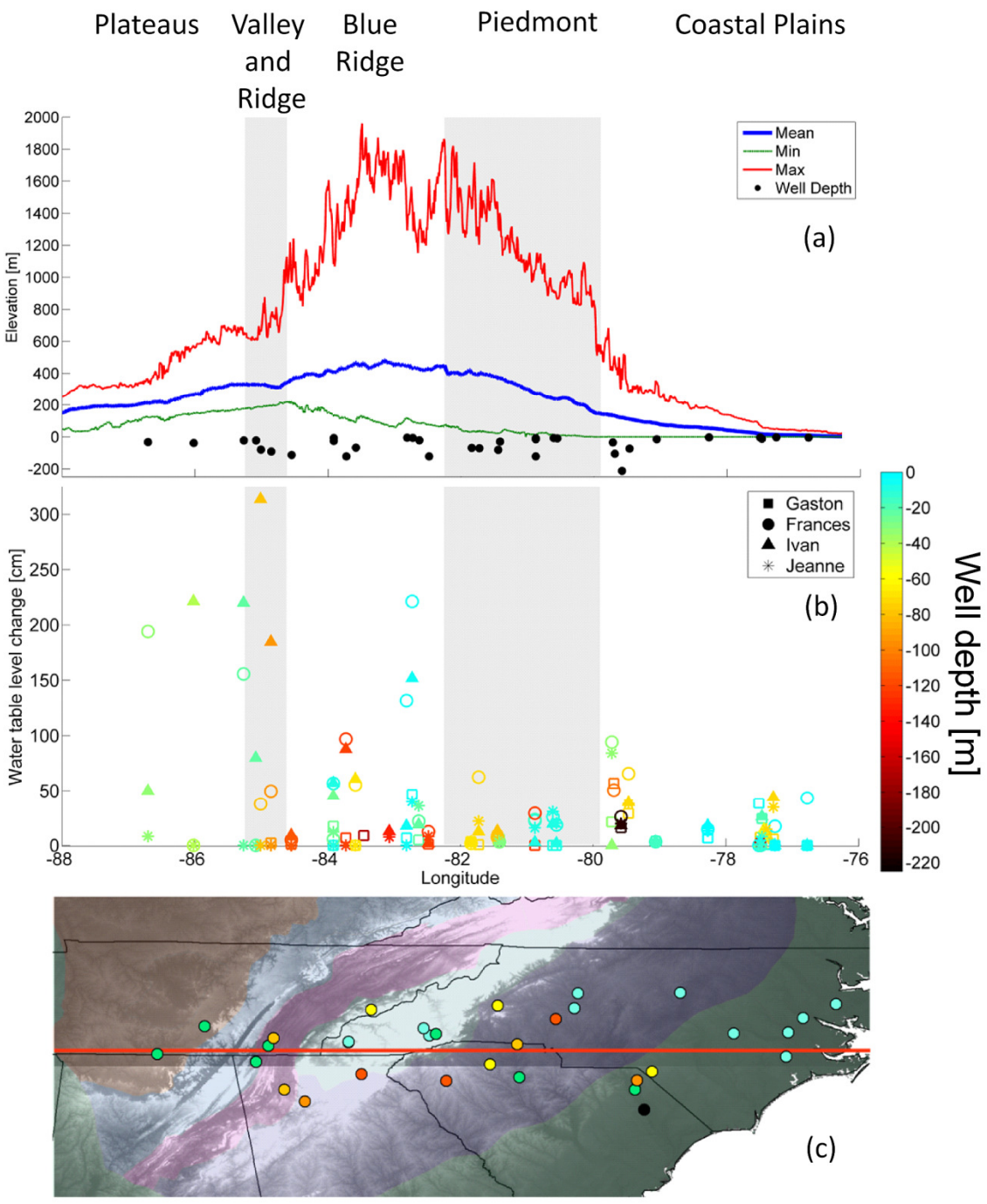

Figure 4-19: Cross-section W-E from the Appalachians to the Coastal plains. (a) Elevation and wells depth, (b) Water table level variations for the successive TCs of the hurricane season 2004. The wells were classified in different categories in respect to their depth., (c) overview of the wells (dots color-coded in respect to well depth) and cross-section locations (red line).

Appendix A.1 shows the time-series of well height for six specific wells along the same cross-section. The horizontal bars correspond to the landfall of the different TCs that passed within 500km of the cross-section. In 2004 the coastal well was more impacted by Charlie, Bonnie and Gaston. The Appalachians wells were strongly impacted by Frances and especially Ivan due to its track that passed directly over this area. The most western wells were only impacted by Ivan. The increase in water level in the aftermath of these major hurricanes is among the sharpest of the time-series with the exception of 2006 for well #3.

4.4.6 Regional Water Storage Changes

At the regional scale, the analysis of well data to interrogate the contribution of TCs to recharge is challenging due to the small number of wells, which tend to be clustered at a small number of locations, and the variations in well depth. For this purpose, we therefore rely on gridded water storage anomalies from the GRACE (Gravity Recovery and Climate Experiment) satellite to qualitatively investigate the spatial and temporal changes in terrestrial water storage at the regional scale.

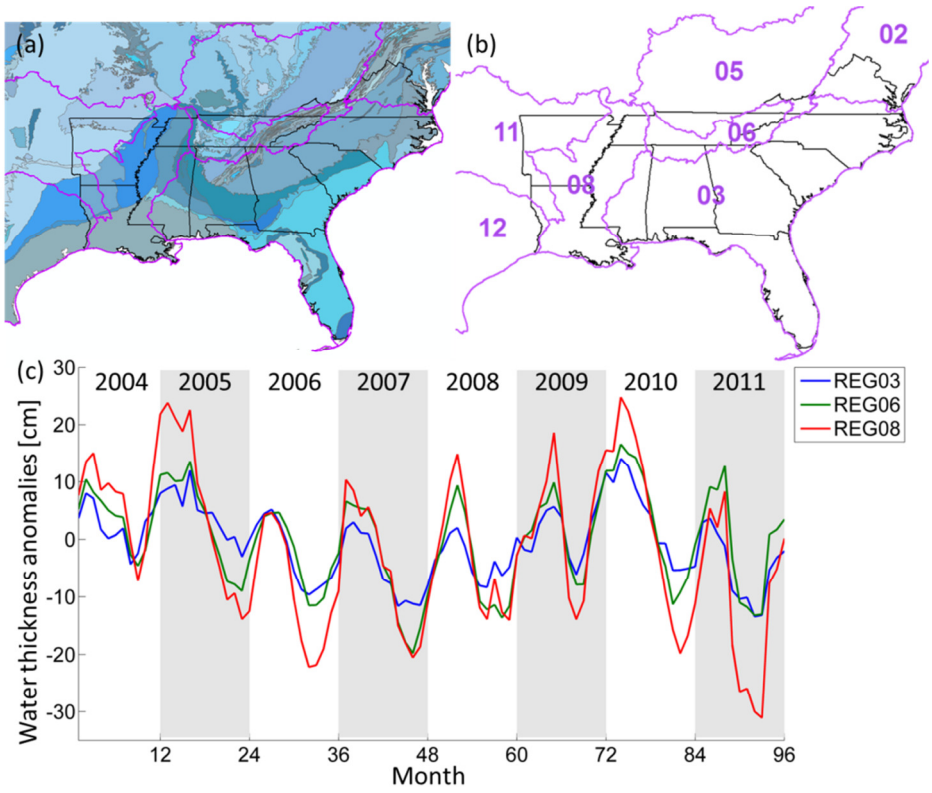

Figure 4-20: Major aquifers of the southeast US (a), hydrologic regions (03 – South Atlantic-Gulf; 06 – Tennessee, 08 – Lower Mississippi) as defined by the USGS (b), and GRACE anomalies regional average time-series from 2004 to 2011 for the major regions of the SE.

Figure 4-20 shows that the hydrological region with the largest annual variations in water storage anomalies is the Lower Mississippi (02). In the South Atlantic-Gulf region (03), the core region for this study, 2007 and 2011 are the two years with the highest deficit in water thickness equivalent at the end of the summer. 2005 and 2010 are the winters with the largest water storage. 2005 follows the highly active hurricane season 2004 and 2009 was one of the wettest years during our period of study (Figure 4-3).

The maps in Figure 4-21 display in red the areas where a deficit in water storage compared to the climatological average for the same month was observed in 2004, whereas the blue color indicates a surplus. In August there was a strong deficit over Georgia and Florida.

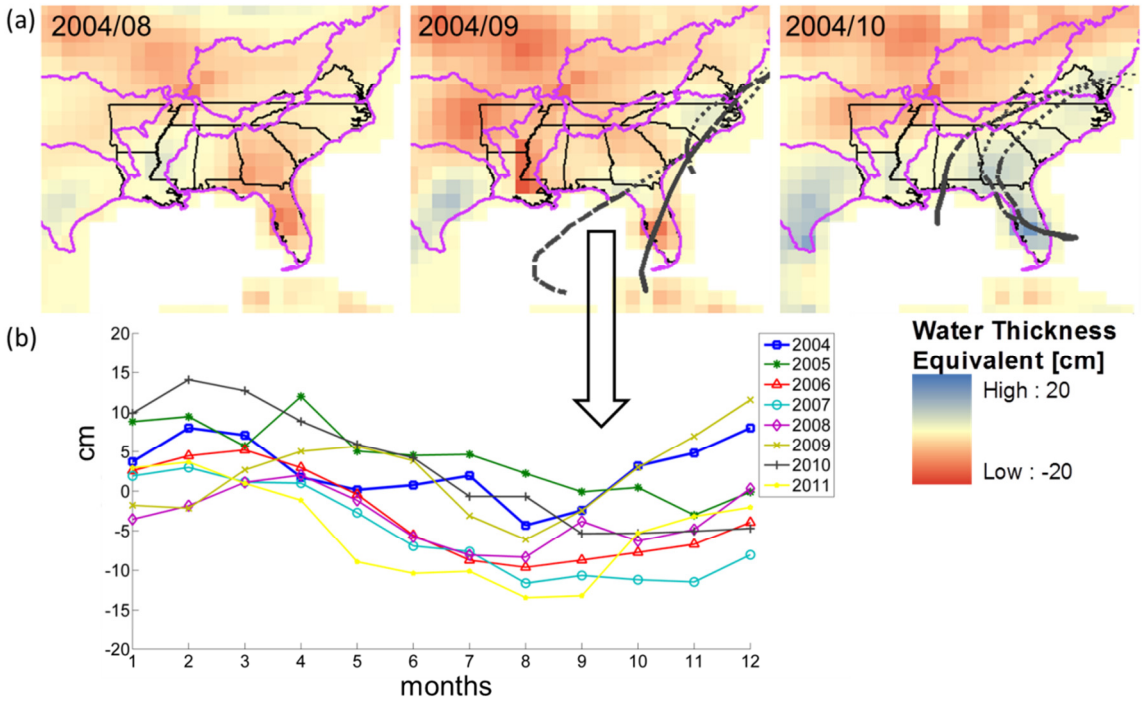

Figure 4-21: Ground water recharge anomalies change in the aftermath of TC during hurricane season 2004 (a), and corresponding regional average variation for the southeast hydrological region (b)

In September, this deficit was reduced in the aftermath of the tropical cyclones landfalling during August and early September 2004. By October, after the landfall of hurricanes Frances, Ivan and Jeanne, most of the SE was in surplus. The 2004 precipitation deficit before the hurricane season in the South-Atlantic-Gulf region was redressed therefore over a short period of time in the late hurricane season. Note that the temporal evolution of water storage in 2009, which was a wet year with low TC

activity, is similar to 2004 in the second part of the year suggesting that non tropical late precipitation can produce a similar recharge response to reduced drought leading to the largest wintertime water storage in the wintertime of our period of study.

Appendix A.2 shows the monthly average change in the wells water level along the cross-section used in Figure 4-18 for the different years. Over the Coastal plains, the well #1 shows an increase in water level starting in August in accordance to GRACE following Bonnie Charley and Gaston. For well #4 and #6, that are close from each other – the sharp increase starting September 2004 following the series of major hurricanes is very different from the other years. The response of that last well of the cluster (well #5) seems to be slower and is still increasing in October. The monthly variations of the most western wells do not show specific changes, suggesting a rapid decrease of water level certainly due to groundwater flow movement. Appendix A.3 shows similar monthly average in the wells water level for a cluster of wells with different depth located on the Coastal plains of Georgia. The response at the different depth show similar variations in time, suggesting an homogenous recharge. In 2004, the groundwater level is decreasing during the month of August (except for well #1) followed by an increase starting September related to the high precipitation produced by the major hurricanes of the season. Note that for wells #2,3,4,5, the groundwater levels are among the highest of the 10 years observation. This suggests that the recharge following the hurricane season 2004 was consequent over this part of the Coastal plains.

4.4.7 Vegetation response

To examine if this increase in water storage in late 2004 translated to vegetation activity, the MVDP averages at the watershed scale has been computed (Figure 4-22). Comparing the average MVDP patterns with the annual depth of precipitation and precipitation deficit (Figure 4-3 and Figure 4-10) suggests that at the watershed scale the drought signal is dominant. This is due to the fact that drought signal in the MVDP, although less persistent than strong disturbance such as wind damage, is more widespread combined with the fact that the drainage areas upstream of coastal streamgages are generally large, thus smoothing the coastal disturbance signal close to landfall. The strong drought signal present over Alabama matches the area where the precipitation deficit of 2004 was not closed by TC precipitation, suggesting that TCs acted as drought busters elsewhere during 2004. In 2005, the watersheds located near Katrina's landfall have an average MVDP of 16 and more, although the 2006 accumulated precipitation over this area is not particularly low, suggesting an extensive disturbance in the forested area related to mechanical damages due to Katrina's strong winds and storm surge.

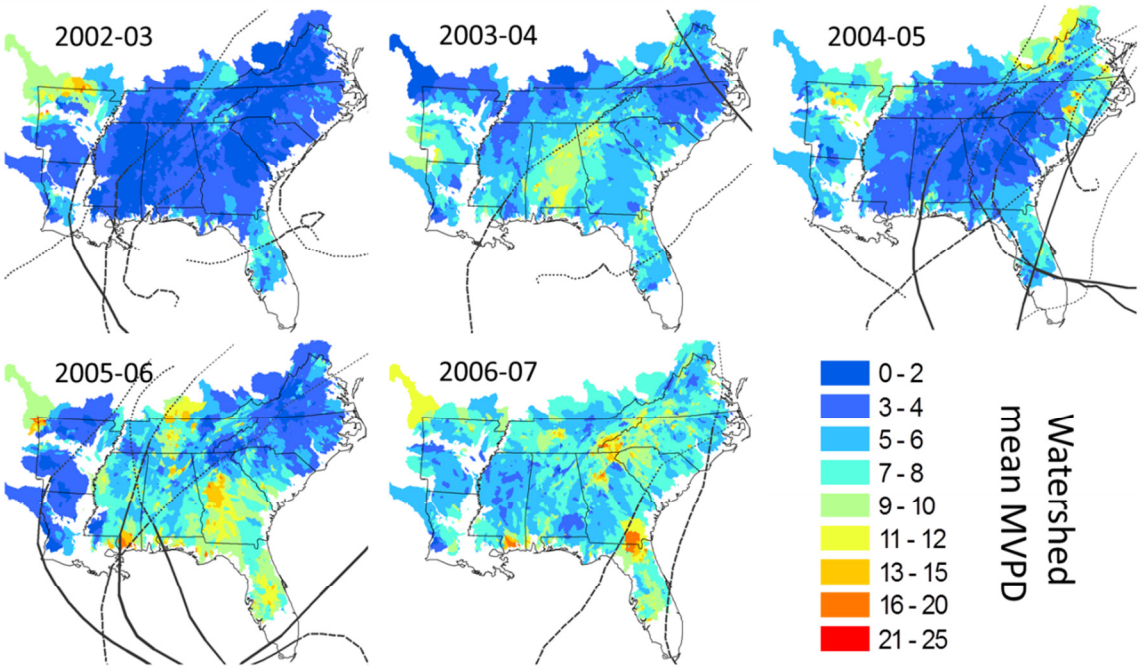

Figure 4-22: MVDP average per watershed. The black lines represent TC tracks for the first calendar year of MVDP water year accumulation.

4.5 Discussion

Regarding the contribution of TCs to the annual precipitation and its distribution across at the drainage basins, the overland path and landfall locations seem to be the most determining factors in regards to total rainfall produced by a TC over the entire SE than the intensity of the storm. Since the total rainfall of the tropical cyclone has been shown to be highly related to the precipitation associated with the inner core (Cerveny and Newman, 2000) and that maximum surface wind classes can explain 94% of the total variance in precipitation, another storm characteristic that can play an important role in the precipitation totals is the size of the TC. In 2004 and 2005, there were 2 major hurricanes with a very limited spatial extent: Charley in 2004 and Dennis in 2005. In the

case of Dennis, despite its small size, the cloud shield preceding the system did produce important precipitation further east from landfall.

Our analysis shows that the hurricane season can bring precipitation totals up to 65% at the basin scale (in 2004) and frequently goes to 30% close to the TC tracks. This fraction is larger from what have been found previously with TCs contribution to annuals precipitation was generally accounted for 4 to 15% in the SE US (Konrad, 2001, Rodgers et al., 2001, Knight and Davis, 2009, Konrad and Perry, 2010, Maxwell et al., 2012, Prat and Nelson, 2012). The peak contribution of TC to precipitation annual totals is during the month of September past the mid-point of the hurricane season (Nogueira and Keim, 2011, Prat and Nelson, 2012). During our period of study (2002-2011), September was effectively the month with the strongest TC activity and precipitation totals; 2004 with 3 major hurricanes (France, Ivan and Jeanne) as the extreme case.

The precipitation deficit analysis shows the large precipitation deficits at the beginning of the 2004 and 2005 hurricane seasons were redressed by TC activity. In 2002 and 2008, the contribution of TCs in reducing the deficit was also significant, despite the reduced number of storms. Slow moving Tropical Storm Fay in 2008 was a drought buster over Florida and South Georgia. In 2006, 2007 and 2010, the contribution of TC was more moderate and these years were also the driest of our period of study. Indeed, the 2007 drought was carried over from 2006 till 2008, in which constituted a multi-year regional drought in the Atlantic States. This highlights the relationship between late summer/early fall TC activity and drought severity, and drought extension.

Complex topography is the dominant factor for runoff generation where TC precipitation is enhanced by orographic effects. Over the Piedmont and the Coastal Plains, the recharge is dominant and more heterogeneity in rainfall-runoff response is observed since the recharge processes are function of land cover, soil composition and geology (Wolock et al., 2004). Generally, the observed runoff partitioning at regional scale is consistent with previous single basin studies suggesting that surface runoff generated by TC is due to strong precipitation and antecedent soil moisture conditions (Sturdevant-Rees et al., 2001). For the series of hurricanes in 2004, especially over the Coastal Plains, there is an increase in the runoff ratio for the later storms (Ivan and Jeanne), although the precipitation totals were lower than Frances. The rainfall apportionment over the Southern Appalachians, with an R/P ratio close to 1, also suggests potential underestimation of precipitation totals from Stage IV over mountainous areas where the raingauge network is sparse. Note that the focus on daily and longer time-scales in hydroclimatic studies puts aside important TC impacts more directly associated with rainfall intensity such as flashfloods, debris flows, and landslides.

GRACE regional spatio-temporal patterns show a consequent recharge of terrestrial reservoir over the Coastal Plains following the 2004 hurricane season. The wells time-series analysis also shows increase in water table starting in August over the coastal plains and in September with sharp response over mountainous region Appendix A.4 shows the location of the major dams and lake across or area of interest. Over the coastal plains the dams are generally scarce, except over South Carolina, and of

moderate reservoir capacity. Also few major lakes are present This combined with the wells time-series analysis suggest that the changes observed in terrestrial water storage are s linked to groundwater reservoir changes and not only changes in surface reservoir and vegetation water content. Over South Carolina and South Florida, the presence of lake and numerous dams make it is more challenging to relate terrestrial water storage variations in the aftermath of TCs to groundwater recharge.

The strong precipitation deficit at the beginning of the hurricane season translated into vegetation stress as suggested by the high MVDP values over Alabama that persisted into the winter because the precipitation deficit was not redressed in the region. By contrast, TC precipitation participated in relieving drought conditions over a large portion of the SE in 2004.

4.6 Conclusion

In summary, first we relied on gauged watersheds as defined by the USGS to investigate the contribution of TCs to the annual precipitation totals over the Southeast US at the seasonal and storm scales during the 2002-2011 period. Second, using these gauged watersheds, we examined the role of TC precipitation in meteorological drought mitigation on a watershed by watershed basis over a wide range of scales. Third, we studied the environmental response to TC precipitation in terms of generated runoff and recharge across the different physiographic regions. The main conclusions of this study are:

- At the drainage basin scale, TC precipitation during the hurricane season can reach as high as 65 % of the annual total of specific watersheds.
- 2004 is clearly the year with the highest relative and quantitative amount of precipitation produced by TCs. Despite a very active hurricane season, precipitation totals were much lower in 2005. These differences are explained by the Atlantic versus Gulf alignments of the storm trajectories. Orographic effects have been shown to enhance greatly the precipitation totals when TC tracks are aligned closely with or cross over the Appalachians.
- In our period of study (2002-2011), Frances in 2004 was the hurricane which produced the highest amount of precipitation producing up to 20% of the annual totals over coastal and mountain basins. Similarly high annual precipitation fractions were reached for Jeanne (2004), Katrina and Rita (2005) over limited areas. Note that, in the case of Katrina, the maxima were reached over Tennessee, and not close to the landfall as for the other two.
- The large precipitation deficit existing at the beginning of the 2004 and 2005 hurricane seasons was entirely redressed by the end of the season. In 2002 and 2008, the contribution of TCs in reducing the deficit was also significant.
- There is a strong gradient in the runoff partitioning of precipitation across the different physiographic regions with the surface runoff being dominant in the mountains and the recharge to the groundwater system being dominant in Piedmont and Coastal Plains. Nevertheless, as the topographic gradients fade toward the coast, the signal becomes more disparate suggesting that other eco-

physiological parameters such as land cover, soil properties and geomorphology play a central role in rainfall-runoff processes integrated by the runoff fraction metric.

- Serial storms enhance runoff response, especially in basins where meteorological drought was redressed by earlier storm activity, highlighting the role of antecedent moisture conditions in rainfall-runoff processes, and consequently in the partition of TC precipitation between the surface and the groundwater system.
- The highly active hurricane season 2004 participated in relieving drought conditions. GRACE and well time-series suggest a consequent recharge of terrestrial water reservoir at the regional scale, with local groundwater response among the sharpest between August and October during our period of observation.

The frequency and intensity of Tropical Cyclone (TCs) landfall are tightly linked to the hydroclimatology of the SE United States. Despite their destructive potential associated with wind damage, flooding, landslides and debris flows, TCs are an important source of freshwater that plays an essential role in regulating regional drought. Therefore changes in frequency, seasonal timing and intensity of TCs in the future are expected to strongly impact the regional water cycle, and in particular water resources. Here, we focused on characterizing the contribution of TCs to the water budget, flood response and drought mitigation of 3,211 watersheds over the SE US over the last decade (2002-2011). The objective is to understand the range of spatial and

temporal variability of regional hydroclimatology that can be attributed to TCs for current climate, which can subsequently be used as a baseline toward mapping regional vulnerabilities to projected climate change at the basin scale. This work documents strong spatial and inter-annual variability in the annual cycle of precipitation that can be attributed to TCs ranging from below 5% everywhere in 2011 to values as high as 65% in the highly active seasons of 2004 and 2005, with a regional-scale range of 15-40%. The data indicate that, with average return periods of (1-3 years), the frequency and timing of landfalling TCs is the key agent of warm-season drought demise in the SE. Intense multi-year droughts develop in dry years with weak frontal and convective system activity that also see weak TC activity in the warm season (e.g. 2006-2007-2008-2010). Away from the coastal zone, the flood response and drought mitigation impacts of TCs are stronger for storms with terrestrial tracks predominantly on the Atlantic region and, or aligned with the Appalachian Mountains where orographic effects are evident in precipitation amounts, runoff ratios and groundwater recharge. Regarding the runoff partitioning of precipitation across the different physiographic regions, a west-east gradient is observed with the surface runoff being dominant in the Blue Ridge and adjacent regions in the Piedmont. As expected, the river response to TC rainfall tends to increase over time during the hurricane season when inter-storm arrivals are very close (< two weeks), but the effect of increased antecedent precipitation decreasing available soil moisture storage capacity as the summer progresses, and is stronger in the Piedmont and Coastal Plain peaking past mid-point of the hurricane season. Away from the Coastal Plain, the maximum runoff-rainfall ratios do not exceed the 0.6-0.7

range independently of initial soil moisture conditions consistent with regional hydrogeology controls of recharge. The association between TC activity and drought mitigation is reflected in the hydroclimatology of flood response in the continental SE US, although river stages tend to be in the 90 percentile of the historical record, they remain below flood stage and flood peaks rarely exceed the 5-year flood magnitude for watersheds away from landfall, generally remaining below the magnitude of the 2-year bank-full event.

5 Impact of tropical cyclones precipitation on the SE US gross primary productivity (GPP)

Tropical Cyclones not only influence the water cycle through precipitation, they also modulate the response of the environment to future events through vegetation changes (wind damage, storm surge, floods or erosion), consequently modifying the land cover. Effectively, previous studies have indicated that TCs, along with drought and fires, are the main causes of GPP inter-annual variability in the US (Mackay et al., 2003).

In this part of the study, the Land Surface Eco-Hydrological Model (LEHM), a coupled hydrology-dynamic vegetation model (Garcia-Quijano and Barros, 2005) that has been proven to work well across different biomes and climatic regions (Gebremichael and Barros, 2006), is used to investigate the changes in vegetation productivity related to TC precipitation in the South Eastern United States and study the processes that lead to changes in the vegetation activity at inter-annual, annual, and seasonal scales. First the model is evaluated against data from Ameriflux towers in the SE US to assess the model's ability to capture the energy, water, and carbon cycles for different biomes. Next, a dynamic phenology parameterization is introduced and the model simulated phenology is evaluated against satellite-based MODIS (Moderate Resolution Imaging Spectroradiometer) products, which provide a further opportunity to assess the consistency among physical and biophysical processes in the mode. Finally, a 10 year regional model run of GPP (used as a proxy measure of ecohydrological

impacts) using normal atmospheric forcing will be compared with a similar run in which the atmospheric forcing has been replaced by same-day climatology during each TC path over the region of study. Precipitation produced by each TC is removed from the forcing as well as radiation and wind.

5.1 Background

Terrestrial gross primary productivity (GPP) is the total photosynthetic uptake or carbon assimilation by plants (net ecosystem exchange of CO_2 – ecosystem respiration) and is a key component of terrestrial carbon balance and a link between the hydrological and carbon cycles. A proper representation of the hydrological cycle and its link to the energy cycle and to biogeochemical processes including the carbon cycle is therefore necessary to describe quantitatively soil–vegetation–atmosphere (SVAT) interactions. At any given place, GPP depends on climate, climate variability, disturbance history, water and nutrient availability, soil type, species composition, and community structure. Understanding how these factors interact and influence GPP remains a challenge due to complex feedbacks and the difficulty in quantitatively measuring GPP directly at various temporal and spatial scales (Beer et al., 2010; Schaefer et al., 2012). Estimates of GPP have only become available at eddy covariance flux tower sites for the past decade, so we depend on models to estimate GPP over long periods of time at regional and global scales.

GPP models can be classified in two main categories: enzyme-kinetic (also called biochemical) and light-use efficiency (LUE). The biochemical models represent leaf-scale

enzyme-kinetics where the CO_2 assimilation is a function of the carboxylation and oxygenation velocities, photosynthetic electron transport and dark respiration. Numerous model schemes in this category (e.g. Friend, 1995; Friend and Kiang, 2005; Harley and Sharkey, 1991; Leuning, 1995; Sellers et al., 1986) are based on variations of the photosynthesis model proposed by Farquhar et al. (Farquhar et al., 1980). In this representation, the photosynthesis rate is typically taken as the lowest among the rates calculated for each of the main photosynthetic factors (i.e., Rubisco carboxylation and Ribulose-1,5 biphosphate (RuBP) regeneration rates). The limitation of this approach is that often the moisture availability controls in the atmosphere (water vapor pressure) and soil (soil water content) are not explicitly taken into account. Another limitation is that several parameters such as nitrogen content of the plant are necessary for this parameterization (Kattge et al., 2011), and the dependence of kinetic parameters on temperature is still not fully understood (Medlyn et al., 2002). Most stomatal conductance models are based on empirical correlations between conductance, photosynthesis, and either relative humidity or vapor pressure deficit (VPD). Although recent work demonstrated that analytical modeling of stomatal optimization is apt to simulate field-scale conditions (e.g. Katul et al., 2010; Manzoni et al., 2011), this approach has not been yet implemented in ecological models. In the other category of GPP models, LUE models, such as that used to generate the MODIS product used here (see section 5.4.2 for more details), estimate either GPP or net primary productivity (NPP) by multiplying incident photosynthetically active radiation (PAR) by a remotely sensed fraction of PAR absorbed by the vegetation (FPAR) and an energy to biomass conversion

parameter, typically referred to as the light use efficiency (e.g. Prince and Goward, 1995; Xiao et al., 2010; Yuan et al., 2007; Zhao et al., 2005). The effects of soil water stress are generally not included explicitly, leading to potential overestimation of carbon assimilation when soil moisture is below the level necessary to reach potential assimilation rates.

Schafer et al. (2012) conducted an extensive comparison of 26 models against estimated GPP at 39 eddy covariance flux towers across the United States and Canada. On average, models overestimate GPP in winter, spring, and fall, and underestimate GPP in summer. Models overpredicted GPP under dry conditions and for temperatures below 0 °C. They did not find any statistically significant differences in performance due to model structure (i.e. enzymatic versus light use efficiency), mainly due to the large spread in performance among models and across sites. Schafer et al. concluded that the poor overall model performance resulted primarily from inadequate representation of actual LUE. The LUE simulated in models is controlled by the leaf-to-canopy scaling strategy and a small set of model parameters that define the maximum potential GPP, both of which carry potential shortcomings due to heterogeneity of land-cover, soils, and micro to meso-climate.

Traditional physically based hydrological models represent vegetation controls of transpiration either in terms of one bulk stomatal resistance, or using a series of resistances from the root system to the leaves, where each resistance is described by a semi-empirical function based on field data or remote sensing observations. Thus, the biological control of evapotranspiration (ET) is passive and depends entirely on physical

variables, neglecting feedbacks involving photosynthesis, soil moisture and transpiration. Even when the temporal evolution of vegetation parameters is taken into consideration via data assimilation of remote-sensing products, the interaction between soil and vegetation in the models is unidirectional: vegetation changes affect soil moisture dynamics via evapotranspiration, and the surface energy balance via albedo and surface roughness changes, but soil moisture does not affect photosynthesis, and therefore primary productivity (Yildiz and Barros, 2005).

5.2 Land Eco-Hydrology model (LEHM)

Note: The description of the hydrological and energetic modules of the model is based on Devonec (2002). The coupled photosynthesis module is described in detail by Garcia-Quijano and Barros (2005). Here a brief overview is provided.

A one-dimensional land surface model, originally developed by Barros (1995) and later modified by Devonec and Barros (2002) to incorporate snowpack simulation, was coupled to a photosynthesis activity leaf model to incorporate canopy physiological processes to the hydrological model (Garcia-Quijano and Barros, 2005)and estimate gross primary production (Gebremichael and Barros, 2006). The land surface model consists of three major elements: an energy balance module, a water balance module (including snow), and a photosynthesis activity module. The conceptual model consists of an atmospheric boundary layer and a soil column, which can be discretized into any number of layers depending on the availability of ancillary data (Figure 5-1). A thin superficial layer (4-10 cm) functions as the interface between the ground and the atmosphere. The deeper soil layers store water and energy. The surface of the soil column can be subdivided into vegetated and bare soil areas, both of which can be covered by snow in winter. A detailed description of the model is presented next.

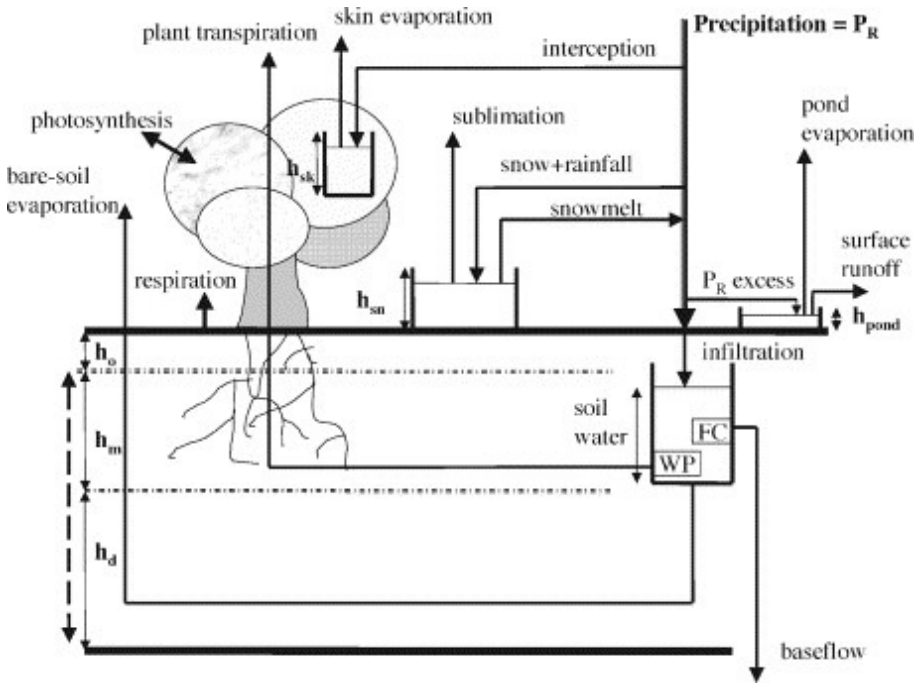

Figure 5-1: Conceptual depiction of essential water fluxes and reservoirs in the land surface hydrology model (LSHM) [from Devonec and Barros, 2002]

5.2.1 Energy balance

The surface energy balance is defined by:

$$C * h_o \frac{\partial T_o}{\partial t} = F_R + S_h + L_h + G_h \qquad (5.1)$$

in which the left-hand term represents the change in heat storage in the superficial soil layer, F_R is the total radiative flux comprising net shortwave and longwave radiation, S_h is the sensible heat flux, L_h is the latent heat flux, and G_h is the ground heat flux calculated as follows:

$$G_h = -C * h_d \frac{\partial T_d}{\partial t} \qquad (5.2)$$

where C* is the volumetric heat capacity of the soil surface, h_o and h_d are respectively the thickness of the superficial and deep soil layers, while T_d and T_o are the temperatures of

the deep and superficial soil layers respectively. C* is corrected in the presence of a snow cover as follows:

$$C^* = (1 - C_{sn})C + C_{sn}C_i \tag{5.3}$$

where C is the heat capacity of the soil, C_i is the heat capacity of ice, and C_{sn} is the areal extent of the snow cover.

The total radiative flux F_R consists of the contribution of net solar shortwave radiation F_s, outgoing longwave radiation emitted by the Earth's surface F_{lo}, and the contribution of incoming longwave radiation F_{li} originates by clouds, aerosols and greenhouse gases, and thus it is written as:

$$F_R = F_s + F_{li} + F_{lo} \tag{5.4}$$

The net solar radiation flux is equal to the downward incoming flux F_{si} minus the reflected fraction:

$$F_s = (1 - a_g)F_{si} \tag{5.5}$$

in which a_g is the effective land surface albedo red from forcing data.

The longwave radiation is determined based on the Stefan-Boltzmann radiative law for a gray body:

$$F_l = F_{li} - F_{lo} = \sigma(\varepsilon_a T_a^4 - \varepsilon_g T_o^4) \tag{5.7}$$

where ε_a and ε_g are the emissivities of the atmosphere and the ground surface; T_a and T_o are the air and ground temperatures (^oK), respectively; and σ is the Stefan-Boltzmann constant ($WK^{-4}m^{-2}$).

The sensible and latent heat fluxes (i.e., S_h and L_h) are estimated based on the Monin-Obukhov similarity theory which has primary assumptions of homogeneity and quasi stationarity of the horizontal flow field, and independence of turbulent fluxes from the height of the surface layer (Brutsaert, 1982; Arya, 1988). The theory provides dimensionless variables expressing the buoyancy effects resulting from the vertical

density gradients in the stable atmosphere. If the molecular boundary layer is neglected, the sensible and latent heat fluxes can be expressed as follows:

$$S_h = C_p \rho_a C_H |U_1| (T_1 - T_o) \tag{5.8}$$

$$L_h = L_v \rho_a C_W |U_1| (q_1 - q_{sat}) \tag{5.9}$$

where the subscript 1 shows a reference height in the boundary layer at which the horizontal wind U_1, the temperature T_1, and specific humidity q_1 are known (i.e., measured) and precise physical meaning. T_o is the ground surface temperature, q_{sat} is the saturated vapor pressure at the ground surface, ρ_a is the density of the air, C_p is the heat capacity of the air at constant pressure, L_v is the latent heat for water vaporization, and C_H and C_W are the heat and water aerodynamic drag coefficients for heat transfer, which are estimated following the approach of Louis (1979) given as:

$$C_H = a \left\{ 1 - \left[\frac{bR_i}{1 + cR_i^{1/2}} \right] \right\} \tag{5.10}$$

with:

$$a = \frac{k^2}{\left[\ln \left[\frac{z}{z_r} \right] \right]^2} \tag{5.11}$$

in which z is the roughness height, z_r is the reference height, $R_i(z)$ is the bulk Richardson number, and b and c are coefficients depending on stability conditions.

Equation (5.9) applies only to surfaces for which evapotranspiration takes places at its potential rate. Over the continental areas, evapotranspiration generally occurs at much slower rates due to resistances of soil, vegetation, and snow cover. Therefore, correction factors are applied to the equation in order to convert the potential estimates of latent heat fluxes to actual values. At saturation, the specific humidity is calculated by using the equation derived by Raudkivi (1979):

$$q_{sat}(T_o, P_o) = \frac{P_b}{P_o} \exp\left(\frac{17.67 T_o}{T_o + 243.5} \right) \tag{5.12}$$

where the ground surface temperature is in degrees centigrade ($-35^oC<T_o<35^oC$), P_b is a constant that is assigned the value $P_b=0.622*e_{sat}(T=0^oC)=0.622*6.11=366.72$ Pa, and P_o is the surface pressure.

As suggested by Marth and Sun (1995), a "subgrid velocity scale" is added to the average wind velocity in order to account for subgrid mesoscale motions generating turbulent fluxes. The measured velocity profile, therefore, corrected by the addition of the subgrid velocity scale term V_{sg}:

$$U = U_1 + V_{sg} \tag{5.13}$$

with:

$$V_{sg} = C\left(\frac{g}{T_o} \Delta T \Delta x \right)^{1/2} \tag{5.14}$$

where g is the gravity acceleration constant (9.8 ms^{-2}), T_o is the surface temperature, ΔT is a measure of the variation of surface temperature, Δx is the grid size, and C is a function of the wind speed U_1 expressed by:

$$C = C(0)\exp\left(-\frac{U_1}{U_{crit}} \right) \tag{5.15}$$

in which the constants are estimated as: C(0)=0.015, and U_{crit}=3.9 ms^{-1}. Marth and Sun (1995) field measurements suggest that V_{sg} should have a typical minimum value of about 0.5 ms^{-1} for data sets where surface heterogeneity has low effects, but it can be higher when compared with Equation (5.33).

5.2.2 Water balance

The total evaporation E_t is expressed as a combination of the partial evaporation fluxes from the vegetation, skin and bare soil:

$$E_t = E_{sk}^{total} + C_v E_v + (1 - C_v) E_b \tag{5.16}$$

in which E_t, E_{sk}, and E_v are the total evaporation, skin evaporation, evapotranspiration and bare soil evaporation, respectively; and C_v measures the fraction of the grid box covered with vegetation. Given the total evaporation rate, the latent heat flux L_h is defined as:

$$L_h = L_v E_t \tag{5.17}$$

where L_v is the latent heat of vaporization.

The skin evaporation is determined based on the classic Monin-Obukhov theory to estimate evaporation from a free surface of water:

$$E_{sk} = \rho_a C_H \left| U_1 \right| \left[q_1 - q_{sat}(T_o, P_o) \right] \tag{5.18}$$

where ρ_a is density of the air, C_H is the aerodynamic drag coefficient U_1 is the horizontal wind velocity, q_1 is the specific humidity, and q_{sat} is the saturated vapor pressure at the ground surface adjusted for the presence of snow in winter. The skin reservoirs function as buckets of pre-established capacities. This flux is limited to the actual contents of the individual reservoirs, as expressed by the superscripts in Equation (5.18), and multiplied by the weighting areal coefficient. Therefore, the total skin evaporation is given as:

$$E_{sk}^{total} = C_{pond} E_{sk}^{pond} + C_v E_{sk}^{can} + C_{sn} E_{sk}^{snow} \tag{5.19}$$

where C_{pond}, C_v, and C_{sn} measure the fraction of the grid box covered with pond, vegetation, and snow, respectively.

Bare soil evaporation is calculated using a modified threshold approach by which the saturated specific humidity at the ground surface $q_{sat}(T_o,P_o)$ is multiplied by a correction factor f_w. This factor depends on the actual surface wetness W_o and the soil wetness at saturation W_{sat}.

$$E_b = \rho_a C_W |U_1| \left[q_1 - f_w q_{sat}(T_o, P_o) \right] \tag{5.20}$$

where fw takes values between zero and one:

$$f_w = 0.5 \left[1 - \cos\pi(W_o / W_{sat}) \right] \tag{5.21}$$

Evapotranspiration is estimated based on the simplified Monteith formulation as proposed by Rowntree (1991):

$$E_v = \rho_a \frac{q_1 - q_{sat}(T_o, P_o)}{r_a + r_c} \tag{5.22}$$

where r_a is the aerodynamic resistance defined as:

$$r_a = \frac{1}{U_1 C_H} \tag{5.23}$$

and r_c is the canopy resistance which is the integral mean of the resistance of the individual leaves, and is estimated in the model with a complex scheme that takes into account the roles of moisture and light availability, temperature conditions and total leaf surface area. When the soil moisture is below the wilting point, plant resistance takes its

maximum value and evaporation is effectively shut off. At night time, the canopy resistance is simply defined as a function of leaf area index (LAI):

$$r_{c|nightime} = \frac{r_{c,\min}}{LAI} \tag{5.24}$$

During the day, the canopy resistance formulation is based on a minimal stomatal resistance value, which is modulated by the influence of the limiting factors:

$$r_{c|daytime} = \frac{r_{c,\min}}{G(W)G(F_{si})G(T)(1-0.6\ln D)(1-\delta)} \tag{5.25}$$

in which G represents conductance functions that take care of the action of the limiting factors with values ranging between zero and one. The factor in the denominator represents the stomatal resistance to the vapor pressure deficit (D) empirically derived by (Oren et al., 1999). δ is a species-specific parameter that describes the sensitivity of stomatal conductance to water vapor pressure.

The relative conductance of plants as a function of moisture availability is expressed as:

$$G(W) = \frac{W - W_{wp}}{W_{cr} - W_{wp}} \tag{5.26}$$

where W is the moisture contained in the root zone, W_{wp} is the wilting point, and W_{cr} is a critical value above which evapotranspiration takes its maximum rate. W_{cr} is comprised between wilting point and field capacity. Given these, if $W<W_{wp}$ then G(W)=0, and if $W_{cr}<W$ then G(W)=1. The empirical equations that relate plant conductance to incoming solar radiation (i.e., $G(F_{si})$), and to temperature (i.e., G(T)) are obtained from Stewart (1988):

$$G(F_{si}) = \frac{46225\ F_{si}}{41870\ F_{si} + 104.4} \tag{5.27}$$

$$G(T) = \frac{T_o (40 - T_o)^{1.18}}{691} \tag{5.28}$$

in which F_{si} is given in cal cm^{-2} s^{-1} , and T_o in degree centigrade.

5.2.3 Photosynthesis

For this model component, an integrated model of leaf photosynthesis, transpiration and conductance developed by Friend (1995) was modified to capture the diurnal cycle of carbon assimilation in the simulation of photosynthesis, including coupling with the water balance of the land surface hydrological model (Garcia-Quijano and Barros, 2005). Detailed formula describing photosynthesis, respiration and stomatal conductance processes and controls are presented below.

The LEHM assumes that photosynthesis is not affected by leaf water status until low relative water content is reached. For each set of conditions, the CO2 flux is governed by three different factors. Two are associated with the Calvin cycle and take place at the chloroplast level:

The Rubisco carboxylation-limited rate:

$$A_{carb} = \frac{V_{c,\max}\left(C_{i,carb} - \Gamma_*\right)}{C_{i,carb} + K_c\left(1 + \frac{O_i}{K_0}\right)} \tag{5.29}$$

Where:

V_{cmax} = max. rate of carboxylation [mol m^{-2} s^{-1}]

$C_{i,carb}$ = concentration of CO_2 in leaf air spaces [mol m^{-3}]

Γ = photosynthesis compensation concentration in leaf air spaces [mol m^{-3}]

K_c *and* K_o = Michaelis-Menten constant of Rubisco for CO_2 and O_2

O_i = concentration of O_2 in leaf [mol m^{-3}]

Rd = mitochondrial respiration [mol m^{-2} s^{-1}]

The ribulose-1,5-bisphosphate (ARuBP) regeneration-limited rate:

$$A_{RuBP} = \frac{J\left(C_{i,RuBP} - \Gamma_*\right)}{4.5C_{i,RuBP} + 10.5} - R_d \tag{5.30}$$

Where:

A_{RuBP} = regeneration-limited rate of net photosynthesis [mol m^{-2} s^{-1}]

J = potential electron rate [mol m^{-2} s^{-1}]

$C_{i,RuBP}$ = concentration of CO_2 in leaf air spaces [mol m^{-3}]

The third one is the stomatal conductance at the leaf level:

$$A_{rc} = \frac{C_{air} - C_i}{rc} - \frac{C_{air} + C_i}{rc} \times \frac{ER\bar{T}}{P} \tag{5.31}$$

Where:

C_{air} = concentration of CO_2 in air [mol m^{-3}]

C_i = concentration of CO_2 in leaf air spaces [mol m^{-3}]

rc = total resistance to CO_2 flux from outside leaf boundary layer to outside mesophyll liquid phase [s m^{-1}]

E = transpiration [mol m^{-2} s^{-1}]

R = gas constant [8.3144 J $K^{-1}mol^{-1}$]

P = atm. pressure [Pa]

T = avg. temperature between air and leaf [°K]

The above three equations are solved by computing analytically the internal CO_2 concentrations ($C_{i,carb}$ and $C_{i,RuBP}$) at steady-state for a given r_c.

$$g_c = \frac{1}{r_c} \tag{5.32}$$

$$\nu = K_c\left(1+\frac{O_i}{K_o}\right) \tag{5.33}$$

$$x = \frac{1}{4.5} \tag{5.34}$$

$$y = \frac{E}{2}\cdot\frac{R\bar{T}}{P} \tag{5.35}$$

$$z = \frac{10.5}{4.5}\Gamma_* \tag{5.36}$$

$$a = g_c + y \tag{5.37}$$

$$b_{carb} = g_c\cdot\left(\nu - C_{air}\right) + y\cdot\left(\nu + C_{air}\right) + V_{c,\max} - R_d \tag{5.38}$$

$$b_{RuBP} = g_c\cdot\left(z - C_{air}\right) + y\cdot\left(z + C_{air}\right) + x\cdot\left(J - 4.5R_d\right) \tag{5.39}$$

$$d_{carb} = \nu\cdot C_{air}\cdot\left(y - g_c\right) - V_{c,\max}\cdot\Gamma_* + R_d\cdot\nu \tag{5.40}$$

$$d_{RuBP} = z\cdot C_{air}\cdot\left(y - g_c\right) - x\cdot\left(J\cdot\Gamma_* + 10.5\Gamma_*\cdot R_d\right) \tag{5.41}$$

$$C_{x,i} = \frac{-b_x + \sqrt{b2_x - 4ad_x}}{2a} \quad (5.41)$$

Finally, the co-limited photosynthetic rate (*A*) is calculated:

$$A = \frac{b - \sqrt{b - 4\theta c}}{2\theta} \quad (5.43)$$

With:

b = $A_{carb} + A_{RuBP}$

c = $A_{carb} \times A_{RuBP}$

θ = empirical co-limitation factor [0:1]; set at 0.95 in our model run

The interactions between soil water, transpiration and carbon assimilation during photosynthesis are represented via the relationship between soil water potential ψ_{soil} and root water potential ψ_{root}, which in turn modulates the leaf water potential ψ_{leaf} that regulates carbon assimilation rate at the leaf level (*Al*):

$$Al(t) = fleaf(t) \times A(t) \quad (5.44)$$

With:

$$fleaf(t) = f[\psi leaf(t), \psi root(t), \psi soil(t)] \quad (5.45)$$

Finally, the gross carbon assimilation rate (*Ac*) is scaled from the leaf to the canopy level using to the leaf area index (LAI):

$$Ac(t) = LAI(t) \times Al(t) \times k \quad (5.46)$$

In the absence of a phenology module, time-varying LAI from satellite imagery is directly assimilated into the LSHM at every time-step during model simulation. k is as a constant of proportionality (Friend, 1995).

5.3 LEHM improvements

5.3.1 Implementation of temperature effect on kinetic rates

Enzymatic properties of Rubisco as a function of temperature should be better represented in the model (Leuning, 1997). Here we focus on the Michaelis-Menton coefficients of Rubisco for CO_2 and O_2 that are known to be strongly temperature depend, but species independent since directly related to the Rubisco enzyme. To implement the change of reaction rate as a function of temperature we relied on the work of Medlyn et al (2002), that follows the work of Bernacchi et al (2001). Bernacchi's study has the advantage to be based on the in vivo measurement of transgenic Tobacco's Rubisco activity rates, thus decreasing the leaf disturbance, and should therefore represent more accurately activity within the leaf (Medlyn et al., 2002):

$$K_c = 404.9 \exp\left(\frac{79430\left(T_k - 298\right)}{298 R T_k}\right) \tag{5.47}$$

Where Kc is the Michaelis-Menten coefficient of Rubisco for carbon (μmol/mol), R is the ideal gas constant, and Tk is the leaf temperature (K). In the LEHM, the air temperature at 2m is used as leaf temperature.

$$K_o = 278.4 \exp\left(\frac{36380\left(T_k - 298\right)}{298 R T_k}\right) \tag{5.48}$$

As recommended by Medlyn et al. (2002), we also adapted the formulation of the photorespiratory compensation point of CO_2 in absence of mitochondrial respiration:

$$\Gamma^* = 42.75e^{\left[\frac{37830(Tk-298)}{298RTk}\right]} \quad (5.49)$$

The formulation of the Assimilation rate RuBP limited was also updated as follows:

$$Arub = \frac{J}{4} \times \frac{(Ci-\Gamma^*)}{(Ci+2\Gamma^*)} \quad (5.50)$$

Figure 5-2 shows the impact of these changes for a range of temperatures under non-limited light and water conditions (ideal conditions for the carboxylation rate). The new formulation induces a shift of 12 degrees in the peak rates of carbon assimilation, which will allow a better representation of the vegetation dynamics in the SE US, especially during the cold season.

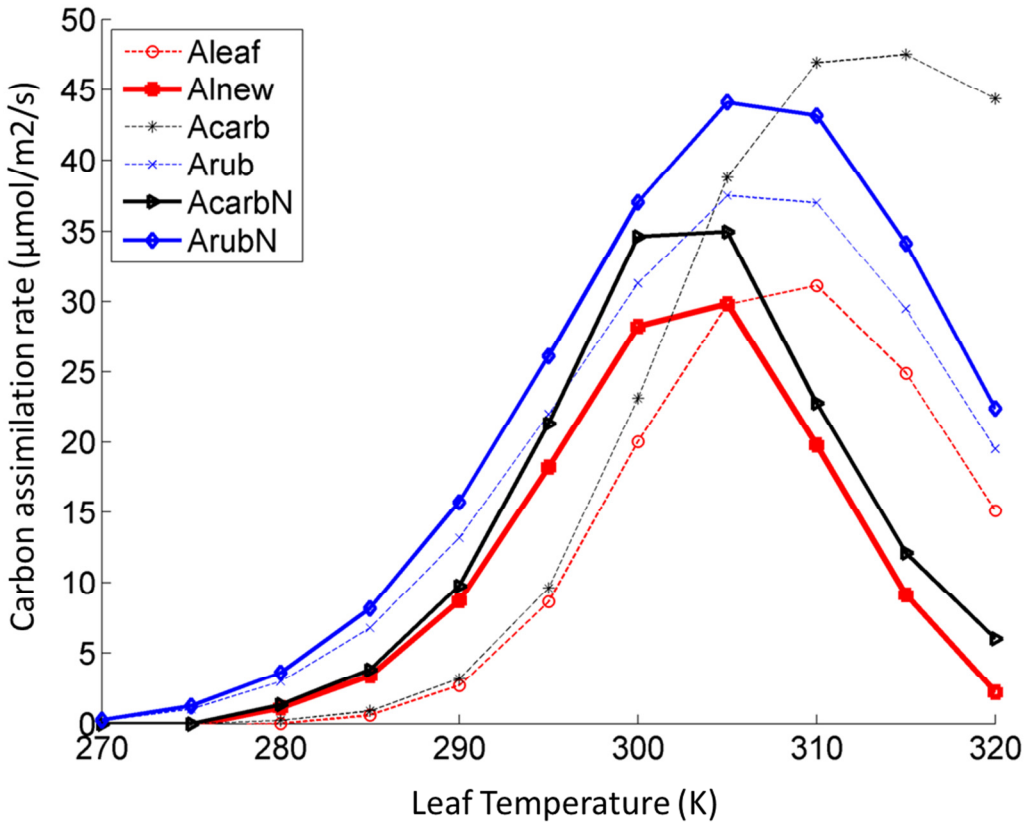

Figure 5-2: Leaf level carbon assimilation rates (red), Carboxylation limited (black) and RuBP limited (blue) as a function of temperature (K). Plain lines show new formulation of the Michaelis-Menten coefficients and photorespiration point; the previous model response to temperature is in dashed lines.

5.3.2 Specific parameterization of Vcmax and Jmax

Due to the regional scale of this study, the ability to model vegetation activity for different types of plant functional types (PFT) is paramount. Vcmax and Jmax are the key species dependent parameters in these processes. Here, we also follow Medlyn et al. (2002), who fitted A-C_i curves derived from measurements for various species (Dreyer et al., 2001). They used a peaked function as follows:

$$f\left(T_k\right) = k_{opt} \frac{H_d \exp\left(\frac{H_a\left(T_k - T_{opt}\right)}{RT_k T_{opt}}\right)}{H_d - H_a\left(1 - \exp\left(\frac{H_d\left(T_k - T_{opt}\right)}{RT_k T_{opt}}\right)\right)} \tag{5.51}$$

Where $f\left(T_k\right)$ represent either Vcmax of Jmax for a specific leaf temperature, k_{opt} the Vcmax and Jmax at 25°C; H_a gives the rate of exponential increase of the function below optimum; H_d describes the rate of decrease of the function above optimum and T_{opt} is the optimum temperature. Figure 5-3 shows the different Vcmax and Jmax obtained using this formulation for the species provided by Medlyn et al. (2002).

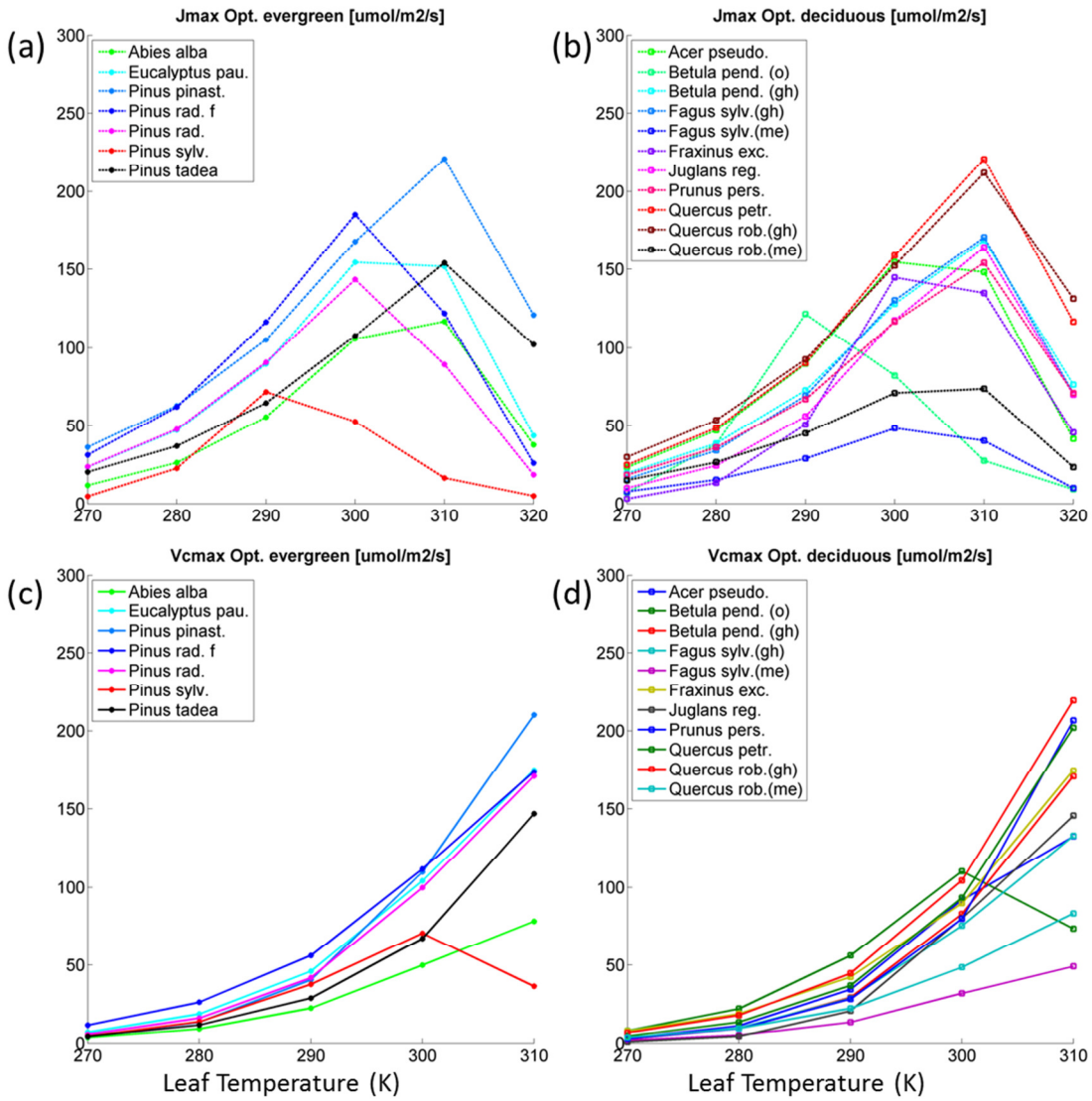

Figure 5-3 Jmax (a-b) and Vcmax (c-d) optimal rates as function of temperature for different species. Left-hand panels: evergreen trees; right-hand panels: deciduous trees.

5.3.3 Canopy scaling – Beer's law

The LEHM is essentially a "big leaf" type model, meaning it computes the canopy level photosynthesis by scaling the leaf level rate to the canopy. Previously the scaling was achieved through remote-sensed LAI by directly multiplying the carbon rate computed at the leaf level by the LAI, however, if this direct-scaling assumption of the big leaf

scaling is correct for low vegetated areas (i.e. low LAI), it becomes less accurate over vegetated area with dense and thick canopies, i.e. high LAI, due to radiation attenuation through the canopy as per Beer's law. Here, we rely and the canopy scaling as proposed by Clark et al. (2011), assuming that the leaf-level photosynthetic capacity varies proportionally with the vertical distribution of irradiance (Sellers et al., 1992) and the leaf photosynthesis can also be expressed as a function of the top of the canopy leaf photo synthesis.

$$A_c = \int_0^L A_l dl = A_o \frac{1 - \exp(-kLAI)}{k} \quad (5.52)$$

Where Ac is the canopy photosynthesis rate, A_o is the leaf photosynthesis rate at the top of the canopy, beneath the canopy, Leaf Area Index (LAI), and k is a light extinction coefficient dependent of the plant functional type. We used the extinction coefficient of 0.5 for all PFTs except for grassland (0.45) and evergreen needleleaf (0.35) (Clark et al., 2011; Thérézien et al., 2007).

5.3.4 Predictive phenology module

5.3.4.1 Framework

In its original version, the LEHM lacked a dynamic representation of the phenology and relied on direct assimilation of the MODIS Fraction of Absorbed Photosynthetically Active Radiation (FPAR) and Leaf Area Index (LAI) products to implicitly represent phenology. However, LAI and FPAR are impacted by the mechanical destruction of vegetation induced by TCs. There is therefore interest in implementing an explicit

representation of phenology to distinguish GPP changes related to the vegetation destruction at the event time-scale from the ones induced by hydrological feedbacks.

A literature review was conducted to select the phenology scheme that best addresses the research needs and that fits well with the LEHM structure. A framework based on the Growing Season Index (GSI) proposed by Jolly et al. (2008) was selected. GSI diagnoses the state of vegetation by use of three major climatic drivers serving as surrogates for the underlying controls on vegetation phenology: minimum temperature (Tmin), evaporative demand (vapor pressure deficit, VDP), and photoperiod (either the number of daylight hours, or the average incoming shortwave radiation). In other words, the GSI can be interpreted as a metric of potential phenological state under current meteorological conditions, and it is used to update green biomass productivity:

$$GSI = f\left(T\min\right) f\left(Light\right)\left(1 - f\left(VPD\right)\right) \tag{5.53}$$

With *f(x)* defined as

$$f\left(x\right) = \begin{cases} 0 & \text{if } x \le x_{\min} \\ \dfrac{x - x_{\min}}{x_{\max} - x_{\min}} & \text{if } x_{\min} \le x \le x_{\max} \\ 1 & \text{if } x \ge x_{\max} \end{cases} \tag{5.54}$$

where x = [T_{min}, photoperiod, VPD] are multiday running mean averages (21-day) to avoid abrupt changes. Air temperature and the radiation forcing are already used in the LEHM. The LEHM computes VPD directly for the stomatal resistance calculation, and it will be used to compute the GSI as well.

The GSI framework was extended to a local prognostic phenology model that predicts the biophysical vegetation states of FPAR and LAI by Stockli et al. (2008). In this context, the prognostic phenological stage (P) is defined as:

$$P = \frac{FPAR - FPAR_{\min}}{FPAR_{\max} - FPAR_{\min}} \tag{5.55}$$

$$LAI = \frac{Ln\left(1 - \frac{FPAR}{f_v}\right)}{Ln\left(1 - FPAR_{sat}\right)} f_v LAI_{\max} \tag{5.56}$$

$$\delta GSI = GSI - P \tag{5.57}$$

$$\frac{\partial FPAR}{\partial t} = \gamma \delta GSI \cdot P\left(1 - P\right) \tag{5.58}$$

$$\frac{\partial LAI}{\partial t} = \frac{\partial LAI}{\partial FPAR} \cdot \frac{\partial FPAR}{\partial t} \tag{5.59}$$

Where:

f_v = fraction of vegetation cover

γ = maximum growth rate

$P\left(1 - P\right)$ = logistic growth function to prevent unrealistic phenology switching between leaves-on and leaves-off states.

$FPAR_{sat}$ = FPAR value for maximum LAI

$FPAR_{min,max}$ = scaling structural parameters (biome dependant)

A semi-implicit numerical scheme was developed by Stockli et al. (2008, 2011) to integrate this set of equations forward in time over time steps Δt by solving the leaf

growth ($FPAR/\Delta t$) with updated meteorological conditions used to compute GSI^{t+1} and the previous biophysical state ($FPAR^t$):

$$P^t = \frac{FPAR^t - FPAR_{min}}{FPAR_{max} - FPAR_{min}} \quad (5.60)$$

$$\Delta GSI = GSI^{t+1} - P^t \quad (5.61)$$

$$\frac{\Delta FPAR}{\Delta t} = \gamma \, \Delta GSI \, P^t \, (1 - P^t) \quad (5.61)$$

$$FPAR^{t+1} = FPAR^t + \frac{\Delta FPAR}{\Delta t} \quad (5.62)$$

$$LAI^{t+1} = \frac{\ln(1 - FPAR^{t+1}/f_v)}{\ln(1 - FPAR_{sat})} LAI_{max} f_v \quad (5.63)$$

This local framework was generalized by splitting the mixed landscape into a discrete set of plant functional types (PFTs) and elevation classes (HGTs). Relying on the Ensemble Kalman Filter (EnKF) for data assimilation, climate controls ($T_{min,max}$; $VPD_{min,max}$; $SWin_{min,max}$), structural parameters ($FPAR_{min,max}$; γ ; LAI_{max}; $FPAR_{sat}$) of the phenology Evensen (2009) estimated growth and senescence rates for a large set of natural and anthropogenic biomes, which will be used here in the form of a lookup table (Table 5-7). This framework has the advantage to link well with the LEHM and to offer great flexibility, because it can be used in prognostic mode and/or integrate data assimilation if needed to constrain the results in the possible ranges of specific biomes.

5.4 Data

5.4.1 Model forcing

Table 5-1 summarizes the different forcing used to run the LEHM during our study. All the datasets were interpolated linearly to a 30min time-step and a grid of 4km. The North America Land Data Assimilation System is the primary forcing for energy and atmospheric forcing, with the exception of rain to which the Stage IV product was preferred since it better captures heavy precipitation (Villarini et al., 2011). For the vegetation in formation, we rely on MODIS (MOD15) Leaf area index (LAI) and the Fraction of Absorbed Photosynthetically Active radiation that a plant canopy absorbs for photosynthesis (FPAR). MODIS land cover (MOD12Q1) was also in combination of look-up-table (LUT) to determine the minimal stomatal resistance, the critical leaf water potential and roughness length. Soil properties were set using the CONUS-soil dataset. This dataset is a multi-layer soil characteristics dataset based on the USDA State Soil Geographic Database (STATSGO) that was specifically developed for model applications, such as SVAT, climatology, hydrology, and other environmental applications (Miller and White, 1998).

Table 5-1: Source of datasets used in LEHM simulations.

Variable	Units	Datasets	Versions
Precipitation	[kg/m2/s]	NLDAS-2	forcingB
Pressure	[Pa]	NLDAS-2	forcingA
Air Temperature @2m	[K]	NLDAS-2	forcingA
Specific Humidity	[Kg/Kg]	NLDAS-2	forcingA
Wind velocity	[m/s]	NLDAS-2	forcingA
Wind direction	[degree]	NLDAS-2	forcingA
Down short wave	[w/m2]	NLDAS-2	forcingA
Down long wave	[w/m2]	NLDAS-2	forcingA
Vegetation fraction	-	NLDAS-1	Mosaic
albedo	-	NLDAS-1	Mosaic
FPAR	-	MODIS	MOD15
LAI	-	MODIS	MOD15
Minimum stomatal resistance	[s/m]	LUT	NLDAS
Roughness length	[m]	LUT	WRF
Land cover	classes	MODIS	MOD12Q1
Soil texture	classes	CONUS soil	STATSGO
Hydraulic conductivity at saturation	[mm/s]	LUT	Dingman (2005)
n number	-	LUT	Dingman (2005)
Soil porosity	[m^3/m^3]	CONUS soil	STATSGO
Field capacity	[m^3/m^3]	LUT	Dingman (2005)
Wilting point	[m^3/m^3]	LUT	Dingman (2005)

5.4.1.1 North America Land Data Assimilation System (NLDAS-2)

In this study, the LEHM is run at a spatial resolution of 4km and at a 30min time-step over a period of 10 years. Note that the spatial and temporal resolutions are limited by the forcing data and not by the model itself. A summary of the different datasets used to force the LEHM is presented in Table 5-1.

The atmospheric forcing of the LEHM is derived from The North America Land Data Assimilation System (NLDAS-2). This framework provides data at 12.5km spatial resolution and at hourly temporal resolution over the entire US. In turn, the land-surface

forcing fields for NLDAS-2 are derived from the analysis fields of NARR. NARR analysis fields are available at 32-km spatial resolution and 3-hourly temporal frequency. These NARR fields are spatially interpolated to match the NLDAS grid and then temporally disaggregated to the NLDAS-2 hourly frequency, as presented by Cosgrove et al. (2002). Additionally, the fields of surface pressure, surface downward longwave radiation, near-surface air temperature and near-surface specific humidity are adjusted vertically to account for the vertical difference between the NARR and NLDAS fields of terrain height. These NLDAS data are linearly interpolated to 30min. Here, the precipitation forcing will be interpolated from the hourly NCEP Stage IV (similar to the one use in Chapter 4), since NAAR precipitation tends to underestimate extremes.

Mo et al. (2012) evaluated drought monitoring systems over the continental United States based on the NLDAS. They found that the discrepancies in soil moisture were due to the difference between model forcing, with NLDAS precipitation being underestimated. They also highlighted discrepancies in radiative forcing, especially after 2002 when the NCEP system transitioned to use the real-time North American Regional Reanalysis (NARR). The latter is the forcing used in our study, therefore in order to address this issue of precipitation underestimation, Stage IV data were used here instead of NLDAS precipitation. Note that this may raise question of consistency in atmospheric forcing

5.4.1.2 MODIS leaf Area Index (LAI) and Fractional Absorbed Photosynthetically Active Radiation (FPAR).

Regarding the vegetation parameterization, we rely on MODIS LAI and FPAR for the forcing. LAI is used to scale the original version of the LEHM from the leaf to the canopy level as well as representing the phenology. FPAR is necessary to the computation of the electron flux implicated in the light part of photosynthesis and necessary to compute the ribulose-1,5-bisphosphate limited carbon flux (Arub). MODIS Gross Primary Production product (MOD17A2) is provided at 1-km spatial resolution using a 8-day composite time step. As stated earlier, LAI defines an important structural property of a plant canopy, namely the one-sided leaf area per unit ground area, and it is used in the LEHM to scale the carbon assimilation rate computed at the leaf level to the canopy level. FPAR measures the proportion of available radiation in the photosynthetically active wavelengths (400 to 700 nm) that the canopy absorbs. Despite its 8-day interval this product has been proven to be impacted by atmospheric conditions. A quality flag is provided on a pixel basis to help the user to estimate the accuracy of the provided data. Based on this quality information, the software TIMESAT was used to remove bad quality data from the time series and fill in the gaps (Jonsson and Eklundh, 2002). For the FPAR, an adaptive Savitzky-Golay filtering was selected since it matches the closest the variations of FPAR. This is important because low values of FPAR are due to cloud cover and should not be removed from the forcing, as this has an important feedback on GPP. Regarding the LAI, the same filter was used but a larger

window of 8 (2 for FPAR) was used. Finally, FPAR and LAI were averaged to a 4km resolution and interpolated linearly to a 30min time-step.

5.4.1.3 Look-up-table for environmental parameters

We rely on different look-up-tables to define parameters as a function of soil texture and as a function of land cover. Table 5-2 summarizes the parameters used to infer soil properties from the soil texture as provided by the CONUS-soil database. These parameters are based on the literature review of Dingman (2005) and the Handbook of Hydrology (Rawls et al., 1993), and Tao and Barros (2013).

Table 5-2: Soil look-up-table used in the model simulation.

TCODE	NAME	Ksat [mm/s]	Field Capacity	Wilting Point	n	Suction Front [mm]
1	Sand	0.0654	0.091	0.033	6	49.50
2	Loamy sand	0.0166	0.125	0.055	7	61.30
3	Sandy loam	0.0061	0.207	0.095	8	110.10
4	Silt loam	0.0019	0.330	0.133	12	166.80
5	Silt	0.0007	0.380	0.140	11	127.85
6	Loam	0.0037	0.270	0.117	11	88.90
7	Sandy clay loam	0.0607	0.255	0.148	9	218.50
8	Silty clay loam	0.0758	0.366	0.208	14	273.00
9	Clay loam	0.0580	0.318	0.197	11	208.80
10	Sandy clay	0.0664	0.339	0.239	12	239.00
11	Silty clay	0.0812	0.387	0.250	16	292.20
12	Clay	0.0879	0.396	0.272	15	316.30
13	Organic materials	0.0222	0.150	0.040	6	100.00

Based on MODIS land cover, we inferred several parameters related to the vegetation presented in Table 5-3. The leaf water potential values were derived from a database based on literature review compiled by Manzoni et al. (2011).

Table 5-3: Vegetation and land surface look-up-table used in the model simulation.

Class	LC Code	Rcmin [s/m]	Critical leaf water potential [Pa]	Roughness length [m]
evergreen needleleaf forest	1	175	-2500	0.5
evergreen broadleaf forest	2	150	-3000	0.5
deciduous needleleaf forest	3	175	-2500	0.5
deciduous broadleaf forest	4	150	-3000	0.5
mixed forest	5	175	-2500	0.4
closed shrubland	6	175	-2500	0.15
open shrubland	7	180	-3000	0.07
woody savanas	8	170	-2500	0.25
savannas	9	170	-4000	0.1
grasslands	10	150	-3500	0.09
permanent wetlands	11	120	-3000	0.05
croplands	12	100	-1800	0.1
urban and built-up	13	250	-1000	0.5
cropland/natural vegetation mosaic	14	150	-2000	0.15
barren or sparsely vegetated	16	175	-2000	0.05

5.4.2 MODIS Gross Primary Production product (MOD17A2)

5.4.2.1 MOD17A2 algorithm

The MODIS GPP/NPP product (Running et al., 2004) is the first continuous satellite-driven dataset monitoring global vegetation productivity and therefore offers the longest time-series. This product is available globally at 1km resolution at an aggregated time-step of 8-day. The algorithm is based on the original logic of Monteith (1972), suggesting that NPP under non-stressed conditions is linearly related to the amount of Absorbed Photosynthetically Active Radiation (APAR) during the growing season. In reality, vegetation growth is subject to a variety of stresses that tend to reduce the potential growth rate, especially stresses resulting from climate (temperature,

radiation, and water availability). The interaction of these primary abiotic controls imposes complex and varying limitations on vegetation activity in different parts of the world.

To determine the efficiency at which the plants transform the incoming energy into organic material, the MODIS algorithm relies on a biome look-up table (BLUT) defining the plant efficiency for specific biomes as defined in the MODIS land cover product. This table was first derived using a global simulation of the general ecosystem model BIOME-BCG (Zhao et al., 2005). The look-up table was recalibrated using MODIS FPAR/LAI and DAO data for version 5 (Zhao et al., 2006).

To implement the impact of suboptimal meteorological conditions, the potential maximum light-use efficiency of specific biome is modulated using linear ramp functions of vapor pressure deficit (VPD) and daily minimum air surface temperature (Tmin). These two parameters are retrieved from the NASA Data Assimilation Office (DAO), model which assimilates surface weather observations globally every 3 hours at spatial resolution of 1°x1.25°. Finally, MODIS FPAR/LAI product (MOD15A2) and incoming shortwave radiation from the DAO are used to infer APAR. Note the discrepancy between DAO resolution and MODIS product.

5.4.2.2 MOD17A2 uncertainties

There are several potential sources of uncertainties in MODIS GPP. Some are related to uncertainties associated with the input data, and some are inherent to assumptions made in the algorithm. Regarding the input data, the MODIS land cover accuracy is a primary concern, since the misclassification of a pixel will lead to the use of

the incorrect biome light-efficiency parameter. In addition, the land cover classes are somewhat vague with regard to vegetation type. For example the class "cropland" covers numerous categories of plants with very different light-use efficiency coefficient. There are also additional uncertainties in BLUT itself. Concerning the DAO data there are two concerns. First, it is an assimilated dataset with potential systematic bias in different parts of the globe. For example, Gebremichael and Barros (2006) identified systematic bias against tower data in the Himalayas and in the Sonora desert. Second, its coarse spatial resolution introduces uncertainties in terms of geolocation, spatial interpolation and representativeness of local conditions at the MODIS 1km grid scale. A comparison of the use of different meteorological reanalysis datasets has shown that bias results in substantial error in GPP estimation (Myneni et al., 2002). Finally, the FPAR/LAI MODIS product is not exempt of cloud contamination even at the 8-day time-step creating erroneously low values of FPAR (e.g. Fensholt et al., 2006; Heinsch et al., 2006; Kanniah et al., 2009). Turner et al. (2006) comparing so-called Bigfoot Data - digital maps of 25km^2 around flux tower combining Landsat and ground measurements to estimate LAI, NPP and GPP – and tower measurements to MODIS GPP product conclude that the overestimation was related to problems with MODIS FPAR in addition to problems related to land cover classification (Heinsch et al., 2006), and the atmospheric forcing used to implement the vegetation stress factor (Zhao et al., 2006). In the last version used here (v5.5) the temporal interpolation of FPAR has been improved (Zhao et al., 2005) removing more low values of FPAR assumed to be due to cloud contamination.

Uncertainty analysis of the MODIS GPP product is challenging mostly due to the difficulty in directly measuring GPP. However it is a crucial task since the quantification of carbon fluxes between the biosphere and the atmosphere is of scientific importance to the understanding of climate change. Therefore numerous studies have been conducted to evaluate MODIS derived GPP/NPP products. They can be classified in two main categories: studies relying on eddy covariance flux tower observations (Chen et al., 2011; Coops et al., 2009; Heinsch et al., 2006; Nightingale et al., 2007; Turner et al., 2006; Xiao et al., 2010), and studies conducted using models (Gebremichael and Barros, 2006; Yang et al., 2007; Zhao et al., 2011). The MODIS GPP algorithm was designed for global-scale applications, and thus discrepancies at local places are expected; previous studies indicate that the algorithm robustness varies strongly with biome type, generally underestimating GPP in semi-arid regions and overestimating GPP in forested areas (Zhao et al. 2011). More recently comparing the Ameriflux data with MODIS GPP estimates to develop a support vector approach of continental scale GPP estimates, Yang et al. (2007) found an error of 50.3% in MODIS GPP estimates for non-forest eco-systems and 21.5% over forested areas.

In response to published studies identifying systematic biases and errors, the algorithm has been revised several times. At the date of this work, MOD17A2 was recently updated to versions 5 (official NASA product) and 5.5. Beginning with version 5, the Biome Property Look-Up Table (BPLUT) parameters were calibrated to better agree with GPP derived from measurements at eddy flux towers and synthesized Net Primary Production (NPP) (Kang et al., 2005). The algorithm to interpolate spatially

coarse resolution meteorological data to the 1-km MODIS pixel level has been modified from a nearest neighbor sampling to a more complex non-linear formulation (Zhao and Running, 2010). The version 5.5 is currently available and needs to be downloaded directly from the Numerical Terradynamic Simulation Group of the University of Montana. The main enhancement of v5.5 is that FPAR/LAI data with bad quality flag have been replaced by temporally interpolated FPAR/LAI annual time-series to remove cloud contamination. This dataset has been proven to be suitable for time-series (Zhao and Running, 2010) and will be the one used in this study.

5.5 Ameriflux tower comparison

In this section, the GPP simulated by the LEHM for the period of 2002-2010 at a time-step of 30min is compared with the MODIS GPP product version 5.5 and AmeriFlux tower data (Baldocchi et al., 2001). For the energy and water budgets, NLDAS MOSAIC model (Koster and Suarez, 1994) results and available tower estimates are used to evaluate the LEHM run. A persistent challenge that arises from using multiple data sources is the scale discrepancy between point measurements and gridded product of various spatial resolutions. Originally, the plan was to force the model with the tower data. However, numerous gaps in time series and difficulties in identifying towers that provided the necessary forcings at similar time periods and intervals proved to be a substantial limitation. Instead, a comparison was made by forcing the model using the NLDAS-2 data linearly interpolated to 4km. The MODIS product LAI and FPAR were used at their original spatial resolution of 1km due to the variability of land

cover around the sites, which caused discrepancies between the 4km average product created for the regional run. Finally, soil properties were inferred from the texture and other information provided in the site description using Table 5-2.

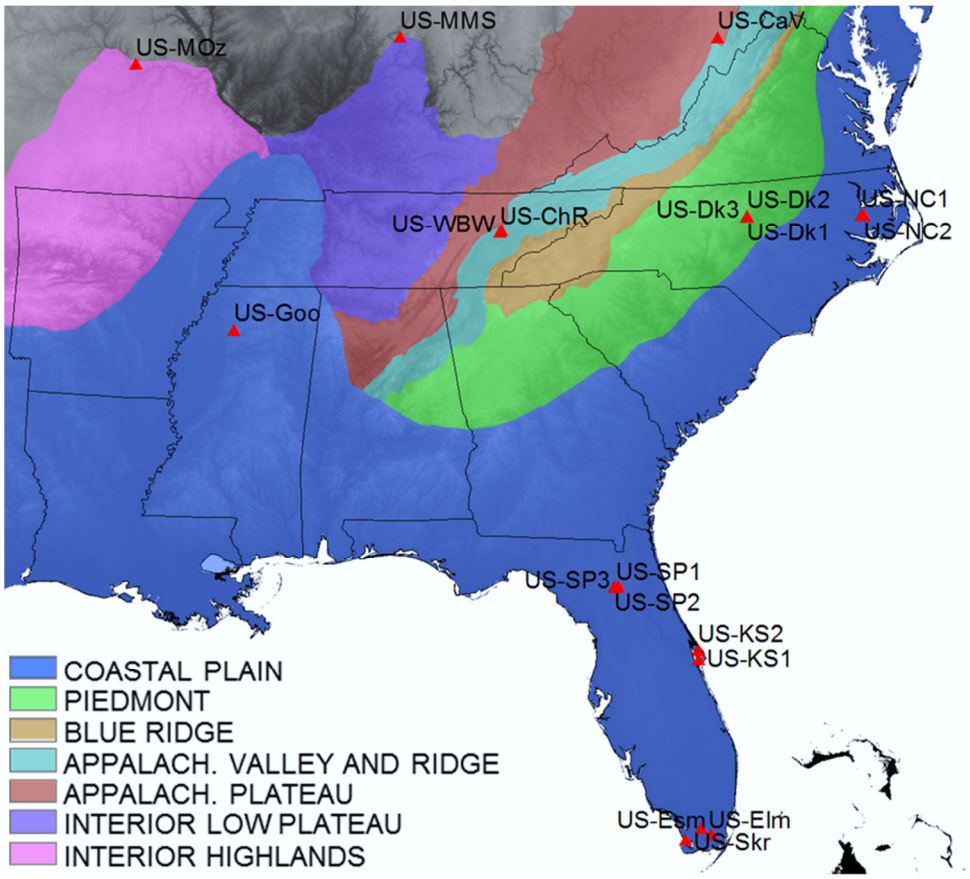

Figure 5-4: Spatial distribution of the AmeriFlux towers in the SE US. USGS physiographic regions (colored) and elevation (grayscale) are used as background.

Figure 5-4 shows the spatial distribution of the AmeriFlux towers providing GPP estimates in the SE US. The AmeriFlux network was established in 1996. The network provides continuous observations of ecosystem level exchanges of CO_2, water, energy and momentum spanning diurnal, synoptic, seasonal, and inter-annual time scales and is currently composed of sites in North America, Central America, and South America

(http://public.ornl.gov/ameriflux/). Tower estimates are provided at a 30-minute time-step. GPP is computed as the difference between the Net Ecosystem Exchange (NEE) and the Ecosystem Respiration (RE). These fluxes are inferred from eddy covariance measurements. Note that these measurements require a considerable amount of processing, implying gap-filling techniques, and that the intrinsic spatial variability of ecosystems can account for up to 50% uncertainties on NEE estimates (Oren et al., 2006; Wilson et al., 2001). There are also limitations with the hydrometeorological data overall, such as the well-documented difficulty in closing the energy budget at the flux towers(Foken, 2008): while the eddy covariance technique captures small-scale turbulent fluxes at spatial scales smaller than 1 km, it underestimates latent and sensible heat fluxes due to large-scale eddies on the order of 10 km. Thus, estimates NEE may be 15 to 20% lower than the actual values.

Table 5-4: Ameriflux towers used in the comparison including the type of vegetation

ID	Name	Elevation (m)	Tower height (m)	Vegetation Type
US-CaV	Canaan_Valley	994	4	GRA (grassland)
US-ChR	Chestnut Ridge	286	60	DBF (Deciduous broadleaf forest)
US-Dk1	Duke_Forest_Open_Field	168	6	GRA
US-Dk2	Duke_Forest_Hardwoods	168	42	MF (Mixed Forest)
US-Dk3	Duke_Forest_Pine	163	22	MF
US-Goo	Goodwin_Creek	87	4	GRA
US-NC1	North_Carolina_Clearcut	5	6	OSH (open shrubland)
US-NC2	North_Carolina_Loblolly_Pine	12	23	ENF (Evergreen needleleaf forest)
US-SP1	Austin_Cary	44	32	ENF
US-SP2	Mize	43	18.5	ENF
US-SP3	Donaldson	36	24.3	ENF
US-SP4	Rayonier	47	15	ENF
US-WBW	Walker_Branch	343	44	DBF

Table 5-4 summarizes information about the different sites used in this study. Note that the Kennedy Space center towers and the stations in the Everglades in Florida were removed from this analysis because the land-cover class is water at 4km resolution. Two levels of data were used in this study. Level-4, which is gap-filled with an artificial neural network method and daily accumulated for the estimation of gross primary productivity and total ecosystem respiration terms (http://public.ornl.gov/ameriflux/level4data.html), and Level-2, which contains formatted and homogenized data with a check for units consistency. For GPP, all the data were at the Level-4 except for the Duke tower, where Level-2 are available. Level-2 data are provided at 30min time-step in standard local time (LST) and Level-4 data are provided at a daily time-step. Note that data from few towers are available concurrently during our period of observation, and many exhibit large data gaps (see Table 5-5).

Table 5-5: Timeline of available measurements at the Ameriflux towers over our area of study. The numbers correspond to the highest level of processing available.

ID	Name	2002	2003	2004	2005	2006	2007	2008	2009	2010	2011
US-CaV	Canaan_Valley			2	2	2	2	2	2	2	
US-ChR	Chestnut Ridge				2	2	2	2	2		
US-Dk1	Duke_Forest_Open_Field	2	2	2	2	2	2	2			
US-Dk2	Duke_Forest_Hardwoods	2	2	2	2	2	2	2			
US-Dk3	Duke_Forest_Pine	2	2	2	2	2	2	2			
US-Goo	Goodwin_Creek	4	4	4	4	4					
US-NC1	North_Carolina_Clearcut				4	4	2	2	2		
US-NC2	North_Carolina_Loblolly_Pine				4	4	2	2	2		
US-SP1	Austin_Cary	4	4	2	4	4	2	2	2	2	2
US-SP2	Mize	4	4	4	2	2	2	2			
US-SP3	Donaldson	4	4	4	2	2	2	2	2	2	
US-SP4	Rayonier										
US-WBW	Walker_Branch	2	2	2	2	2	2				

Table 5-5 does not fully represent the actual data availability as there are many interruptions due to sensor failures or lack of maintenance; therefore numerous gaps are present in the time-series. Furthermore, tower maintenance, including sensor calibration, can vary greatly with time, which introduces uncertainties that are difficult to quantify objectively (MacDonald, 1972). Next we focus our analysis on the evaluation of the model performance organized in terms of PFT.

5.5.1 Atmospheric forcing

Figure 5-5 shows scatter plots of the different atmospheric forcings used to drive the model at tower site US-WBW – which representative of forcing discrepancies among the other sites - for the NLDAS and StageIV 4km grid pixel corresponding to the tower location. The Ameriflux over measurements of level-2 are provided at a 30min time-step matching the linear interpolation implemented on the original hourly time-step of NLDAS-2. Those discrepancies are expected when comparing gridded products with point measurements, strong discrepancies are present. Note there is no correlation between the two rainfall datasets. It was expected due to the large spatial and temporal variability in rainfall. The 2 meter air temperature is in good agreement with an R of 0.86. Note also the large variability in incoming shortwave radiation. These discrepancies will therefore induce differences between the model and tower estimates due to different representations of the atmospheric conditions.

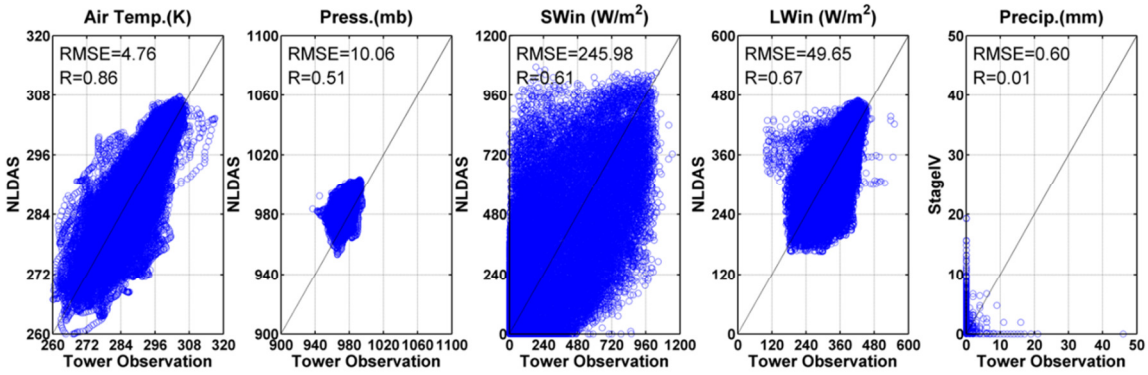

Figure 5-5: Comparison between Tower observations (x-axis) and NLDAS-2 resample at 4km spatial and 30min resolution and Stage IV data for the tower location US-WBW over the period 2002-2011.

5.5.2 Evergreen needleleaf

Across the SE, evergreen needleleaf is the vegetation type that is best monitored by the Ameriflux network with 3 distinct sites: Duke Forest, North Carolina Coastal Plains and North Florida.

Figure 5-6 shows the comparison between tower MODIS and LEHM GPP estimates over the period 2002 to 2011. In terms of similarities in phenology and amplitude between MODIS and the model are attributable to the fact that the forcing for light availability (FPAR) and the scaling from canopy to leaf (LAI) come from the same MODIS products that are used in the GPP algorithm. In Figure 5-6 (c), we see that the annual amplitude of GPP calculated by the model agrees well with MODIS, but that tower estimates in the only four years of data available are higher both in winter and summertime. The annual cycle in GPP shows that this site is a mixed forest. Note that the model is capturing the water stress during the second part of the summer during the severe drought in 2007. This suggests that the model can simulate water stress related variation in GPP over evergreen needleleaf vegetation.

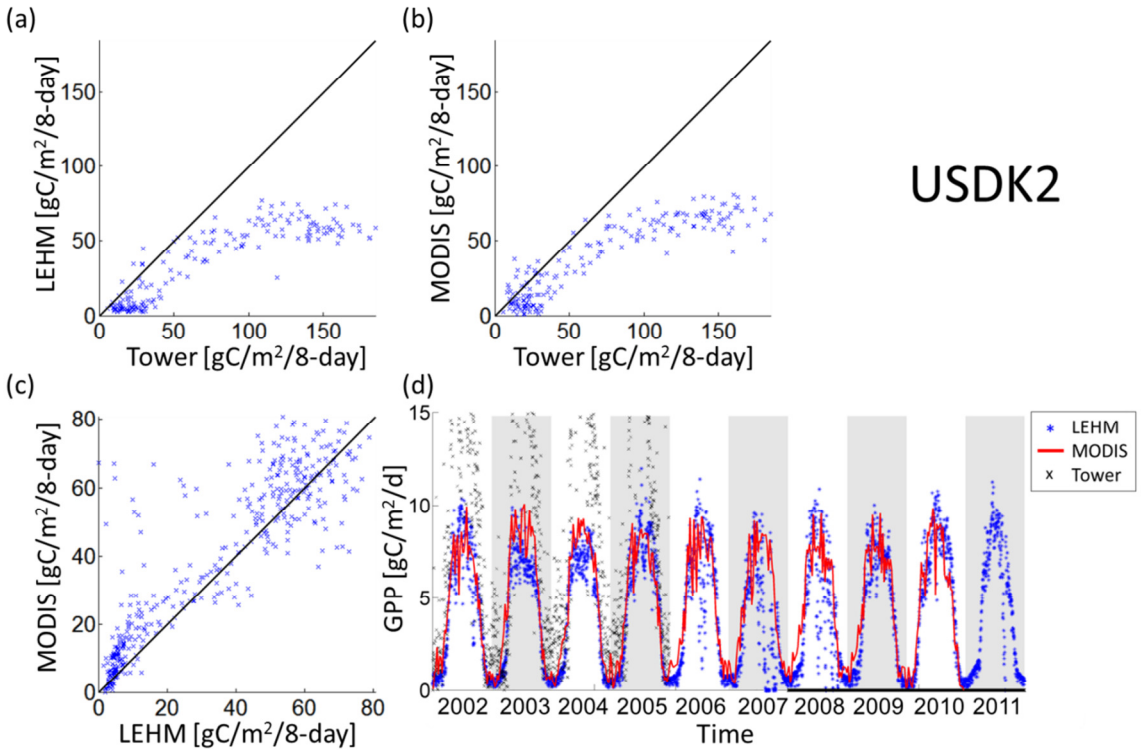

Figure 5-6: Duke tower – US-DK2; (a)-(c) scatter plots of 8-day GPP accumulation (gC/m²/8-day) LEHM results against tower and MODIS GPP estimates; (d) 10 years GPP (gC/m²/day) estimates for the LEHM, MODIS and Tower (level-2) from 2002 to 2011. The LEHM is forced using NLDAS and Stage IV resampled products at 4km spatial resolution and 30min time-steps. MODIS LAI and FPAR are used at original 1km spatial resolution and linearly interpolated to 30min.

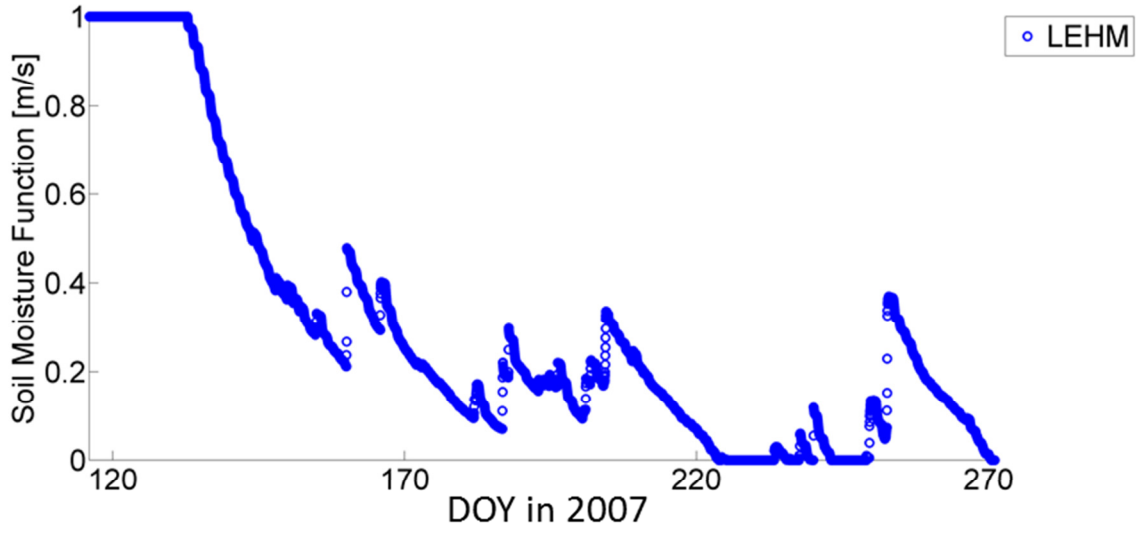

Figure 5-7: Soil moisture function used in the canopy resistance computation during the summer 2007.

Figure 5-7 shows the soil moisture as calculated by the model during the onset of water stress in 2007. These severe conditions strongly limit the evaporation rate starting in June (DOY 150) and completely shut down evapotranspiration by the beginning of August (DOY 220). This extreme model behavior in August reflects the fact that the model does not represent the role of deep trees roots in accessing soil moisture at lower soil depths and close to the water table as its level lowers during drought. Although proven suitable to estimate the impact of drought on GPP (Zhao and Running, 2010), the MODIS GPP time-series does not capture this decrease in vegetation activity at the end of the summer 2007. This discrepancy during the 2007 drought is attributable to the fact that the MODIS algorithm relies on the VDP (Heinsch et al., 2003) and not soil water content to estimate plant water status.

To compare the water and energy budgets, tower measurements and LEHM simulations were compared with the MOSAIC model (Koster and Suarez, 1992, 1994)of the NLDAS system. The MOSAIC-NLDAS land surface model computes energy and water fluxes from the land surface in response to meteorological forcing. The scheme includes a canopy interception reservoir and three soil reservoirs: a thin layer near the surface, a middle layer that encompasses the root zone, and a deep layer for long term storage. The model represents environmental stresses such has high temperature and dry soil through modification of the canopy resistance decreasing transpiration. MOSAIC was originally derived from the SiB model of Sellers et al. (1986). The subgrid variability is represented by tiling vegetation and bare soil type using observed vegetation distributions.

Figure 5-8 shows the comparison between the soil moisture measured at 10cm depth at the tower site, the MOSAIC model of the NLDAS system soil water content for the first top soil layer (10cm) and the LEHM top soil moisture (8cm); the soil moisture content for the tower site at 20cm, the MOSAIC (10-50cm) and the LEHM (8-50cm); at the bottom, the comparison between the MOSAIC and LEHM total soil moisture in the three top soil layers. The comparison with the tower measurement is difficult due to the strong variation in the time-series. The LEHM shows a larger variability in the top soil layer than MOSAIC. The variations in time and the values in the medium and total 1m soil column are in pretty good agreement between the LEHM and MOSAIC, with the LEHM being slightly dryer in the total column. Note that MOSAIC is generally wetter in the deeper soil layer than MOSAIC. Besides model differences, note that the soil

parameterization is different too. In the case of the LEHM the soil properties are defined using the soil type as describe at the tower site using the look-up table (Table 5-1) for soil parameterization and assuming an homogenous soil in the column. In the case of MOSAIC, the soil properties are changing in function of soil layer using the NLDAS soil properties datasets.

Figure 5-9 shows the comparison between the MOSAIC-NLDAS and LEHM models for the different components of the evapotranspiration. The bare soil evapotranspiration is in better agreement between the two models. Note that the LEHM allows dew formation (positive values), which is not the case for the MOSAIC over bare soil. The transpiration rate is higher in the LEHM than in MOSAIC. The skin evaporation rate tends to be larger in the MOSAIC with sensitivity to seasonality that is lower. This can be explained by the use of MODIS LAI to force the LEHM phenology.

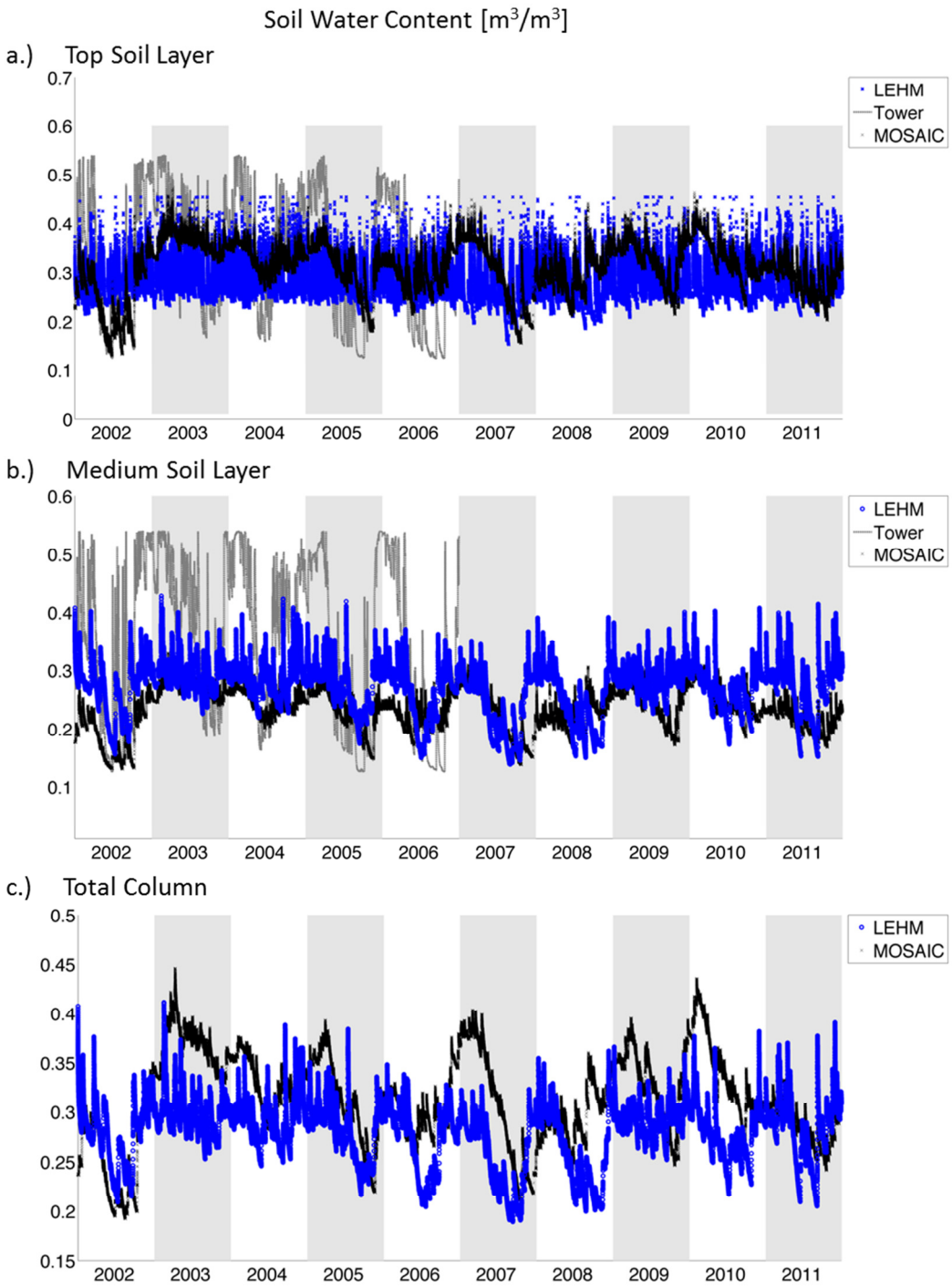

Figure 5-8: Soil water content [m³/m³] comparison between tower US-DK2 measurement in grey, MOSAIC model (12.5km) of the NLDAS in black and the LEHM (4km) in blue: (a) the top soil layer, (b) the medium soil layer and (c) 1m soil column.

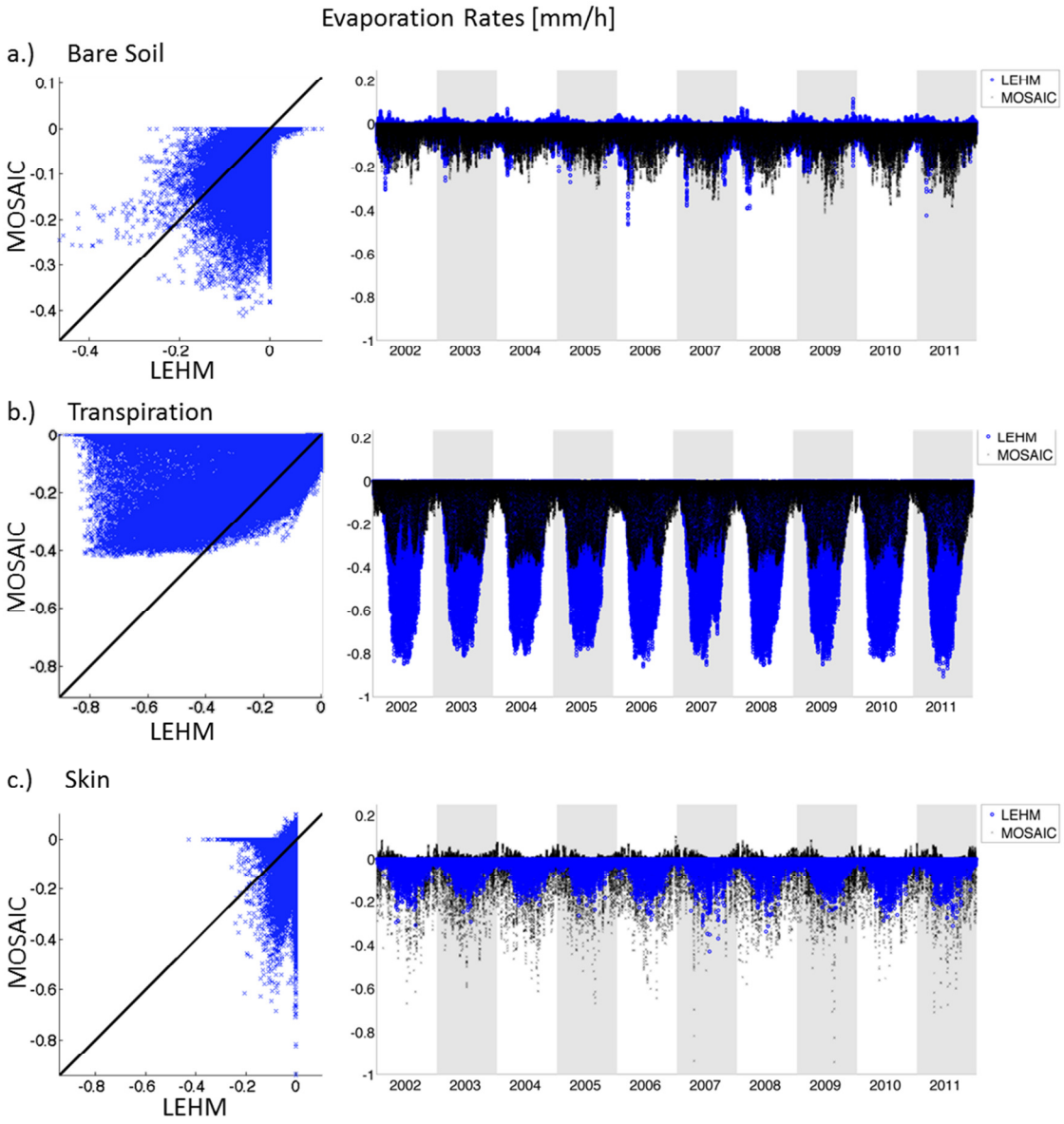

Figure 5-9: Comparison of the evapotranspiration rates [mm/h] the MOSAIC model (12.5km) of the NLDAS (black) and the LEHM (blue): (a) bare soil, (b) transpiration and (c) the skin evaporation from the interception reservoir.

Figure 5-10 to 12 show the energy budget comparison for the latent, sensible and ground heat fluxes. The MOSAIC-NLDAS model produces large ground heat fluxes that are about two times larger than the LEHM. The tower measurements, when available,

are close to the LEHM simulated values. In terms of latent heat flux, the LEHM values are around 600-700 W/m^2 during the summertime, when the MOSAIC-NLDAS estimates are closer to 400-550 W/m^2. Consequently, the sensible heat flux of MOSAIC-NLDAS simulations is larger than the LEHM peaking at 600 W/m^2 during the summertime, while the LEHM values are around 400 W/m^2 which is in better agreement with tower measurements.

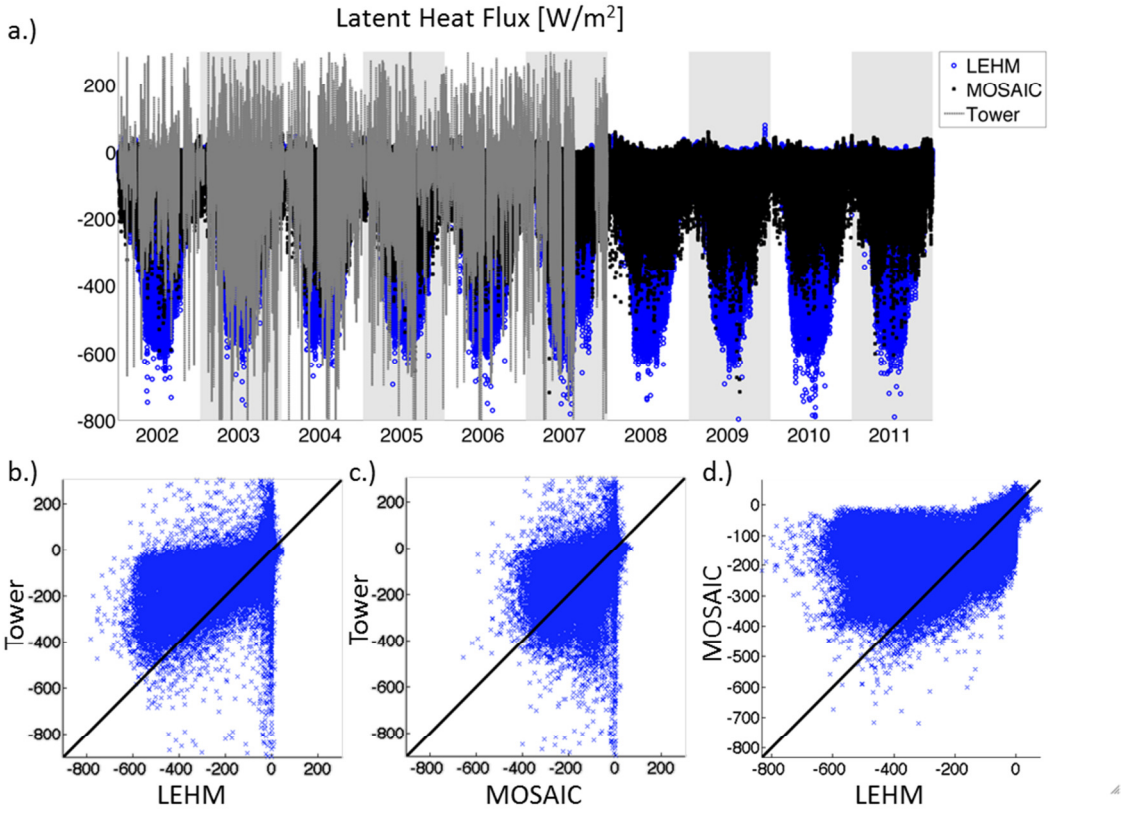

Figure 5-10: Comparison for the latent heat flux between the tower US-DK2 measurement in grey, MOSAIC-NLDAS model (12.5km) of the NLDAS in black and the LEHM (4km) in blue: (a) time-series, (b)-(d) scatterplots.

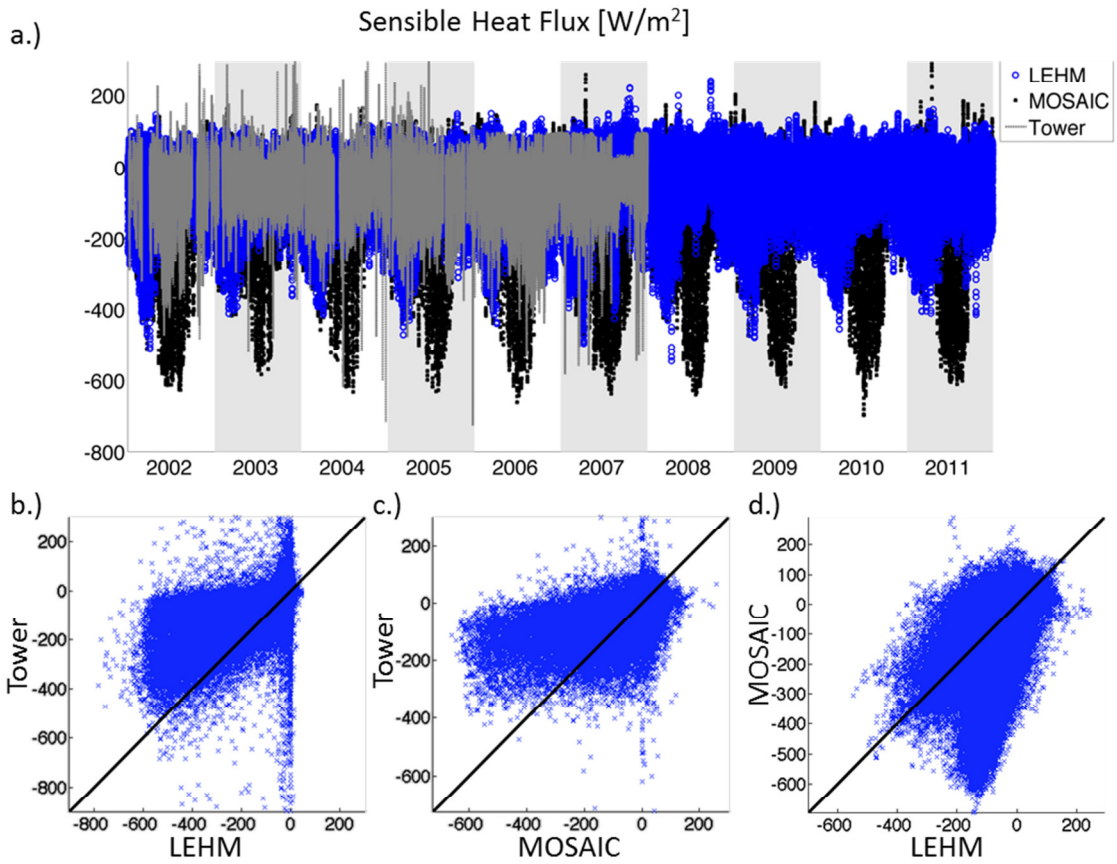

Figure 5-11: Comparison for the sensible heat flux between the tower US-DK2 measurement in grey, MOSAIC-NLDAS model (12.5km) of the NLDAS in black and the LEHM (4km) in blue: (a) time-series, (b)-(d) scatterplots.

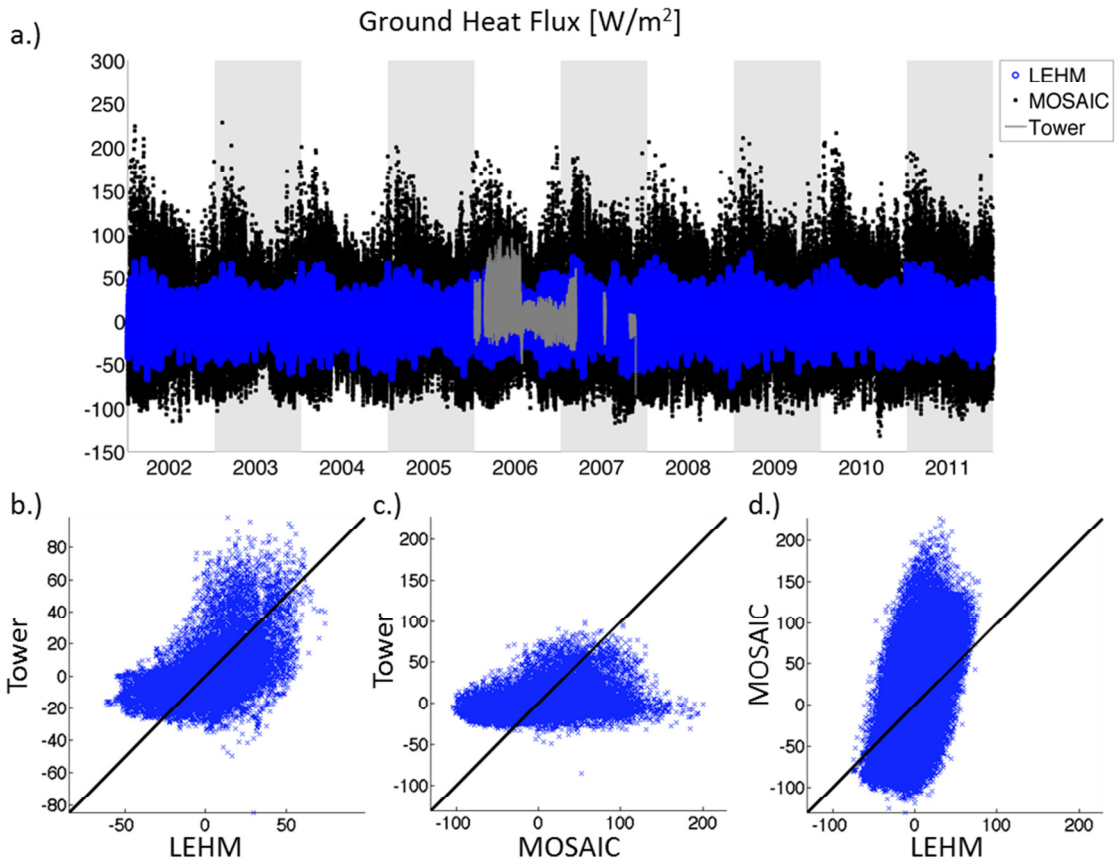

Figure 5-12: Comparison for the ground heat flux between the tower US-DK2 measurement in grey, MOSAIC-NLDAS model (12.5km) of the NLDAS in black and the LEHM (4km) in blue: (a) time-series, (b)-(d) scatterplots.

Figure 5-13 andFigure 5-14 show the comparison for the top soil temperature. The tower measurements and both models are in good agreement in terms of seasonal cycle and range of variability. However the diurnal cycle is stronger in both models for the top soil layer. The deep soil temperatures agree well.

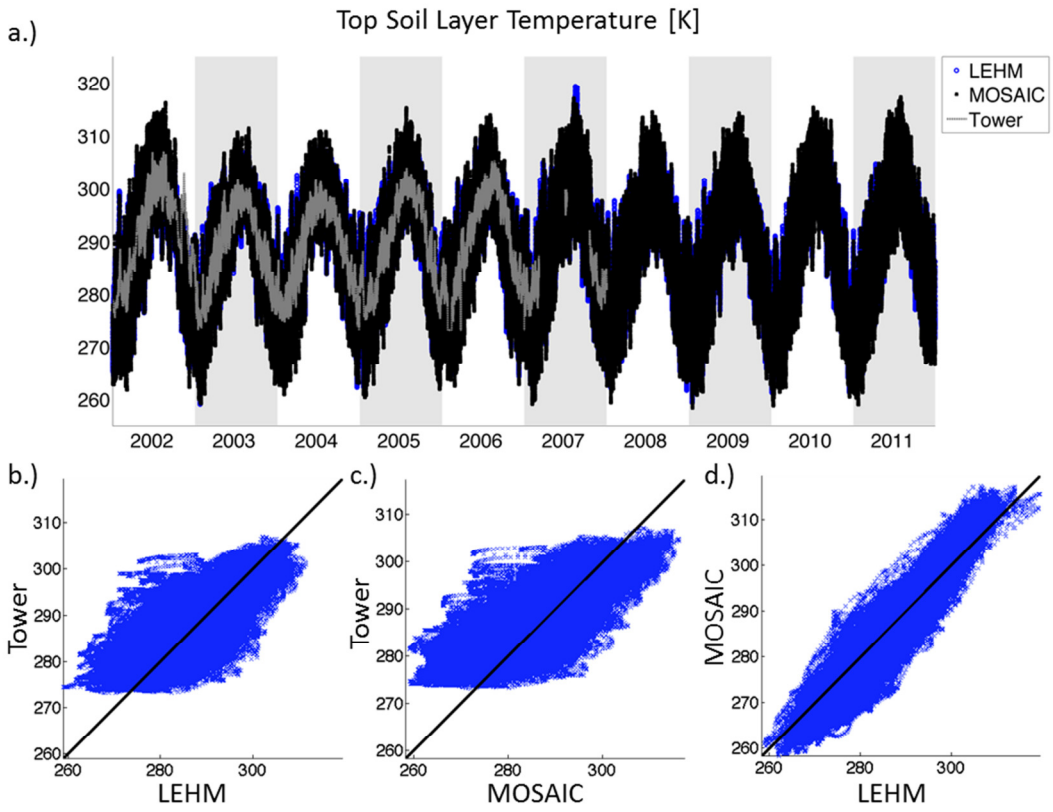

Figure 5-13: Comparison of the soil temperature for the top soil layer between the LEHM (blue), the MOSAIC-NLDAS model of NLDAS (black) and the tower data (grey): (a) time-series over 10 years, (b), (c), (d) scatterplots.

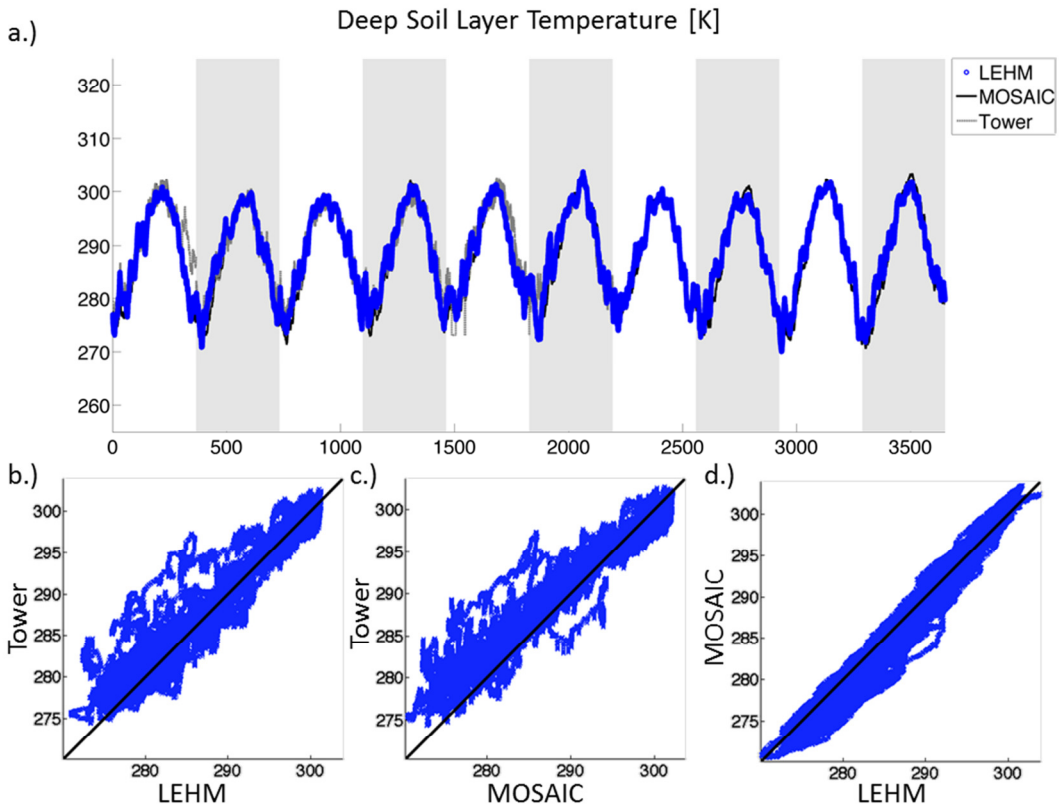

Figure 5-14: : Comparison of the soil temperature for the deep soil layer between the LEHM (blue), the MOSAIC-NLDAS model of NLDAS (black) and the tower data (grey): (a) time-series over 10 years, (b), (c), (d) scatterplots.

Scatterplots shown in Figure 5-15 (a-c) show that the LEHM represents the full range of GPP as measured by the tower, with a low bias. During the winter, the LEHM underestimates vegetation activity with generally 1 $gC/m^2/d$ compared to 2-2.5 for MODIS and the tower.

f

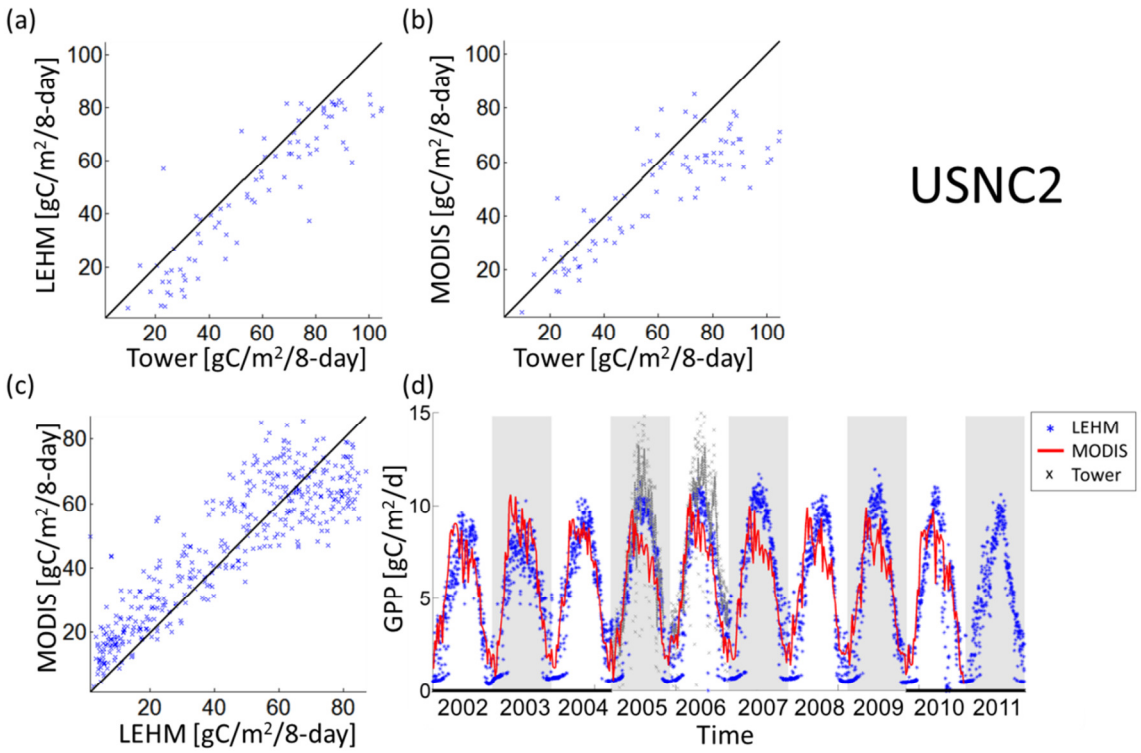

Figure 5-15: US-NC2 site; (a)-(c) scatter plots of 8-day GPP accumulation (gC/m²/8-day) LEHM results against tower and MODIS GPP estimates; (d) 10 years of GPP (gC/m²/day) estimates for the LEHM, MODIS and Tower (level-4; the grey dashed line corresponds to the 10-day running average) from 2002 to 2011. The LEHM is forced using NLDAS and Stage IV resample at 4km spatial resolution and 30min time-steps. MODIS LAI and FPAR at original 1km spatial resolution and linearly interpolated to 30min.

Figure 5-16 through Figure 5-18 show the comparison for the 3 towers in North Florida. The towers are very close in terms of spatial location and, in fact, US-SP2 and US-SP3 fall in the same MODIS 1km pixel, and US-SP1 in the adjacent pixel. Therefore, the model results and the MODIS product exhibit the same behavior. Whereas it is not possible to determine whether fluctuations in tower estimates reflect real variations in

vegetation activity or measurement uncertainty, this example demonstrates well the scaling challenges between tower estimates and the MODIS footprint.

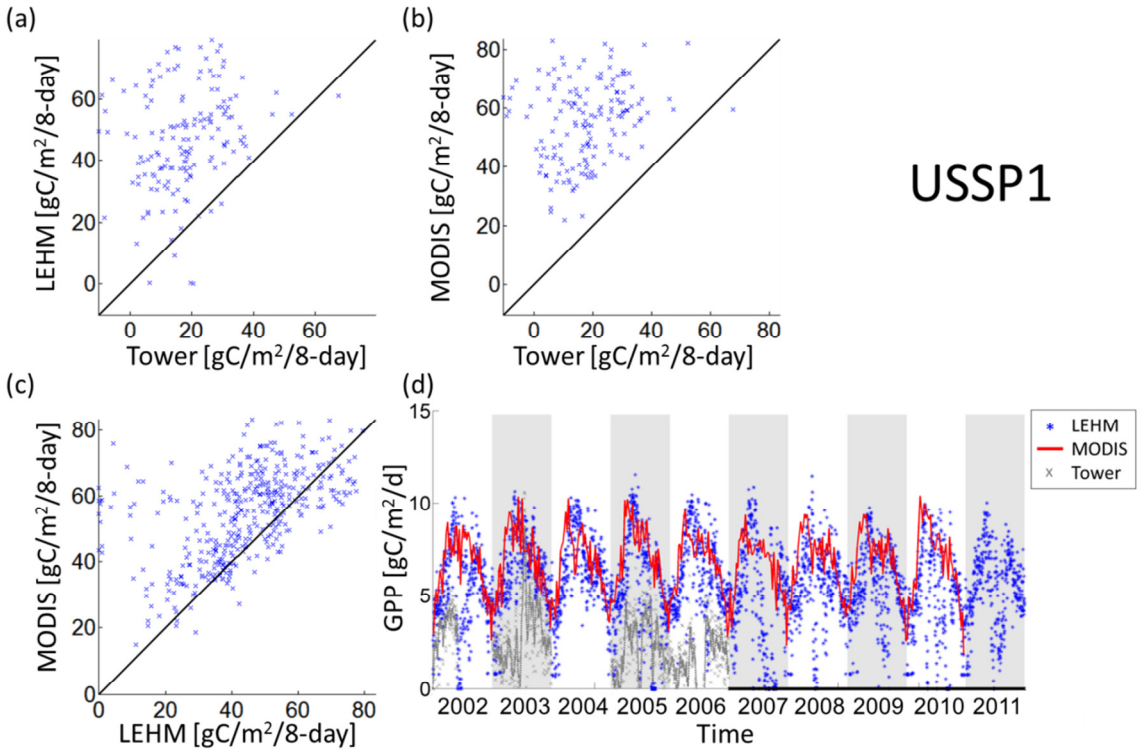

Figure 5-16: Same as Figure 5-15 but for station US-SP1.

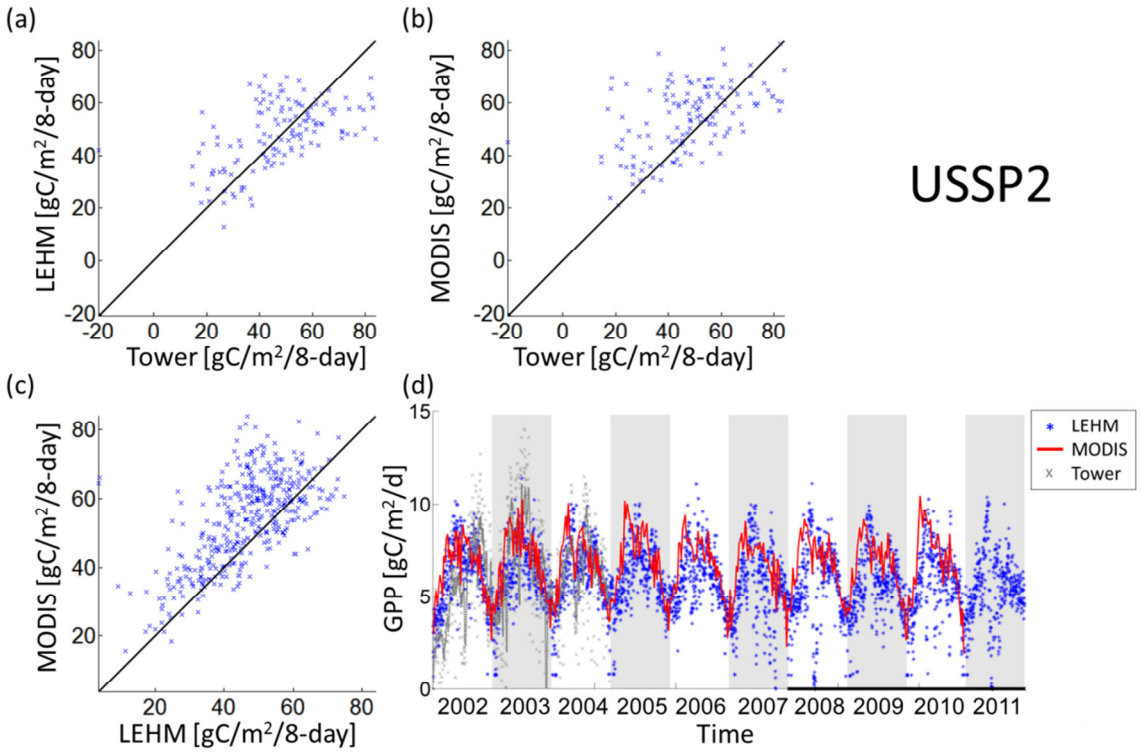

Figure 5-17: Same as Figure 5-15 but for station US-SP2.

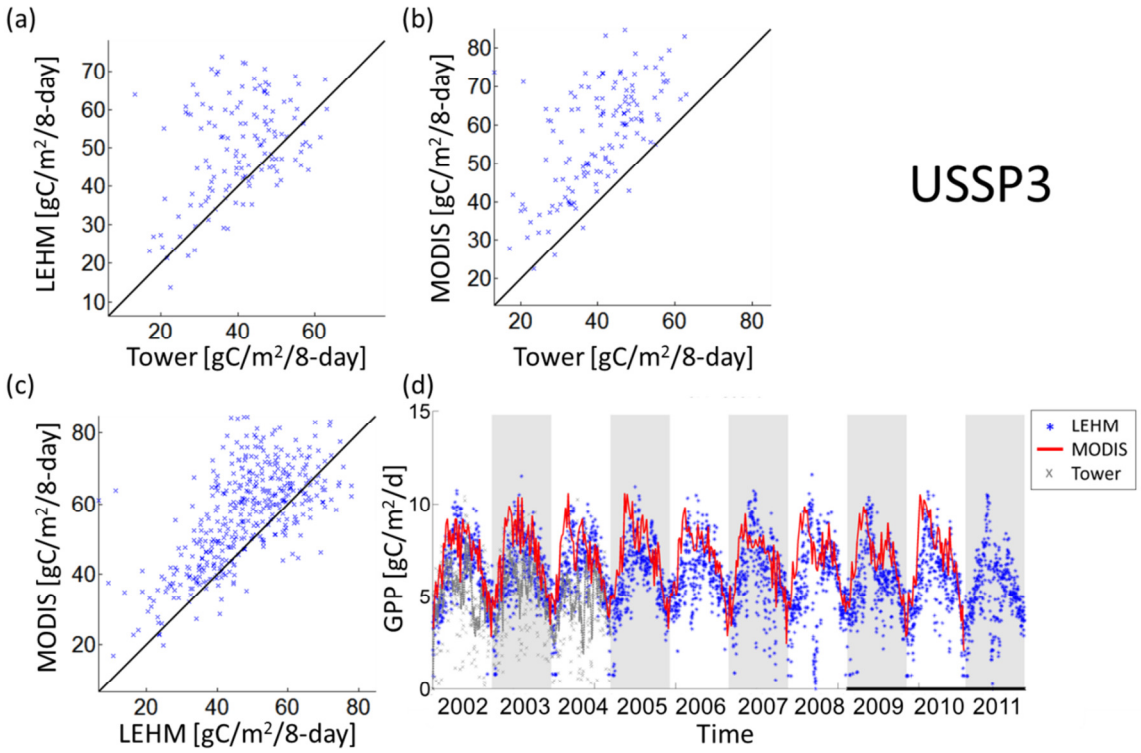

Figure 5-18: Same as Figure 5-15 but for station US-SP3.

In summary, the LEHM generally captures well the phenology and amplitude of vegetation activity over evergreen needleleaf sites. The scatterplots suggest an underestimation of low GPP values during the wintertime compared to the MODIS product. Table 5-6 shows the annual GPP average and standard deviation for the 10 years of simulation. The bold numbers correspond to the year with the highest productivity. At the USSP towers, the MODIS product is systematically the highest estimate (> 7 gC/m²/day). Neither the tower estimates nor the model results exceed 6.45 gC/m²/day, which suggests that MODISS GPP is overestimated at these sites. However, the large variability among the USSP towers despite their geographic proximity highlights the impact of large spatial heterogeneity and footprint length-scale on eddy

covariance estimates. Note also the large standard deviation up to 100% of the annual average. With only one full year of measurements, it is difficult to interpret the results of USNC2.

Table 5-6: Annual GPP mean and standard deviation for the tower, MODIS and the LEHM from 2002 to 2010.

Site	Year	Tower mean	MODIS mean	LEHM mean	Site	Year	Tower mean	MODIS mean	LEHM mean
USNC2	2002	--	5.49	4.87	USSP2	2002	5.36	6.54	**6.09**
	2003	--	**6.10**	5.10		2003	**6.45**	6.87	6.08
	2004	--	5.69	5.39		2004	6.18	6.71	6.08
	2005	6.97	5.46	5.72		2005	--	**6.97**	6.00
	2006	**7.46**	6.03	6.03		2006	--	6.77	5.96
	2007	--	5.70	**6.10**		2007	--	6.46	5.61
	2008	--	5.62	5.39		2008	--	6.74	5.59
	2009	--	5.62	5.68		2009	--	6.74	5.63
	2010	--	5.51	4.61		2010	--	6.73	5.55
USSP1	2002	**3.26**	6.66	5.36	USSP3	2002	5.15	7.03	**6.31**
	2003	2.75	6.85	**6.22**		2003	**5.45**	**7.29**	6.25
	2004	--	6.76	6.15		2004	4.69	7.02	6.25
	2005	2.15	**7.02**	5.45		2005	--	7.26	6.08
	2006	1.47	6.83	6.18		2006	--	7.10	6.19
	2007	--	6.59	4.68		2007	--	6.84	6.10
	2008	--	6.84	5.47		2008	--	7.07	5.82
	2009	--	6.84	5.53		2009	--	7.07	5.70
	2010	--	6.74	4.67		2010	--	7.05	5.68

One of the main advantages of the LEHM is that the coupling between the hydrological processes and photosynthetic activity is dynamic. The soil content water status, the energy balance, and the photosynthesis activity are updated every time-step (30min in our case), thus allowing to fully capture the diurnal cycle of vegetation activity and its response to the water and energy status. Figure 5-19 shows the monthly

averaged diurnal cycle of GPP for the tower US-SP2 for the different years of simulation from 2002 to 2011. The decrease in GPP rate in the afternoon is related to the stomatal conductance limitation. Note the impact of the dry conditions in 2008 and 2011 on the GPP due to low soil moisture and large VPD, which illustrates well the advantage of the fully coupled approach.

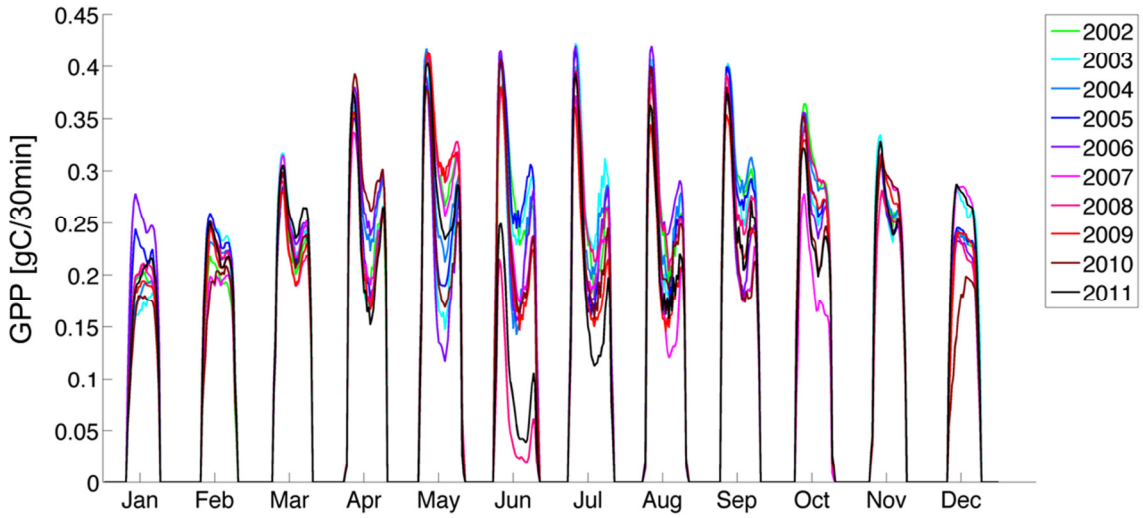

Figure 5-19: simulated GPP Monthly averaged diurnal cycle for the 10 years simulation at the evergreen needleleaf site US-SP2.

5.5.3 Deciduous broadleaf

There are two towers available at locations representative of broadleaf vegetation, and neither Walker Branch (US-WBW) nor Chestnut Ridge (US-ChR) datasets contain GPP estimates during our period of study. Therefore, the inter-comparison presented below is limited to the LEHM and MODIS products. The model represents well both amplitude and phenology over these two sites compared to MODIS. The scatter plots (Figure 5-20a and c) show that MODIS estimates are generally higher than the LEHM

simulation with lower values during the winter time and GPP 8-day accumulation more generally. The inter-annual variability of GPP amplitude is stable with 2007 being the summer with lowest productivity at the Chestnut site.

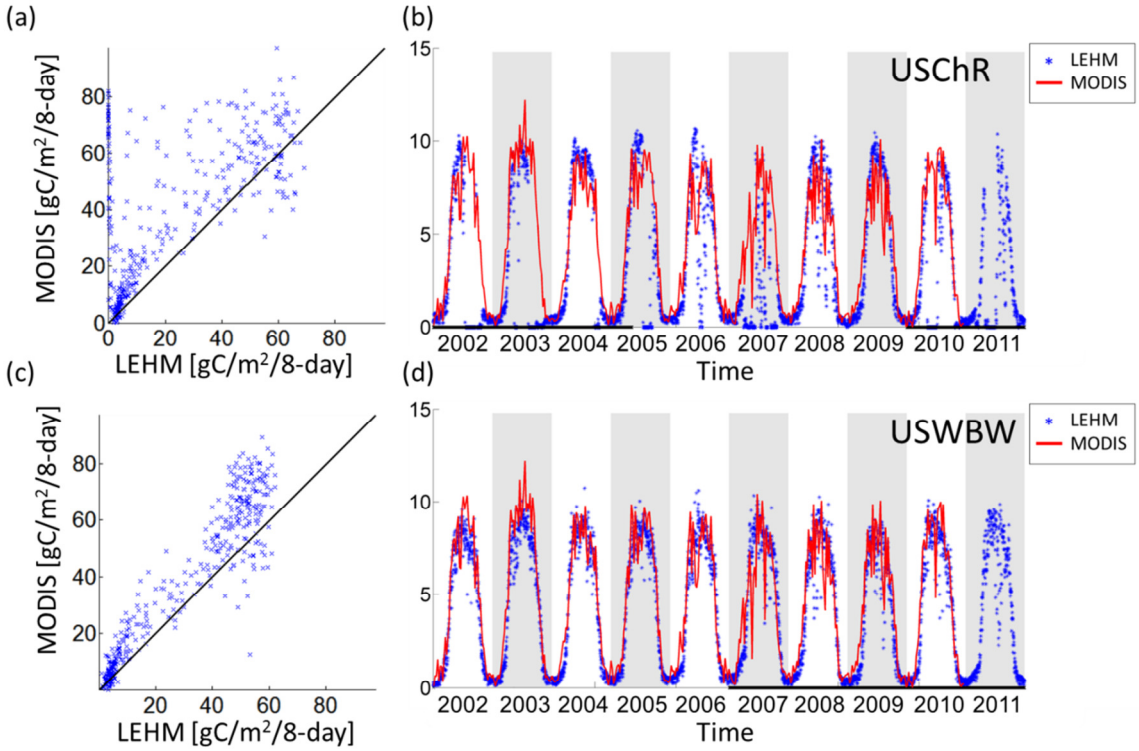

Figure 5-20: Comparison of model and MODIS GPP estimates over deciduous broadleaf trees at the Ameriflux sites: Chestnut ridge – US-ChR (a) scatter plot of 8-day GPP accumulation (gC/m²/8-day) LEHM results against MODIS GPP estimates; (b) 10 years GPP (gC/m²/day) from 2002 to 2011; Walker Branch – USWBW (c) scatter plot of 8-day GPP accumulation (gC/m²/8-day) LEHM results against tower and MODIS GPP estimates; (d) 10 years of GPP (gC/m²/day) estimates for the LEHM and MODIS from 2002 to 2011. The LEHM is forced using NLDAS and Stage IV products resampled at 4km spatial resolution and 30min time-steps. MODIS LAI and FPAR at original 1km spatial resolution and linearly interpolated to 30min.

5.5.4 Grassland

Three towers, US-CaV, US-Dk1 and US-Goo, are located over grassland. Figure 5-21 summarizes the 10-year run over the Cannan Valley site. The model GPP estimates are generally higher during the summer than the MODIS product (again, no tower data are available for comparison). During summer 2006, there is a strong water stress induced decrease that is also moderately captured by the MODIS time-series. The large peak during summer 2007 is due to LAI and FPAR reported by MODIS and it does not represent a true increase in vegetation in the Cannan Valley region. This highlights the importance of the model's dependence on the MODIS LAI product. Nevertheless note that there is not a systematic bias between the LEHM and MODIS, which is the result of nonlinear soil-vegetation-atmospheric interactions.

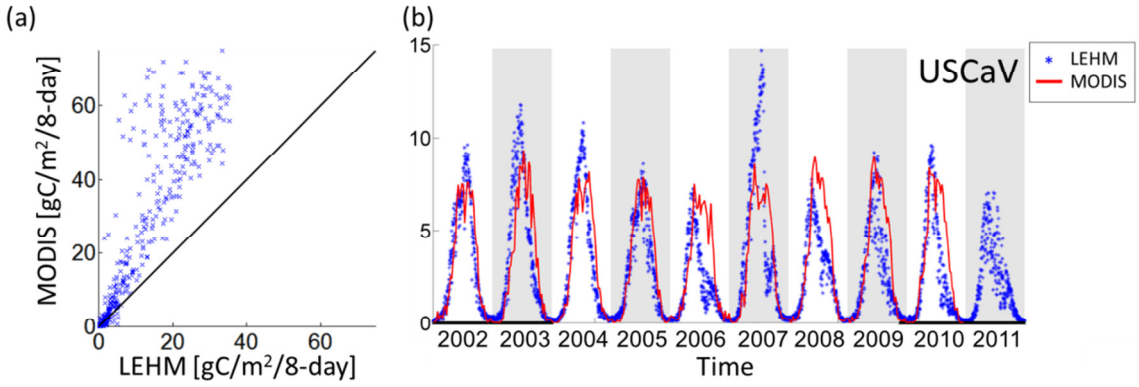

Figure 5-21: Canaan Valley – US-CaV; (a) scatter plot of 8-day GPP accumulation (gC/m²/8-day) LEHM results against and MODIS GPP estimates; (b) 10 years of GPP (gC/m²/day) estimates for the LEHM and from 2002 to 2011. The LEHM is forced using NLDAS and Stage IV resample at 4km spatial resolution and 30min time-steps. MODIS LAI and FPAR at original 1km spatial resolution and linearly interpolated to 30min.

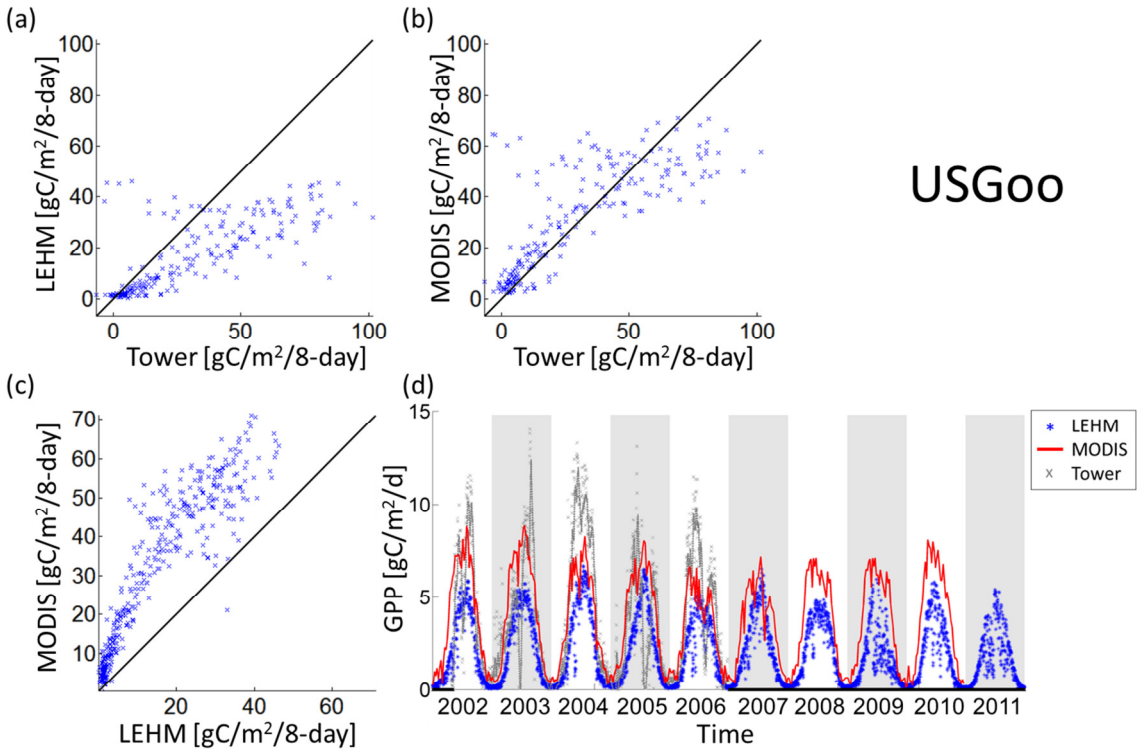

Figure 5-22: Goodwin Creek tower – US-Goo; (a)-(c) scatter plots of 8-day GPP accumulation (gC/m²/8-day) LEHM results against tower and MODIS GPP estimates; (d) 10 years of GPP (gC/m²/day) estimates for the LEHM, MODIS and Tower (level-4; the grey dashed line corresponds to the 10-day running average) from 2002 to 2011. The LEHM is forced using NLDAS and Stage IV resample at 4km spatial resolution and 30min time-steps. MODIS LAI and FPAR at original 1km spatial resolution and linearly interpolated to 30min.

Over the US-Goo station, the simulation strongly underestimates the GPP peak during summertime by almost a factor of 2 compared to tower estimates and by a factor of 1.5 compared to MODIS. In addition to the LAI scaling effect, a number of other factors may also be responsible for the simulated values. First, the kinetic models based on Farquhar's work have been designed for C3 plants and not the C4 plants that are present in grassland. Second, Medlyn et al. (2002) did not provide information for

Vcmax and Jmax for grass, but recommended to keep their A/Ci curve fitting. Therefore, average values from the information provided for cropland were used here. This choice was motivated by the fact that in the SE US cropland and natural vegetation are often a mosaic that will be averaged at the 4km spatial resolution used for the regional run.

Discrepancies between the US-Goo tower measurements and NLDAS and Stage IV were also investigated. There are large differences in climate forcing as illustrated by the scatter plots in Figure 5-23. There is little to no agreement between the Stage IV rainfall and that reported at the tower; the air temperature is significantly higher in NLDAS (up to 10 K); and there is a large bias in incoming shortwave radiation. The shortwave incoming radiation (SWin) is limited to 400 W/m^2 in the NLDAS, but goes up to 600 W/m^2 at the tower. The positive bias in air temperature and negative bias in shortwave radiation indicate that the energy budget cannot be well simulated by the model using the NLDAS forcing. In addition, PAR is calculated as a ratio of the SWin, and thus this will further lead to lower GPP in the model as the Arub rate is artificially decreased (see Section 5.4.1.2).

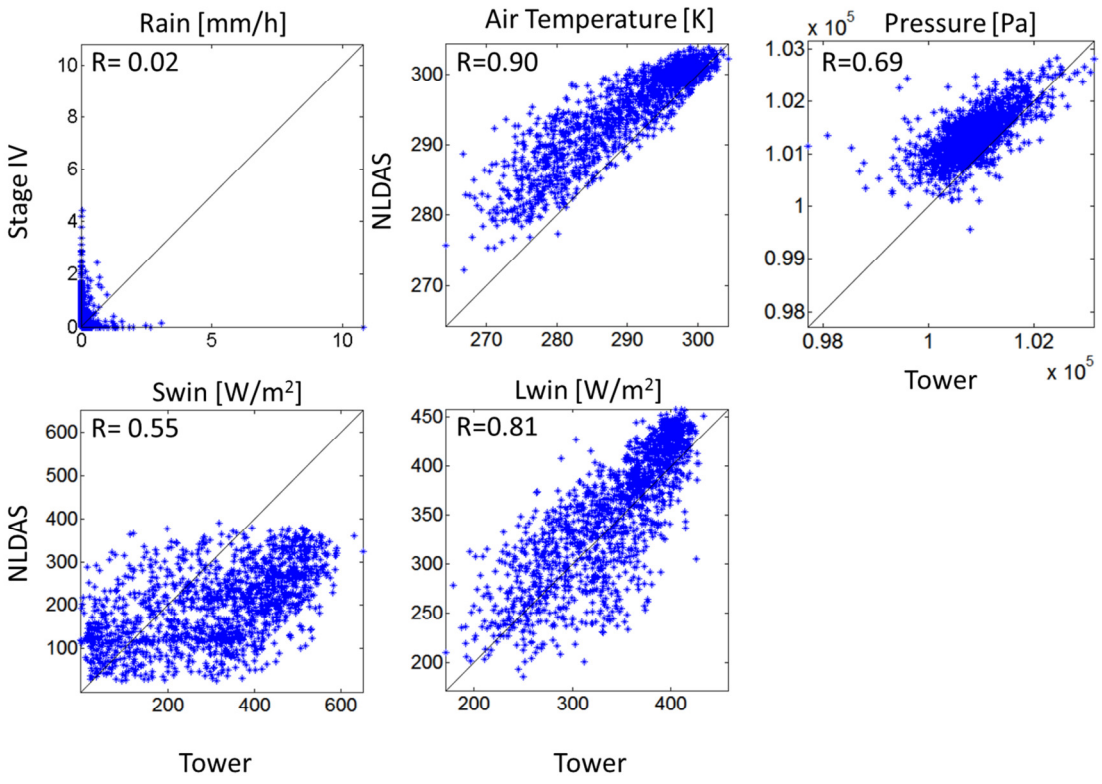

Figure 5-23: Comparison between the tower measurements and the NLDAS forcing used to run the model at USGoo site.

Another major forcing is the use of MODIS LAI and FPAR to represent the phenology in the LEHM. The US-Goo site is a good example of the implications of the spatial variability of LAI around a site. Figure 5-17a shows the spatial variability of MODIS LAI in the 7x7km^2 centered on the tower. Figure 5-17b shows the time-series of gap-filled/smoothed LAI time-series using TIMESAT at 1km at the tower location, the minimum LAI time-series and maximum in the 7x7km^2.

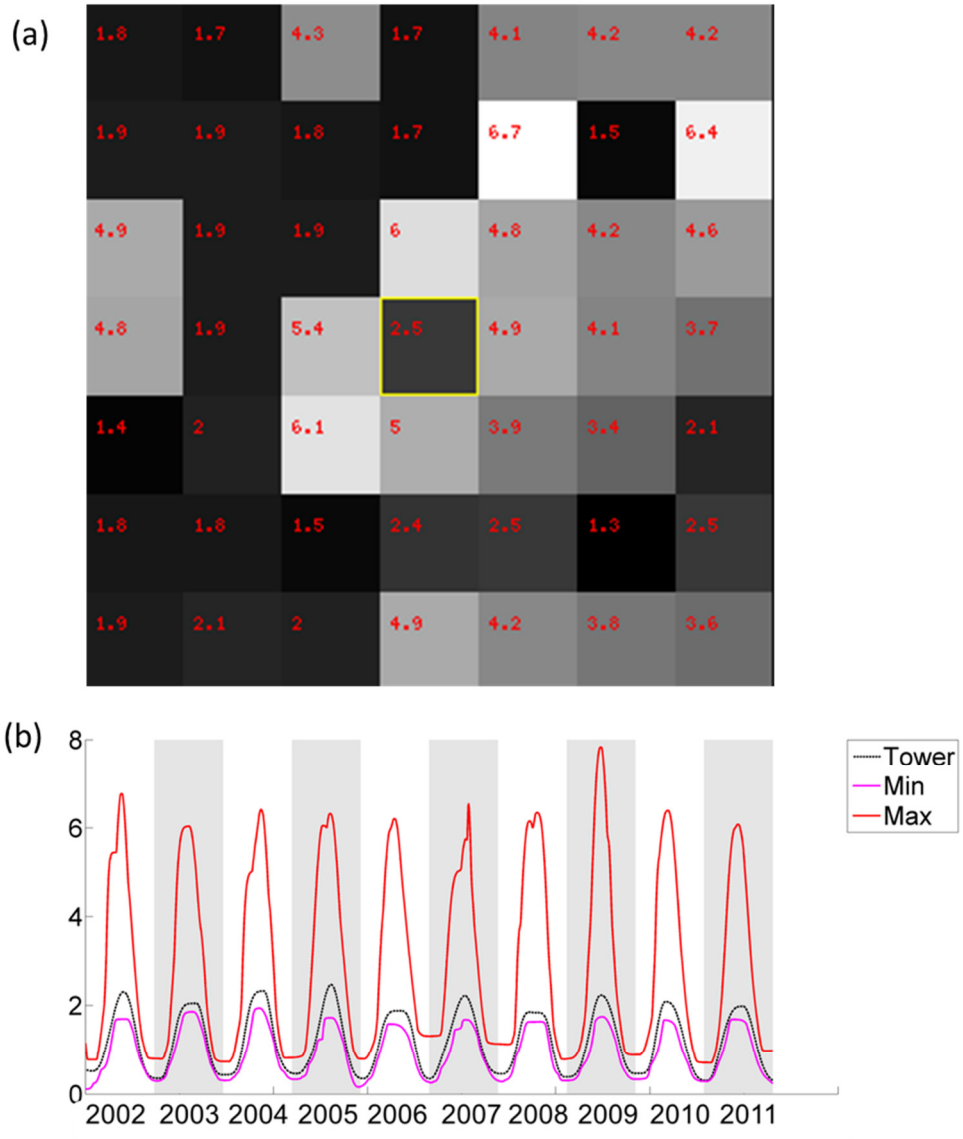

Figure 5-24: (a) Spatial variability of LAI in a 7km squared area around the US-Goo tower (yellow square) for the period of Aug. 5, 2003 - Aug. 12, 2003 (source: http://daac.ornl.gov/cgi-bin/MODIS/GR_col5_1/grid.slim.pl); (b) LAI time-series variability from 2002 to 2011 for the pixel above the tower (black line), the minimum LAI in the 7x7km² area (magenta line), and the maximum (red line).

Due to the scaling from leaf-scale processes to the whole canopy, this variability has a large impact on GPP estimates. Figure 5-25 shows the impact of LAI and FPAR variability on the LEHM simulation showing the corresponding range of GPP

simulation. The maximum LAI/FPAR time-series produced GPP estimates above the tower and MODIS estimates with a seasonal peak of 13 gC/m²/d, while the minimum LAI time-series produces a seasonal peak of 4.5gC/m²/d. The minimum time-series is closer to the pixel tower based simulation, suggesting the tower estimates is in the higher range of LAI. This example illustrates well –the challenge of comparing tower estimates having a certain footprint, with remote sensing and numerical model estimates due to the large spatial variability surrounding the tower sites.

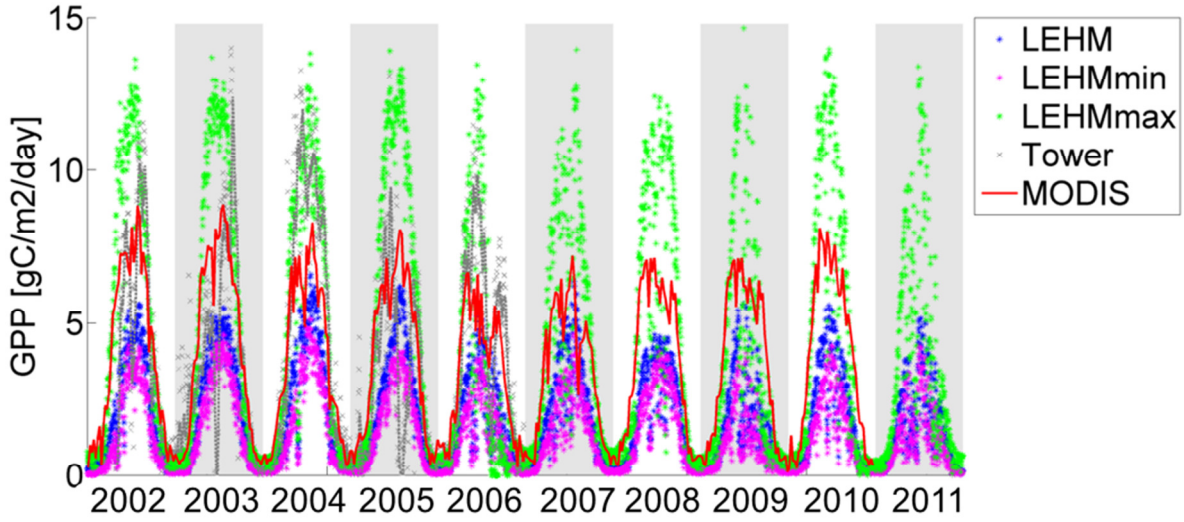

Figure 5-25: Impact of LAI variability on GPP simulations. The magenta and the green time-series from 2002 to 2011 correspond to GPP simulations that were forced using respectively the minimum and maximum LAI and the corresponding FPAR time-series in the 7x7km² area centered on the US-Goo tower.

Although classified as grassland, the open field Duke site (US-DK1) is surrounded by forested areas that appear to strongly impact the simulation and MODIS, since the GPP magnitude and temporal evolution are similar to those reported for the forest towers. The LEHM and MODIS estimates tend to remain below 10 gC/m²/day (i.e. about 80gC/m²/8-day) whereas the tower estimates as are high as 120 gC/m²/8-day.

During the winter, the model consistently yields lower GPP values compared to MODIS estimates and tower measurements. Note there is higher within season variance in the tower estimates during the summer and the winter, and some unrealistically low or high values are reported but no quantitative assessment of uncertainty is provided with the data.

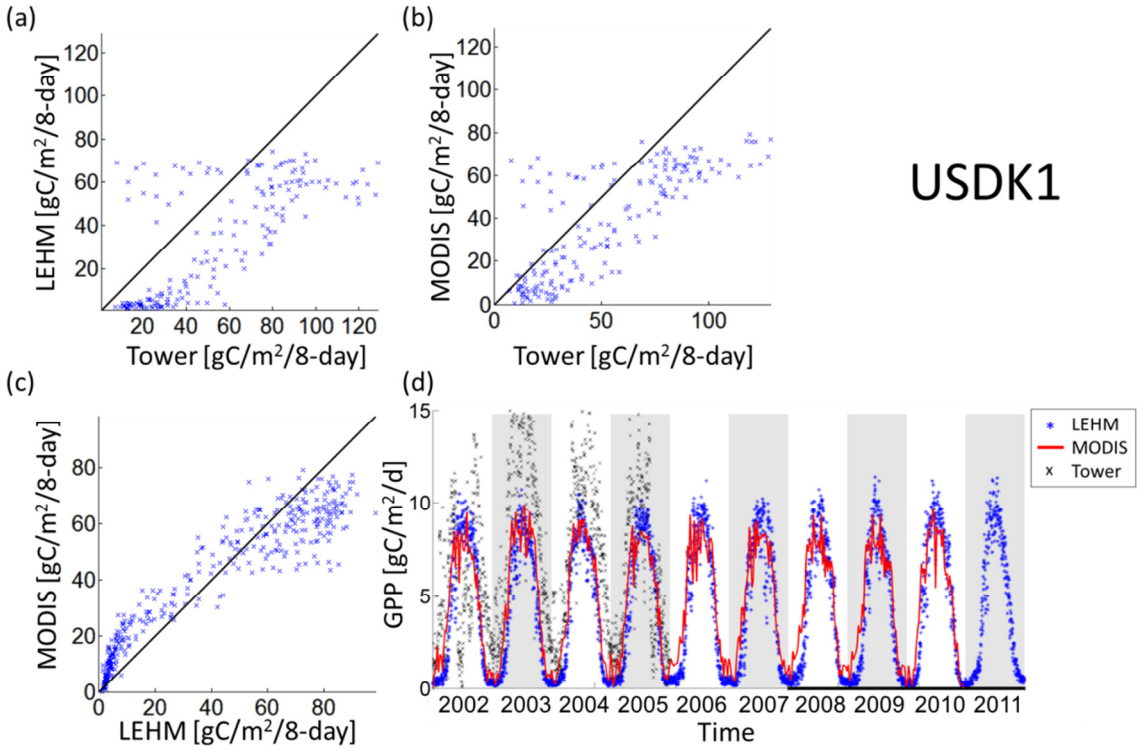

Figure 5-26: same as Figure 5-22 for Duke tower US-DK1

Thus, we expect the model to tend to underestimate GPP over grassland and cropland areas, with this effect being dependent on LAI.

5.5.5 General comparison

Figure 5-27 shows the comparison between the tower and LEHM annual averaged GPP at each site: between tower estimates and LEHM (a), tower and MODIS

(b) and MODIS and LEHM (c). MODIS and the LEHM are generally in good agreement with a Root Mean Square Error (RMSE) difference of 1.42 gC/m²/day, where the LEHM estimates are lower than MODIS. Concerning the towers, the comparison is limited to the years when data are available. The RMSE between MODIS and the towers is 2.45gC/m²/day, and between the LEHM and the towers is 2.13 gC/m²/day. The four lowest points correspond to the USGoo grassland site, where the large discrepancies were attributed to atmospheric forcing. The LEHM results compare favorably with other estimates from uncalibrated models (e.g. Chen et al. 2011 and Yang et al. 2007 with RMSEs slightly above 3.0gC/m²/day). Note however that previous studies did not typically use SE Ameriflux towers for validation of GPP models.

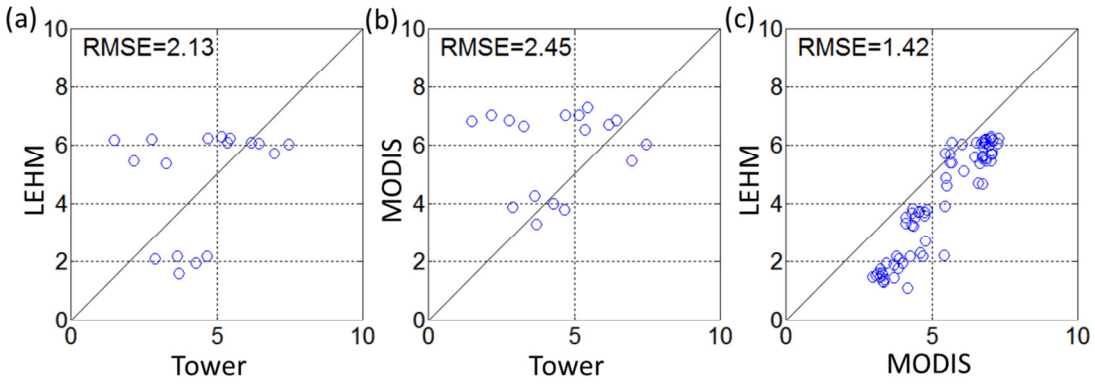

Figure 5-27: Annual averaged GPP comparison for the tower and the LEHM (a), the tower and MODIS (b), and MODIS and the LEHM (c) for all the towers with GPP level-4 data. Units are gC/m²/day.

5.6 Phenology Module Implementation

5.6.1 Description

The link between the phenology module and the model is the vapor pressure deficit as computed by the model, incoming shortwave radiation, and the 2m air temperature necessary to the computation of GSI.

MODIS FPAR and LAI are also used on a pixel basis to extract the necessary $FPAR_{\min}$, $FPAR_{\max}$, and $FPAR_{sat}$ from the 10years MODIS time-series used to force the Model so far. The $FPAR_{\min}$ is taken as the average from January to February for each of the 10 years climatology, and not the absolute min, since the very low values due to atmospheric conditions in the winter time induce instabilities in the numerical solution. The $FPAR_{\max}$ is taken as the maximum of the 10 years climatology, and the $FPAR_{sat}$ as the absolute maximum of the 10 years.

5.6.1 Phenology model evaluation

The module was tested over 3 Ameriflux sites that cover different PFTs: US-Goo for grassland, US-ChR for deciduous broadleaf and US-SP2 for the evergreen needleleaf. The growth and senescence factors were taken from Table 5-7 (adapted from Stockli et al., 2011) as mentioned earlier. Figure 5-28a shows the GSI index from 2002 to 2011 and the three functions used to compute it: fTM represent the sensitivity to air temperature, fRg to the incoming the radiative forcing and fVDP to the vapor pressure deficit.

Table 5-7: Coefficient used for growth γg and senescence γd factors (Stockli et al., 2011)

PFT	γ_g (days^{-1})	γ_d (days^{-1})
Trees: temperate evergreen needleleaf	0.19 ± 0.02	0.19 ± 0.02
Trees: temperate evergreen broadleaf	0.45 ± 0.04	0.05 ± 0.00
Trees: temperate deciduous broadleaf	0.57 ± 0.03	0.42 ± 0.02
Shrubs: evergreen broadleaf	0.36 ± 0.04	0.31 ± 0.04
Shrubs: temperate deciduous broadleaf	0.49 ± 0.04	0.43 ± 0.03
Grass: non-Arctic c3	0.47 ± 0.02	0.37 ± 0.02
Grass: c4	0.55 ± 0.03	0.13 ± 0.01

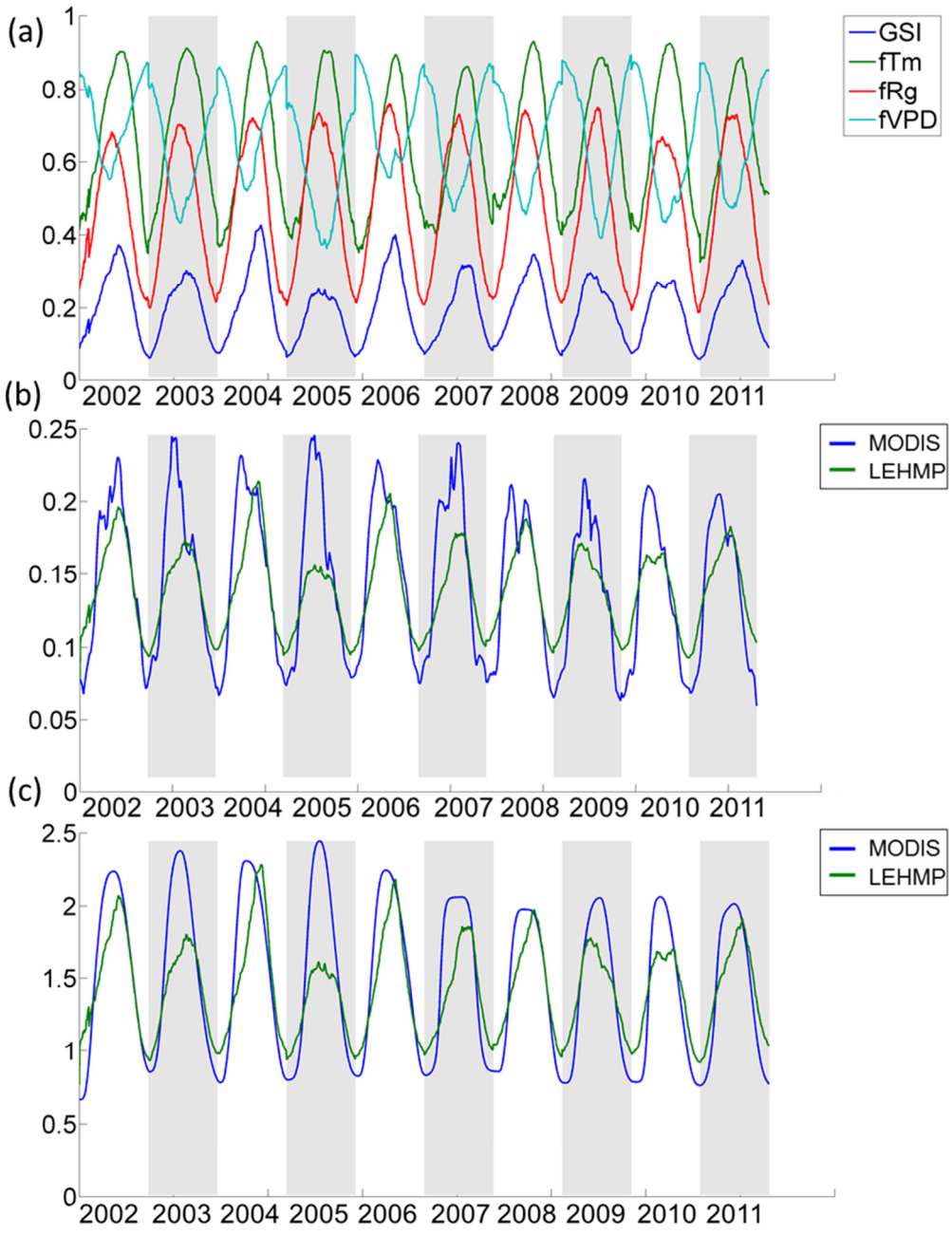

Figure 5-28: Phenology simulation over US-Goo (GRA); (a) GSI and its component, (b) FPAR from MODIS (in blue) and model results (in green), (c) LAI (in blue) and model results (in green).

Figure 5-28b-c compare the MODIS FPAR and LAI (in blue) to the simulated FPAR and LAI (in green). Over grassland, the model tends to simulate an accurate start and end of the growing with generally a late peak in the summer that MODIS

measurement. The range of the modeled FPAR and therefore LAI is smaller with a peak reaching 0.2 when MODIS estimates go to 0.25. In the winter time, the simulated FPAR is generally higher than MODIS. I can be due to the fact we did not used the absolute minimum but the average over January and February. The inter-annual variability of the model, which is dependent on the GSI (Figure 5-28a), does not match MODIS variations. For example the low values during the summer, which are due to VPD, did not translate into an observed vegetation stress.

Figure 5-29 shows the comparison for the US-SP2 over evergreen needleleaf forest. The range of the modeled FPAR agrees well with the MODIS estimates during the first years, after that MODIS range tends to be larger. The phenology is captured with correct timing. The modeled LAI is larger than MODIS suggesting the computed vegetation fraction is compensating the lower FPAR values. Interannual variability is limited in both MODIS and the modeled parameters.

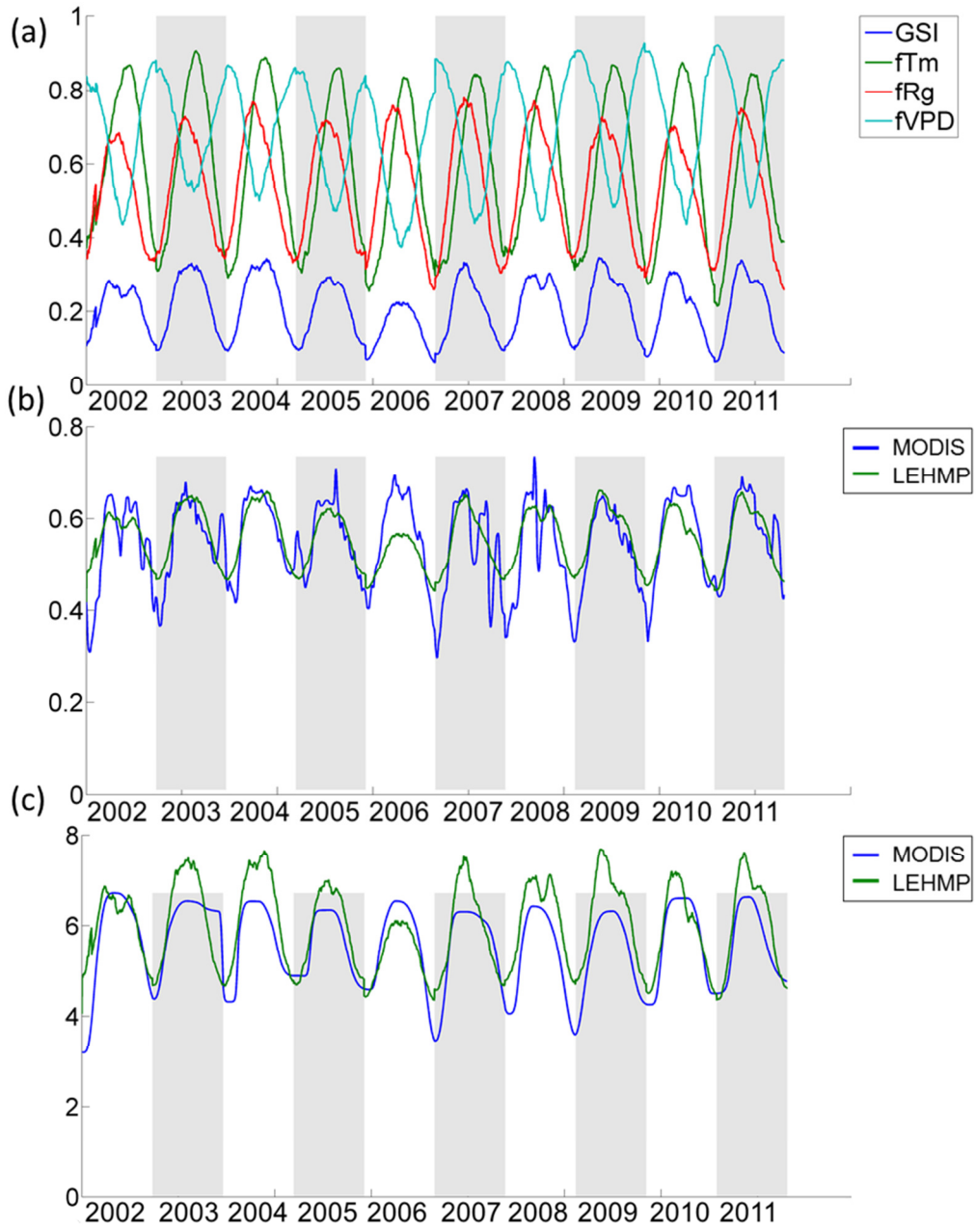

Figure 5-29: Phenology simulation over US-SP2 (ENF); (a) GSI and its component, (b) FPAR from MODIS (in blue) and model results (in green), (c) LAI (in blue) and model results (in green).

Figure 5-30 shows the same comparison but for the US-ChR over deciduous broadleaf forest. The same patterns are observed as for grassland, with a narrower ranges of variability, lower peak values and higher winter values. Again the modeled

FPAR inter-annual variability is mainly due to the VPD limitations during the summer time.

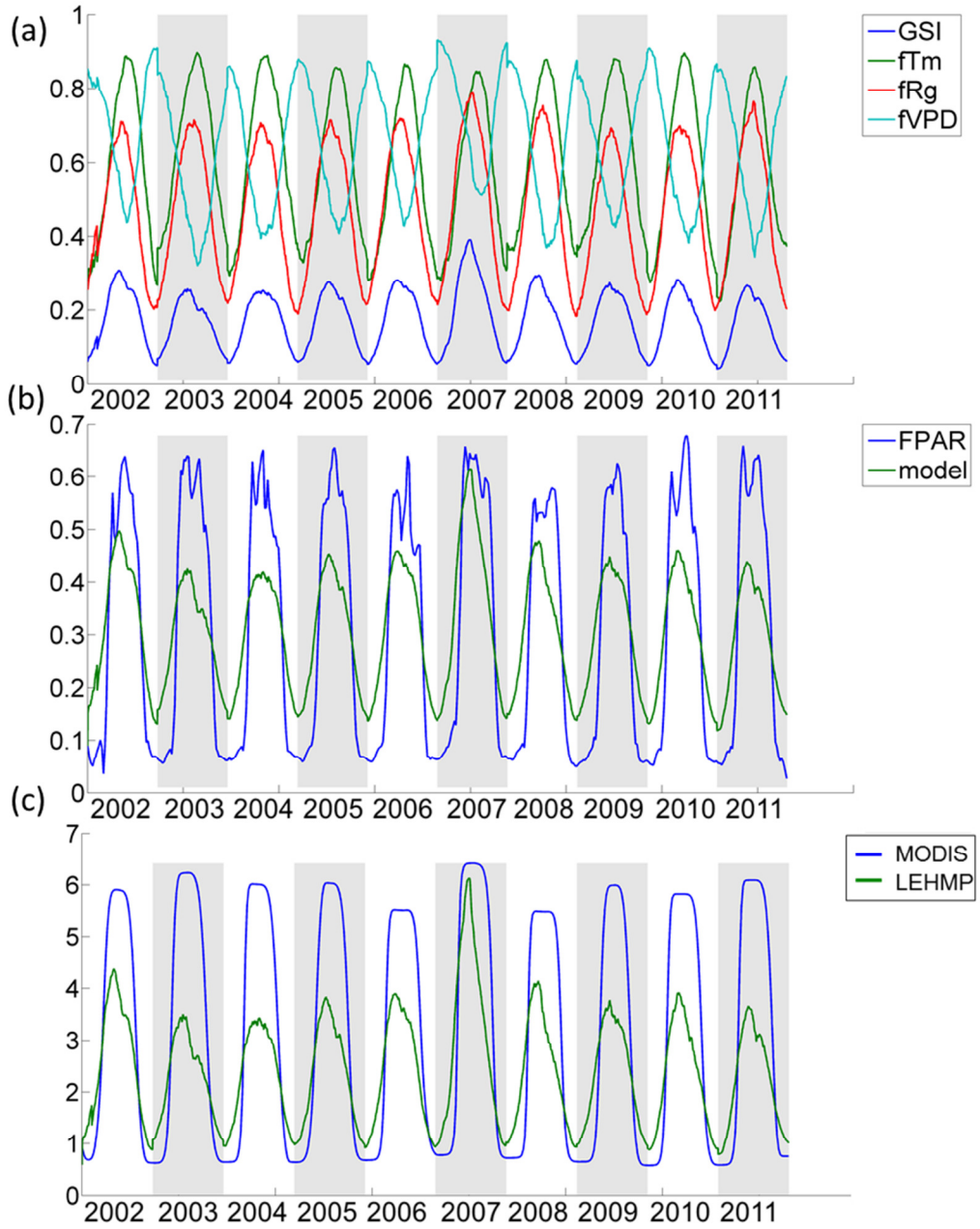

Figure 5-30: Phenology simulation over US-ChR (DBF); (a) GSI and its component, (b) FPAR from MODIS (in blue) and model results (in green), (c) LAI (in blue) and model results (in green).

Generally, the simulated FPAR varies over a narrower range than the MODIS FPAR. The inter-annual variability is strongly dependent on the VPD, suggesting that species dependent coefficients are necessary to better represent stomatal behavior. Sensitivity analysis with regard to the growth and senescence rates (not shown) indicated limited response. We also tested the sensitivity of the scaling from FPAR to LAI which is dependent of the vegetation fraction, and the sensitivity to the vegetation fraction. Figure 5-31 illustrates the impact of the vegetation fraction on the LAI estimation. The green shaded area represents the variations in LAI when the vegetation faction is reduced to 85% of its original value computed as the ratio $FPAR_{max}/FPAR_{sat}$. Note that in this approach the vegetation represents the maximum vegetation fraction and it does not vary with time. For the same FPAR, a decrease of vegetation fraction is compensated by an increase of LAI to conserve biomass. In other words with a vegetation fraction of 1, the model estimates the minimum LAI.

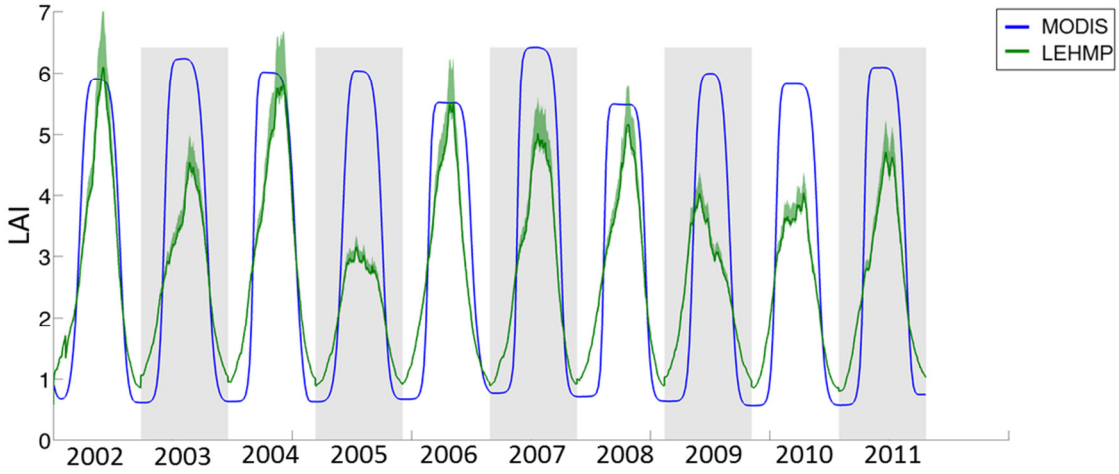

Figure 5-31: Sensitivity of simulated LAI by the LEHMP to the vegetation fraction. The green area represents LAI variability as function of 85% variation of vegetation fraction.

5.6.1 LEHM with phenology

An independent test was conducted to use the simulated FPAR and LAI to force the LEHM at the USChR tower. Figure 5-32 shows the 10-year LEHM simulation with predicted phenology (LEHM-P) as compared to the simulation using MODIS phenology (LEHM). There is a net underestimation of the GPP during the growing season due to the lower LAI values computed by the model. However, in the wintertime, the combination of the higher FPAR and LAI values increase the model GPP even above MODIS estimates producing more realistic behavior. Note that GSI uses similar stress functions as those used in the algorithm of MODIS GPP product based on minimal daily temperature and vapor pressure deficit.

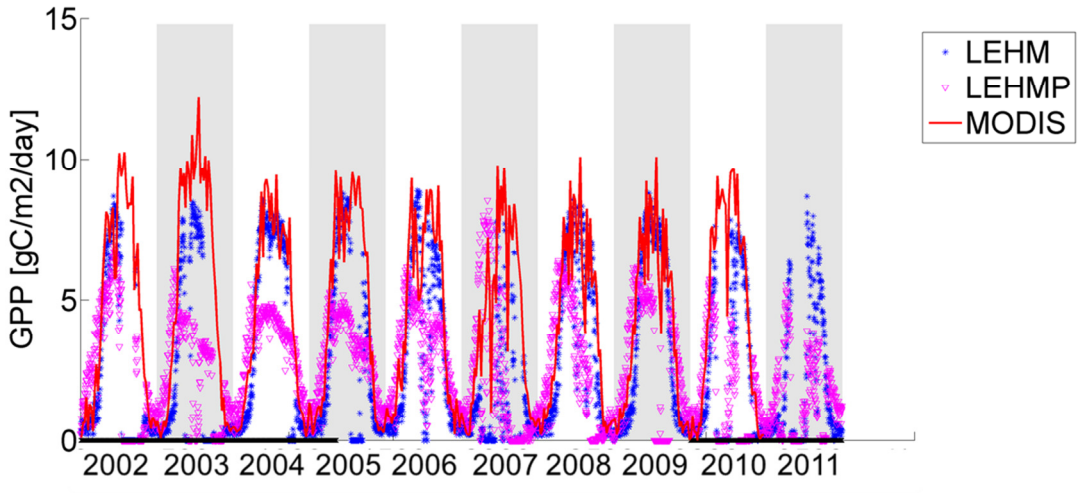

Figure 5-32: Model simulation using the FPAR and LAI computed by the phenology module over the US-ChR site. Red line MODIS, blue stars LEHM forced with MODIS, magenta triangle LEHM using the phenology module (LEHMP).

Figure 5-33 shows the simulated GPP forcing the LEHM with the simulated FPAR and LAI at US-SP2. At this location, the model results follow closely the tower

estimates. The higher FPAR values during winter time compared to the MODIS values (Figure 5-29) explain the increase in the simulated GPP during winter time.

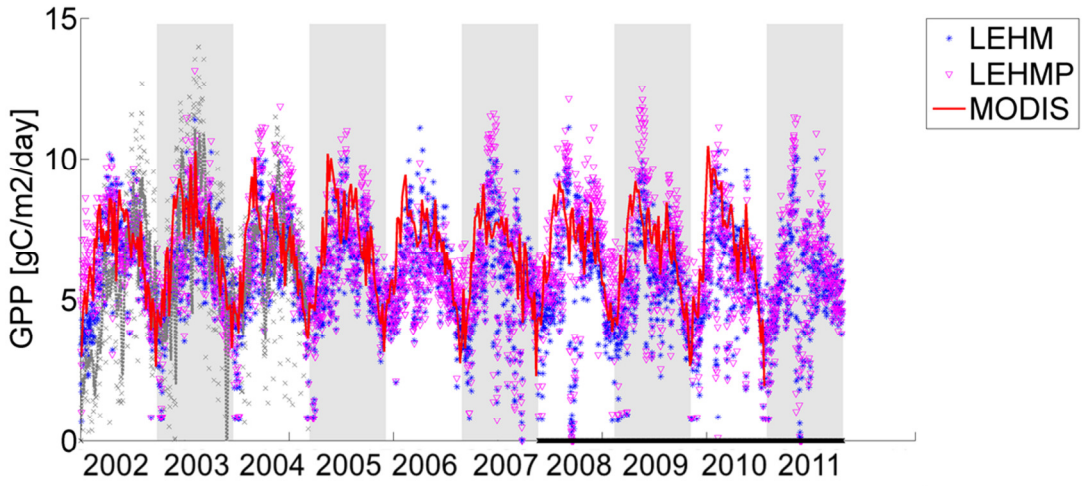

Figure 5-33: Model simulation using the FPAR and LAI computed by the phenology module over US-SP2. Red line MODIS, blue stars LEHM forced with MODIS, magenta triangle LEHM using the phenology module (LEHMP).

Figure 5-34 shows the same simulation using the FPAR and LAI computed by the phenology module at USGoo. As discussed previously, the distinctive LEHM performance (strong underestimation) at this location reflects the inconsistency of the NLDAS-Stage IV atmospheric forcing and the local hydroclimate as reported at the tower. We can see the impact of the smaller range of FPAR limiting the scaling of photosynthetic activity during the active period and but increasing the activity during the cold season. The simulated FPAR also introduces an earlier start of the growing season and delays the ending.

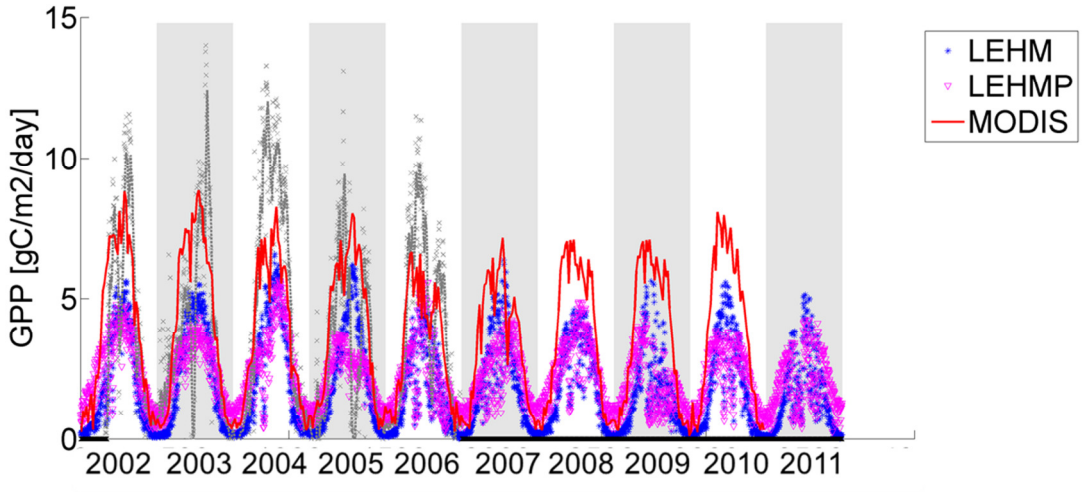

Figure 5-34: Model simulation using the FPAR and LAI computed by the phenology module over US-Goo. Red line MODIS, blue stars LEHM forced with MODIS, magenta triangle LEHM using the phenology module (LEHMP).

Although further investigation will be needed to enhance the scaling of the FPAR as a function of plant functional types, the GSI combined with FPAR and LAI climatology from MODIS and NLDAS atmospheric forcing captures well the start and the end of the growing season. The sensitivity to VPD during the summer induces inter-annual variability in simulated FPAR time-series that is not present in the MODIS estimates. However, since VPD is already implemented in the model stomatal function, modification of the GSI to avoid possible double-counting the influence of VDP should be conducted.

5.7 LEHM Regional-Scale Simulations

It is important to stress that the coupling between the water and energy balance and the photosynthetic activity in LEHM is principally driven by the stomatal conductance, which is a function (among other parameters, see Equation 5.25) of water

availability in the soil and water vapor deficit. Therefore, discrepancies between the LEHM simulated GPP and the MODIS GPP product are expected not only because of differences in hydrometeorological forcing, but also because the MODIS GPP algorithm does not capture soil moisture feedbacks, and the light use efficiency parameter is a function of the minimum air temperature and the vapor pressure deficit from the NASA Data Assimilation Office (DAO) products at much coarser resolution. It is also well established that satellite-based products have large uncertainties over mountainous regions principally due to shade and other sun angle effects, combined with DAO dataset potential bias regarding orographic precipitation, temperature, and cloudiness among others (Gebremichael and Barros, 2006).

Another critical, source of variability is the spatial heterogeneity (topography, soils, vegetation cover), that affects the surface water and energy budgets, surface radiometric properties and soil moisture distributions which pose a major challenge for upscaling biophysical and hydrological processes to the spatial resolution of GPP products and the LEHM simulations. As mentioned earlier, the soil texture and the land cover are used in combination of different look-up-tables to derive the necessary parameters for the LEHM. However the aggregation to larger scales of thematic data such as land cover is always challenging and is expected to impact the model capabilities. In addition, LAI averaging to 4km is expected to decrease significantly the GPP simulated at the regional scale. This is illustrated by the example shown in Figure 5-35 for an open grass field at Duke Forest (US-DK1 tower). At this site, and using the rule of the predominance, the land cover at 4km resolution is described as evergreen needle-leaf forest instead of an

open field as it is in reality, which impacts the choice of Vcmax, Jcmax, minimal stomatal resistance and the roughness length parameters. The soil properties are also different. The soil at the tower is described as a sandy loam texture, but at 4km it is classified as a clay loam. Note that in the warm season the 4km LEHM grid simulation exhibits a systematic bias of about 3 gC/m²/day. In the cold season, model GPP is controlled by hydrometeorological forcing which is the same here except for spatial interpolation.

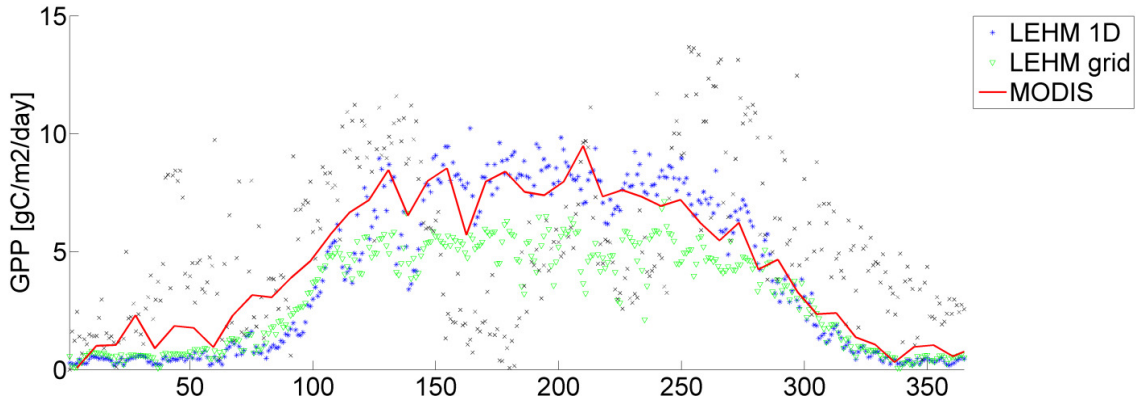

Figure 5-35: Scaling effects due to spatial heterogeneity between the LEHM simulation using the soil and vegetation types as described in the metadata for the Ameriflux Duke tower 1 (USDK1) and the MODIS FPAR and LAI products at 1 km (in blue) compared to LEHM results at 4km resolution using the predominance criterion for aggregation of categorical data and the spatial average for quantitative attributes (in green), and MODIS 1km GPP product (in red).

5.7.1 GPP inter-annual variations

Figure 5-36 shows the annual accumulated GPP in kgC/m²/year for the 10-year simulation effectuated using the model in a grid mode. Note that in this version of the LEHM there is no lateral flow routing (Yildiz and Barros, 2005; Yildiz and Barros, 2007), each pixel being an independent column, therefore underestimation of soil moisture in the alluvial plain is expected during heavy rainfall events when interflow and

subsurface flow processes redistribute moisture in the landscape. Croplands areas exhibit limited annual GPP compared to the natural vegetation (<0.3 kgC/m^2/year), see Figure 2-1 for land cover spatial distribution. This is due to a shorter growing season due to harvest. Earlier, the intercomparison among MODIS, LEHM and Tower EC-based (Eddy–Correlation) estimates indicated that the model tends to underestimate the GPP over agricultural lands. The Atlantic Coastal Plains, which are mainly a mosaic of natural, urban and cropland, show comparatively low annual GPP. Over North Florida and forested areas north of New-Orleans as well as west of the Mississippi are the most productive areas with a total annual GPP reaching 2.5 kgC/m^2/year. In the central southeast the modeled GPP ranges between 0.8-1.3 kgC/m^2/year. Table 5-8 summarizes the annual GPP statistics per land cover class for the 10-year simulation. As mentioned eralier, the evergreen forested areas are the most productive. Evergreen broadleaf forest is the land cover that produces the highest GPP simulated by the LEHM with a 10-year average of 1.34 kgC/m^2/year followed by the evergreen needle-leaf forest. Permanent wetlands, cropland and sparse vegetation are the three land cover classes with the lowest productivity. Across all the land cover classes, 2003 is the most productive year (sometimes equally with 2004). 2002, 2009 and 2011 are the three years with the lowest productivity reflecting severe water stresses in the warm season.

Table 5-8: Land cover statistics for the annual GPP simulated by LEHM

Land cover	2002	2003	2004	2005	2006	2007	2008	2009	2010	2011	Mean	SD
evergreen needle-leaf forest	1.11	1.16	1.14	1.14	1.10	1.12	1.11	1.01	1.07	1.02	1.10	0.05
evergreen broadleaf forest	1.35	1.41	1.39	1.39	1.36	1.36	1.36	1.25	1.31	1.24	1.34	0.06
deciduous needle-leaf forest	0.66	0.70	0.70	0.70	0.68	0.65	0.65	0.66	0.68	0.64	0.67	0.02
deciduous broadleaf forest	1.07	1.11	1.10	1.11	1.08	1.07	1.07	1.03	1.08	1.04	1.07	0.03
mixed forest	1.02	1.07	1.06	1.07	1.03	1.03	1.03	0.94	1.00	0.94	1.02	0.05
shrubland	0.85	0.90	0.89	0.89	0.85	0.84	0.84	0.78	0.82	0.78	0.84	0.04
woody savannas	1.05	1.12	1.11	1.10	1.05	1.05	1.07	0.98	1.02	0.95	1.05	0.05
grasslands	1.01	1.09	1.11	1.06	0.98	1.05	1.07	0.96	1.00	0.88	1.02	0.07
permanent wetlands	0.48	0.51	0.51	0.50	0.47	0.49	0.46	0.43	0.47	0.46	0.48	0.03
croplands	0.40	0.43	0.45	0.42	0.40	0.40	0.42	0.39	0.39	0.36	0.40	0.03
cropland/natural vegetation mosaic	0.72	0.76	0.76	0.76	0.73	0.70	0.72	0.67	0.70	0.67	0.72	0.03
barren or sparsely vegetated	0.30	0.36	0.34	0.34	0.32	0.32	0.29	0.30	0.30	0.30	0.32	0.02

To further investigate the inter-annual variations in GPP, the relative difference between each year and 2003 was computed. The year 2003 was selected, because it was a very wet year during which hurricane activity contributed only modestly to the precipitation totals (Brun and Barros, 2013; see Figure 4-4). Figure 5-37 shows the relative difference between GPP in all other years and 2003 values, where warm colors indicate an increase of GPP compared to 2003, and cold colors indicate a decrease. The strong variations in the Mississippi alluvial plain are attributed to low values of NDVI and LAI due to the small values of GPP for cropland. The constant increase of GPP in the northwest sector of the study domain for all the years reflects the low GPP baseline over the area in 2003. The year 2002 which is at the end of the first major drought of the 21st century shows generally lower GPP over the Coastal Plains; whereas 2004 and 2005 exhibit a slight decrease in annual GPP compared to 2003; and in 2007, which was a very dry year in the SE, there is a moderate decrease in GPP over most of the Coastal Plains and especially in the central part. In 2009 and 2011, the GPP decrease is more pronounced than in 2007 for the Coastal Plains reflecting summertime drought, and over Texas in response to the big drought of 2011.

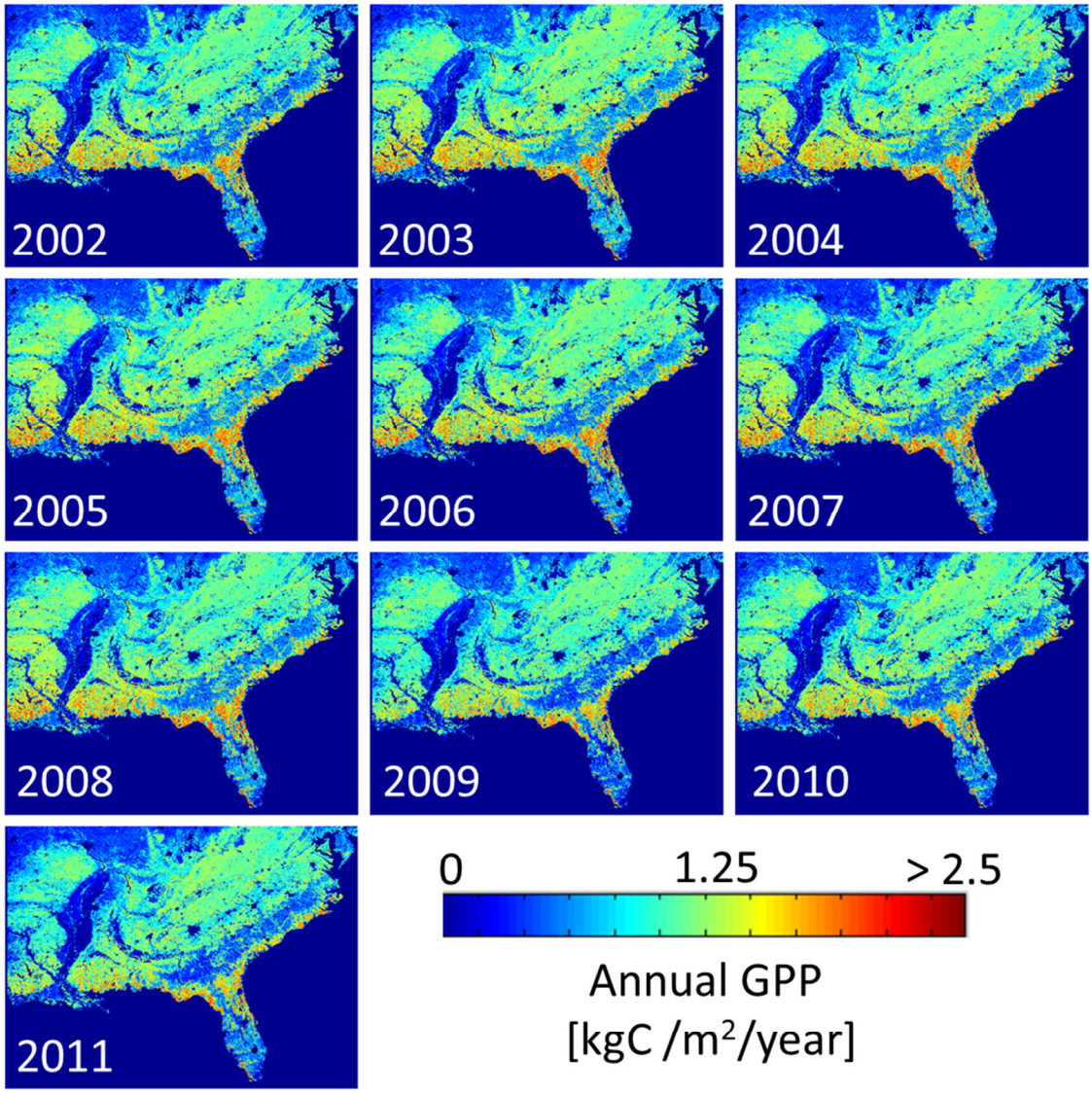

Figure 5-36: Model simulated yearly accumulated GPP (kgC/m²/year) from 2002 to 2010.

Note the larger decrease in GPP for the three-year period 2009-2011 as compared to the meteorological and hydrological droughts of 2006-2007. This shows the importance of precipitation timing and nonlinear eco-hydrological interactions in determining vegetation impacts (see Appendix B for monthly soil water content maps).

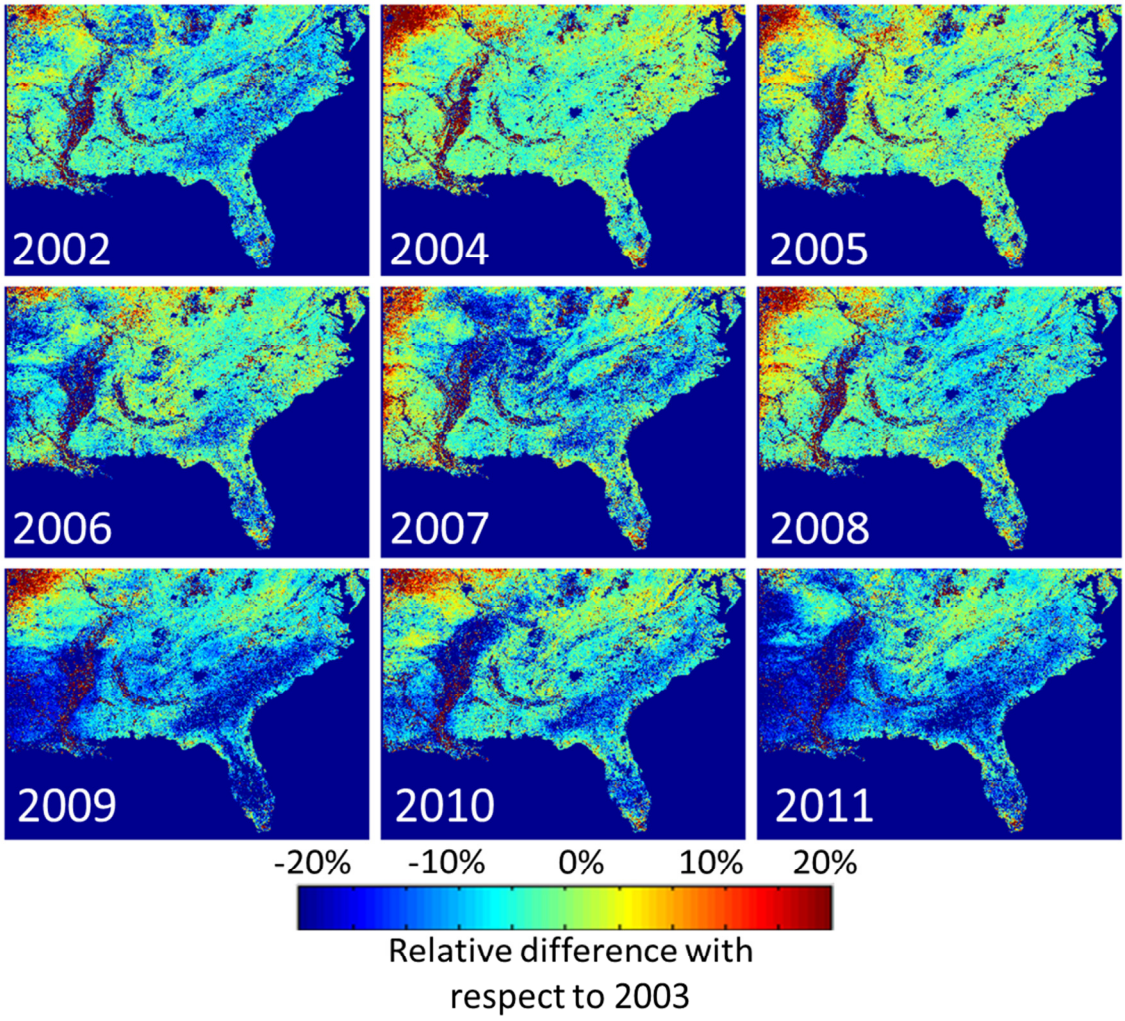

Figure 5-37: Relative difference in annual GPP as modeled by the LEHM with respect to 2003. Warm colors indicate an increase in GPP compare to 2003 and cold color a decrease.

To investigate the processes associated with seasonal and inter-annual GPP variations, the relative deviations are also shown for the yearly averaged soil water content in the 1m soil column (Figure 5-38), the yearly averaged latent heat flux (Figure 5-39) and the average net radiation (Figure 5-40). During 2007, there is a significant decrease in soil water content in the Piedmont and in the Appalachians explaining the observed GPP decrease in the central SE. Likewise the pattern of GPP decrease over

Texas in 2011 and more generally along the Gulf Coast is also in accord with low soil water content and with the extreme and severe drought patterns published by US Drought Monitor NOAA (e.g.: http://drougtmonitpor.unl.edu). This is not the case in 2009, when soil wetness in Alabama, North Florida and Georgia is higher than in 2003.

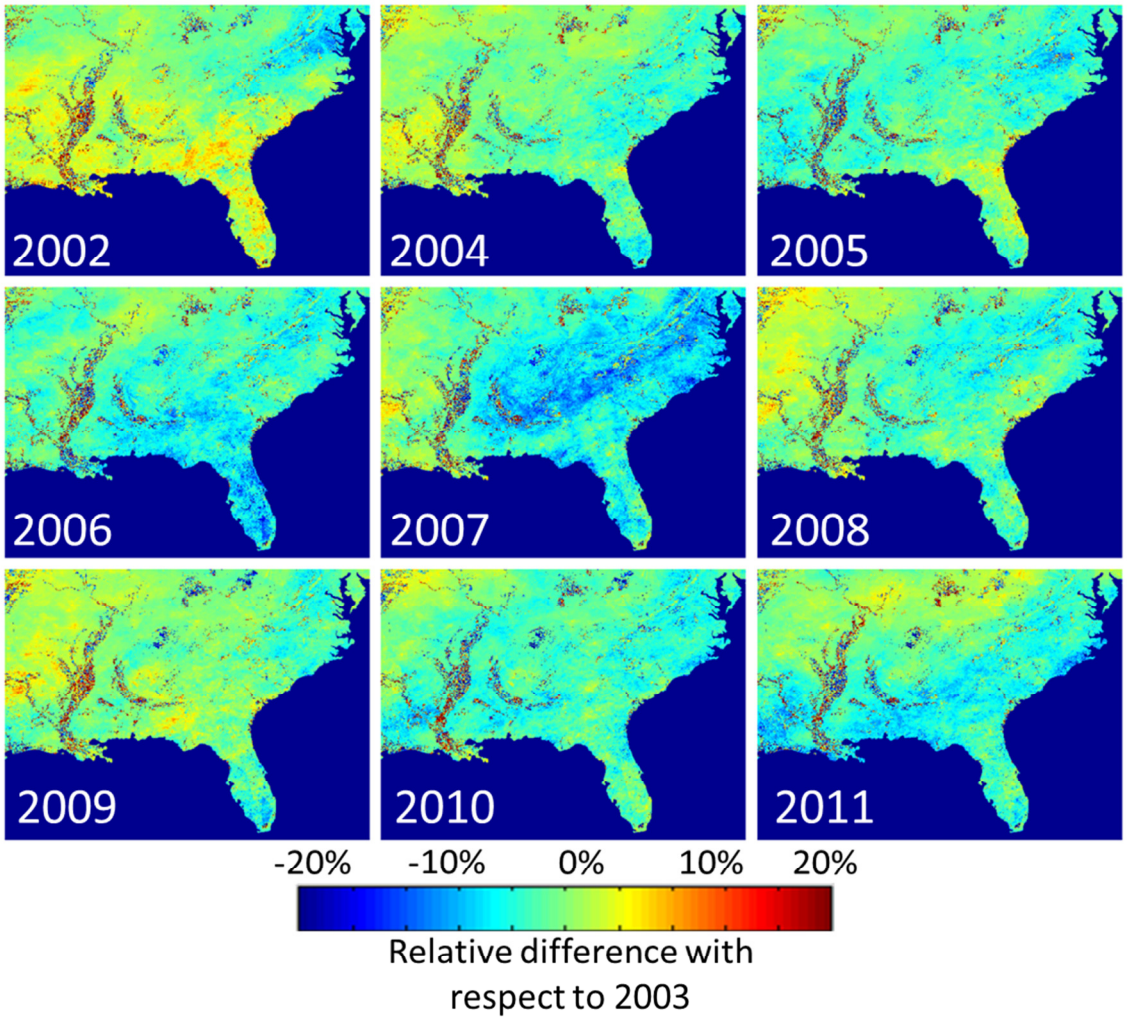

Figure 5-38: Relative difference in yearly average soil water content (m^3/m^3) in the 1m soil column with respect to 2003. Warm colors indicate an increase in soil moisture compare to 2003 and cold color a decrease.

As mentioned in Chapter 4, a large amount of the 2009 annual precipitation was concentrated at the end of the year, and therefore water availability was reduced during the warm season even if the annual amounts do not show evidence of water stress (see Appendix B for monthly analysis).

The high net radiation over the Coastal Plain in 2007 and 2011 is consistent with the predominance of fair weather conditions, and thus lower cloudiness, and rainfall deficits during these two years.

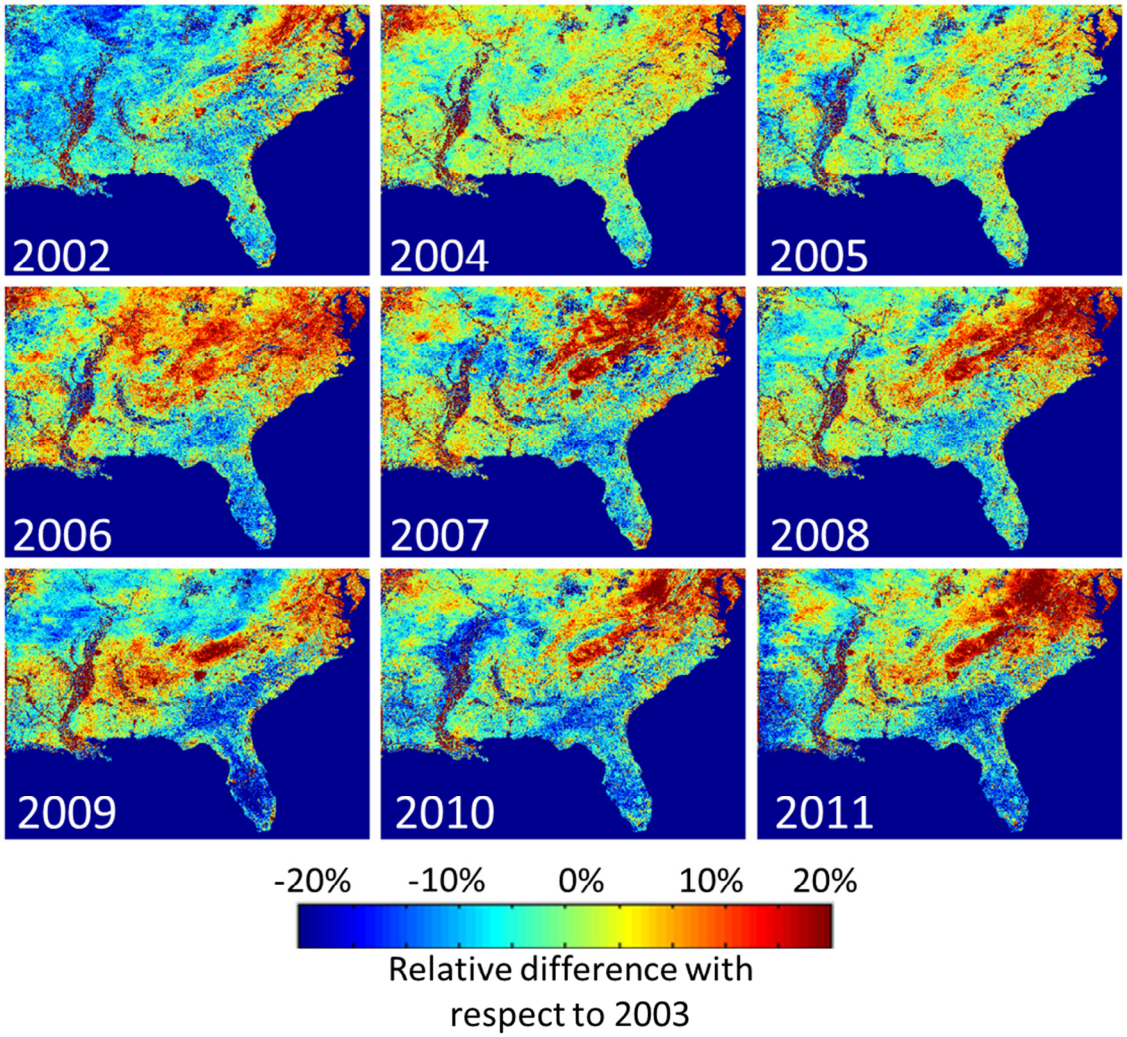

Figure 5-39: Relative difference in average latent heat flux with respect to 2003. Warm colors indicate an increase in latent heat flux compare to 2003 and cold color a decrease.

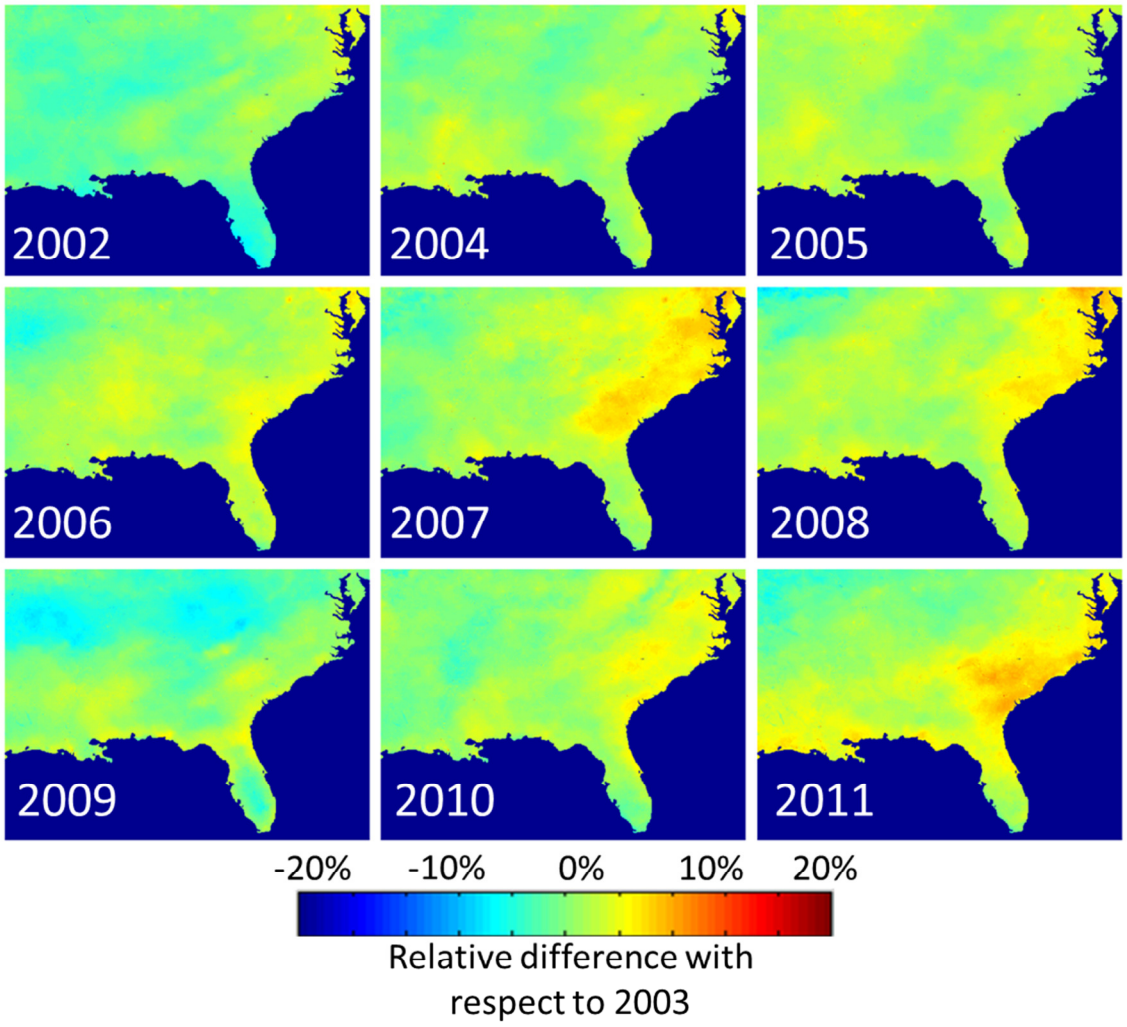

Figure 5-40: Relative difference in average net radiation with respect to 2003. Warm colors indicate an increase in net radiation compare to 2003 and cold color a decrease.

Figure 5-41 shows the annual GPP estimates extracted from the MOD17A3 (version5.5) and resampled at 4km spatial resolution to match the LEHM grid. Although the spatial patterns are similar between our simulations and MODIS estimates, MODIS annual estimates exceed LEHM estimates by 85% at regional scale (compare Table 5-8 and Table 5-9). Higher values are expected from MODIS because the maximum value for LAI and FPAR over a 8-day period to filter out cloud contamination, and if this is not

available, unreliable or missing 8-day values of LAI and FPAR are replaced by the seasonal value in the current version of the MODIS algorithm, which artificially increases GPP estimates. In addition, meteorological data at the daily time-scale are used as forcing, which averages out the effects of the diurnal variations of water stress and radiative forcing, including the underestimation of the impact of cloud cover on the GPP estimates. In particular, note the very high values over mountainous regions

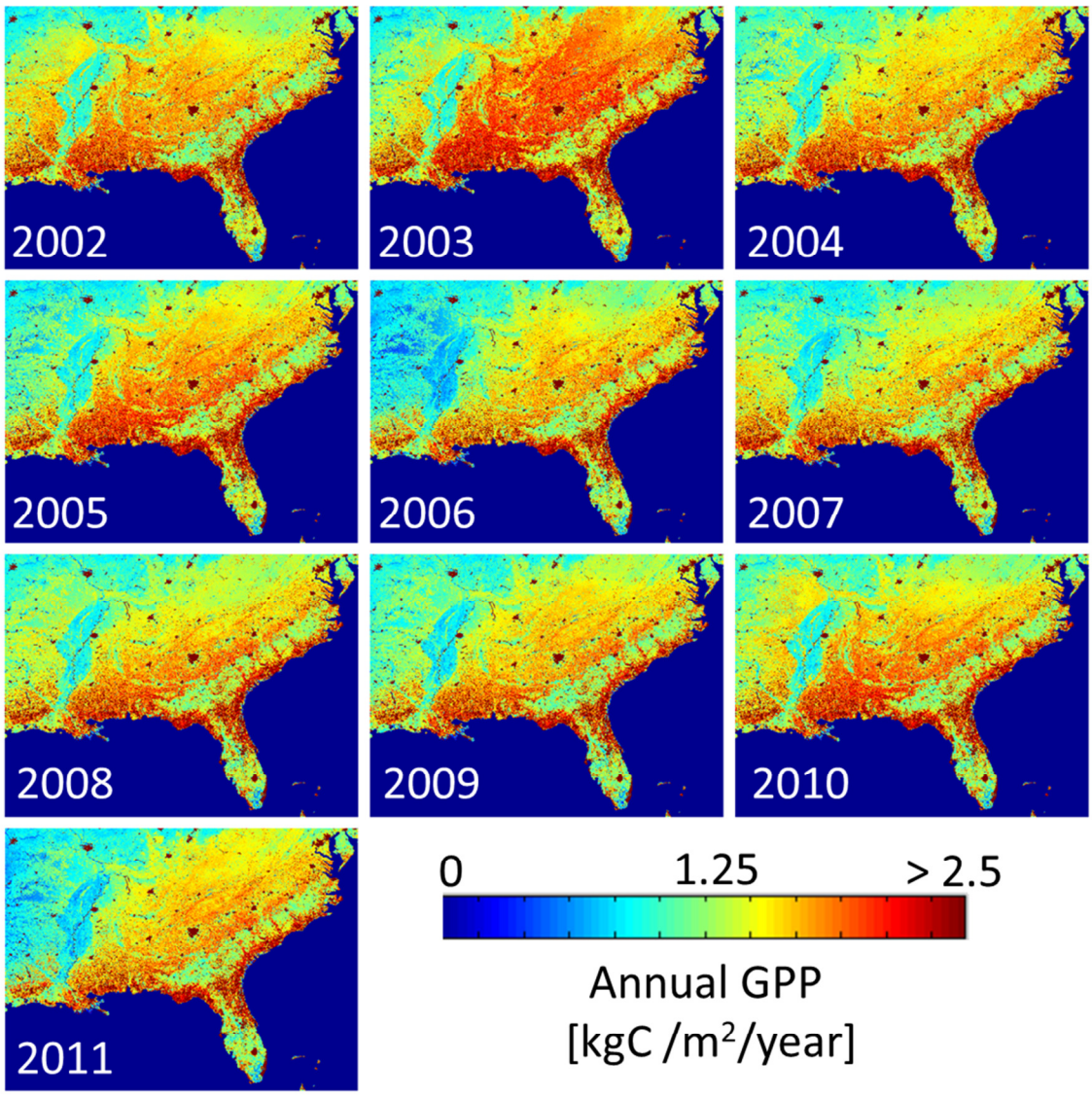

Figure 5-41: MODIS GPP yearly accumulation (MOD17A3) estimates averaged at 4km from 2002 to 2011.

in the South Appalachians and in the ridge-valley region of Tennessee, where persistent low level clouds are known to be present. Indeed, recent work by Tao and Barros (2013) suggests large uncertainties in other MODIS products, such as albedo, in the region.

Table 5-9: Land cover statistics for the annual GPP estimates of MODIS

Land cover	2002	2003	2004	2005	2006	2007	2008	2009	2010	2011	Mean	SD
evergreen needleleaf forest	2.11	2.19	2.13	2.12	2.02	2.08	2.10	2.04	2.13	2.02	2.09	0.05
evergreen broadleaf forest	2.22	2.34	2.25	2.26	2.13	2.18	2.23	2.16	2.25	2.12	2.21	0.07
deciduous needleleaf forest	2.89	2.98	2.89	2.85	2.74	2.82	2.83	2.83	2.92	2.76	2.85	0.07
deciduous broadleaf forest	1.55	1.72	1.52	1.51	1.34	1.41	1.46	1.48	1.55	1.46	1.50	0.10
mixed forest	1.82	1.93	1.79	1.79	1.64	1.74	1.77	1.72	1.84	1.67	1.77	0.08
shrubland	1.76	1.86	1.78	1.76	1.66	1.72	1.72	1.69	1.77	1.66	1.74	0.06
woody savannas	1.76	1.85	1.75	1.73	1.58	1.70	1.72	1.67	1.77	1.60	1.71	0.08
grasslands	1.48	1.52	1.46	1.41	1.27	1.45	1.45	1.38	1.49	1.29	1.42	0.08
permanent wetlands	1.96	2.02	2.00	1.97	1.91	1.95	1.93	1.91	1.97	1.92	1.95	0.04
croplands	1.21	1.26	1.24	1.18	1.10	1.17	1.19	1.16	1.23	1.11	1.19	0.05
cropland/natural vegetation mosaic	1.50	1.61	1.51	1.51	1.43	1.43	1.48	1.45	1.52	1.45	1.49	0.05
barren or sparsely vegetated	2.46	2.53	2.46	2.44	2.34	2.38	2.38	2.38	2.44	2.35	2.41	0.06

Table 5-9 shows the land cover statistics for the MODIS annual GPP averaged to 4km resolution to facilitate comparison with the LEHM. Surprisingly, deciduous needle-leaf forest is the land cover type with the highest annual productivity (10-year average: 2.85 kgC/m^2/year) followed by barren or sparsely vegetation (10-year average: 2.41 kgC/m^2/year) and evergreen broadleaf forest (10-year average: 2.21 kgC/m^2/year). This confirms that MODIS GPP product accuracy is dependent of the type of vegetation as previous studies have shown (Gebremichael and Barros, 2006; Yang et al., 2007; Zhao et al., 2005), as it seems unlikely that the high GPP estimates in sparse vegetation and deciduous needle-leaf reflect accurately those biomes. Despite higher productivity estimates ranging from 40 to 105% depending on land cover class (excluding croplands and wetlands where the LEHM strongly underestimates GPP compared to MODIS as expected), the distributions of the high and low GPP land cover classes are similar between the two estimates. In terms of inter-annual variability, 2003 is also the most productive year of our period of simulation followed by 2004 and 2010, 2010 being a highly productive year as per MODIS, which is not the case in LEHM simulation. The less productive years in the MODIS GPP product are 2006 followed by 2011. While 2011 is also the year with lowest overall GPP for most land-cover types for the LEHM simulation, 2006 is year with close to normal productivity. Although 2006 was a dry year (see Figure 4-3), the contribution of seasonal TC precipitation to the annual cycle is significant (Figure 4-4). In particular, the timing (early June) and tropical storm Alberto were such that the soil moisture storage in the Coastal Plain was significantly higher in the growing season than in 2007 (see Appendix B), which explains the LEHM results.

Similar behavior occurred in 2007 in response to tropical storm Barry in the Atlantic Coastal Plain.

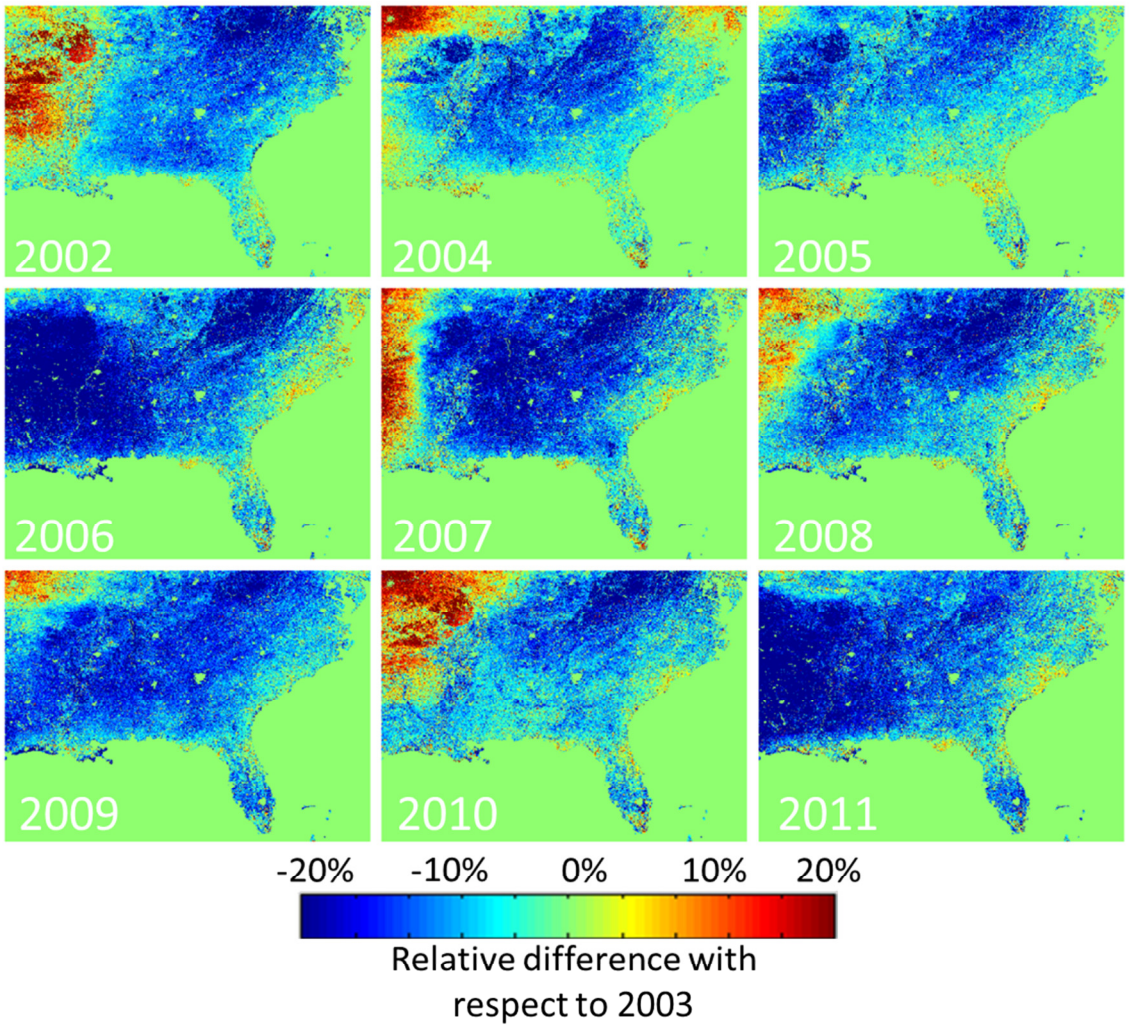

Figure 5-42: Relative difference in MODIS annual GPP averaged at 4km with respect to 2003. Warm colors indicate an increase GPP compare to 2003 and cold color a decrease

Figure 5-42 shows the relative MODIS time-series of annual accumulated GPP in respect to the 2003. The negative relative difference indicates that 2003 is indeed the year with the highest vegetation activity. In contrast to the LEHM simulation, which captures the spatial variability of land-use, soil heterogeneity, and topography, there is only one

dominant regional-scale pattern in MODIS suggesting that the GPP estimation methodology relying on coarse meteorological forcing used to infer the temperature and VPD controls on photosynthesis does not capture critical local water availability limitations as the LEHM does. This is well demonstrated by inspecting Figure 3-4 which displays the spatial patterns of MVDP from 2001-2007. Although the maps in Figure 3-4 at displayed at 500 m resolution, there is strong spatial organization in the signature of drought that is consistent with Figure 5-37 for the LEHM simulation and in contrast with Figure 5-42 for MODIS.

5.7.2 Model experiment: TC atmospheric signature removal

5.7.2.1 Hybrid forcing

The hybrid forcing was built by substituting the standard meteorological forcing (precipitation, pressure, wind speed, specific humidity, temperature) and radiative forcing (incoming short and longwave radiation) by the equivalent monthly North American Regional Reanalysis (NARR) climatology dataset (Mesinger et al., 2006) during the periods of TC activity as defined in Table 5-10 from NCEP's Environmental Modeling Center (EMC). The NARR climatology is available for the 25-year period from 1979 to 2001. The NARR climatology dataset provides a typical diurnal cycle for each specific month. In the hybrid simulations, the days with no TC activity were left identical as extracted from the NLDAS and Stage IV forcing previously, and the days with TC activity were replaced with the diurnal cycle from the NARR climatology. Note that Table 5-10 is different from the Table used in Chapter 4. This is due to the fact that

the true climate forcing and the NARR climatology were sum-averaged to avoid abrupt shifts in meteorological forcing from one day to the next, and for days with TC activity in the SE the replacement was implemented for the entire region of study. The underlying assumption is that other synoptic activity is weak and the precipitation is relatively small in terms of precipitation contribution compared to the tropical system itself.

The advantage is that this approach removes the cloud shield leading hurricanes landfall (such as in case of Dennis for example), which can produce heavy precipitation far away from the main system track, and would not have been produced in the absence of the tropical system. In addition, a replacement limited to a band along the storm track would have had the shortcoming of introducing artificial spatial patterns.

Table 5-10: Summary of the start and the end of the substitution for each storm that have made landfall

ID	Year	TC name	TC landfall	timez	TC catIn	TC exit	timez	TC catOut
1	2002	BERTHA	4-Aug	18.00	TS	9-Aug	6.00	TD
2	2002	EDOUARD	1-Sep	6.00	TS	5-Sep	6.00	TS
3	2002	HANNA	12-Sep	0.00	TS	15-Sep	6.00	--
4	2002	ISIDORE	25-Sep	0.00	TS	27-Sep	12.00	TD
5	2002	KYLE	9-Oct	12.00	TD	12-Oct	6.00	TD
6	2002	LILI	2-Oct	0.00	H1	4-Oct	6.00	TS
7	2003	BILL	29-Jun	12.00	TD	2-Jul	18.00	ET
8	2003	HENRI	3-Sep	18.00	TD	8-Sep	12.00	TD
9	2003	ISABEL	17-Sep	12.00	H2	19-Sep	6.00	H1/TS
10	2004	BONNIE	11-Aug	12.00	TS	13-Aug	18.00	TD
11	2004	CHARLEY	13-Aug	6.00	H4	15-Aug	0.00	TD/ET
12	2004	GASTON	27-Aug	18.00	H1	31-Aug	6.00	TS
13	2004	FRANCES	3-Sep	0.00	H2	9-Sep	6.00	TD
14	2004	IVAN	14-Sep	18.00	H3	19-Sep	6.00	TD/ET
15	2004	JEANNE	25-Sep	0.00	H3	29-Sep	6.00	ET
16	2005	ARLENE	11-Jun	0.00	TS	12-Jun	18.00	TD
17	2005	CINDY	5-Jul	6.00	H1	8-Jul	13.00	ET
18	2005	DENNIS	8-Jul	18.00	H3	13-Jul	12.00	TD
19	2005	KATRINA	24-Aug	0.00	H4/H3	31-Aug	0.00	TD
20	2005	TAMMY	5-Oct	0.00	TS	7-Oct	12.00	--
21	2005	RITA	20-Sep	0.00	H3	26-Sep	0.00	TD
22	2005	WILMA	23-Oct	6.00	H3/H2	25-Oct	0.00	H3
23	2006	ALBERTO	11-Jun	0	TS	14-Jun	18	ET
24	2006	ERNESTO	28-Aug	18	TS	3-Sep	6	ET
25	2007	BARRY	1-Jun	18	TS	4-Jun	12	ET
26	2007	GABRIELLE	9-Sep	0	TS	10-Sep	6	TS
27	2008	FAY	18-Aug	6	TS	28-Aug	0	ET
28	2008	HANNA	5-Sep	0	TS	7-Sep	0	TS
29	*2008*	*GUSTAV*	*1-Sep*	0	*H2*	*4-Sep*	12	*ET*
30	*2008*	*IKE*	*11-Sep*	12	*H2*	*14-Sep*	12	
31	2009	CLAUDETTE	16-Sep	0	TD	18-Sep	0	--
32	2009	IDA	9-Nov	12	TS/ET	11-Nov	0	--
33	2010	BONNIE	23-Jul	0	TS	26-Jul	0	TD
34	*2011*	*IRENE*	*25-Aug*	12	*H1*	*28-Aug*	6	*H1*
35	2011	LEE	2-Sep	18	SS	7-Sep	0	--

5.7.3 Impact of TC on the regional GPP

Figure 5-43 shows the annual averaged relative difference in soil volumetric water content in the soil column between the true climate (used as reference in the normalization) and the hybrid simulations. Clear patterns corresponding to hurricane tracks of the different seasons can be identified present: the impact of hurricane Isabel over North Carolina in 2003; the strong precipitation of Gaston, Frances, Ivan and Jeanne over all the Atlantic Coastal Plain and the Piedmont in 2004; the recharge impact of soil reservoir of Dennis, Katrina and Rita along the Mississippi River in 2005; and the footprint of Cindy in the soil moisture at the border of North Carolina and Virginia in 2005. Note the agreement between the relative contribution to annual precipitation (Figure 4-4) and the estimated soil moisture difference, though the contribution of Cindy per se was not determined significant in terms of contribution to annual totals. In 2006, there is a clear footprint of tropical storms Alberto and Ernesto on the soil moisture in the Atlantic Coastal Plain. Tropical Storm Barry had a local impact at the border of Georgia and South Carolina in 2007. The slow moving Fay impacted most of the central southeast in 2008. West of the Mississippi, although Ike's rainfall was not a significant fraction of annual precipitation (Figure 4-4), the soil moisture increased by more than 5% of the annual average. In 2009, moderate recharge was produced over the central Atlantic Coastal Plains by tropical storm Claudette. There were no significant effects in 2010. Finally, in 2011 tropical storm Lee a system that produced heavy precipitation and floods along its terrestrial path up to Pennsylvania, impacted most of the SE and Irene over coastal North Carolina and Virginia in 2011.

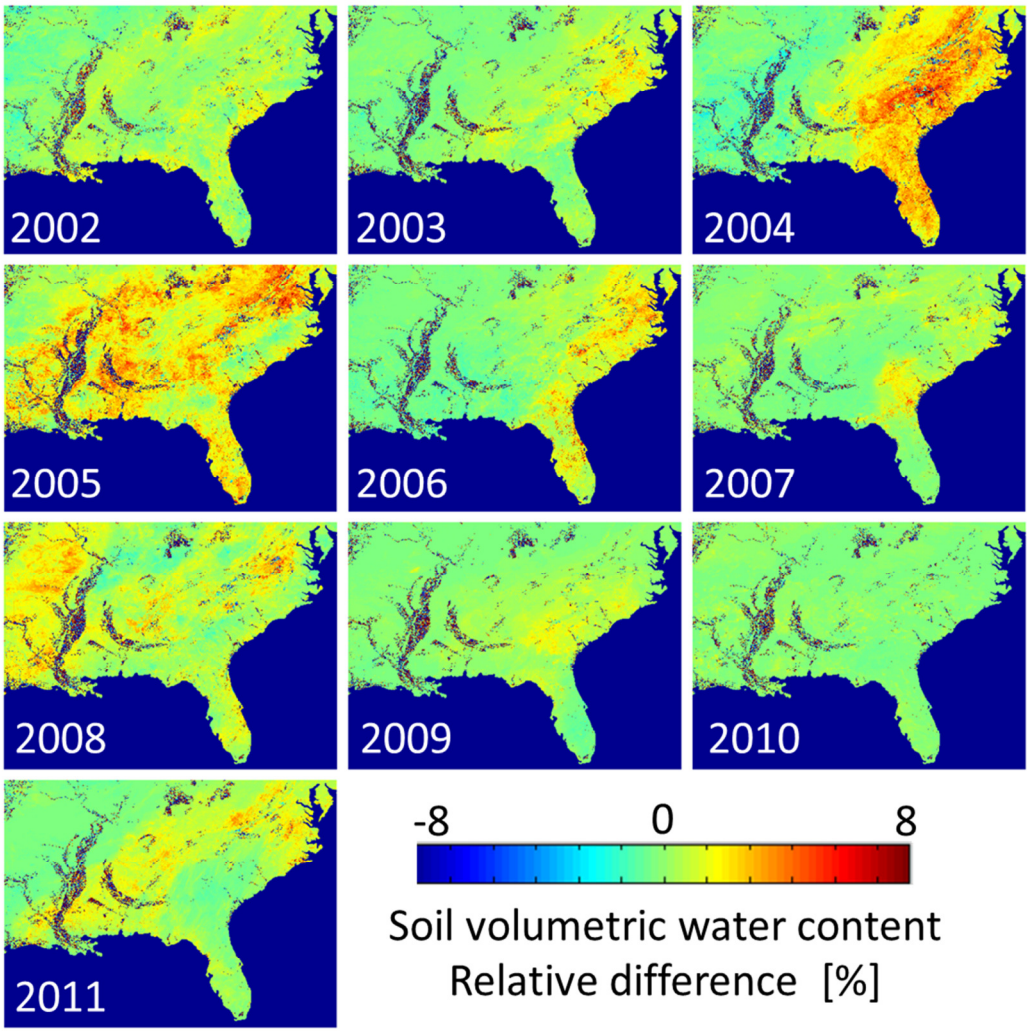

Figure 5-43: Relative difference in annual average soil volumetric water content between the real climate simulation and the hybrid simulation over the 10 years period.

Appendix B shows the monthly evolution of the relative difference in soil volumetric water content for each year. This shows that even if the storm terrestrial track lasted generally a few days the contribution of TC precipitation to soil moisture does last up to several (1-3) months with a monthly average increase exceeding 15% in the case of major events such as the end of 2004 and 2005 hurricane seasons. These results suggest that the hydrological and eco-hydrological impacts of TCs take place at two time-scales:

a short-scale immediately after landfall and along the terrestrial track as the storm transits to the mid-latitudes, and a longer time-scale that reflects the persistence of nonlinear eco-hydrological interactions.

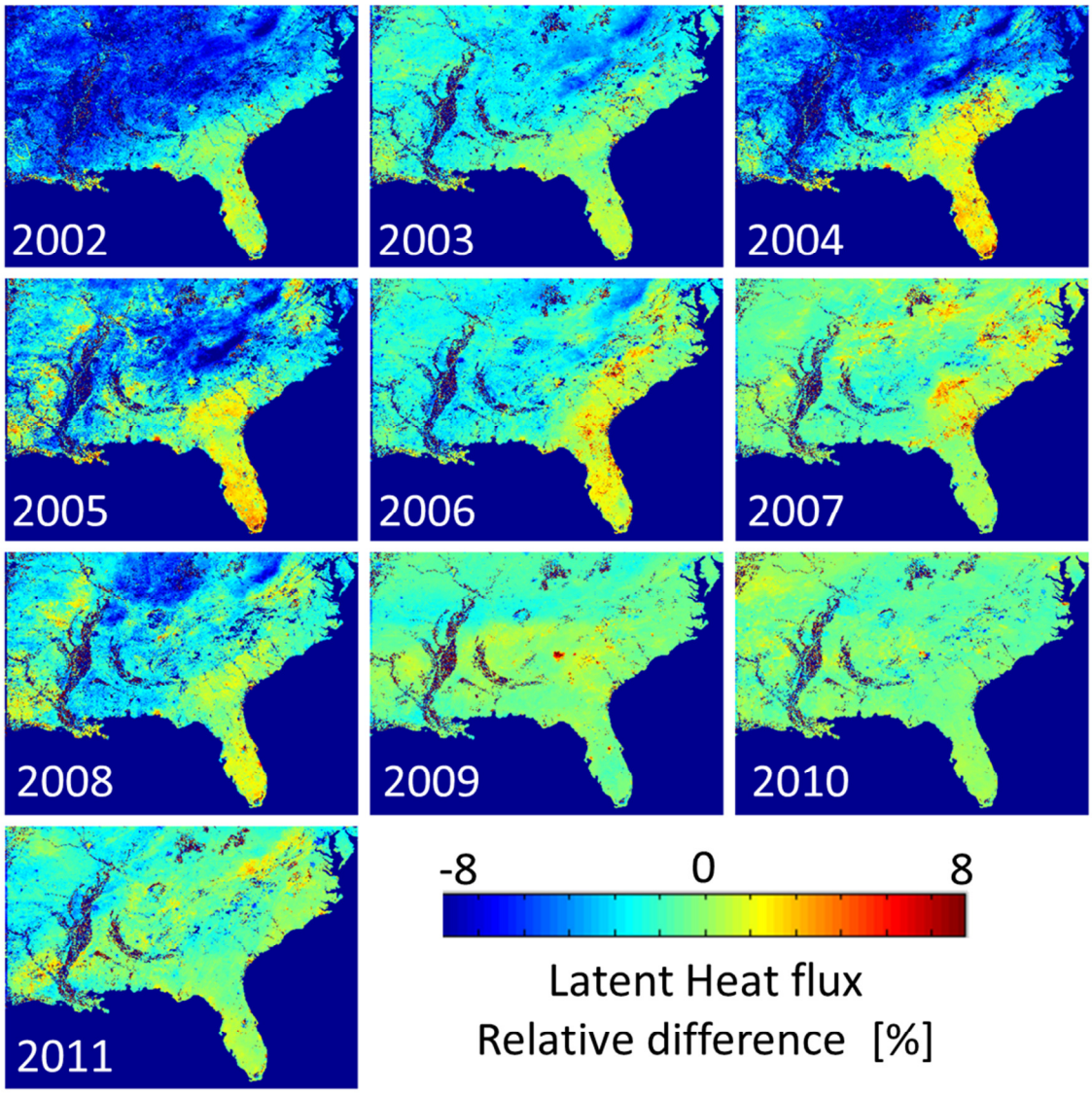

Figure 5-44: Relative difference in annual average latent heat flux between the real climate simulation and the hybrid simulation over the 10 years period.

Figure 5-44 shows of relative difference in annual average latent heat flux and how the increase in soil water availability due to TC precipitation affects the water and

energy budgets through evapotranspiration. The years 2004, 2005 and 2006 exhibit strong decrease in evapotranspiration when the TC precipitation is removed from the water cycle. This decrease is mainly apparent over Florida and the Atlantic Coastal Plains where rainfall was abundant and vegetation is generally dense. The year 2007 also exhibits more localized higher evapotranspiration over Georgia and South Carolina. Since this year was a very dry year, this difference is important suggesting the meteorological drought conditions would have been worse in absence of TC landfall. The mild (< 2% in annual average) but widespread change in soil moisture in 2009 does reflect the general increase in evapotranspiration compared to the simulation without TC. There are also extensive areas in 2002, 2004 and in 2005 that exhibit larger latent heat fluxes in the simulation without TC. These regions of large latent heat flux are regions where soil moisture increase was not observed following the TC landfall. Since the radiative forcing was also replaced by climatology, we expect to have more incoming energy in the simulation without TC compared to the TC simulation in which cloud cover is large and the incoming radiation at the surface lower. Therefore, in the absence of water stress or soil water limitations, the latent heat is expected to be higher due to the increase of incoming energy in the system.

Figure 5-45 shows the relative difference in annual GPP. The spatial patterns are more complex than for the previous variables, since the GPP is function of evapotranspiration, water availability in the soil, air temperature and vapor pressure deficit as well as incoming radiation for the electron rate estimates. Generally, the real climate simulation does have higher productivity on the order of 10-18% over large

areas of the Southeast US. This shows that even if the storm persistence is short, that is the number of days is small never exceeding two weeks, the contribution of the TC precipitation to the recharge of ground reservoirs does translate into more water availability for vegetation over longer time-scales. Hydrologic processes therefore amplify the impact of tropical cyclones well beyond their passage. This is the case of tropical cyclone Bill in 2003, which made landfall in late June and explains about 10% increase in annual GPP over nearly 2/3 of SE US area, and especially the Atlantic Coastal Plain and Florida during the same year. The large change in soil moisture water content due to hurricanes Frances, Ivan and Jeanne during September 2004 did translate into a moderate increase in GPP over the Atlantic Coastal Plain and the Piedmont due to the late input of freshwater at the end of the growing season In 2005 the impact of early TCs, Cindy and Dennis, the latter with a cloud shield producing strong precipitation eastward from its landfall, impacted more the annual GPP than the late season TC's Katrina and Rita with only moderate impact along the Mississippi alluvial plains. This, highlights the importance of the timing of the input of freshwater in terms of impact on the vegetation productivity. Recall that, in this case, the predominant land-use is cropland, and as discussed in Chapter 3, flooding and erosion altered significantly modified the landscape. Even though TC activity was relatively weak in 2006 and 2007, note the higher productivity in the Appalachians in 2006 and 2007. This suggests that the 2007 drought would have been much more severe in the SE US in the absence of TCs. In 2008, the contribution of Tropical Storm Fay to GPP in the southern part of our region of study is visible in the same year since its landfall occurred mid- august.

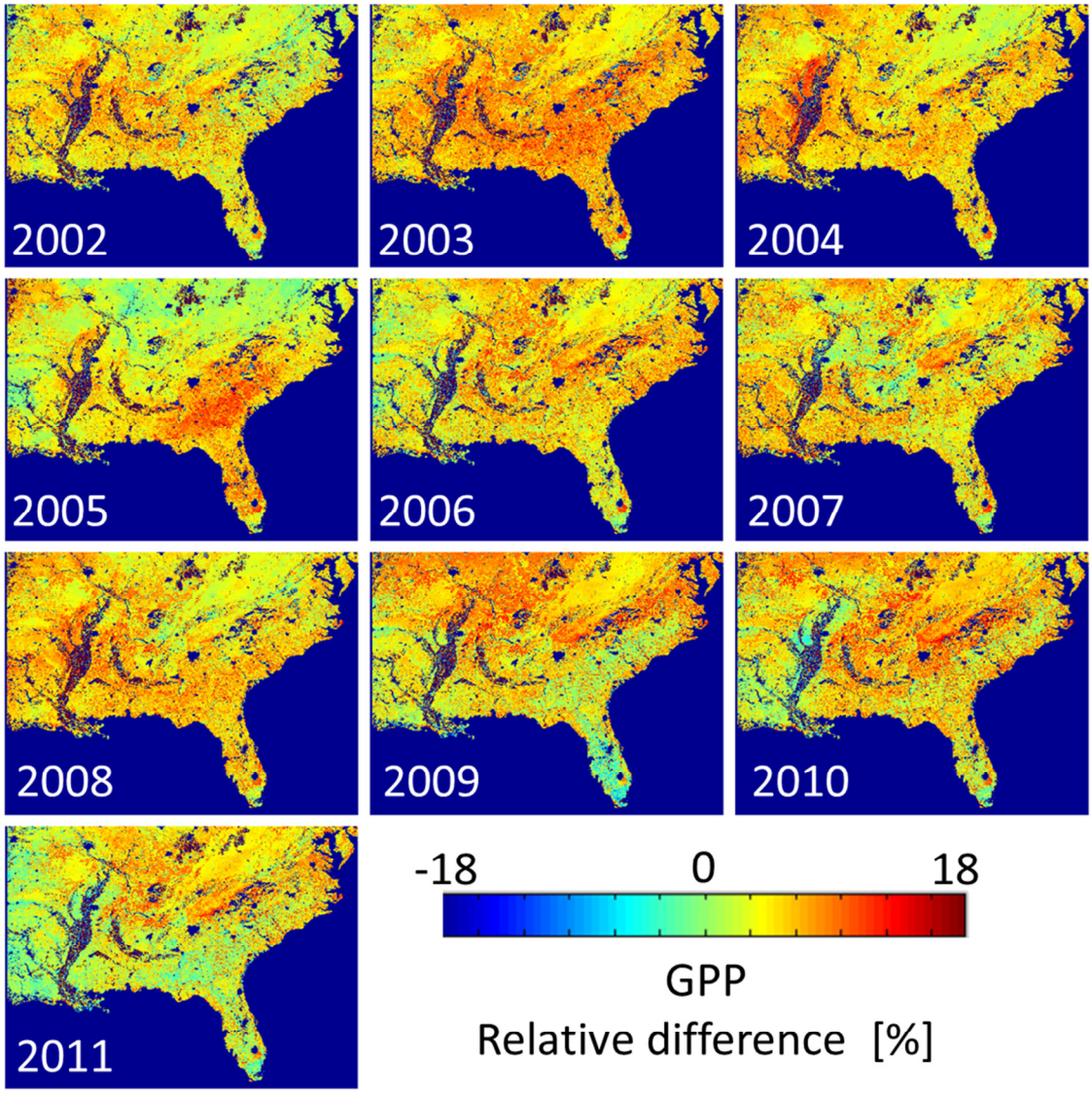

Figure 5-45: Relative difference in annual GPP between the real climate simulation and the hybrid simulation over the 10 years period.

Also in the same year, TC Ike in mid-September can be linked to the 2009 GPP enhancement. Note the spatial mismatch between the soil moisture (Figure 5-43) and GPP patterns in 2009 over the Coastal Plain and Florida. This can be explained by the late landfalls in 2009 (mid-September for Claudette and early November for Ida). In 2010, the contribution of TCs in terms of soil moisture content was quasi null (Figure 5-43).

Nevertheless, the GPP is regionally enhanced, especially inland. The change could be due to the enhanced soil moisture at the end of 2009 in the Atlantic Coastal Plain and Florida, and the timely inland passage of Bonnie in late July to explain the differences estimated in the Appalachians and valley and Ridge regions.

5.8 Discussion and conclusions

Comparison of GPP estimates is challenging due to discrepancies in the footprint of the observed area (Turner et al., 2006; Yang et al., 2007), spatial heterogeneity, spatio-temporal scaling of nonlinear processes, and high uncertainties in the estimates (Oren et al., 2006). During our period of study, 6 Ameriflux towers provided GPP estimates in the SE US, 3 of which were located in North Florida. This lack of spatial coverage combined with the fact that tower measurements were only available for evergreen needle leaf forest and grassland make it difficult to fully evaluate the different vegetation dynamics and climate-vegetation feedbacks present across the Southeastern US. Over broadleaf deciduous vegetation, the LEHM simulates phenology similar to MODIS in terms of timing and in terms of annual amplitude. The LEHM tends to start the growing season later than MODIS, but it has been shown that the lack of soil temperature dependencies in the MODIS algorithm tends to advance the seasonality (Turner et al., 2006). Over grassland, the LEHM seasonal peak reaches 5-6 $gC/m^2/day$ whereas MODIS estimates are as high as 8 $gC/m^2/day$. The choice of parameter of Vcmax and Jmax in the LEHM could be a source of error. The generally low value of LAI over this type of vegetation is another limitation on the canopy scaling of the modeled leaf processes. The values over

the Duke open field (US-DK1) and US-ChaV towers are in better agreement, mainly due to higher value of LAI in MODIS consistent with the presence of forest in the direct neighborhood of the towers. The introduction of the new scheme for Vcmax and Jmax has greatly improved the representation of GPP over evergreen needleleaf forests. During the cold season, the LEHM simulates lower GPP than MODIS or the tower estimates. Cloud contamination in the FPAR and LAI products are a possible source of this underestimation, in the same way that the corrected MODIS algorithm tends to overestimate GPP due to the type of approach used to correct for cloud contamination (replacing low values by seasonal values), as well as the temperature function used in the Michaelis-Menten coefficient calculation. Nevertheless, the LEHM captures well the timing phenology.

Overall, the phenology module based on the GSI and integration of FPAR and LAI climatology from the 10 years of MODIS have shown a good predictive ability to estimate the start and the length of the growing season. However the estimates of FPAR over deciduous broadleaf and grassland vegetation types have a lower annual variability underestimating FPAR than observed during the active period and overestimating FPAR during the wintertime. This leads to strong underestimation of GPP when used to force the model since the correction also affects LAI estimates. Sensitivity analysis has shown that phenology is relatively insensitive to the growth and senescence factors, suggesting that the scaling of FPAR will need the introduction of further specificity related to the type of vegetation. Over evergreen forests, the simulations provided results in good agreement with MODIS and the tower. The inter-

annual variations suggest that the dependence of the GSI on the VPD should be reduced since the VDP already constrain the canopy resistance in the LEHM.

At the regional scale, the model has shown that the dependence of the scaling on the LAI combined with the use of look-up table base on coarse grid tends to produce lower GPP estimates than MODIS at the regional scale. The model does also underestimate the grassland productivity, and especially the cropland. Since the version of the LEHM used here lacks representation of water-table dynamics, and the soil depth is likely too shallow (a heritage from previously applying the model to very large scales), the role of deep roots in alleviating the signature of drought especially in forest ecosystems is not modeled. Consequently, the sensitivity to water stress during severe drought may be overestimated in the LEHM as compared to actual conditions.

The accuracy of the MODIS algorithm has been shown to be strongly dependent of the type of vegetation and the related light efficiency coefficient, and previous research indicates that MODIS tend to overestimate GPP by 20-30% (Heinsch et al., 2006). It has been also highlighted that high values of FPAR in the MODIS algorithm can lead to overestimation of GPP (Turner et al., 2006). In addition, in the GPP product version used in this study, the use of the maximum FPAR could be introducing an overestimation over certain vegetation type with strong annual dynamic. Effectively since version 5.5 of the MODIS GPP annual accumulation product (MOD17A3) was released, the FPAR and LAI at 8-day time period has been processed to remove low values assuming they are related to cloud contamination and not to vegetation variations (Zhao et al., 2005; Zhao and Running, 2010), this in addition to the fact that

the original 8-day product already using the maximum acquired value over the time period. Although these assumptions might be adequate over tropical evergreen forests, there is no reason this should be the case in general, especially for vegetation with strong phenology. Also note that averaging the original MODIS GPP from 1km to 4km for the comparison is different than averaging the LAI/FPAR to 4km before computing the GPP due to the strong sensitivity of the LEHM to LAI/FPAR as shown in section 5.5.4. Finally, the MODIS algorithm works at the daily time-scale, relying on daily – scale response functions and threshold values, being constrained only by mid-day observations at the peak of the diurnal cycle, which in the absence of cloud contamination should overestimate GPP all other factors being equal.

By contrast, the LEHM simulates the diurnal cycle fully including soil temperature and soil water stress effects on GPP production and effects of cloudiness and variability in VPD, and therefore should produce lower estimates of GPP than the MODIS algorithm. The model has shown very good skill in simulating the difference between wet and dry periods during 2002-2011. The relative differences suggest that 2003 was the most productive year during our period of study. The Atlantic coastal plains and Piedmont show vegetation stress in 2009 and 2011 and 2002. The inter-annual patterns of MODIS GPP differences relative to 2003 lack spatial structure exhibit large regional variations related to the coarse meteorological forcing used in the algorithm to represent the different vegetation stresses, since this product is produced at the global scale. However the main regional patterns are similar in the LEHM simulation and

MODIS product with the exception of 2006 that was estimated to have lower vegetation activity in the western part of the MODIS product.

The comparison of the 10 years simulations with and without TCs has shown that the impact of TC precipitation on the soil water content as simulated by the LEHM can be as high as 8% of the annual average and up to 15% at the monthly scale in the regions along the TC tracks. The late and highly active 2004 hurricane season, which contributed the most to the precipitation annual totals over the Coastal Plains and the Piedmont during our period of study (Brun and Barros, 2013; Knight and Davis, 2009; Prat and Nelson, 2012), recharged the ground water reservoir by 3% to 8% of the annual average over most of this area. This late recharge had however a limited impact on the GPP of 2004 due to the late landfalls at the end of the growing season. In 2005, TCs Cindy and Dennis in July increased significantly the GPP over the Coastal Plains and the Piedmont. The contribution to soil moisture of the late TCs Katrina and Rita is more centered on the western part of the SE due to the clustering of landfalls along the Gulf of Mexico. Katrina has also strongly contributed the increase in soil moisture in the northeastern sector of our region. Recently, Kam et al. (2012) conducted an modeling study using NARR Climatology and the Variable Infiltration Capacity (VIC) land surface hydrologic model to simulate soil moisture and estimate the role of hurricanes in redressing drought. Besides the model, the main difference between the two experiments is that only TC precipitation was removed from the forcing by tracking the position of the storm and taking a buffer of 500km along the storm track, but leaving all the other forcings identical in Kam et al. (2012). They found a decrease from 50% to 25%

in the spatial extent of drought during the period 2004-05. They conclude TCs will impact drought through late initiation, early recovery, smaller spatial extent and shorter duration primarily along the coastline. Note that since they did not modify the other forcing, their experiment might have overestimated the difference between the two simulations by drying up the simulation without TC precipitation due to the high evaporation related to the strong winds during the TC. Our results show that effectively 2004 and 2005 are the years in which soil moisture difference are the largest in terms of relative difference. However, 2003, 2008 and 2011 also show that slow moving tropical storms that cross the entire region have a large impact regionally, which in turn strongly impacts GPP at the regional scale. Overall the model results also confirm the findings of Chapter 4 using data analysis. Recharge is mainly located in the Piedmont and Coastal Plains, the hurricane season 2004 helped alleviate hydrologic drought conditions. However due to its late timing the impacts in terms of GPP are moderate. That is the impacts are different for hydrological and eco-hydrological droughts. Note that since in this version of the model there is no routing of the surface and lateral flow we do expect to underestimate the recharge especially at lower elevations. McGrath et al. (2012) showed that TC plays an important role in vegetation dynamics and drought relief in Australia. Our results suggest that the change in soil moisture does translate into increase of evapotranspiration and GPP at the regional scale. Although the spatial patterns of latent heat flux are clearly co-localized with the soil moisture difference, the spatial patterns in GPP are different. This can be explained by the timing of the storm. Effectively, late storms with landfall in September will recharge the soil moisture

reservoirs, but will not impact the vegetation activity significantly. Finally, landfalls early in the hurricane season such as the case of Bill in 2003 can have a huge impact for the current harvest season, and therefore directly impact the GPP for the same year. The GPP spatial extent also suggests that GPP is not only modified on the coast, but across the entire SE making the impact on the carbon cycle larger than expected. Note that the substitution of the radiative forcing by the NAAR climatology also has an impact on the GPP estimates.

In summary, the 10-year model simulation shows that, despite the short duration for the events per se, the impact of TCs on the regional GPP through enhancement of water availability is of the order of 10% with localized differences going up to 18%. This has important implications for the regional carbon cycle that go beyond the destructive carbon footprint of hurricanes (Chambers et al., 2007; Zeng et al., 2009) due to their localized nature. Beside the highly active season 2004 and 2005 that strongly increased the water availability, tropical storms moving slowly across the entire US such as Bill (2003), Fay (2008) and Lee (2011) have an important impact on GPP at the regional scale. Note that as in any other model experiment limitations of the study have to be stressed. The fact the lateral and surface flows are not routed can lead to underestimation of hurricane recharge capacity since the large runoff produced is not routed to the lower regions of the landscape. Nevertheless, the timing of the storm is critical. For example the large recharge of 2004 did not have significant impact on GPP due to the late landfall of the major TCs. This is in contrast with the significant impact of early TCs in 2006 and 2007 despite the low overall rainfall. These results confirm that TCs play an important

role in the SE ecohydrology and therefore changes in the frequency, path or intensity and timing of TCs can impact the spatial and quantitative distributions of water, regularly and consequently on the regional carbon cycle.

These results also have implications in terms of climate change mitigation suggesting that changes in timing of TCs should have a strong impact on GPP at the regional scale. The 10-year simulation demonstrates that early season TCs, and generally weak and slow moving TCs, induced the largest increase in GPP. Thus any change in timing of TC landfall induced by climate change could produce an important change in water availability and vegetation dynamics in the SE US.

6 Summary and Conclusions

6.1 Research summary

The main goal of this research was to investigate the role of tropical cyclones (TCs) in the SE hydrometeorology and evaluate how it feeds back on the carbon cycle by modulating vegetation activity by mechanical damage during the transit of TCs overland or by affecting soil water availability and soil-atmosphere-vegetation interactions. This study sets the basis for a quantitative evaluation of the role of TCs in the SE ecohydrology at the regional scale and allows to better understand for potential changes in TC activity due to climate change (Emanuel, 2005; Michener et al., 1997; Pielke et al., 2005; Shepherd and Knutson, 2007).

Previously, most studies relating vegetation impacts to hurricane activity focused on the mechanical damage caused by winds, storm surge and flooding, especially over forested areas (e.g. Chambers et al., 2007; Gresham et al., 1991; Weishampel et al., 2007). The contribution of TCs to the precipitation of the SE US has received great attention and detailed assessment (Knight and Davis, 2009; Knutson et al., 2010; Konrad and Perry, 2010; Nogueira and Keim, 2011; Prat and Nelson, 2012), but the environmental impact of this heavy precipitation has often focused on the flash floods and landslides (Smith et al., 2010; Tao and Barros, 2013; Villarini et al., 2011). Thus, so far, an integrated regional assessment of the ecohydrological impacts of TC over SE in terms of hydroclimatic controls on vegetation dynamics is lacking.

For this purpose, we first concentrated on monitoring the impact of hurricanes and tropical storms on vegetation activity along their terrestrial tracks over the entire southeastern US by the development of a remote sensed metric based on MODIS Enhanced Vegetation Index (EVI) that would allow detection and attribution of vegetation stress; next, a watershed-based GIS framework was developed to generate a quantitative atlas of the role of TC precipitation in meteorological drought mitigation, and the environmental response to TC precipitation in terms of runoff response and recharge across the different physiographic regions in the SE. Finally, the impact of TCs on vegetation dynamics from inter-annual to sub-diurnal time-scales was investigated using GPP (Gross Primary Productivity) as a metric, and model simulations using a land surface eco-hydrological mode (LEHM) with and without TC atmospheric impact in the forcing. Data analysis and modeling were conducted for the first decade of the MODIS era (2001-2011), which allows concerted examination of hydrologic and vegetation processes at unprecedented spatial and temporal resolutions.

This dissertation addresses the following specific scientific questions:

1. What is the spatial distribution and persistence of the impacts of land-falling hurricanes in the SE US? This question is addressed in Chapter 3 through a new metric, the MODIS Vegetation Disturbance Persistence (MVDP) (Brun and Barros, 2012).
2. What is the fractional contribution of TCs to SE hydroclimate, and what are the spatial fingerprints of TC activity on the hydrologic regimes of SE

watersheds at multiple scales? This question is addressed in Chapter 4 using a water balance approach applied to over 3,200 catchments (Brun and Barros, 2013b).

3. What is the impact of TC precipitation on vegetation activity at regional scale in the SE US? This question is addressed in Chapter 5 using a coupled hydrology-vegetation dynamics model and remote sensing data (Brun and Barros, submitted).

The major research findings are described in Section 6.2 and recommendations for further work are discussed in Section 6.3.

6.2 Major research findings

- A new vegetation disturbance metric based on MODIS EVI anomalies (MVDP) shows robust skill in detecting broad disturbance patterns caused by drought stress conditions, as well as organized localized disturbances due to specific storm events.
- The MVDP allows detection of phenology shifts in addition to changes in vegetation activity.
- The MVDP facilitates physical attribution of vegetation disturbances to soil water availability such as in 2001 to 2003 coinciding with years with weak hurricane activity, especially in areas of short rooted vegetation such as grasslands and agriculture.

- The magnitude of vegetation disturbances due to hurricanes is larger than that for drought (high MVDP value in the range of 30 to 46) and spatially clustered and organized according to the governing hydrological process.
- Low lying areas along the terrestrial track of hurricanes are the most affected, and coastal disturbances at or in in the vicinity of landfall are the most persistent lasting up to two years as shown in the case studies of Isabel and Katrina.
- The temporal evolution of the recovery suggests that mechanical sediment removal and salt intrusion associated with the storm surge may be more important than tree uprooting and, or decrowning in terms of long term ecosystem recovery.
- Salt contamination of the subsurface due to infiltration during the storm surge appears to cause vegetation morbidity in the coastal zone for a period from 1 to 2 years.
- Generally, watersheds suffering major direct impact are on the right flank of the storm track, or in the case of large river basins that have their headwaters and major tributaries on the right flank, downstream floodplains on the left flank also show severe impact due to flood propagation.
- Alluvial plains with intense agricultural activities seem to be particularly vulnerable to flooding events in the aftermath of major tropical storms that last well into the year following the event due to erosion and de-capping of the upper soil layers.

- Precipitation produced by moderate and intense TCs provides significant recharge to groundwater and soil moisture reservoirs, erasing the signature of water stress that dominates in the absence of significant Tropical Cyclone activity.
- At the catchment scale, the contribution of TC precipitation during the hurricane season can be as high as 65 % of the annual total for specific watersheds.
- For individual events, in our period of study (2002-2011), Frances in 2004 was the hurricane which produced the highest amount of precipitation corresponding up to 20% of the annual totals over coastal and mountain basins due to orographic enhancement effects. Similarly high annual precipitation fractions were reached for Jeanne (2004), Katrina and Rita (2005) over limited areas. Note that, in the case of Katrina, the maxima were reached over Tennessee, and not close to the landfall as for the other two.
- The large precipitation deficit (meteorological drought) existing at the beginning of the 2004 and 2005 hurricane seasons was entirely redressed by the end of the season. In 2002 and 2008, the contribution of TCs in reducing the deficit was also significant.
- There is a strong gradient in the runoff partitioning of precipitation across the different physiographic regions with streamflow response dominating in the mountains, and groundwater recharge being dominant in Piedmont and Coastal Plains. Nevertheless, as the topographic gradients fade toward the coast, the hydrologic response is complex revealing the signature of nonlinear effects due to heterogeneity in land cover, soil properties and geomorphology that play an

important role in rainfall-runoff processes integrated by the runoff fraction metric.

- Not unexpectedly, serial storms enhance runoff response, especially in basins where meteorological drought was redressed by earlier storm activity, highlighting the role of antecedent moisture conditions in rainfall-runoff processes, and consequently in the partition of TC precipitation between the surface and the groundwater system.
- At the regional scale, the LEHM simulated GPP exhibits spatial variability related to water stress at inter-annual time-scales which is not captured by the coarse MODIS GPP patterns.
- Inter-annual relative difference variations in the LEHM simulated annual GPP show that the impact of TCs on redressing meteorological, hydrological and eco-hydrological droughts occurs at different time-scales extending to periods of 1-3 months in the case of the latter depending on storm timing .
- The comparison of the 10-year simulations with and without TC meteorology has shown that the impact of TCs on soil water content as simulated by the LEHM can be as high as 8% of the annual average soil water content and up to 15% of the monthly average along the TC tracks.
- The excess soil moisture availability attributed to TCs is coupled to an increase of GPP over large areas ranging between 5 and 15%.

- Isolated events, such as tropical storms and generally weak TCs moving slowly across the SE US such as Bill (2003), Fay (2008) and Lee (2011) can have an important impact on GPP at the regional scale.
- The timing of the landfall is critical in terms of impact on the GPP, with early season TCs such as Alberto and Barry having a more significant impact on GPP than TCs happening near and past the mid-point of the hurricane season. Therefore any shift in season related to climate change should have an important impact on water availability and vegetation dynamics in the SE US.

6.3 Limitations and recommendations for further research

The limitations of this research stem from data used for analysis, to specify model parameters, and to evaluate model results, and from model shortcomings proper. The most difficult to address in future research are those associated with data uncertainty associated with measurements, measurement scale and sampling, and spatial and temporal consistency among observational data sets that is required for climate scale studies. One clear example is the dearth of Ameriflux towers with long, robust and representative observations of SE ecosystems, and the lack of quantitative science-grade data sets of the integrated water and carbon cycles at the existing locations. Scaling methods to bridge resolution gaps among data sets struggle to represent nonlinearity. The scaling of vegetation activity is especially challenging, in particular the representation of canopy behavior changes in space and time. Climate data are equally

sparse, and complex terrain in particular remains a major challenge in assessing water and carbon budgets even at annual scales.

This work also shows the challenges in conducting uncertainty analysis using multi-sensor, multi-platform datasets, which are further amplified through discrepancies of temporal and spatial resolution among ground-based, remote sensing and model data that such regional approach requires. This is well illustrated by Figure 5-35. Remote sensing has great potential to be used as extrapolation envelope to improve the monitoring of space-time heterogeneity. Also efforts to build large databases about vegetation species behavior, such has the TRY plant traits database (http://www.try-db.org/TryWeb/About.php), should greatly enhance the further development of eco-hydrological model.

Regarding model simulations of GPP, nutrient controls were not taken into consideration (i.e. nitrogen availability was always assumed optimal), despite the fact that there is nutrient washout associated the TC runoff causing eutrophication in the lower part of the river system and estuaries (Paerl et al., 2006). This is mainly due to lack of spatial information about nitrogen in soils, and that nitrogen dynamics in soil and its distribution in plants remains a challenging problem.

Salt intrusion during the storm surge has an important impact on coastal and inland ecosystems. Through their role of environmental buffer, these wetlands ecosystem are however key inter of shoreline protection as well as water quality. The effect of salt intrusion on vegetation response in the storm aftermath was not investigated. This

requires a salt intrusion model to determine the spatial patterns of salinity, as well as a parameterization of salt concentration controls on vegetation processes.

Not unlike other Land Surface Models (LSM) used in similar regional scale studies, the version of the LEHM used here does not represent deep water table variations and regional scale water flows which are a critical source of water to trees during drought, and therefore GPP deficits during extreme water stress conditions such as the 2007 drought are necessarily overestimated. Future research should incorporate the 2.1/2D parsimonious version of the coupled surface-groundwater hydrologic model (Yildiz and Barros, 2007; Tao and Barros, 2013). In addition, in its present form, the LEHM does not include representation of agricultural activity, such as planting, growth and harvest phases, and most importantly irrigation. The latter is especially important in that meteorological drought translates into soil water stresses that are exacerbated in irrigated croplands, thus explaining at least in part the underestimation of GPP in such areas as compared with approaches that do not explicitly couple GPP to soil water stress.

Further research is needed in terms of monitoring regional terrestrial recharge in the aftermath of TCs, and to quantify how it translates into groundwater recharge. The GRACE satellite provides an interesting synoptic view of terrestrial water storage change that is difficult to obtain from the local wells measurements. In this study, it was used in a qualitative way to understand spatial patterns and temporal trend. Its use for a more quantitative approach will require characterizing the partitioning of the terrestrial water storage changes between groundwater and surface reservoirs including vegetation water content. Remote sensing is a suitable tool to monitor vegetation water

content among which the Normalized Difference Water Index (Gao, 1996) and advanced microwave scanning radiometer for the Earth observation system (AMSR-E) on MODIS (Njoku and Chan, 2006; Reginald and Vladimir, 2009) have shown great potential. In terms of surface reservoirs, dam regulation can contribute to changes in terrestrial depending on the number and the capacity of dams. It is possible to estimate the variation in volume (difference in water level x reservoir area) and therefore their contribution to the water thickness equivalent changes. For the lakes, it will be more difficult to estimate changes, although lake levels are often monitored, high resolution bathymetry will be required to estimate the change in water volume. Using the same period of observation as GRACE, it will be possible to compute the anomalies on these different datasets to better estimate the changes among the surface reservoirs. This will enable estimation of the fraction of the GRACE signal due to groundwater changes. Combined with well data, it will provide a quantitative evaluation of groundwater recharge related to TC precipitation.

In summary, long-term monitoring of vegetation is needed to fully capture the ecohydrological impacts of climate extremes. Remote sensing techniques offer an important synoptic approach that complemented with field ground calibration can provide spatio-temporal comprehension of vegetation dynamics. However maintaining consistent remote sensing time-series is challenging. Models provide a virtual laboratory to test hypothesis and begin realistic quantitative assessments of water and carbon cycles at regional scales, ultimately leading to a better understanding of the underlying biophysical processes. By combining models and remote sensing tools, and taking

advantage of increasingly available computational power to improve spatial and temporal resolution, further advances in the understanding in vegetation dynamics and the role of meteorological extremes and their impact on water availability will allow to better manage our environment and therefore anticipate variability and changes in natural resources as a consequence of climatic change.

Appendix A.1

USGS wells water level time-series in meters during the hurricane seasons from 2002 to 2011. The black lines represent TC landfalls.

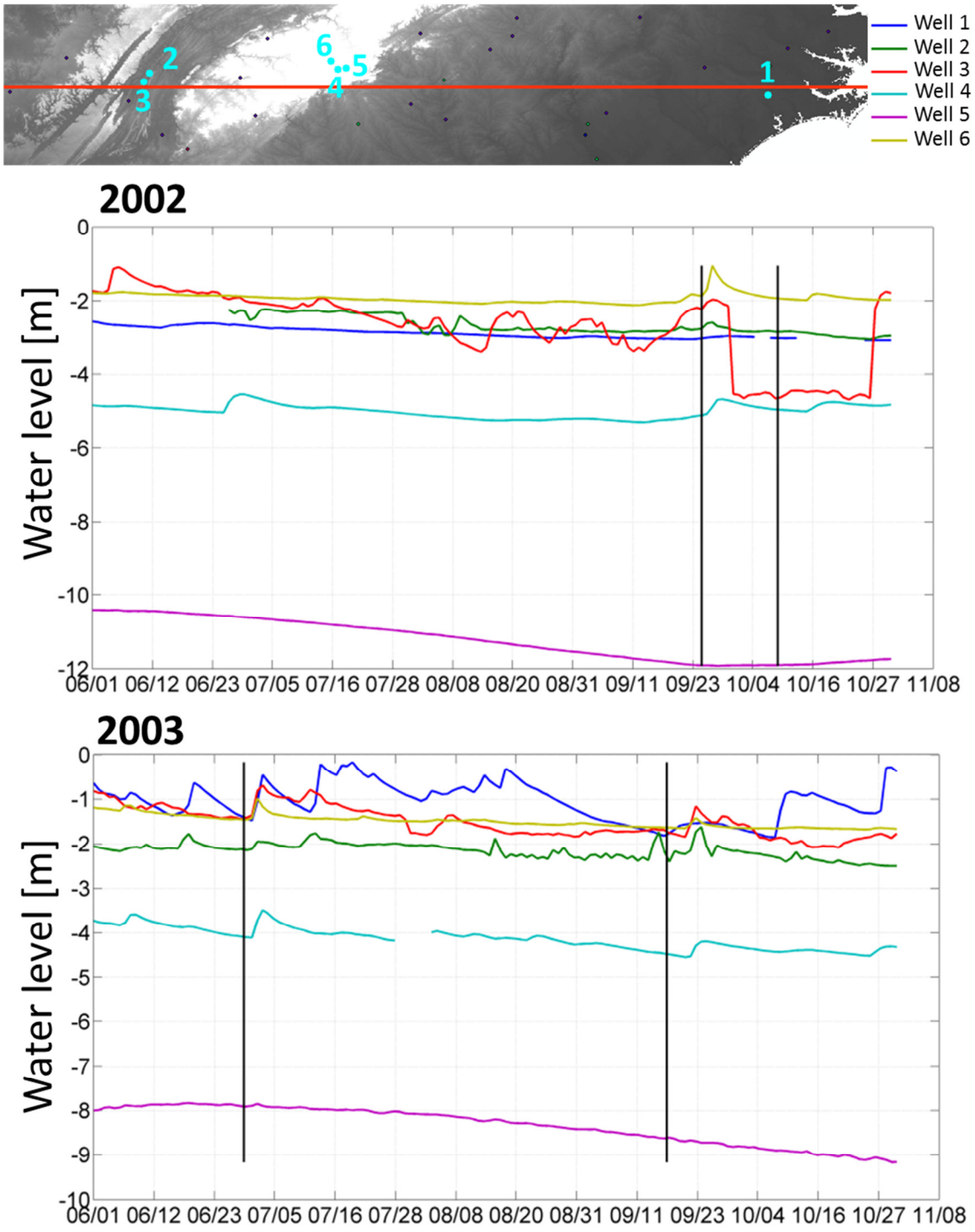

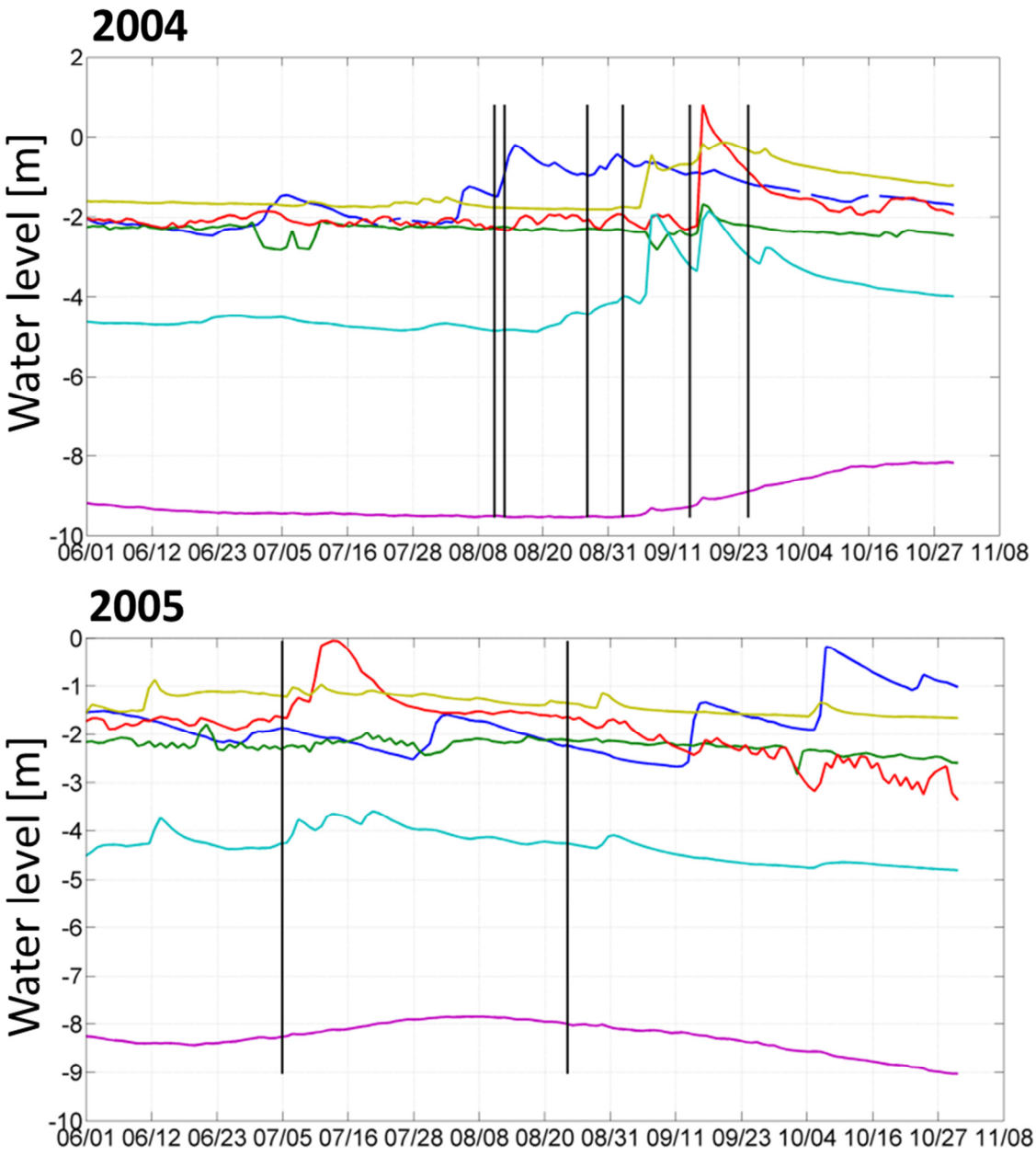
2004
Water level [m]
2
0
-2
-4
-6
-8
-10
06/01 06/12 06/23 07/05 07/16 07/28 08/08 08/20 08/31 09/11 09/23 10/04 10/16 10/27 11/08
2005
Water level [m]
0
-1
-2
-3
-4
-5
-6
-7
-8
-9
-10
06/01 06/12 06/23 07/05 07/16 07/28 08/08 08/20 08/31 09/11 09/23 10/04 10/16 10/27 11/08

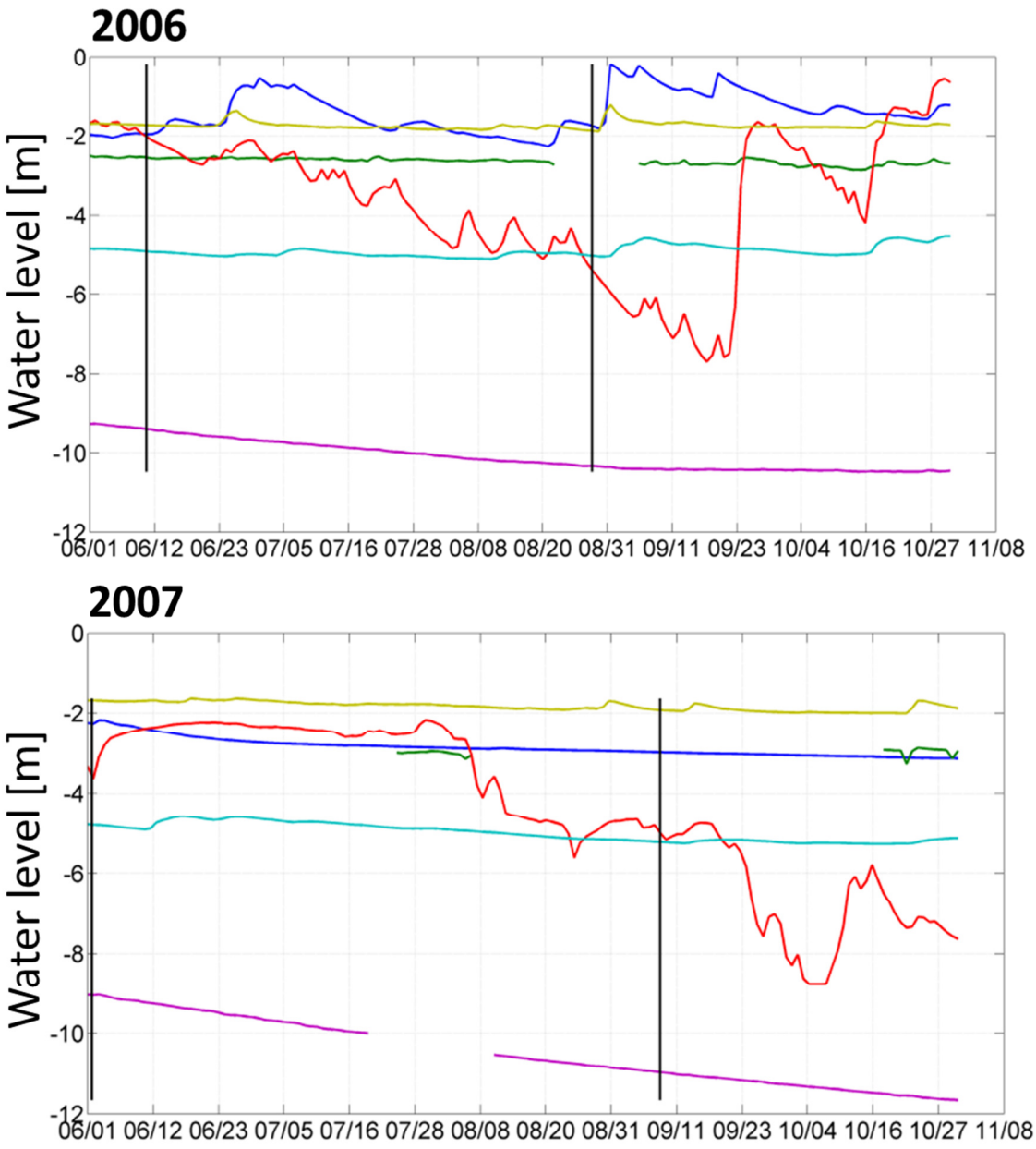
2006
Water level [m]
0
-2
-4
-6
-8
-10
-12
06/01 06/12 06/23 07/05 07/16 07/28 08/08 08/20 08/31 09/11 09/23 10/04 10/16 10/27 11/08
2007
Water level [m]
0
-2
-4
-6
-8
-10
-12
06/01 06/12 06/23 07/05 07/16 07/28 08/08 08/20 08/31 09/11 09/23 10/04 10/16 10/27 11/08

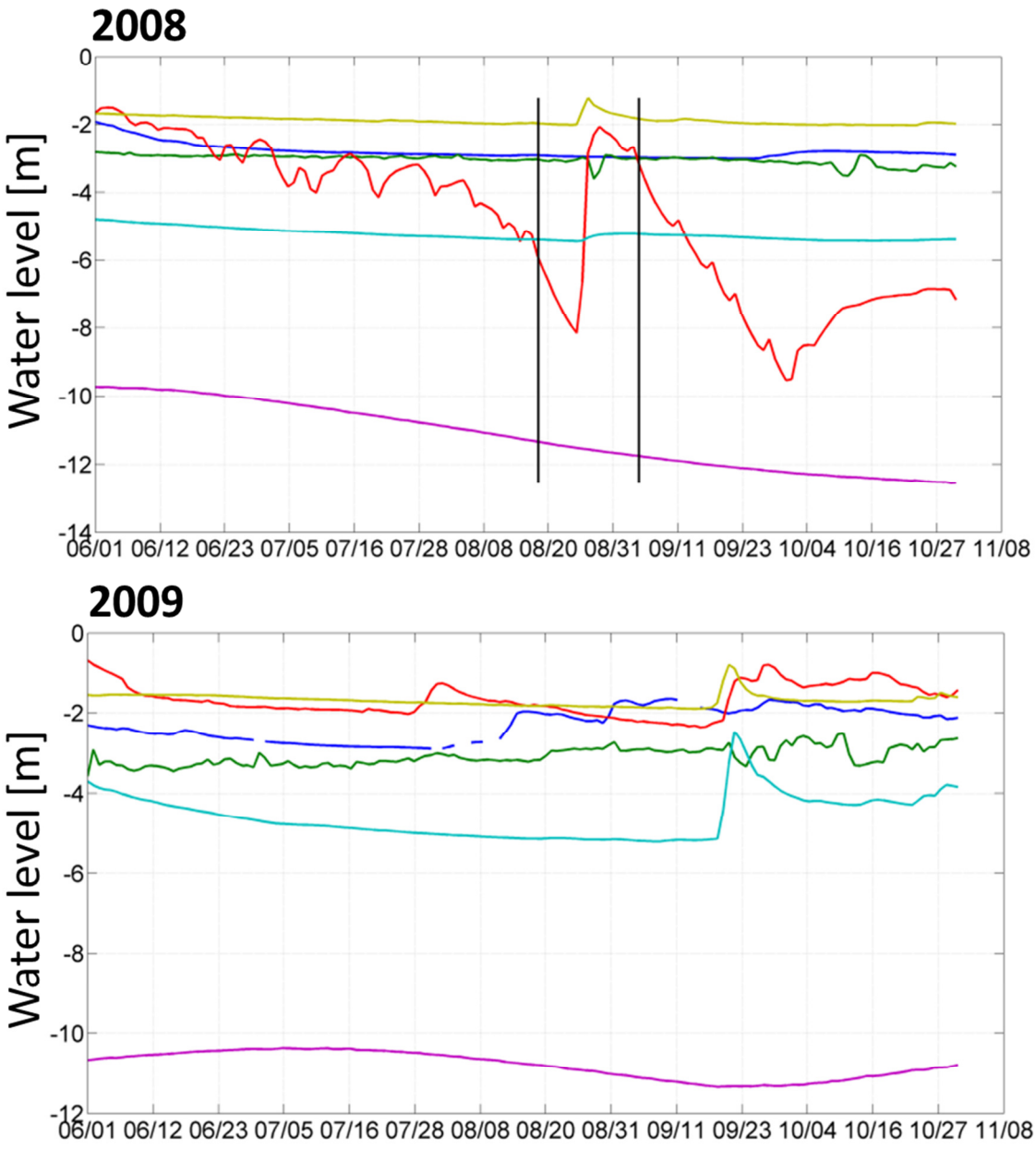
2008
Water level [m]
0
-2
-4
-6
-8
-10
-12
-14
06/01 06/12 06/23 07/05 07/16 07/28 08/08 08/20 08/31 09/11 09/23 10/04 10/16 10/27 11/08
2009
Water level [m]
0
-2
-4
-6
-8
-10
-12
06/01 06/12 06/23 07/05 07/16 07/28 08/08 08/20 08/31 09/11 09/23 10/04 10/16 10/27 11/08

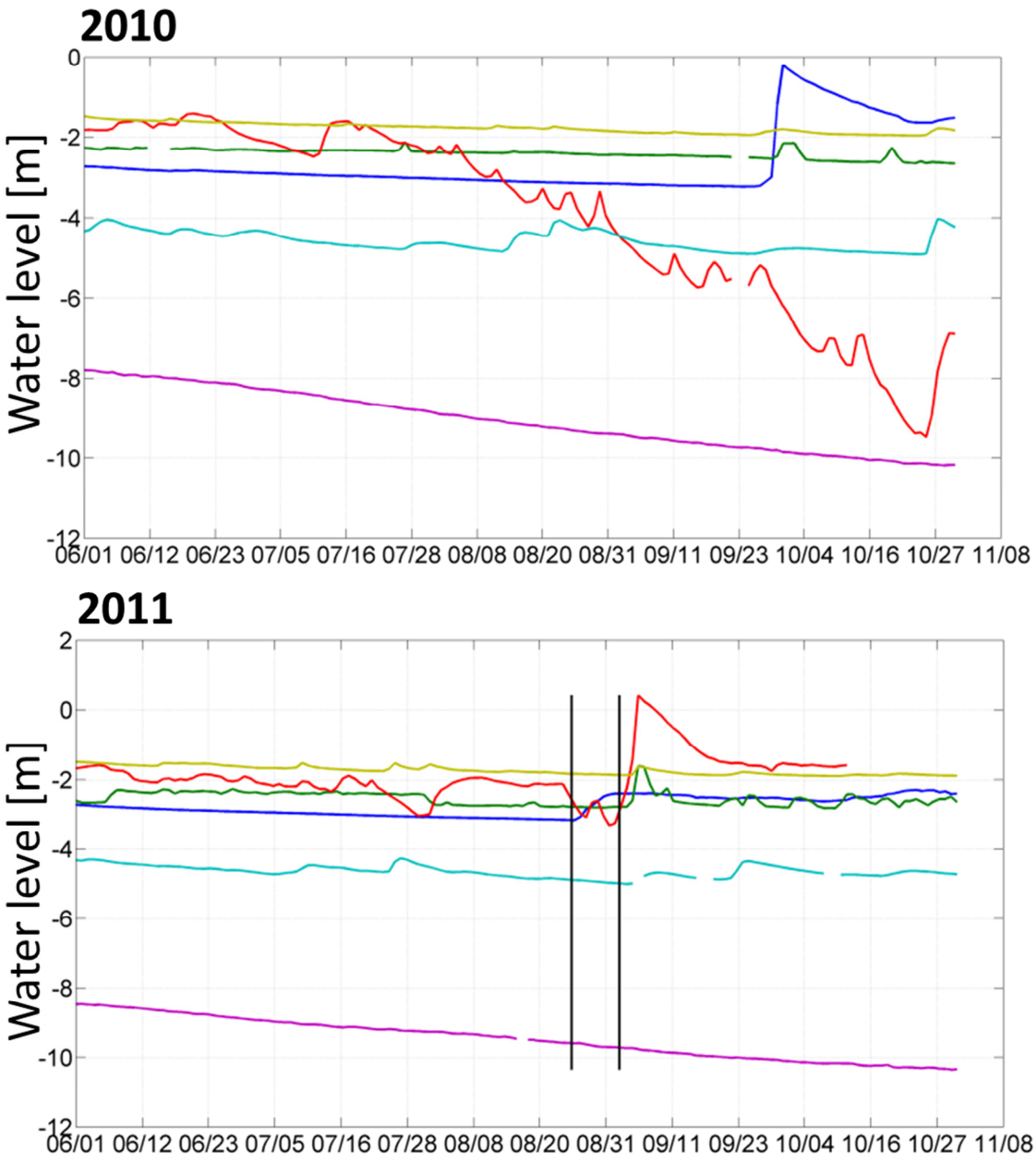
2010
Water level [m]
0
-2
-4
-6
-8
-10
-12
06/01 06/12 06/23 07/05 07/16 07/28 08/08 08/20 08/31 09/11 09/23 10/04 10/16 10/27 11/08
2011
Water level [m]
2
0
-2
-4
-6
-8
-10
-12
06/01 06/12 06/23 07/05 07/16 07/28 08/08 08/20 08/31 09/11 09/23 10/04 10/16 10/27 11/08

Appendix A.2

USGS wells monthly average water table height [m] time-series during the hurricane seasons from 2002 to 2011.

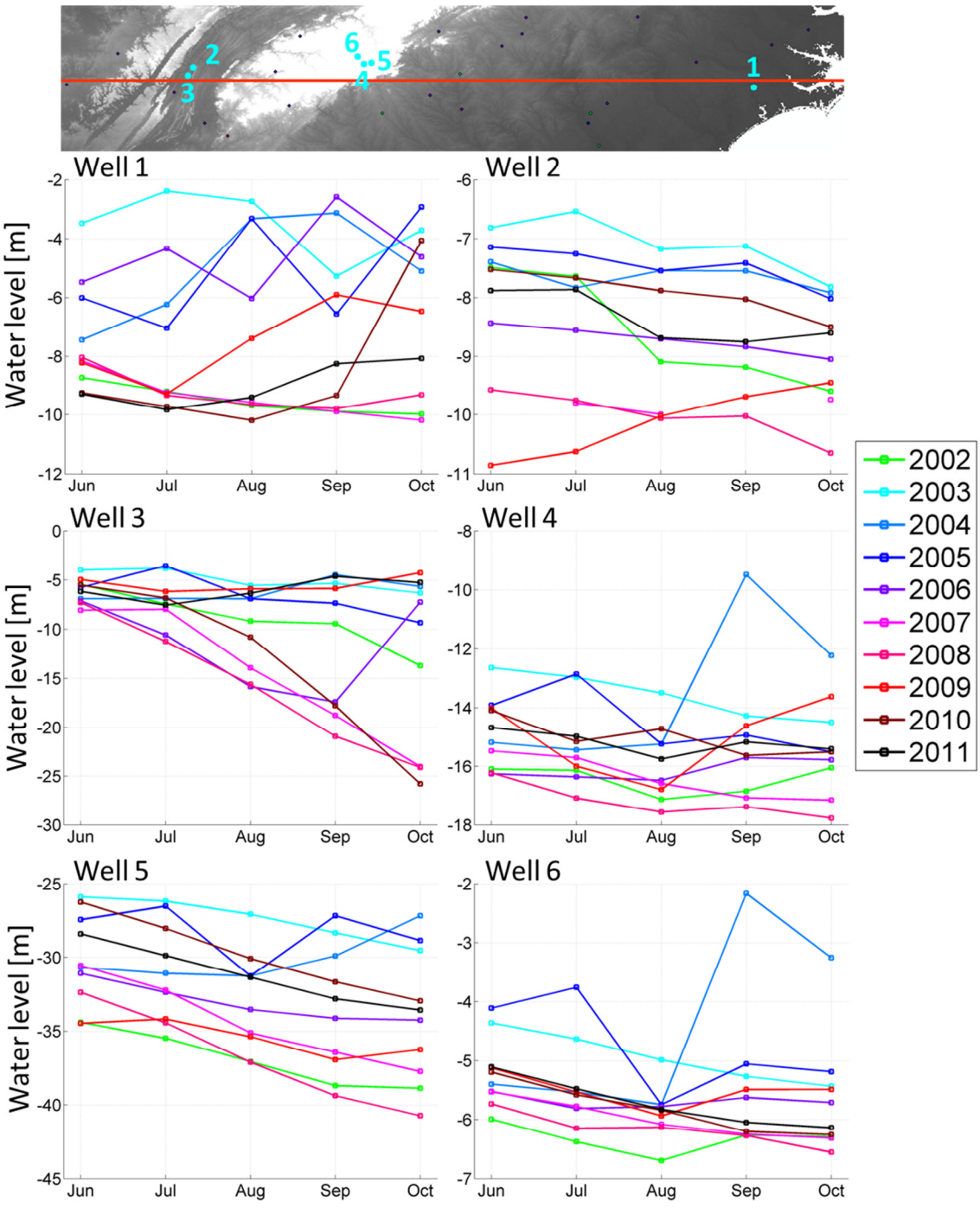

Appendix A.3

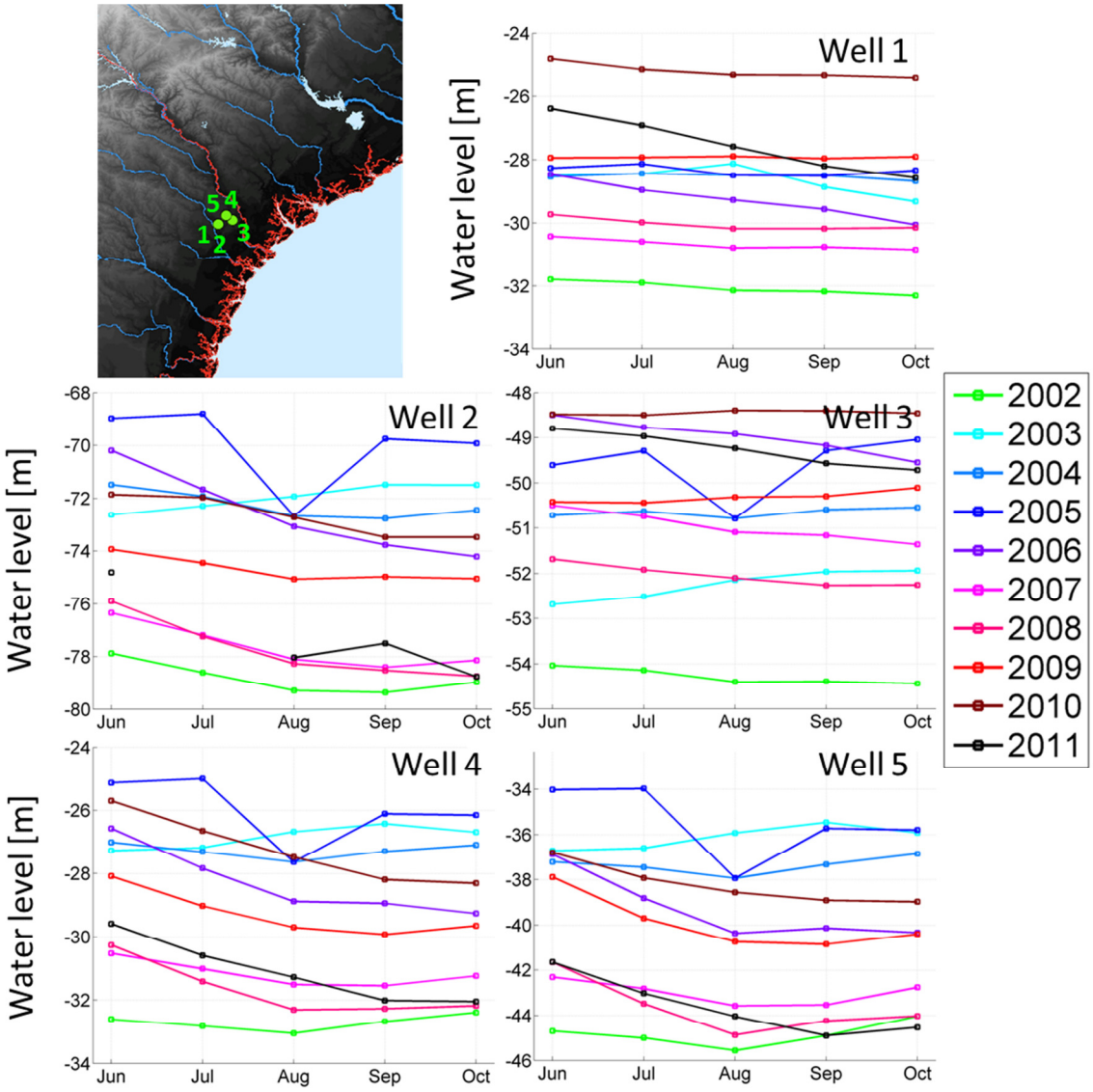
Well 1
Well 2
Well 3
Well 4
Well 5
Water level [m]
Water level [m]
Jun
Jul
Aug
Sep
Oct
2002
2003
2004
2005
2006
2007
2008
2009
2010
2011

Appendix A.4

The blue lines represent the major rivers, the light blue polygons the major lakes and the red dots the dam location over the Southeast US. The dot size is proportional to the dam capacity (i.e. bigger dots represent dams with large capacity of storage).

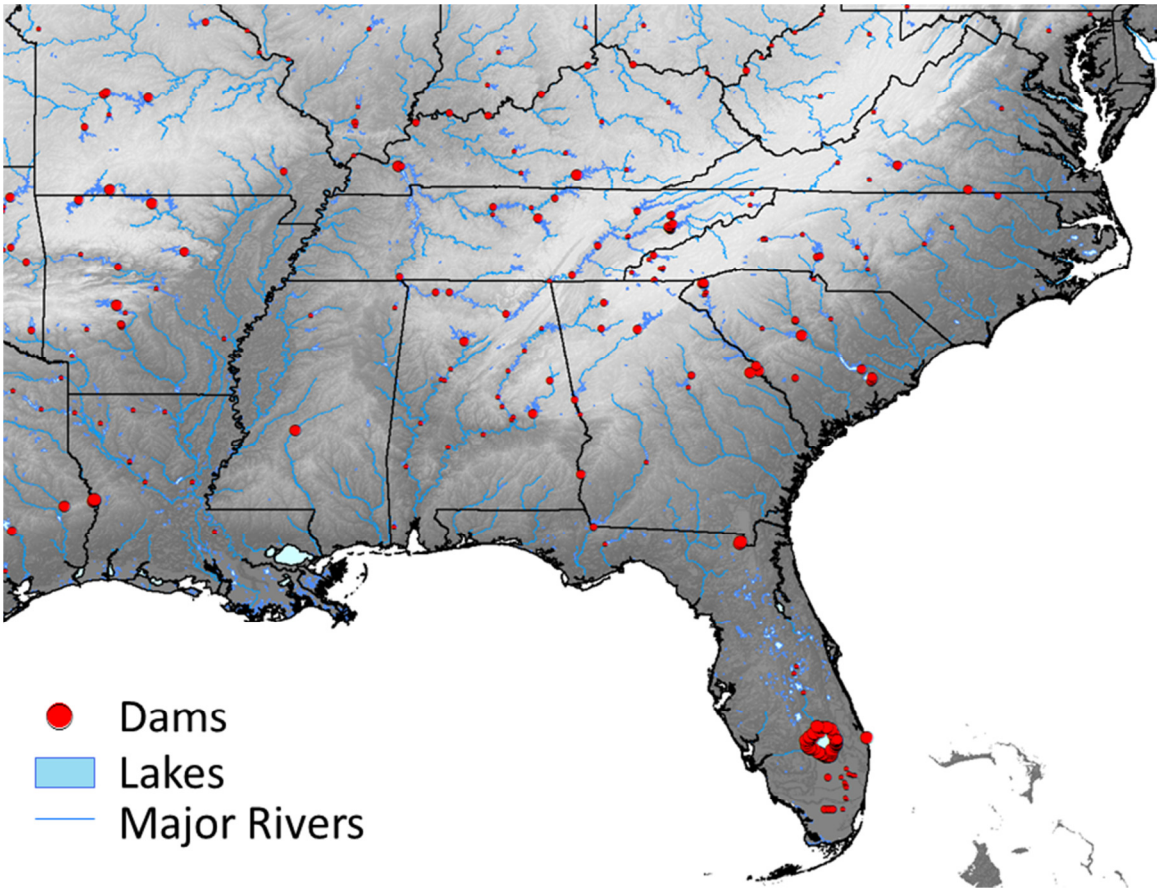

Appendix B

Monthly averaged total soil volumetric water content relative difference of the 1m soil column between the simulation with and without TCs for the 10 years long simulation from Jan 1st 2002 to Dec 31st 2011. The black lines represent the TC tracks.

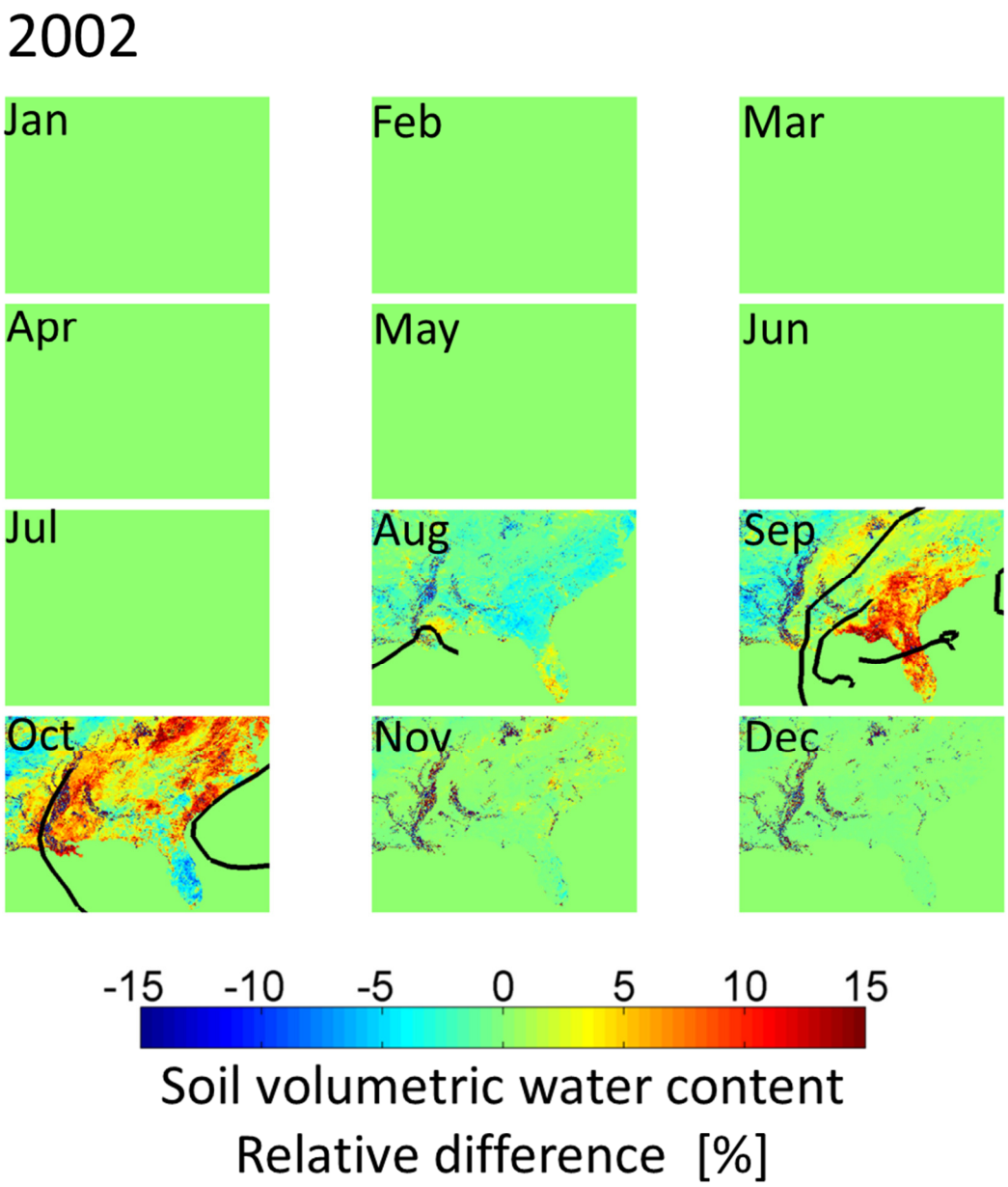

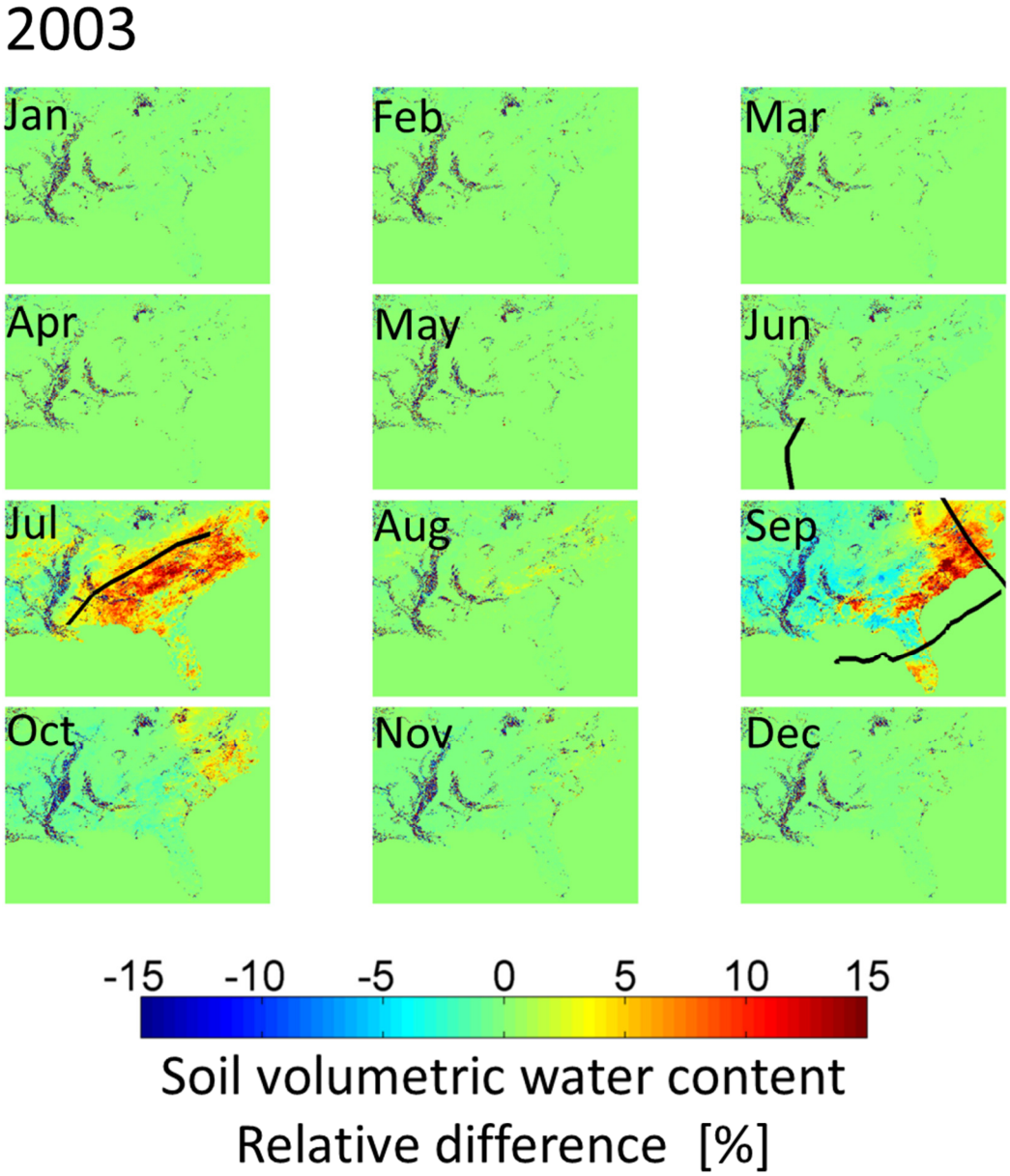
2003
Jan
Feb
Mar
Apr
May
Jun
Jul
Aug
Sep
Oct
Nov
Dec
-15
-10
-5
0
5
10
15
Soil volumetric water content
Relative difference [%]

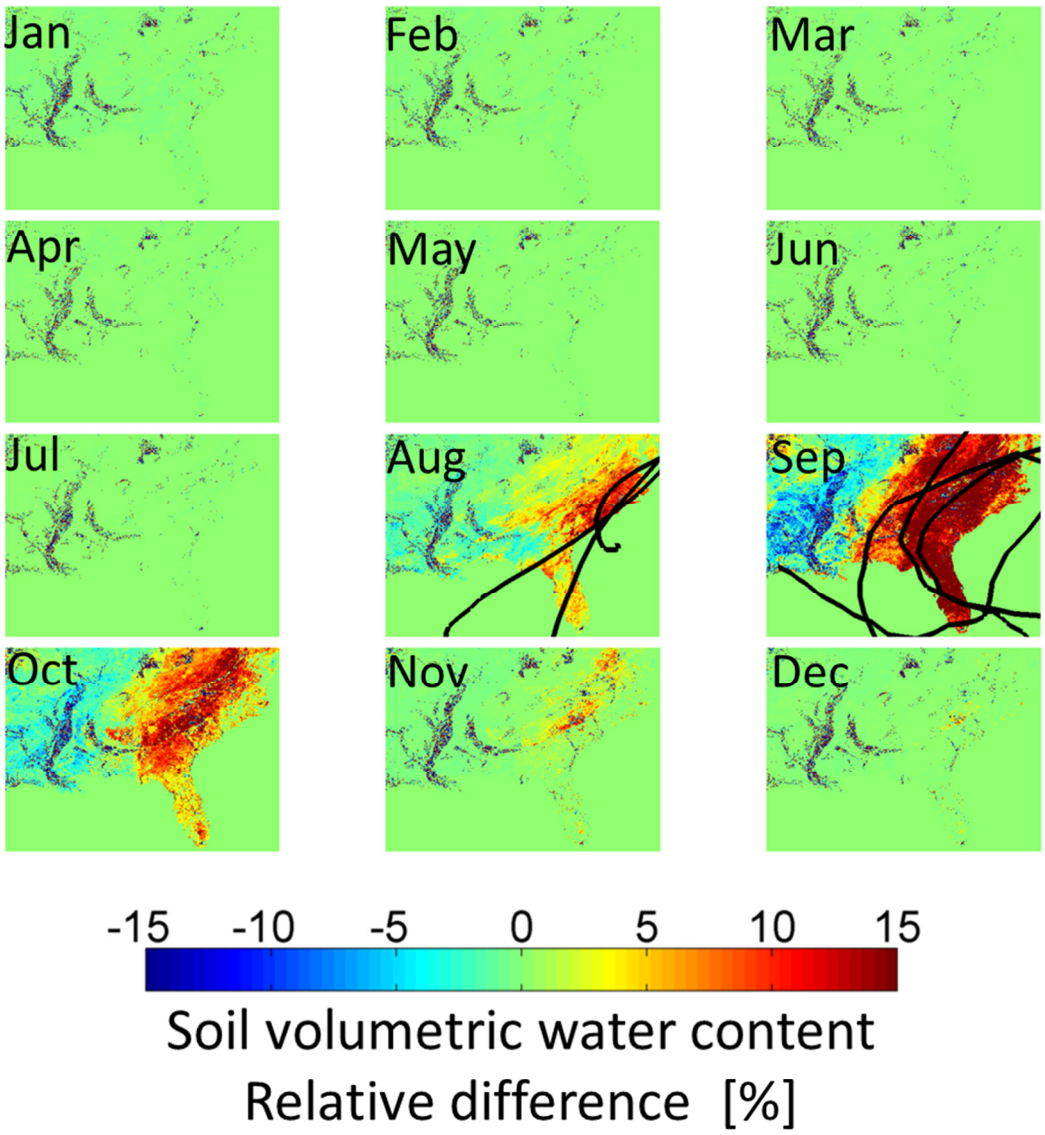
2004
Jan
Feb
Mar
Apr
May
Jun
Jul
Aug
Sep
Oct
Nov
Dec
-15
-10
-5
0
5
10
15
Soil volumetric water content
Relative difference [%]

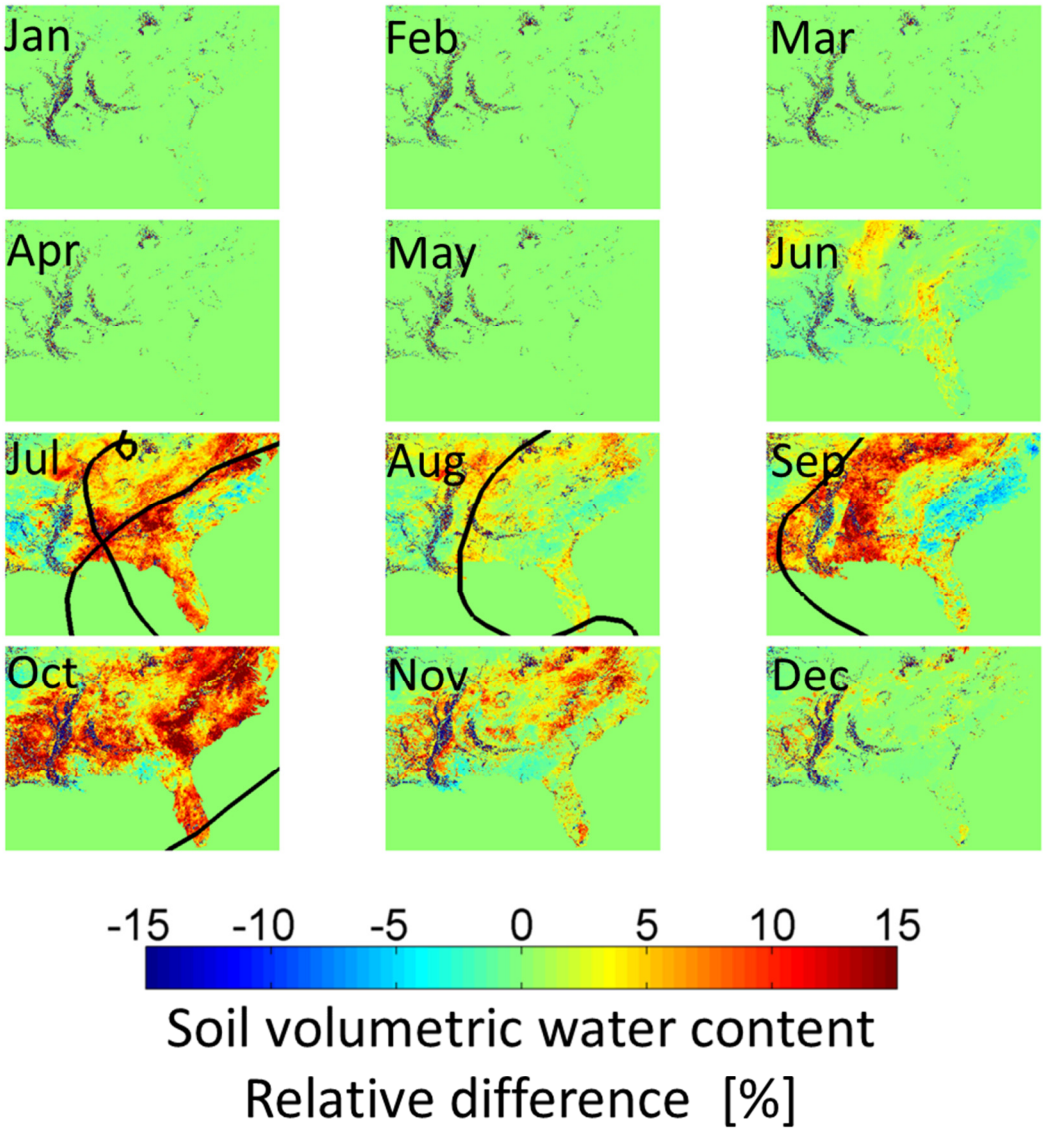
2005
Jan
Feb
Mar
Apr
May
Jun
Jul
Aug
Sep
Oct
Nov
Dec
-15
-10
-5
0
5
10
15
Soil volumetric water content
Relative difference [%]

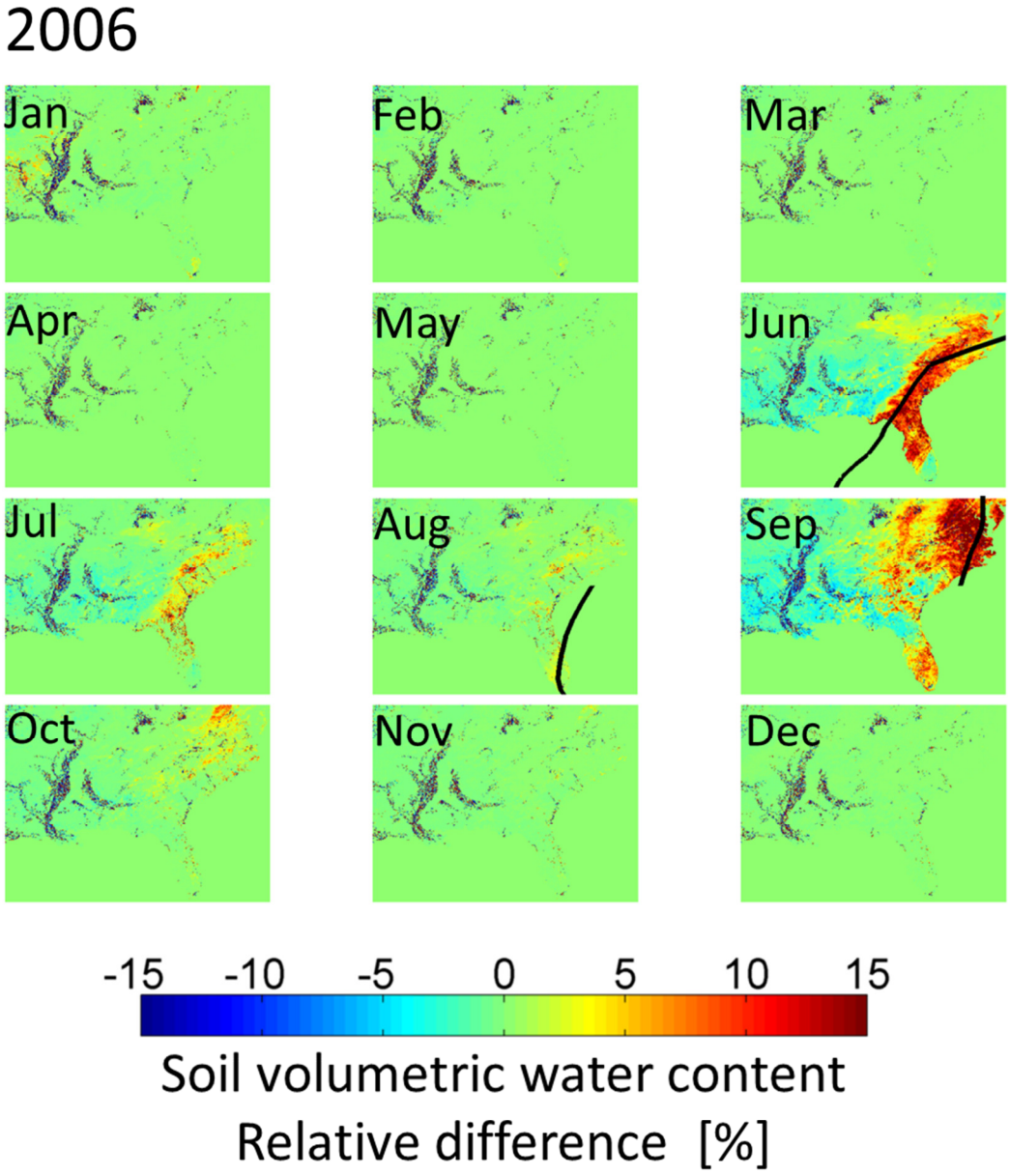
2006
Jan
Feb
Mar
Apr
May
Jun
Jul
Aug
Sep
Oct
Nov
Dec
-15
-10
-5
0
5
10
15
Soil volumetric water content
Relative difference [%]

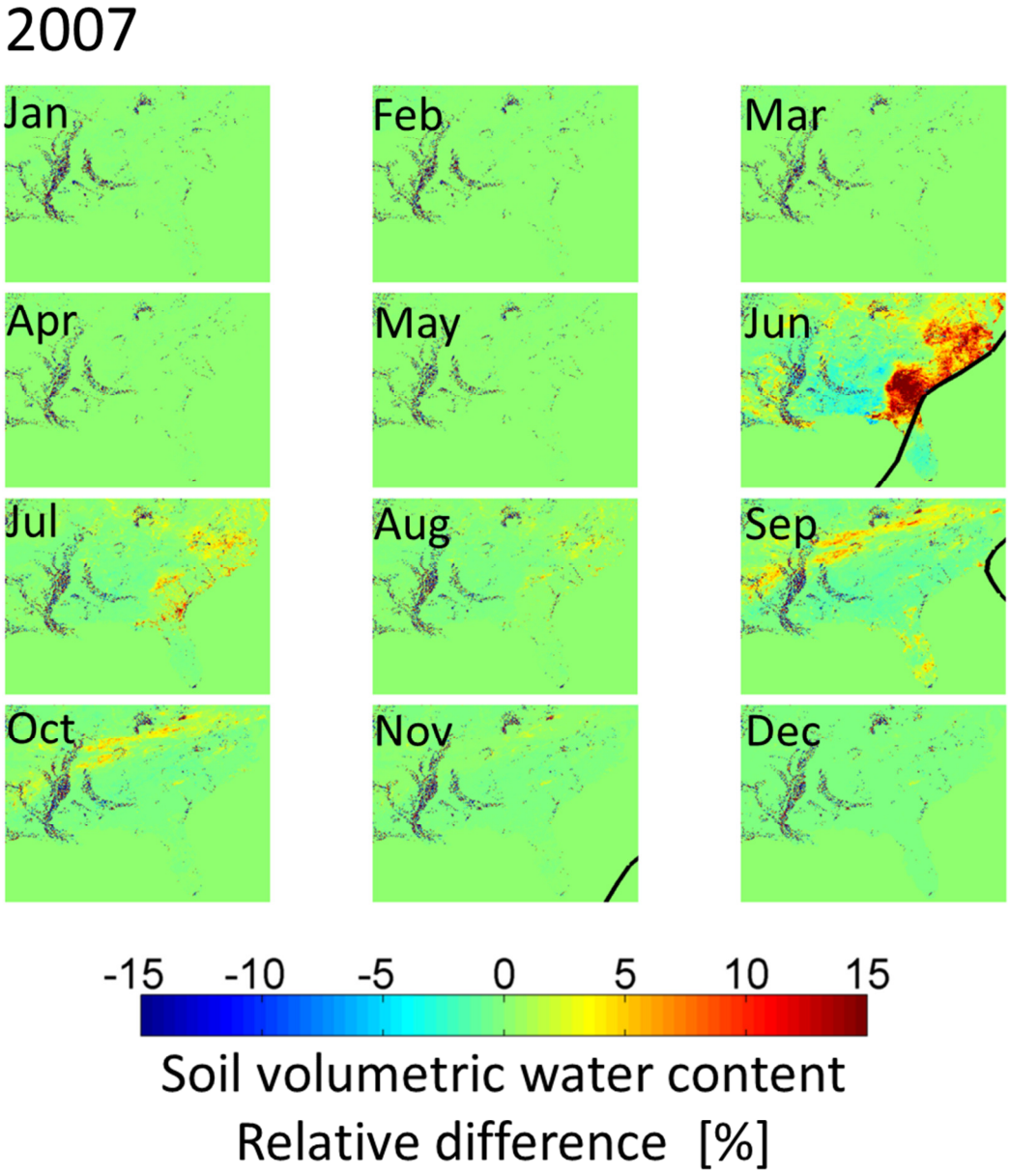
2007
Jan
Feb
Mar
Apr
May
Jun
Jul
Aug
Sep
Oct
Nov
Dec
-15
-10
-5
0
5
10
15
Soil volumetric water content
Relative difference [%]

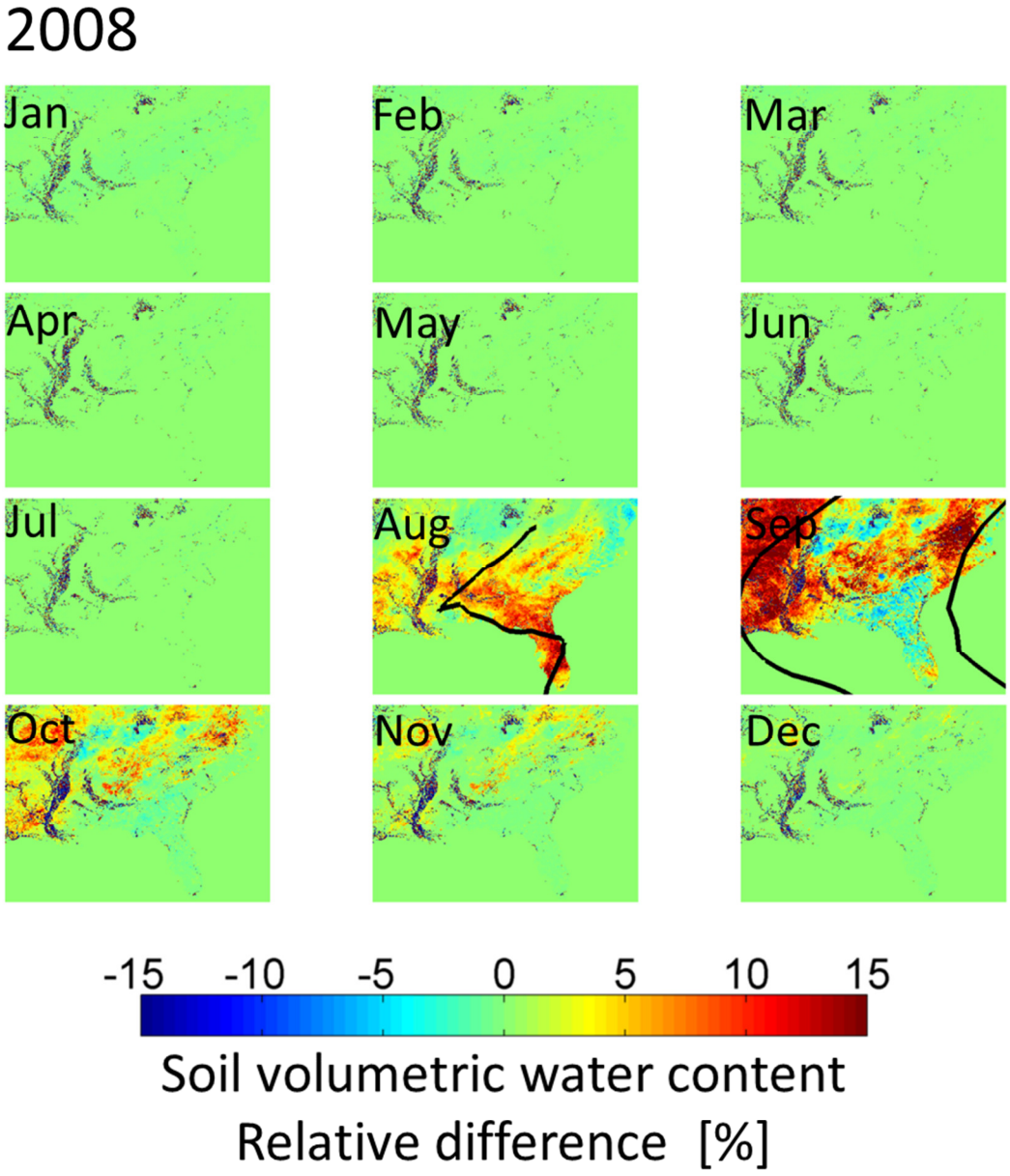
2008
Jan
Feb
Mar
Apr
May
Jun
Jul
Aug
Sep
Oct
Nov
Dec
-15
-10
-5
0
5
10
15
Soil volumetric water content
Relative difference [%]

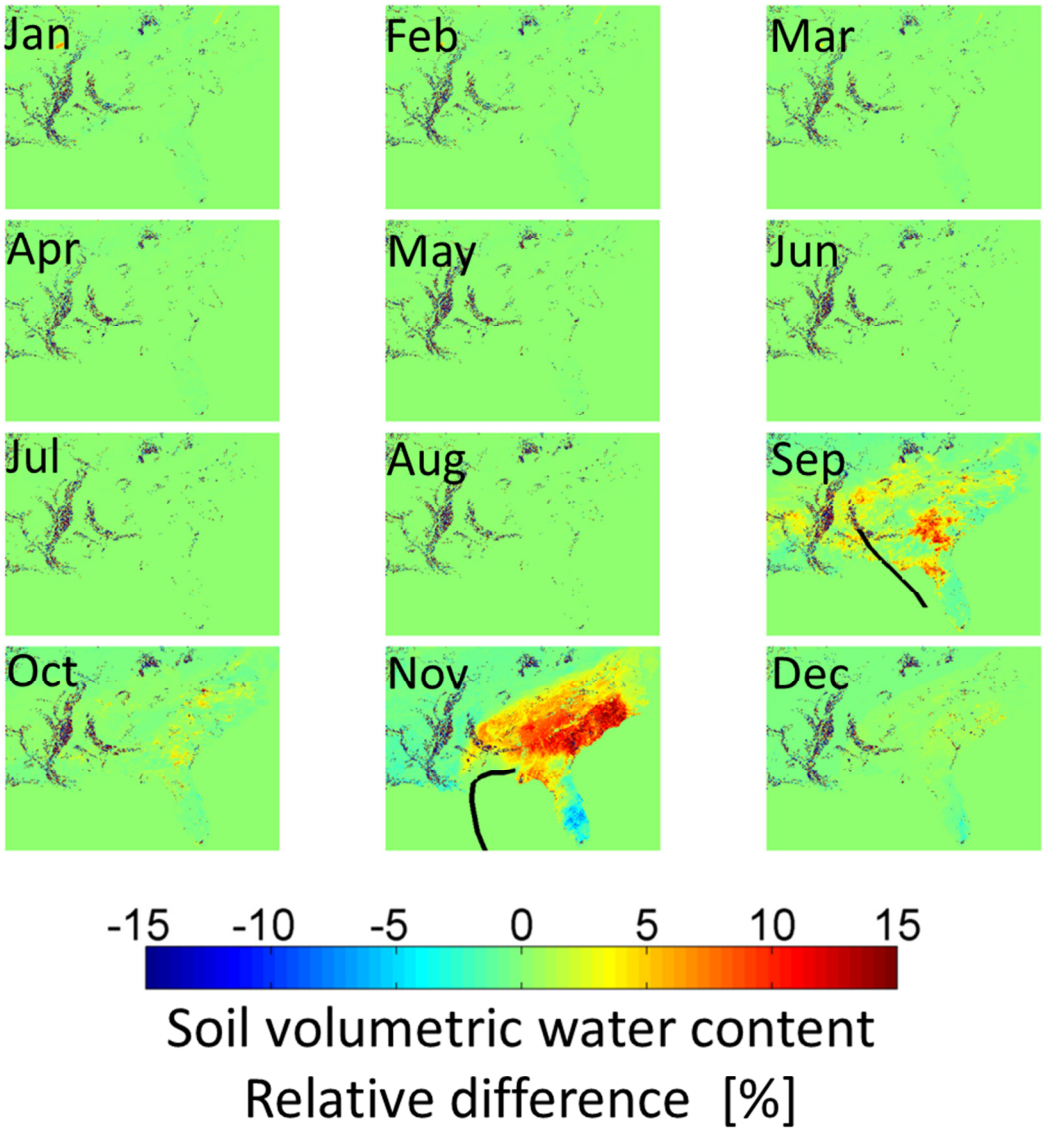
2009
Jan
Feb
Mar
Apr
May
Jun
Jul
Aug
Sep
Oct
Nov
Dec
-15
-10
-5
0
5
10
15
Soil volumetric water content
Relative difference [%]

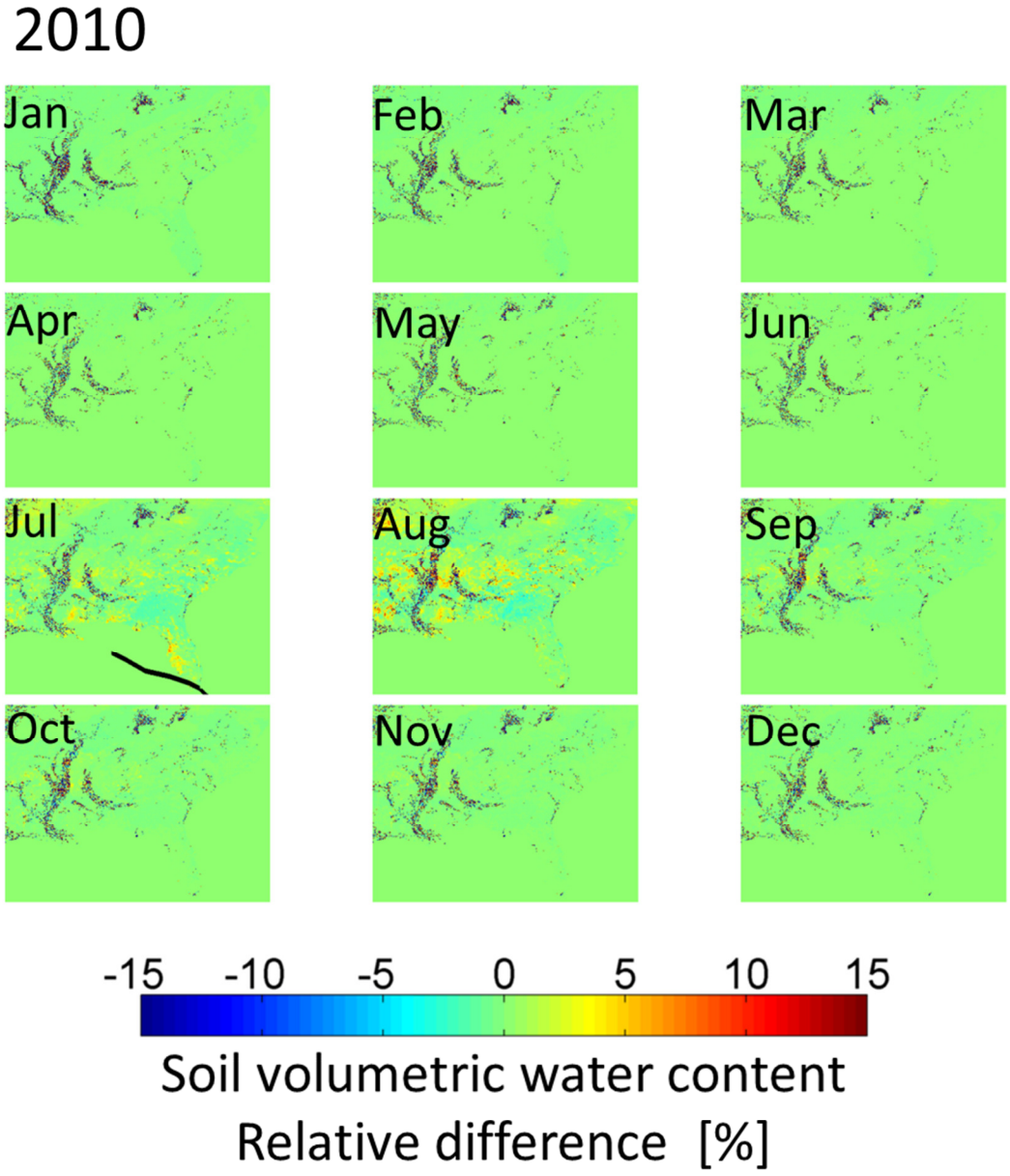
2010
Jan
Feb
Mar
Apr
May
Jun
Jul
Aug
Sep
Oct
Nov
Dec
-15
-10
-5
0
5
10
15
Soil volumetric water content
Relative difference [%]

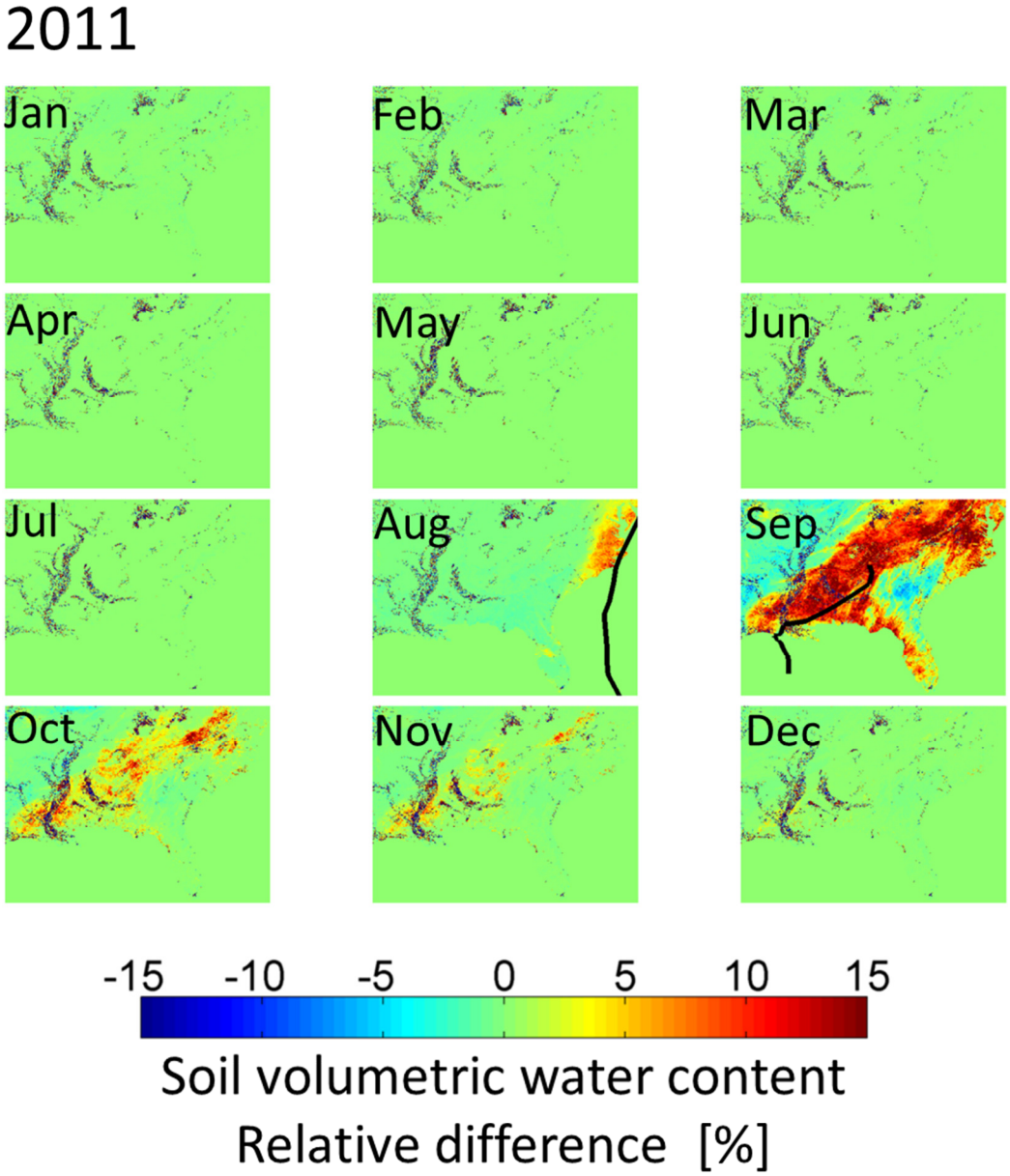
2011
Jan
Feb
Mar
Apr
May
Jun
Jul
Aug
Sep
Oct
Nov
Dec
-15
-10
-5
0
5
10
15
Soil volumetric water content
Relative difference [%]

7 Bibliography

Abramowitz, M., Stegun, I.A., 1972. Handbook of mathematical functions with formulas, graphs, and mathematical tables. National Bureau of Standards : For sale by the Supt. of Docs., U.S. G.P.O., Washington, D.C.

Asbjornsen, H., Goldsmith, G.R., Alvarado-Barrientos, M.S., Rebel, K., Van Osch, F.P., Rietkerk, M., Chen, J., Gotsch, S., Tobon, C., Geissert, D.R., Gomez-Tagle, A., Vache, K., Dawson, T.E., 2011. Ecohydrological advances and applications in plant-water relations research: a review. Journal of Plant Ecology 4, 3-22.

Atallah, E., Bosart, L.F., Aiyyer, A.R., 2007. Precipitation Distribution Associated with Landfalling Tropical Cyclones over the Eastern United States. Monthly Weather Review 135, 2185-2206.

Atallah, E.H., Bosart, L.F., 2003. The Extratropical Transition and Precipitation Distribution of Hurricane Floyd (1999). Monthly Weather Review 131, 1063-1081.

Baldocchi, D., Falge, E., Gu, L., Olson, R., Hollinger, D., Running, S., Anthoni, P., Bernhofer, C., Davis, K., Evans, R., Fuentes, J., Goldstein, A., Katul, G., Law, B., Lee, X., Malhi, Y., Meyers, T., Munger, W., Oechel, W., Paw, K.T., Pilegaard, K., Schmid, H.P., Valentini, R., Verma, S., Vesala, T., Wilson, K., Wofsy, S., 2001. FLUXNET: A New Tool to Study the Temporal and Spatial Variability of Ecosystem–Scale Carbon Dioxide, Water Vapor, and Energy Flux Densities. Bulletin of the American Meteorological Society 82, 2415-2434.

Baldwin, M.E., Mitchell, K.E., 1998. Progress on the NCEP hourly multi-sensor U.S. precipitation analysis for operations and GCIP research, 2nd Symposium on Integrated Observing Systems, 78th AMS Annual Meeting, pp. 10-11.

Barlow, M., 2011. Influence of hurricane-related activity on North American extreme precipitation. Geophys. Res. Lett. 38, L04705.

Barnes, C.F., Fritz, H., Jeseon, Y., 2007. Hurricane Disaster Assessments With Image-Driven Data Mining in High-Resolution Satellite Imagery. Geoscience and Remote Sensing, IEEE Transactions on 45, 1631-1640.

Barros, A.P., 1995. ADAPTIVE MULTILEVEL MODELING OF LAND-ATMOSPHERE INTERACTIONS. Journal of Climate 8, 2144-2160.

Basnet, K., Likens, G.E., Scatena, F.N., Lugo, A.E., 1992. Hurricane Hugo: Damage to a Tropical Rain Forest in Puerto Rico. Journal of Tropical Ecology 8, 47-55.

Beard, K.H., Vogt, K.A., Vogt, D.J., Scatena, F.N., Covich, A.P., Sigurdardottir, R., Siccama, T.G., Crowl, T.A., 2005. Structural and Functional Responses of a Subtropical Forest to 10 Years of Hurricanes and Droughts. Ecological Monographs 75, 345-361.

Beer, C., Reichstein, M., Tomelleri, E., Ciais, P., Jung, M., Carvalhais, N., Rödenbeck, C., Arain, M.A., Baldocchi, D., Bonan, G.B., Bondeau, A., Cescatti, A., Lasslop, G., Lindroth, A., Lomas, M., Luyssaert, S., Margolis, H., Oleson, K.W., Roupsard, O., Veenendaal, E., Viovy, N., Williams, C., Woodward, F.I., Papale, D., 2010. Terrestrial Gross Carbon Dioxide Uptake: Global Distribution and Covariation with Climate. Science 329, 834-838.

Beniston, M., 2012. Impacts of climatic change on water and associated economic activities in the Swiss Alps. Journal of Hydrology 412, 291-296.

Bernacchi, C.J., Singsaas, E.L., Pimentel, C., Portis Jr, A.R., Long, S.P., 2001. Improved temperature response functions for models of Rubisco-limited photosynthesis. Plant, Cell & Environment 24, 253-259.

Blake, E.S., Rappaport, E.N., Landsea, C.W., 2007. The Deadliest, Costliest, and Most Intense United States Tropical Cyclones From 1851 to 2006 (and Other Frequently Requested Hurricane Facts), in: NOAA (Ed.), NOAA Technical Memorandum. NOAA / NHC Miami, p. 37.

Boose, E.R., Foster, D.R., Fluet, M., 1994. Hurricane Impacts to Tropical and Temperate Forest Landscapes. Ecological Monographs 64, 370-400.

Boutet, J., Weishampel, J., 2003. Spatial pattern analysis of pre- and post-hurricane forest canopy structure in North Carolina, USA. Landscape Ecology 18, 553-559.

Bren, L., Lane, P., Hepworth, G., 2010. Longer-term water use of native eucalyptus forest after logging and regeneration: The Coranderrk experiment. Journal of Hydrology 384, 52-64.

Brokaw, N.V.L., Jason, S.G., 1991. Forest Structure Before and After Hurricane Hugo at Three Elevations in the Luquillo Mountains, Puerto Rico. Biotropica 23, 386-392.

Brokaw, N.V.L., Walker, L.R., 1991. Summary of the Effects of Caribbean Hurricanes on Vegetation. Biotropica 23, 442-447.

Brown, M.E., Pinzon, J.E., Didan, K., Morisette, J.T., Tucker, C.J., 2006. Evaluation of the consistency of long-term NDVI time series derived from AVHRR,SPOT-vegetation, SeaWiFS, MODIS, and Landsat ETM+ sensors. Geoscience and Remote Sensing, IEEE Transactions on 44, 1787-1793.

Brun, J., Barros, A.P., 2008. Mapping the History of Environmental Impacts of Land-Falling Hurricanes in The Southeastern United States – A Demonstration for Isabel, in:

IEEE (Ed.), 2008 IEEE International Geoscience and Remote Sensing Symposium. IGARSS 2008., Boston, MA.

Brun, J., Barros, A.P., 2012. Vegetation activity monitoring as an indicator of eco-hydrological impacts of extreme events in the southeastern USA. International Journal of Remote Sensing 34, 519-544.

Brun, J., Barros, A.P., 2013. Mapping the role of tropical cyclones on the hydroclimate of the southeast United States: 2002–2011. International Journal of Climatology, n/a-n/a.

Burkholder, J., Eggleston, D., Glasgow, H., Brownie, C., Reed, R., Janowitz, G., Posey, M., Melia, G., Kinder, C., Corbett, R., Toms, D., Alphin, T., Deamer, N., Springer, J., 2004. Comparative impacts of two major hurricane seasons on the Neuse River and western Pamlico Sound ecosystems. Proceedings of the National Academy of Sciences of the United States of America 101, 9291-9296.

Chambers, J.Q., Fisher, J.I., Zeng, H., Chapman, E.L., Baker, D.B., Hurtt, G.C., 2007. Hurricane Katrina's Carbon Footprint on U.S. Gulf Coast Forests. Science 318, 1107-.

Chen, K.S., Crawford, M.M., Gamba, P., Smith, J.S., 2007. Introduction for the Special Issue on Remote Sensing for Major Disaster Prevention, Monitoring, and Assessment. Geoscience and Remote Sensing, IEEE Transactions on 45, 1515-1518.

Chen, M., Zhuang, Q., Cook, D.R., Coulter, R., Pekour, M., Scott, R.L., Munger, J.W., Bible, K., 2011. Quantification of terrestrial ecosystem carbon dynamics in the conterminous United States combining a process-based biogeochemical model and MODIS and AmeriFlux data. Biogeosciences 8, 2665-2688.

Clark, D.B., Mercado, L.M., Sitch, S., Jones, C.D., Gedney, N., Best, M.J., Pryor, M., Rooney, G.G., Essery, R.L.H., Blyth, E., Boucher, O., Harding, R.J., Huntingford, C., Cox, P.M., 2011. The Joint UK Land Environment Simulator (JULES), model description – Part 2: Carbon fluxes and vegetation dynamics. Geosci. Model Dev. 4, 701-722.

Colin, P., David, C., 2005. Drought, Climate Change, and Vulnerability, Drought and Water Crises. CRC Press, pp. 215-245.

Coops, N.C., Ferster, C.J., Waring, R.H., Nightingale, J., 2009. Comparison of three models for predicting gross primary production across and within forested ecoregions in the contiguous United States. Remote Sensing of Environment 113, 680-690.

Coppin, P., Jonckheere, I., Nackaerts, K., Muys, B., Lambin, E., 2004. Digital change detection methods in ecosystem monitoring: a review. International Journal of Remote Sensing 25, 1565-1596.

Devonec, E., Barros, A.P., 2002. Exploring the transferability of a land-surface hydrology model. Journal of Hydrology 265, 258-282.

Dingman, S.L., 2002. Physical hydrology. Prentice Hall, Upper Saddle River, N.J.

Douglas, E.M., Barros, A.P., 2003. Probable Maximum Precipitation Estimation Using Multifractals: Application in the Eastern United States. Journal of Hydrometeorology 4, 1012-1024.

Dreyer, E., Le Roux, X., Montpied, P., Daudet, F.A., Masson, F., 2001. Temperature response of leaf photosynthetic capacity in seedlings from seven temperate tree species. Tree Physiology 21, 223-232.

Dupigny-Giroux, L.-A., 2001. Towards Characterizing and Planning for Drought In Vermont-Part I: A Climatological Perspective. JAWRA Journal of the American Water Resources Association 37, 505-525.

Emanuel, K., 2005. Increasing destructiveness of tropical cyclones over the past 30 years. Nature 436, 686-688.

Evans, J.L., Hart, R.E., 2003. Objective indicators of the life cycle evolution of extratropical transition for Atlantic tropical cyclones. Monthly Weather Review 131, 909-925.

Everham, E.M., III, Brokaw, N.V.L., 1996. Forest Damage and Recovery from Catastrophic Wind. Botanical Review 62, 113-185.

Farquhar, G.D., Caemmerer, S.V., Berry, J.A., 1980. A BIOCHEMICAL-MODEL OF PHOTOSYNTHETIC CO2 ASSIMILATION IN LEAVES OF C-3 SPECIES. Planta 149, 78-90.

Farris, G.S., Smith, G.J., Crane, M.P., Demas, C.R., Robbins, L.L., LaVoie, D.L., 2007. Science and the storms - the USGS response to the hurricanes of 2005, U.S. Geological Survey Circular. USGS, p. 283.

Fensholt, R., Sandholt, I., Rasmussen, M.S., Stisen, S., Diouf, A., 2006. Evaluation of satellite based primary production modelling in the semi-arid Sahel. Remote Sensing of Environment 105, 173-188.

Field, C.B., Mortsch, L.D., Brklacich, M., Forbes, D.L., Kovacs, P., Patz, J.A., Running, S.W., Scott, M.J., 2007. North America. Climate Change 2007: Impacts, Adaptation and Vulnerability. Contribution of Working Group II to the Fourth Assessment Report of the Intergovernmental Panel on Climate Change, in: M.L. Parry, O.F.C., J.P. Palutikof, P.J. van der Linden and C.E. Hanson (Ed.), Cambridge University Press ed. IPCC, Cambridge, UK.

Fisher, J.I., Mustard, J.F., 2007. Cross-scalar satellite phenology from ground, Landsat, and MODIS data. Remote Sensing of Environment 109, 261-273.

Foken, T., 2008. The Energy Balance Closure Problem: An Overview. Ecological Applications 18, 1351-1367.

Frangi, J.L., Lugo, A.E., 1991. Hurricane Damage to a Flood Plain Forest in the Luquillo Mountains of Puerto Rico. Biotropica 23, 324-335.

Frangi, J.L., Lugo, A.E., 1998. A Flood Plain Palm Forest in the Luquillo Mountains of Puerto Rico Five Years After Hurrican Hugo. Biotropica 30, 339-348.

Franklin, J.L., Pasch, R.J., Avila, L.A., Beven, J.L., Lawrence, M.B., Stewart, S.R., Blake, E.S., 2006. Atlantic Hurricane Season of 2004. Monthly Weather Review 134, 981-1025.

Friend, A.D., 1995. PGEN: an integrated model of leaf photosynthesis, transpiration, and conductance. Ecological Modelling 77, 233-255.

Friend, A.D., Kiang, N.Y., 2005. Land Surface Model Development for the GISS GCM: Effects of Improved Canopy Physiology on Simulated Climate. Journal of Climate 18, 2883-2902.

Galarneau, T.J., Bosart, L.F., Schumacher, R.S., 2010. Predecessor Rain Events ahead of Tropical Cyclones. Monthly Weather Review 138, 3272-3297.

Gao, B.-c., 1996. NDWI—A normalized difference water index for remote sensing of vegetation liquid water from space. Remote Sensing of Environment 58, 257-266.

Gao, F., Morisette, J.T., Wolfe, R.E., Ederer, G., Pedelty, J., Masuoka, E., Myneni, R., Bin, T., Nightingale, J., 2008. An Algorithm to Produce Temporally and Spatially Continuous MODIS-LAI Time Series. Geoscience and Remote Sensing Letters, IEEE 5, 60-64.

Garcia-Quijano, J.F., Barros, A.P., 2005. Incorporating canopy physiology into a hydrological model: photosynthesis, dynamic respiration, and stomatal sensitivity. Ecological Modelling 185, 29-49.

Gebremichael, M., Barros, A.P., 2006. Evaluation of MODIS Gross Primary Productivity (GPP) in tropical monsoon regions. Remote Sensing of Environment 100, 150-166.

Goward, S.N., Masek, J.G., Cohen, W., Moisen, G., Collatz, G.J., Healey, S., Houghton, R.A., Huang, C., Kennedy, R., Law, B., Powell, S., Turner, D., Wulder, M.A., 2008. Forest Disturbance and North American Carbon Flux. Eos, Trans. Amer. Geophys. Union 89.

Gresham, C.A., Williams, T.M., Lipscomb, D.J., 1991. Hurricane Hugo Wind Damage to Southeastern U.S. Coastal Forest Tree Species. Biotropica 23, 420-426.

Harley, P., Sharkey, T., 1991. An improved model of C3 photosynthesis at high CO2: Reversed O2 sensitivity explained by lack of glycerate reentry into the chloroplast. Photosynth Res 27, 169-178.

Hart, R.E., Evans, J.L., 2001. A Climatology of the Extratropical Transition of Atlantic Tropical Cyclones. Journal of Climate 14, 546-564.

Heartsill-Scalley, T., Scatena, F.N., Estrada, C., McDowell, W.H., Lugo, A.E., 2007. Disturbance and long-term patterns of rainfall and throughfall nutrient fluxes in a subtropical wet forest in Puerto Rico. Journal of Hydrology 333, 472-485.

Heinsch, F.A., Maosheng, Z., Running, S.W., Kimball, J.S., Nemani, R.R., Davis, K.J., Bolstad, P.V., Cook, B.D., Desai, A.R., Ricciuto, D.M., Law, B.E., Oechel, W.C., Hyojung, K., Hongyan, L., Wofsy, S.C., Dunn, A.L., Munger, J.W., Baldocchi, D.D., Liukang, X., Hollinger, D.Y., Richardson, A.D., Stoy, P.C., Siqueira, M.B.S., Monson, R.K., Burns, S.P., Flanagan, L.B., 2006. Evaluation of remote sensing based terrestrial productivity from MODIS using regional tower eddy flux network observations. Geoscience and Remote Sensing, IEEE Transactions on 44, 1908-1925.

Heinsch, F.A., Reeves, M., Bowker, C., Votava, P., Kang, S., Milesi, C., Zhao, M., Glassy, J., Nemani, R., Running, S., 2003. GPP and NPP (MOD17A2/A3) Products NASA MODIS Land Algorithm. MOD17 User's Guide, 1-57.

IPCC, 2007. Climate change 2007 : mitigation of climate change / edited by Bert Metz ... [et al.]. Cambridge University Press, Cambridge ; New York :.

Jacobs, D.M., 2007. Forest inventory, catastrophic events and historic geospatial assessments in the south, ASPRS 2007 Annual Conference, Tampa, Florida, p. 12.

Jiang, H., Zipser, E.J., 2010. Contribution of Tropical Cyclones to the Global Precipitation from Eight Seasons of TRMM Data: Regional, Seasonal, and Interannual Variations. Journal of Climate 23, 1526-1543.

Jin, S., Sader, S.A., 2005. MODIS time-series imagery for forest disturbance detection and quantification of patch size effects. Remote Sensing of Environment 99, 462-470.

Jones, S.C., Harr, P.A., Abraham, J., Bosart, L.F., Bowyer, P.J., Evans, J.L., Hanley, D.E., Hanstrum, B.N., Hart, R.E., Lalaurette, F., Sinclair, M.R., Smith, R.K., Thorncroft, C., 2003. The Extratropical Transition of Tropical Cyclones: Forecast Challenges, Current Understanding, and Future Directions. Weather and Forecasting 18, 1052-1092.

Jonsson, P., Eklundh, L., 2002. Seasonality extraction by function fitting to time-series of satellite sensor data. Geoscience and Remote Sensing, IEEE Transactions on 40, 1824-1832.

Kagawa, A., Sack, L., Duarte, K.Ä., James, S., 2009. Hawaiian native forest conserves water relative to timber plantation: Species and stand traits influence water use. Ecological Applications 19, 1429-1443.

Kam, J., Sheffield, J., Yuan, X., Wood, E.F., 2012. The Influence of Atlantic Tropical Cyclones on Drought over the Eastern United States (1980–2007). Journal of Climate 26, 3067-3086.

Kang, S., Running, S.W., Zhao, M., Kimball, J.S., Glassy, J., 2005. Improving continuity of MODIS terrestrial photosynthesis products using an interpolation scheme for cloudy pixels. International Journal of Remote Sensing 26, 1659-1676.

Kanniah, K.D., Beringer, J., Hutley, L.B., Tapper, N.J., Zhu, X., 2009. Evaluation of Collections 4 and 5 of the MODIS Gross Primary Productivity product and algorithm improvement at a tropical savanna site in northern Australia. Remote Sensing of Environment 113, 1808-1822.

Karl, T.R., Meehl, G.A., Miller, C.D., Hassol, S.J., Waple, A.M., Murray, W.L., 2008. Weather and Climate Extremes in a Changing Climate. Regions of Focus: North America, Hawaii, Caribbean, and U.S. Pacific Islands. , in: Commerce, D.o. (Ed.). U.S. Climate Change Science Program and the Subcommittee on Global Change Research, Washington, D.C., p. 164.

Kattge, J., Diaz, S., Lavorel, S., Prentice, I.C., Leadley, P., Boenisch, G., Garnier, E., Westoby, M., Reich, P.B., Wright, I.J., Cornelissen, J.H.C., Violle, C., Harrison, S.P., Van Bodegom, P.M., Reichstein, M., Enquist, B.J., Soudzilovskaia, N.A., Ackerly, D.D., Anand, M., Atkin, O., Bahn, M., Baker, T.R., Baldocchi, D., Bekker, R., Blanco, C.C., Blonder, B., Bond, W.J., Bradstock, R., Bunker, D.E., Casanoves, F., Cavender-Bares, J., Chambers, J.Q., Chapin Iii, F.S., Chave, J., Coomes, D., Cornwell, W.K., Craine, J.M., Dobrin, B.H., Duarte, L., Durka, W., Elser, J., Esser, G., Estiarte, M., Fagan, W.F., Fang, J., Fernandez-Mendez, F., Fidelis, A., Finegan, B., Flores, O., Ford, H., Frank, D., Freschet, G.T., Fyllas, N.M., Gallagher, R.V., Green, W.A., Gutierrez, A.G., Hickler, T., Higgins, S.I., Hodgson, J.G., Jalili, A., Jansen, S., Joly, C.A., Kerkhoff, A.J., Kirkup, D., Kitajima, K., Kleyer, M., Klotz, S., Knops, J.M.H., Kramer, K., Kuehn, I., Kurokawa, H., Laughlin, D., Lee, T.D., Leishman, M., Lens, F., Lenz, T., Lewis, S.L., Lloyd, J., Llusia, J., Louault, F., Ma, S., Mahecha, M.D., Manning, P., Massad, T., Medlyn, B.E., Messier, J., Moles, A.T., Mueller, S.C., Nadrowski, K., Naeem, S., Niinemets, Ü., Noellert, S., Nueske, A., Ogaya, R., Oleksyn, J., Onipchenko, V.G., Onoda, Y., Ordonez, J., Overbeck, G., Ozinga, W.A., Patino, S., Paula, S., Pausas, J.G., Penuelas, J., Phillips, O.L., Pillar, V., Poorter, H., Poorter, L., Poschlod, P., Prinzing, A., Proulx, R., Rammig, A., Reinsch, S., Reu, B., Sack, L., Salgado-Negret, B., Sardans, J., Shiodera, S., Shipley, B., Siefert, A., Sosinski, E., Soussana, J.F., Swaine, E., Swenson, N., Thompson, K., Thornton, P., Waldram, M., Weiher, E., White, M., White, S., Wright, S.J., Yguel, B., Zaehle, S., Zanne, A.E., Wirth, C., 2011. TRY – a global database of plant traits. Global Change Biology 17, 2905-2935.

Katul, G., Manzoni, S., Palmroth, S., Oren, R., 2010. A stomatal optimization theory to describe the effects of atmospheric CO2 on leaf photosynthesis and transpiration. Ann Bot-London 105, 431-442.

Kennedy, R.E., Townsend, P.A., Gross, J.E., Cohen, W.B., Bolstad, P., Wang, Y.Q., Adams, P., 2009. Remote sensing change detection tools for natural resource managers: Understanding concepts and tradeoffs in the design of landscape monitoring projects. Remote Sensing of Environment 113, 1382-1396.

Kite, G.W., 1977. Frequency and risk analyses in hydrology. Water Resources Publications, Fort Collins, Colo.

Knight, D., Davis, R., 2007. Climatology of Tropical Cyclone Rainfall in the Southeastern United States. Physical Geography 28, 126-147.

Knight, D.B., Davis, R.E., 2009. Contribution of tropical cyclones to extreme rainfall events in the southeastern United States. J. Geophys. Res. 114, D23102.

Knutson, T.R., McBride, J.L., Chan, J., Emanuel, K., Holland, G., Landsea, C., Held, I., Kossin, J.P., Srivastava, A.K., Sugi, M., 2010. Tropical cyclones and climate change. Nature Geosci 3, 157-163.

Konrad, C.E., 2001. The Most Extreme Precipitation Events over the Eastern United States from 1950 to 1996: Considerations of Scale. Journal of Hydrometeorology 2, 309-325.

Konrad, C.E., Perry, L.B., 2010. Relationships between tropical cyclones and heavy rainfall in the Carolina region of the USA. International Journal of Climatology 30, 522-534.

Koster, R.D., Suarez, M.J., 1992. Modeling the land surface boundary in climate models as a composite of independent vegetation stands. Journal of Geophysical Research: Atmospheres 97, 2697-2715.

Koster, R.D., Suarez, M.J., 1994. The components of a 'SVAT' scheme and their effects on a GCM's hydrological cycle. Advances in Water Resources 17, 61-78.

Kunkel, K.E., Easterling, D.R., Kristovich, D.A.R., Gleason, B., Stoecker, L., Smith, R., 2010. Recent increases in U.S. heavy precipitation associated with tropical cyclones. Geophys. Res. Lett. 37, L24706.

Landerer, F.W., Swenson, S.C., 2012. Accuracy of scaled GRACE terrestrial water storage estimates. Water Resources Research 48, W04531.

Leuning, R., 1995. A critical appraisal of a combined stomatal-photosynthesis model for C3 plants. Plant, Cell & Environment 18, 339-355.

Leuning, R., 1997. Scaling to a common temperature improves the correlation between the photosynthesis parameters J(max) and V-cmax. Journal of Experimental Botany 48, 345-347.

Li, L., Li, W., Kushnir, Y., 2012. Variation of the North Atlantic subtropical high western ridge and its implication to Southeastern US summer precipitation. Clim. Dyn. 39, 1401-1412.

Licata, J.A., Gyenge, J.E., Fernandez, M.E., Schlichter, T.M., Bond, B.J., 2008. Increased water use by ponderosa pine plantations in northwestern Patagonia, Argentina compared with native forest vegetation. Forest Ecology and Management 255, 753-764.

Lin, Y., Mitchell, K.E., 2005. The NCEP Stage II/IV hourly precipitation analyses: development and applications, 19th Conf. on Hydrology. American Meteorological Society, San Diego, CA,.

Lodge, D.J., McDowell, W.H., 1991. Summary of Ecosystem-Level Effects of Caribbean Hurricanes. Biotropica 23, 373-378.

Lu, D., Mausel, P., Brondazio, E., Moran, E., 2004. Change detection techniques. International Journal of Remote Sensing 25, 2365-2401.

Lunetta, R.S., Knight, J.F., Ediriwickrema, J., Lyon, J.G., Worthy, L.D., 2006. Land-cover change detection using multi-temporal MODIS NDVI data. Remote Sensing of Environment 105, 142-154.

Luzum, B.J., Slatton, K.C., Shrestha, R.L., 2005. Analysis of spatial and temporal stability of airborne laser swath mapping data in feature space. Geoscience and Remote Sensing, IEEE Transactions on 43, 1403-1420.

MacDonald, J.R., 1972. Are the Data Worth Owning? Science 176, 1377.

Mackay, D.S., Ahl, D.E., Ewers, B.E., Samanta, S., Gower, S.T., Burrows, S.N., 2003. Physiological tradeoffs in the parameterization of a model of canopy transpiration. Advances in Water Resources 26, 179-194.

Manzoni, S., Vico, G., Katul, G., Fay, P.A., Polley, W., Palmroth, S., Porporato, A., 2011. Optimizing stomatal conductance for maximum carbon gain under water stress: a meta-analysis across plant functional types and climates. Functional Ecology 25, 456-467.

Mas, J.-F., 1999. Monitoring land-cover changes: a comparison of change detection techniques. International Journal of Remote Sensing 20, 139 - 152.

Matyas, C.J., 2010. Associations between the size of hurricane rain fields at landfall and their surrounding environments. Meteorology & Atmospheric Physics 106, 135-148.

Maxwell, J.T., Soulé, P.T., Ortegren, J.T., Knapp, P.A., 2011. Drought-Busting Tropical Cyclones in the Southeastern Atlantic United States: 1950–2008. Annals of the Association of American Geographers 102, 259-275.

McGrath, G.S., Sadler, R., Fleming, K., Tregoning, P., Hinz, C., Veneklaas, E.J., 2012. Tropical cyclones and the ecohydrology of Australia's recent continental-scale drought. Geophys. Res. Lett. 39, L03404.

Medlyn, B.E., Dreyer, E., Ellsworth, D., Forstreuter, M., Harley, P.C., Kirschbaum, M.U.F., Le Roux, X., Montpied, P., Strassemeyer, J., Walcroft, A., Wang, K., Loustau, D., 2002. Temperature response of parameters of a biochemically based model of photosynthesis. II. A review of experimental data. Plant, Cell & Environment 25, 1167-1179.

Meehl, G.A., Stocker, T.F., W.D.Collines, Friedlingstein, P., A.T.Gaye, Gregory, J.M., Kitoh, A., Knutti, R., Murphy, J.M., Noda, A., Raper, S.C.B., Watterson, I.G., Weaver, A.J., Zhao, Z.-C., 2007. Global climate projections. Climate Change 2007: The Physical Science Basis. Contribution of Working Group I to the Fourth Assessment Report of the Intergovernmental Panel on Climate Change, Cambridge University Press ed, Cambridge and NewYork, pp. 747-846.

Mendelsohn, R., Emanuel, K., Chonabayashi, S., Bakkensen, L., 2012. The impact of climate change on global tropical cyclone damage. Nature Clim. Change advance online publication.

Mesinger, F., DiMego, G., Kalnay, E., Mitchell, K., Shafran, P.C., Ebisuzaki, W., Jovi*f*á, D.a., Woollen, J., Rogers, E., Berbery, E.H., Ek, M.B., Fan, Y., Grumbine, R., Higgins, W., Li, H., Lin, Y., Manikin, G., Parrish, D., Shi, W., 2006. North American Regional Reanalysis. Bulletin of the American Meteorological Society 87, 343-360.

Metternicht, G., Hurni, L., Gogu, R., 2005. Remote sensing of landslides: An analysis of the potential contribution to geo-spatial systems for hazard assessment in mountainous environments. Remote Sensing of Environment 98, 284-303.

Michener, W.K., Blood, E.R., Bildstein, K.L., Brinson, M.M., Gardner, L.R., 1997. Climate Change, Hurricanes and Tropical Storms, and Rising Sea Level in Coastal Wetlands. Ecological Applications 7, 770-801.

Miller, D.A., White, R.A., 1998. A Conterminous United States Multilayer Soil Characteristics Dataset for Regional Climate and Hydrology Modeling. Earth Interactions 2, 1-26.

Mo, K.C., Chen, L.-C., Shukla, S., Bohn, T.J., Lettenmaier, D.P., 2012. Uncertainties in North American land data assimilation systems over the contiguous United States. Journal of Hydrometeorology 13, 996-1009.

Monteith, J., 1972. Solar radiation and productivity in tropical ecosystems. Journal of applied ecology 9, 747-766.

Morisette, J.T., 2009. NACP products.

Myneni, R.B., Hoffman, S., Knyazikhin, Y., Privette, J.L., Glassy, J., Tian, Y., Wang, Y., Song, X., Zhang, Y., Smith, G.R., Lotsch, A., Friedl, M., Morisette, J.T., Votava, P., Nemani, R.R., Running, S.W., 2002. Global products of vegetation leaf area and fraction absorbed PAR from year one of MODIS data. Remote Sensing of Environment 83, 214-231.

Neigh, C.S.R., Tucker, C.J., Townshend, J.R.G., 2008. North American vegetation dynamics observed with multi-resolution satellite data. Remote Sensing of Environment 112, 1749-1772.

Nightingale, J.M., Coops, N.C., Waring, R.H., Hargrove, W.W., 2007. Comparison of MODIS gross primary production estimates for forests across the U.S.A. with those generated by a simple process model, 3-PGS. Remote Sensing of Environment 109, 500-509.

Njoku, E.G., Chan, S.K., 2006. Vegetation and surface roughness effects on AMSR-E land observations. Remote Sensing of Environment 100, 190-199.

Nogueira, R.C., Keim, B.D., 2011. Contributions of Atlantic tropical cyclones to monthly and seasonal rainfall in the eastern United States 1960-2007. Theoretical & Applied Climatology 103, 213-227.

O'Connor, J.E., Costa, J.E., 2004. Spatial distribution of the largest rainfall-runoff floods from basins between 2.6 and 26,000 km2 in the United States and Puerto Rico. Water Resour. Res. 40, W01107.

Oren, R., Sperry, J.S., Katul, G.G., Pataki, D.E., Ewers, B.E., Phillips, N., Schäfer, K.V.R., 1999. Survey and synthesis of intra- and interspecific variation in stomatal sensitivity to vapour pressure deficit. Plant, Cell & Environment 22, 1515-1526.

Oren, R.A.M., Hsieh, C.-I., Stoy, P., Albertson, J., McCarthy, H.R., Harrell, P., Katul, G.G., 2006. Estimating the uncertainty in annual net ecosystem carbon exchange: spatial variation in turbulent fluxes and sampling errors in eddy-covariance measurements. Global Change Biology 12, 883-896.

Oswalt, S.N., Oswalt, C.M., 2008. Relationships between common forest metrics and realized impacts of Hurricane Katrina on forest resources in Mississippi. Forest Ecology and Management 255, 1692-1700.

Paerl, H., Valdes, L., Piehler, M., Stow, C., 2006. Assessing the Effects of Nutrient Management in an Estuary Experiencing Climatic Change: The Neuse River Estuary, North Carolina. Environmental Management 37, 422-436.

Palmroth, S., Katul, G.G., Hui, D.F., McCarthy, H.R., Jackson, R.B., Oren, R., 2010. Estimation of long-term basin scale evapotranspiration from streamflow time series. Water Resources Research 46.

Parodi, A., Foufoula-Georgiou, E., Emanuel, K., 2011. Signature of microphysics on spatial rainfall statistics. J. Geophys. Res. 116, D14119.

Parry, M.L., Canziani, O.F., Palutikof, J.P., Linden, P.J.v.d., Hanson, C.E., 2007. Contribution of Working Group II to the Fourth Assessment Report of the Intergovernmental Panel on Climate Change, Cambridge University Press ed, Cambridge and New York.

Pascarella, J.B., Mitchell Aide, T., Zimmerman, J.K., 2004. Short-term response of secondary forests to hurricane disturbance in Puerto Rico, USA. Forest Ecology and Management 199, 379-393.

Pielke, J.R.A., Gratz, J., Landsea, C.W., Collins, D., Saunders, M.A., Musulin, R., 2008. Normalized Hurricane Damage in the United States: 1900--2005. Natural Hazards Review 9, 29-42.

Pielke, R.A., Landsea, C., Mayfield, M., Laver, J., Pasch, R., 2005. Hurricanes and Global Warming. Bulletin of the American Meteorological Society 86, 1571-1575.

Potter, C., Tan, P.-N., Kumar, V., Kucharik, C., Klooster, S., Genovese, V., Cohen, W., Healey, S., 2005. Recent History of Large-Scale Ecosystem Disturbances in North America Derived from the AVHRR Satellite Record. Ecosystems 8, 808-824.

Prat, O.P., Barros, A.P., 2010. Assessing satellite-based precipitation estimates in the Southern Appalachian mountains using rain gauges and TRMM PR. Adv. Geosci. 25, 143-153.

Prat, O.P., Nelson, B.R., 2012. Precipitation contribution of tropical cyclones in the Southeastern United States from 1998 to 2009 using TRMM satellite data. Journal of Climate.

Prince, S.D., Goward, S.N., 1995. Global Primary Production: A Remote Sensing Approach. Journal of Biogeography 22, 815-835.

Rawls, W.J., Ahuja, L.R., Brakensiek, D.L., Shirmohammadi, A., 1993. Infiltration and Soil Water Movement, in: Maidment, D.R. (Ed.), Handbook of Hydrology. McGraw-Hill, New York.

Reginald, R.M., Vladimir, E.R., 2009. Groundwater storage changes in arctic permafrost watersheds from GRACE and in situ measurements. Environmental Research Letters 4, 045009.

Reilly, A.E., 1991. The Effects of Hurricane Hugo in Three Tropical Forests in the U.S. Virgin Islands. Biotropica 23, 414-419.

Riegger, J., Tourian, M.J., Devaraju, B., Sneeuw, N., 2012. Analysis of grace uncertainties by hydrological and hydro-meteorological observations. Journal of Geodynamics 59–60, 16-27.

Rodgers, E.B., Adler, R.F., Pierce, H.F., 2001. Contribution of Tropical Cyclones to the North Atlantic Climatological Rainfall as Observed from Satellites. Journal of Applied Meteorology 40, 1785-1800.

Rogan, J., Schneider, L., Christman, Z., Millones, M., Lawrence, D., Schmook, B., 2010. Hurricane disturbance mapping using MODIS EVI data in the southeastern Yucatán, Mexico. Remote Sensing Letters 2, 259-267.

Running, S.W., Nemani, R.R., Heinsch, F.A., Zhao, M., Reeves, M., Hashimoto, H., 2004. A Continuous Satellite-Derived Measure of Global Terrestrial Primary Production. BioScience 54, 547-560.

Schaefer, K., Schwalm, C.R., Williams, C., Arain, M.A., Barr, A., Chen, J.M., Davis, K.J., Dimitrov, D., Hilton, T.W., Hollinger, D.Y., Humphreys, E., Poulter, B., Raczka, B.M., Richardson, A.D., Sahoo, A., Thornton, P., Vargas, R., Verbeeck, H., Anderson, R., Baker, I., Black, T.A., Bolstad, P., Chen, J., Curtis, P.S., Desai, A.R., Dietze, M., Dragoni, D., Gough, C., Grant, R.F., Gu, L., Jain, A., Kucharik, C., Law, B., Liu, S., Lokipitiya, E., Margolis, H.A., Matamala, R., McCaughey, J.H., Monson, R., Munger, J.W., Oechel, W., Peng, C., Price, D.T., Ricciuto, D., Riley, W.J., Roulet, N., Tian, H., Tonitto, C., Torn, M., Weng, E., Zhou, X., 2012. A model-data comparison of gross primary productivity: Results from the North American Carbon Program site synthesis. J. Geophys. Res. 117, G03010.

Schaller, M.F., Fan, Y., 2009. River basins as groundwater exporters and importers: Implications for water cycle and climate modeling. J. Geophys. Res. 114, D04103.

Sellers, P.J., Berry, J.A., Collatz, G.J., Field, C.B., Hall, F.G., 1992. Canopy reflectance, photosynthesis, and transpiration. III. A reanalysis using improved leaf models and a new canopy integration scheme. Remote Sensing of Environment 42, 187-216.

Sellers, P.J., Mintz, Y., Sud, Y.C., Dalcher, A., 1986. A Simple Biosphere Model (SIB) for Use within General Circulation Models. Journal of the Atmospheric Sciences 43, 505-531.

Shepherd, J.M., Knutson, T., 2007. The Current Debate on the Linkage Between Global Warming and Hurricanes. Geography Compass 1, 1-24.

Shrestha, R.L., Carter, W.E., Sartori, M., Luzum, B.J., Slatton, K.C., 2005. Airborne Laser Swath Mapping: Quantifying changes in sandy beaches over time scales of weeks to years. ISPRS Journal of Photogrammetry and Remote Sensing 59, 222-232.

Smith, J.A., Villarini, G., Baeck, M.L., 2010. Mixture Distributions and the Hydroclimatology of Extreme Rainfall and Flooding in the Eastern United States. Journal of Hydrometeorology 12, 294-309.

Stockli, R., Rutishauser, T., Dragoni, D., O'Keefe, J., Thornton, P.E., Jolly, M., Lu, L., Denning, A.S., 2008. Remote sensing data assimilation for a prognostic phenology model. J. Geophys. Res. 113, G04021.

Sturdevant-Rees, P., Smith, J.A., Morrison, J., Baeck, M.L., 2001. Tropical storms and the flood hydrology of the central Appalachians. Water Resour. Res. 37, 2143-2168.

Sun, X., Barros, A.P., 2009. An Evaluation of the Statistics of Rainfall Extremes in Rain Gauge Observations, and Satellite-Based and Reanalysis Products Using Universal Multifractals. Journal of Hydrometeorology 11, 388-404.

Sun, X., Barros, A.P., 2012. The impact of forcing dataset on the high resolution simulation of Tropical Storm Ivan (2004) in the Southern Appalachians. Monthly Weather Review.

Swain, L.A., Mesko, T.O., Hollyday, E.F., 2004. Summary of the Hydrogeology of the Valley and Ridge, Blue Ridge, and Piedmont Physiographic Provinces in the Eastern United States. U.S. Geological Survey, Denver, CO, p. 23.

Swenson, S., Wahr, J., 2006. Post-processing removal of correlated errors in GRACE data. Geophysical Research Letters 33, L08402.

Tao, J., Barros, A.P., 2013. Prospects for flash flood forecasting in mountainous regions – An investigation of Tropical Storm Fay in the Southern Appalachians. Journal of Hydrology.

Tapley, B.D., Bettadpur, S., Watkins, M., Reigber, C., 2004. The gravity recovery and climate experiment: Mission overview and early results. Geophysical Research Letters 31, L09607.

Temesgen, B., Mohammed, M.U., Korme, T., 2001. Natural hazard assessment using GIS and remote sensing methods, with particular reference to the landslides in the Wondogenet Area, Ethiopia. Physics and Chemistry of the Earth, Part C: Solar, Terrestrial & Planetary Science 26, 665-675.

Tesoriero, A.J., Spruill, T.B., Eimers, J.L., 2004. Geochemistry of shallow ground water in coastal plain environments in the southeastern United States: implications for aquifer susceptibility. Applied Geochemistry 19, 1471-1482.

Thérézien, M., Palmroth, S., Brady, R., Oren, R., 2007. Estimation of light interception properties of conifer shoots by an improved photographic method and a 3D model of shoot structure. Tree Physiology 27, 1375-1387.

Thompson, S.E., Harman, C.J., Troch, P.A., Brooks, P.D., Sivapalan, M., 2011. Spatial scale dependence of ecohydrologically mediated water balance partitioning: A synthesis framework for catchment ecohydrology. Water Resources Research 47.

Tucker, C.J., Pinzon, J.E., Brown, M.E., Slayback, D.A., Pak, E.W., Mahoney, R., Vermote, E.F., Saleous, N.E., 2005. An extended AVHRR 8-km NDVI dataset compatible with MODIS and SPOT vegetation NDVI data. International Journal of Remote Sensing 26, 4485 - 4498.

Turner, D.P., Ritts, W.D., Cohen, W.B., Gower, S.T., Running, S.W., Zhao, M., Costa, M.H., Kirschbaum, A.A., Ham, J.M., Saleska, S.R., 2006. Evaluation of MODIS NPP and GPP products across multiple biomes. Remote Sensing of Environment 102, 282-292.

Villarini, G., Smith, J.A., Baeck, M.L., Marchok, T., Vecchi, G.A., 2011. Characterization of rainfall distribution and flooding associated with U.S. landfalling tropical cyclones: Analyses of Hurricanes Frances, Ivan, and Jeanne (2004). J. Geophys. Res. 116, D23116.

Walker, L.R., 1995. Timing of Post-Hurricane Tree Mortality in Puerto Rico. Journal of Tropical Ecology 11, 315-320.

Wang, F., Xu, Y., 2009. Hurricane Katrina-induced forest damage in relation to ecological factors at landscape scale. Environmental Monitoring and Assessment 156, 491-507.

Wang, W., Qu, J.J., Hao, X., Liu, Y., Stanturf, J.A., 2010. Post-hurricane forest damage assessment using satellite remote sensing. Agricultural and Forest Meteorology 150, 122-132.

Webster, P.J., Holland, G.J., Curry, J.A., Chang, H.-R., 2005. Changes in Tropical Cyclone Number, Duration, and Intensity in a Warming Environment. Science 309, 1844-1846.

Weishampel, J.F., Drake, J.B., Cooper, A., Blair, J.B., Hofton, M., 2007. Forest canopy recovery from the 1938 hurricane and subsequent salvage damage measured with airborne LiDAR. Remote Sensing of Environment 109, 142-153.

Wen, S., Fetcher, N., Zimmerman, J.K., 2008. Acclimation of tropical tree species to hurricane disturbance: ontogenetic differences. Tree Physiol 28, 935-946.

Wilson, K.B., Hanson, P.J., Mulholland, P.J., Baldocchi, D.D., Wullschleger, S.D., 2001. A comparison of methods for determining forest evapotranspiration and its components: sap-flow, soil water budget, eddy covariance and catchment water balance. Agricultural and Forest Meteorology 106, 153-168.

Wolock, D.M., Winter, T.C., McMahon, G., 2004. Delineation and Evaluation of Hydrologic-Landscape Regions in the United States Using Geographic Information System Tools and Multivariate Statistical Analyses. Environmental Management 34, S71-S88.

Wooten, R., Gillon, K., Witt, A., Latham, R., Douglas, T., Bauer, J., Fuemmeler, S., Lee, L., 2008. Geologic, geomorphic, and meteorological aspects of debris flows triggered by Hurricanes Frances and Ivan during September 2004 in the Southern Appalachian Mountains of Macon County, North Carolina (southeastern USA). Landslides 5, 31-44.

Xiao, J., Zhuang, Q., Law, B.E., Chen, J., Baldocchi, D.D., Cook, D.R., Oren, R., Richardson, A.D., Wharton, S., Ma, S., Martin, T.A., Verma, S.B., Suyker, A.E., Scott, R.L., Monson, R.K., Litvak, M., Hollinger, D.Y., Sun, G., Davis, K.J., Bolstad, P.V., Burns, S.P., Curtis, P.S., Drake, B.G., Falk, M., Fischer, M.L., Foster, D.R., Gu, L., Hadley, J.L., Katul, G.G., Matamala, R., McNulty, S., Meyers, T.P., Munger, J.W., Noormets, A., Oechel, W.C., Paw U, K.T., Schmid, H.P., Starr, G., Torn, M.S., Wofsy, S.C., 2010. A continuous measure of gross primary production for the conterminous United States derived from MODIS and AmeriFlux data. Remote Sensing of Environment 114, 576-591.

Yang, F., Ichii, K., White, M.A., Hashimoto, H., Michaelis, A.R., Votava, P., Zhu, A.X., Huete, A., Running, S.W., Nemani, R.R., 2007. Developing a continental-scale measure of gross primary production by combining MODIS and AmeriFlux data through Support Vector Machine approach. Remote Sensing of Environment 110, 109-122.

Yildiz, O., Barros, A.P., 2005. Climate variability, water resources, and hydrologic extremes; modeling the water and energy budgets. John Wiley & Sons, Chichester.

Yildiz, O., Barros, A.P., 2007. Elucidating vegetation controls on the hydroclimatology of a mid-latitude basin. Journal of Hydrology 333, 431-448.

Yilmaz, M.T., Hunt Jr, E.R., Jackson, T.J., 2008. Remote sensing of vegetation water content from equivalent water thickness using satellite imagery. Remote Sensing of Environment 112, 2514-2522.

Yuan, W., Liu, S., Zhou, G., Zhou, G., Tieszen, L.L., Baldocchi, D., Bernhofer, C., Gholz, H., Goldstein, A.H., Goulden, M.L., Hollinger, D.Y., Hu, Y., Law, B.E., Stoy, P.C., Vesala, T., Wofsy, S.C., 2007. Deriving a light use efficiency model from eddy covariance flux data for predicting daily gross primary production across biomes. Agricultural and Forest Meteorology 143, 189-207.

Zeng, H., Chambers, J.Q., Negron-Juarez, R.I., Hurtt, G.C., Baker, D.B., Powell, M.D., 2009. Impacts of tropical cyclones on U.S. forest tree mortality and carbon flux from 1851 to 2000. Proceedings of the National Academy of Sciences 106, 7888-7892.

Zhang, X.Y., Goldberg, M., Tarpley, D., Friedl, M.A., Morisette, J., Kogan, F., Yu, Y.Y., 2010. Drought-induced vegetation stress in southwestern North America. Environmental Research Letters 5, -.

Zhao, M., Heinsch, F.A., Nemani, R.R., Running, S.W., 2005. Improvements of the MODIS terrestrial gross and net primary production global data set. Remote Sensing of Environment 95, 164-176.

Zhao, M., Running, S., Heinsch, F.A., Nemani, R., 2011. MODIS-Derived Terrestrial Primary Production
Land Remote Sensing and Global Environmental Change, in: Ramachandran, B., Justice, C.O., Abrams, M.J. (Eds.). Springer New York, pp. 635-660.

Zhao, M., Running, S.W., 2010. Drought-Induced Reduction in Global Terrestrial Net Primary Production from 2000 Through 2009. Science 329, 940-943.

Zhao, M., Running, S.W., Nemani, R.R., 2006. Sensitivity of Moderate Resolution Imaging Spectroradiometer (MODIS) terrestrial primary production to the accuracy of meteorological reanalyses. Journal of Geophysical Research: Biogeosciences 111, G01002.

8 Biography

Julien Brun was born in 1976 in Geneva, Switzerland. He received his B.S. in Biology in 2000, a M.S. in Environmental Sciences with a specialization in Remote Sensing and Geographic Information system in 2003 both from the University of Geneva, Switzerland. He came to the US in 2007 and started the PhD program in Environmental Engineering at Duke University in 2008.

After obtaining his MS, Julien worked several years as a consultant in remote sensing and Geographic information systems, mostly for governmental and international organizations, such as UNITAR. He joined Prof. Ana P. Barros's research group in August 2007, where he completed his Ph.D. in June 2013. Julien has authored and co-authored three peer reviewed publications in the areas of remote sensing, aerosol detection and hydroclimate in the International Journal of Remote Sensing, and Atmospheric Environment and International Journal of Climatology. One additional publication from his Ph.D. research is in preparation for publication in the Journal of Biogeosciences.

During the graduate studies, Julien received the NASA Earth Science System Fellowship (2009-2012) to pursue his research work. He also received the AMS student poster award during the second symposium in aerosol cloud climate interaction 2009 jointly with Prabhakar Shrestha.